

https://dspace.org/

The optimisation and design of catenary barrel vaults for excessive wind load

Le Roux, Jeandré Stefan

2017

https://hdl.handle.net/10539/24035

Le Roux, Jeandré Stefan (2017) The optimisation and design of catenary barrel vaults for excessive wind load, University of the Witwatersrand, <https://hdl.handle.net/10539/24035>

Downloaded from a DSpace repository. https://dspace.org/

THE OPTIMISATION AND DESIGN OF CATENARY BARREL VAULTS FOR EXCESSIVE WIND LOAD



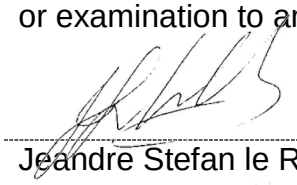
Jeandré Stefan le Roux

A research report submitted to the Faculty of Engineering and the Built Environment, University of the Witwatersrand, Johannesburg, in partial fulfilment of the requirements for the degree of Master of Science in Engineering.

Johannesburg 2017

DECLERATION

I declare that this research report is my own unaided work. It is being submitted to the Degree of Master of Science to the University of the Witwatersrand, Johannesburg. It has not been submitted for any degree or examination to any other University.



Jeandre Stefan le Roux

29th day of September year 2017

ABSTRACT

The present study investigates the possibility of designing a catenary barrel vault, which can be implemented in regions where extreme tropical storms are frequently experienced. It moreover investigated the effect of non-uniform wind loads on catenary barrel vaults, and how to solve for these load conditions efficiently.

The effects of high, non-uniform wind loads were assessed, and possible solutions were explored to determine a structurally efficient solution in resisting the loads applied. Different analysis and design techniques were explored in this research. These techniques included the optimization of the geometry, in resisting the applied loads most efficiently, as well as the structural design of the section in ensuring a durable and safe structure.

The study revealed that the geometry of the structure cannot be optimised to resist the applied loads in a catenary fashion without external aid. By draping the vault in a post-tensioned basalt geogrid mesh, axial compression can be increased in the section and geometry optimisation can be achieved in resisting the applied loads in a catenary fashion. Three post-tensioning techniques were investigated and discussed.

In loving memory of my late mother

Erika le Roux

ACKNOWLEDGEMENTS

I would like to thank:

1. My loving wife, E. le Roux, for her unduly support and encouragement throughout my studies.
2. My loving and supportive mother and father in law, Johan and Hester Norté.
3. My supervisor, Professor M. Gohnert, for the support and encouragement received while undertaking this research.
4. Mr. D. Surat, for the supply of test results regarding basalt geogrid characteristic properties.
5. Hydraform for their willingness in assisting me with the characteristic properties for earth bricks.
6. Eskom Holdings for the funding of my studies.

Table of Contents

DECLERATION ..... **I**

ABSTRACT ..... **II**

ACKNOWLEDGEMENTS ..... **IV**

LIST OF FIGURES ..... **VIII**

LIST OF TABLES ..... **XIX**

1. INTRODUCTION **1**

1.1 GENERAL 1
1.2 TYPHOONS AND THEIR EFFECTS ON THE PHILIPPIAN COMMUNITIES 2
1.2.1 Super Typhoon Haiyan 2
1.2.2 Typhoon Haima 4
1.2.3 A History of Tropical Cyclones 5
1.3 POVERTY IN THE PHILIPPINES 6
1.3.1 Current Poverty Status 6
1.3.2 A History of Poverty 7
1.3.3 Characteristics of the Poor 7
1.3.4 Causes of Poverty in the Philippines 8
1.4 OBJECTIVES 8
1.5 SCOPE 9

2. LITERATURE REVIEW **10**

2.1 AN INTRODUCTION TO ARCHES 10
2.1.1 History of Arches 10
2.1.2 Collapse Mechanism of Arches 11
2.1.3 Design of Arches 13
2.2 CATENARY STRUCTURES 14
2.2.1 The Funicular Form 14
2.2.2 The Catenary Arch 16
2.3 WIND LOAD ON VAULTED STRUCTURES 40
2.3.1 Defining Wind Load 40
2.3.2 Tropical Cyclones 43
2.3.3 Limit State Design Approach 48
2.3.4 Wind loads as per SANS 10160-3:2011 50
2.3.5 Wind Loads on Catenary Vaults 56
2.4 DESIGN OF THE SHELL 57
2.4.1 Dealing with Tensile Stresses 58
2.4.2 Design of the Masonry Section 60
2.5 PRE-STRESSING OF STRUCTURES 80
2.5.1 Mechanics of Pre-stressing 80
2.5.2 Traditional Pre-stressing Materials 84
2.5.3 Basalt Geo-reinforcing 87
2.5.4 Loss of Pre-stress 90

3. FORM FINDING TECHNIQUES **93**

3.1 INTRODUCTION 93
3.1.1 Practical Living Space Definition 93
3.1.2 Design Objectives 94
3.1.3 Alternative Designs 95
3.1.4 Initial Geometry Definition 100
3.2 DESIGN LOAD CONSIDERATIONS 101
3.2.1 Self-weight 102

3.2.2 Wind Load ... 103
3.3 FINDING THE MOST EFFICIENT SHAPE ... 119
3.3.1 Graph Interpretation ... 121
3.3.2 Funicular Curve for Elevated Flat Vaults ... 123
3.3.3 Funicular Curve for Steep Vault ... 128
3.3.4 Post-tensioned Vaults ... 140
3.4 TESTED MATERIALS ... 160
3.4.1 Basalt Geogrid Mechanical Properties ... 160
3.4.2 Earth Bricks Mechanical Properties ... 162
3.5 FEA ANALYSIS ... 164
3.5.1 Introduction ... 164
3.5.2 Traditionally Shaped Post-tensioned Vault ... 165
3.5.3 Five Point Contact Post-tensioned Vault Solutions ... 174
3.5.4 Buckling Analysis ... 225

4. STRUCTURAL DESIGN ... 238

4.1 INTRODUCTION ... 238
4.2 DESIGN LOAD SUMMARY ... 239
4.3 MATERIAL PROPERTIES ... 240
4.4 DESIGN OF SHELL ... 241
4.4.1 250mm Shell Thickness ... 242
4.4.2 335mm Shell Thickness ... 244
4.4.3 350mm Shell Thickness ... 245
4.4.4 Normal Reinforcement ... 246
4.5 POST-TENSION DESIGN ... 251
4.5.1 Introduction ... 251
4.5.2 Transfer Force Application ... 252
4.5.3 Results Interpretation ... 254

5. FINAL SOLUTION ... 257

5.1 3D ISOMETRIC MODELLING ... 257
5.2 EXPLORED METHODS OF POST-TENSIONING ... 258
5.2.1 Uniform Ratchet Tensioning ... 259
5.2.2 Funicular Chain Block Tensioning ... 265
5.2.3 Winch Tensioning ... 274
5.3 GABLE END WALLS ... 276
5.4 POST-TENSION BEARING PADS ... 277
5.5 ERECTION SEQUENCE ... 279

6. CONCLUSIONS AND RECOMMENDATIONS ... 280

6.1 FINDINGS ... 280
6.2 ON THE GEOMETRY OF THE VAULT ... 281
6.3 ON THE PERFORMANCE CRITERIA OF THE VAULT ... 281
6.4 ON POST-TENSIONING SOLUTIONS ... 283
6.4.1 Ratchet Tensioning ... 284
6.4.2 Funicular Cable Tensioning ... 284
6.4.3 Winch Tensioning ... 284
6.5 RECOMMENDATIONS ... 285

APPENDIX A : FINAL GEOMETRY COORDINATES ... 287

APPENDIX B : DESIGN CALCULATION ... 288

B.1 SECTION CAPACITY VERIFICATION FOR 250MM SHELL THICNKESS WITH 22KN POST-TENSION ... 288
B.2 SECTION CAPACITY VERIFICATION FOR 335MM SECTION WITH 13KN POST-TENSION FORCE ... 289

B.3 SECTION CAPACITY VERIFICATION FOR 350MM SECTION WITH 25KN POST-TENSION 290
B.4 BUCKLING LOAD OF 250MM VAULT WITH 22KN POST-TENSION 291
B.5 BUCKLING LOAD OF 335MM VAULT WITH 13.5KN POST-TENSION 292
B.6 BUCKLING LOAD OF 350MM VAULT WITH 25KN POST-TENSION 293
B.7 POST-TENSION DESIGN FOR 350MM VAULT WITH 25KN POST-TENSION FORCE 294

REFERENCES 295

LIST OF FIGURES

Figure 1.1: Super Typhoon Haiyan seen from outer space (Marsh, 2013). 3
Figure 1.2: Residents walking in the street after Super Typhoon Haiyan (Jaramillo, 2013). 3
Figure 1.3: Damaged house after Super Typhoon Haiyan (Jaramillo, 2013). 4
Figure 2.1: Corbelled arch (Cowan, 1977). 11
Figure 2.2: True arch (Cowan, 1977). 11
Figure 2.3: Collapse of a semi-circular masonry arch under a point load (Huerta, 2001). 13
Figure 2.4: Graphical representation of a hanging chain and it's inverted catenary arch shape (Allan *et al.*, 2010). 16
Figure 2.5: Catenary arch for uniform load (Gohnert & Bradley, 2016). ... 17
Figure 2.6: Reactions of a catenary arch subjected to self-weight (Gohnert & Bradley, 2016). 18
Figure 2.7: Growth of the funicular shape, starting with stem element (Gohnert & Bradley, 2016). 20
Figure 2.8: Triangular shape to support a point load in pure compression (Gohnert & Bradley, 2016). 22
Figure 2.9: Shifting of the line of thrust of a masonry vault due to a change in support condition (Huerta, 2001). 23
Figure 2.10: Kern points of rectangular cross section 25
Figure 2.11: Stress condition in section of arch (Curtin *et al.*, 1995). 26
Figure 2.12 : Two buckling modes of a two hinged arch (Jinsan & Yanlin, 2002). 26
Figure 2.13 : Buckling profile of a uniformly compressed circular arch with hinged ends (Timoshenko & Gere, 1963). 29
Figure 2.14 : Buckling profile of a uniformly compressed circular arch with fixed ends (Timoshenko & Gere, 1963). 30
Figure 2.15: Buckling coefficient (β) for in-plane buckling of a monolithic arch system (German Building and Civil

Engineering Standards Committee & German Committee for Structural Steelwork, 1990). 33
Figure 2.16: Buckling coefficient (β) for in-plane buckling of an one hinged arch system (German Building and Civil Engineering Standards Committee & German Committee for Structural Steelwork, 1990). 33
Figure 2.17: Buckling coefficient (β) for in-plane buckling of a two hinged arch system (German Building and Civil Engineering Standards Committee & German Committee for Structural Steelwork, 1990). 34
Figure 2.18: Buckling coefficient (β) for in-plane buckling of a three hinged arch system (German Building and Civil Engineering Standards Committee & German Committee for Structural Steelwork, 1990). 34
Figure 2.19: Buckling of a catenary arch under self-weight (Pedreschi & Theodossopoulos, 2007) 36
Figure 2.20: Design charts for the buckling of catenary arches (Pedreschi & Theodossopoulos, 2007). 37
Figure 2.21: Double cantilever free-standing vault at Refresco del Norte, Uruguay (Pedreschi, 2006). 38
Figure 2.22: Looped pre-stressing steel in vault (Pedreschi, 2006). 39
Figure 2.23: Wind flow near the boundary layer of the earth's surface (Holmes, 2001). 41
Figure 2.24: The apparent Coriolis force due to the earth's rotation (Holmes, 2001). 42
Figure 2.25: Balanced geostrophic flow in the Northern and Southern hemisphere (Holmes, 2001). 43
Figure 2.26: Three-dimensional vortex structure in a developed tropical cyclone (Holmes, 2001). 44
Figure 2.27: Gradient wind speed for Cyclone "Tracy" (Holmes, 2001). .. 45
Figure 2.28: Probability densities for load effects and resistance (Holmes, 2001). 49

Figure 2.29: Map of the fundamental value of the basic wind speed in South Africa (SABS, 2011). 51
Figure 2.30: Terrain categories for the determination of the roughness factor (SABS, 2011). 52
Figure 2.31: Variation of the roughness factor with height above ground level (SABS, 2011). 53
Figure 2.32: Recommended values of external pressure coefficients for vaulted roofs with rectangular bases (SABS, 2011). 55
Figure 2.33: Wind azimuth direction 0/180 degrees (Bradley, Gohnert, Goliger & Mistry, 2016)..... 56
Figure 2.34: Wind azimuth direction 30/45 degrees (Bradley *et al.*, 2016) 57
Figure 2.35: Wind azimuth direction 90/270 degrees (Bradley *et al.*, 2016) 57
Figure 2.36: Factors affecting the compressive strength of masonry (Curtin *et al.*, 1995)..... 60
Figure 2.37: Compressive strength of a variety of masonry units (Curtin *et al.*, 1995). 62
Figure 2.38: Determination of the shape factor of a masonry brick (Curtin *et al.*, 1995)..... 63
Figure 2.39: Mortar requirements according to BS 5628 Part 1 (Curtin *et al.*, 1995). 63
Figure 2.40: Characteristic compressive strength of masonry (fk) for solid bricks having a ratio of height to least horizontal dimension of between 2.0 and 4.0 as per BS 5628 - Table 2d (Curtin *et al.*, 1995)..... 64
Figure 2.41: Partial factors of safety on materials (Curtin *et al.*, 1995). ... 65
Figure 2.42: Capacity reduction factor for load bearing masonry structures (Curtin *et al.*, 1995)..... 67
Figure 2.43: Un-cracked vs cracked masonry sections (Curtin *et al.*, 1995). 69

Figure 2.44: Characteristic flexural strength of masonry (Curtin *et al.*, 1995). 70
Figure 2.45: Exaggerated action of stability moment (Curtin *et al.*, 1995). 72
Figure 2.46: Assumed moment equilibrium in cracked masonry section (Curtin *et al.*, 1995)..... 73
Figure 2.47: Illustration of the difference between normal reinforcement and pre-stressing (Curtin *et al.*, 1995). 75
Figure 2.48: Section through a normally reinforced masonry section (Curtin *et al.*, 1995)..... 76
Figure 2.49: Stress strain relationship in a reinforced masonry section (Curtin *et al.*, 1995)..... 77
Figure 2.50: Partial factor of safety for masonry in reinforced sections in ultimate limit state (Curtin *et al.*, 1995). 77
Figure 2.51: Partial factor of safety on materials – ultimate and accidental damage limit states (Curtin *et al.*, 1995)..... 78
Figure 2.52: Section through a typical post-tensioned masonry column (Curtin *et al.*, 1995)..... 81
Figure 2.53: Stress state in a concentrically pre-stressed element (Curtin *et al.*, 1995)..... 82
Figure 2.54: Stress state of a post-tensioned masonry section before, during and after wind load (Curtin *et al.*, 1995). 83
Figure 2.55: Tensile strength and elongation characteristics of cold drawn stress relieved wires (Raju, 2007). 84
Figure 2.56: Mechanical properties of high-tensile steel bars (Raju, 2007). 84
Figure 2.57: Mechanical properties of high tensile indented wires (Raju, 2007). 85
Figure 2.58: Mechanical properties of uncoated stress-relieved strands (Raju, 2007). 85
Figure 2.59: Stress-strain curves for reinforcing and pre-stress steel (Raju, 2007). 86

Figure 2.60: Mechanical properties of basalt fibres (Sim *et al.*, 2005). 88
Figure 2.61: Characteristic properties of basalt fibres (Saravanan, 2006) 88
Figure 2.62: Typical stress-strain diagram of basalt fibres vs fibre glass (Fiore *et al.*, 2015). 89
Figure 3.1: Elevated flat vault on vertical walls subjected to wind flow. ... 96
Figure 3.2: Steep vault subjected to wind load. 97
Figure 3.3: Traditionally shaped catenary vault - post-tensioned along geometric centroid. 99
Figure 3.4: Optimised catenary vault - post-tensioned by externally placed tendon. 100
Figure 3.5: Resultant pressure force on elevated flat vault - load case 1 104
Figure 3.6: Resultant pressure force on elevated flat vault - load case 2. 104
Figure 3.7: Resultant pressure force on steep vault for normal wind speeds - load case 1 (Bradley *et al.*, 2016). 107
Figure 3.8: Resultant pressure force on steep vault for normal wind speeds - load case 2 (Bradley *et al.*, 2016). 108
Figure 3.9: Resultant pressure force on steep vault for normal wind speeds - load case 3 (Bradley *et al.*, 2016). 108
Figure 3.10: Resultant pressure force on steep vault for normal wind speeds - load case 4 (Bradley *et al.*, 2016). 109
Figure 3.11: Resultant pressure force on steep vault for normal wind speeds - load case 5 (Bradley *et al.*, 2016). 109
Figure 3.12: Resultant pressure force on steep vault for normal wind speeds - load case 6 (Bradley *et al.*, 2016). 110
Figure 3.13: Resultant pressure force on steep vault for 300kph wind speed - load case 1 (Bradley *et al.*, 2016). 113
Figure 3.14: Resultant pressure force on steep vault for 300kph wind speed - load case 2 (Bradley *et al.*, 2016). 114

Figure 3.15: Resultant pressure force on steep vault for 300kph wind speed - load case 3 (Bradley *et al.*, 2016). 114
Figure 3.16: Resultant pressure force on steep vault for 300kph wind speed - load case 4 (Bradley *et al.*, 2016). 115
Figure 3.17: Resultant pressure force on steep vault for 300kph wind speed - load case 5 (Bradley *et al.*, 2016). 115
Figure 3.18: Resultant pressure force on steep vault for 300kph wind speed - load case 6 (Bradley *et al.*, 2016). 116
Figure 3.19: Catenary arch subjected to a 5kN point load at its centreline (Gohnert, 2016). 120
Figure 3.20: Convergence of the funicular curve based on normal pressure load assignments to the curve. 121
Figure 3.21: FLPC for elevated flat vault of 250mm thickness subjected to gravity and wind loads as per Table 10 (LC1). 124
Figure 3.22: FLPC for elevated flat vault of 1000mm thickness subjected to gravity and wind loads as per Table 10 (LC1). 125
Figure 3.23: FLPC for elevated flat vault of 250mm thickness subjected to gravity and wind loads as per Table 10 (LC2). 126
Figure 3.24: FLPC for elevated flat vault of 1000mm thickness subjected to gravity and wind loads as per Table 10 (LC2). 127
Figure 3.25: FLPC for steep vault of 250mm thickness subjected to gravity and wind loads (LC1) as per Table 11. 128
Figure 3.26: FLPC for steep vault of 250mm thickness subjected to gravity and wind loads (LC2) as per Table 11. 129
Figure 3.27: FLPC for steep vault of 250mm thickness subjected to gravity and wind loads (LC3) as per Table 11. 129
Figure 3.28: FLPC for steep vault of 250mm thickness subjected to gravity and wind loads (LC4) as per Table 11. 130
Figure 3.29: FLPC for steep vault of 250mm thickness subjected to gravity and wind loads (LC5) as per Table 11. 130
Figure 3.30: FLPC for steep vault of 250mm thickness subjected to gravity and wind loads (LC6) as per Table 11. 131

Figure 3.31: FLPC for steep vault of 250mm thickness subjected to gravity and wind loads (LC1) as per Table 12. 132
Figure 3.32: FLPC for steep vault of 250mm thickness subjected to gravity and wind loads (LC2) as per Table 12. 133
Figure 3.33: FLPC for steep vault of 250mm thickness subjected to gravity and wind loads (LC3) as per Table 12. 133
Figure 3.34: FLPC for steep vault of 250mm thickness subjected to gravity and wind loads (LC4) as per Table 12. 134
Figure 3.35: FLPC for steep vault of 250mm thickness subjected to gravity and wind loads (LC5) as per Table 12. 134
Figure 3.36: FLPC for steep vault of 250mm thickness subjected to gravity and wind loads (LC6) as per Table 12. 135
Figure 3.37: FLPC for steep vault of 1000mm thickness subjected to gravity and wind loads (LC1) as per Table 12. 136
Figure 3.38: FLPC for steep vault of 1000mm thickness subjected to gravity and wind loads (LC2) as per Table 12. 137
Figure 3.39: FLPC for steep vault of 1000mm thickness subjected to gravity and wind loads (LC3) as per Table 12. 137
Figure 3.40: FLPC for steep vault of 1000mm thickness subjected to gravity and wind loads (LC4) as per Table 12. 138
Figure 3.41: FLPC for steep vault of 1000mm thickness subjected to gravity and wind loads (LC5) as per Table 12. 138
Figure 3.42: FLPC for steep vault of 1000mm thickness subjected to gravity and wind loads (LC6) as per Table 12. 139
Figure 3.43: Simply supported beam with parabolic tendon (Marshall & Robberts, 2000). 143
Figure 3.44: Schematic of vault draped in post-tension tendon and supported at 800mm increments. 144
Figure 3.45: Optimised catenary geometry for externally draped post-tensioned tendon, supported along the vault's arch, and exerting a 10kN point loads along vault surface. 145

Figure 3.46: Optimised catenary geometry for externally draped post-tensioned tendon, supported along the vault's arch, and exerting a uniform 1kN load on vault surface. 146
Figure 3.47: Optimised catenary geometry for externally draped post-tensioned tendon, supported along the vault's arch, and exerting a uniform 1000kN load on vault surface. 147
Figure 3.48: Schematic of vault draped in post-tension tendon and supported along 1000mm of crown. 148
Figure 3.49: Optimised catenary geometry for externally draped post-tensioned tendon, supported along the vault's crown, and exerting a uniform 1kN load on vault surface. 149
Figure 3.50: Hanging chain principle and the effect of uniform and concentrated loads on the chain and inverted arch. 150
Figure 3.51: Optimised catenary geometry for externally draped post-tensioned tendon, supported along the vault's crown, and exerting a uniform 1000kN load on vault surface. 151
Figure 3.52: Schematic of vault draped in post-tension tendon and supported at three definitive locations. 152
Figure 3.53: Optimised catenary geometry for externally draped post-tensioned tendon, supported at three pertinent positions, and exerting a 30kN point load..... 153
Figure 3.54: Schematic of vault draped in post-tension tendon and supported at five definitive locations..... 154
Figure 3.55: Optimised catenary geometry for externally draped post-tensioned tendon, supported at five pertinent positions, and exerting a 5kN point load..... 155
Figure 3.56: Optimised catenary geometry for externally draped post-tensioned tendon, supported at five pertinent positions, and exerting a 30kN point load..... 156
Figure 3.57: Optimised catenary geometry for externally draped post-tensioned tendon, supported at five pertinent positions, and exerting a 1000kN point load..... 156

Figure 3.58: FLPC for five point post-tensioned vault, subjected to all load conditions. 159
Figure 3.59: Isometric view (StaadPro V8i FEA model) of traditional catenary vault with concentrically placed post-tension tendon. . 165
Figure 3.60: Graphical representation of stress reduction vs tendon force increase for data as per Table 17. 172
Figure 3.61: Graphical representation of bending moment reduction vs tendon force increase for data presented in Table 17. 173
Figure 3.62: Five point contact post-tensioned vault (StaadPro V8i model) for no tension allowed in 300kph wind load condition.... 176
Figure 3.63: Convergence of FLPC based on bending moment in section of five point contact optimised vault. 177
Figure 3.64: Five point contact post-tensioned vault (StaadPro V8i model) tendon support loads for no tension allowed in 300kph wind load condition. 182
Figure 3.65: 250mm thick vault post-tensioned to 22kN effective post-tensioning. 186
Figure 3.66: Five point contact post-tensioned vault (StaadPro V8i model) tendon support loads for no tension allowed in service wind load condition - 22kN effective post-tensioning. 188
Figure 3.67: 335mm thick vault post-tensioned to 13kN effective post-tensioning. 200
Figure 3.68: 350mm thick vault post-tensioned to 25kN effective post-tensioning. 213
Figure 3.69: Axial force diagram for five point contact post-tensioned vault without string grouping (Strand7). 227
Figure 3.70: Bending moment diagram for five point contact post-tensioned vault without string grouping (Strand7). 228
Figure 3.71: Buckling mode shapes for dominant load case of vault post-tensioned to pure compression for service loads (Strand7). 229

Figure 3.72: Buckling mode shapes for LC6 as per Table 12 for vault post-tensioned to pure compression for service loads (Strand7). 230
Figure 3.73: Bending moment diagram for five point contact post-tensioned vault with string grouping (Strand7). 231
Figure 3.74: Axial force diagram for five point contact post-tensioned vault with string grouping (Strand7). 232
Figure 3.75: Buckling mode shapes for dominant load case of vault post-tensioned to pure compression for 300kph wind loads (Strand7). 232
Figure 3.76: Buckling mode shapes for LC6 as per Table 12 for vault post-tensioned to pure compression for 300kph wind loads (Strand7). 234
Figure 4.1: Loads applicable to shell section. 242
Figure 5.1: Basic components of the final solution in isometric view. 258
Figure 5.2: Six ratchet post-tensioning jack configuration. 260
Figure 5.3: Edge preparation of basalt geogrid for effective load transfer from load distribution beam to mesh. 261
Figure 5.4: Six ratchet post-tensioning jack configuration. 262
Figure 5.5: 2 Metric ton cable ratchet (“2 Ton Power Puller | TEKTON 5541”, 2016) 263
Figure 5.6: Ratchet configuration - anchor foundation. 264
Figure 5.7: Funicular chain block tensioning configuration. 266
Figure 5.8: Schematic illustration of basalt geogrid mesh’s force application under post-tensioning. 267
Figure 5.9: Bow’s notation on basalt geogrid mesh (Allan *et al.*, 2010). 268
Figure 5.10: Force diagram at transfer. 270
Figure 5.11: Funicular profile for cable tensioning at transfer. 271
Figure 5.12: Funicular cable tensioning anchor foundations. 272
Figure 5.13: Funicular cable tensioning – tied strip footing for anchor foundation and section at foundation level. 273
Figure 5.14: Winch tensioning 275

Figure 5.15: Bending moment, reaction and deflection for equal span beams under uniform load (Davison & Owens, 2008). 275
Figure 5.16: Post-tension bearing pad details. 278
Figure 6.1: Final vault geometry 282
Figure 6.2: Post-tensioning solutions. 283

LIST OF TABLES

Table 1: 10 Deadliest typhoons in the Philippians till 2012 (Padua, 2013). 5
Table 2: Magnitude of poverty in the Philippines population, 1985 – 2000 (Asian Development Bank, 2009). 7
Table 3 : Common Euler buckling equations (Timoshenko & Gere, 1963) 28
Table 4 : Values of the constant ($\gamma 4$) for catenary arches of constant cross section with load uniformly distributed along the arch's axis (Timoshenko & Gere, 1963). 35
Table 5: Saffir-Simpson hurricane wind scale (Rowlett & University of North Carolina, 2000). 46
Table 6: Factors that influence losses or gains in post-tension force (Curtin *et al.*, 1995) 81
Table 7: Causes for the loss of pre-stress (Raju, 2007). 92
Table 8: Stress conditions considered for the design of the vault section. 94
Table 9: Basic Vault Dimensions 101
Table 10: Summary of wind pressures on elevated flat vaults. 105
Table 11: Summary of wind pressure on steep vault for normal wind speeds 111
Table 12: Summary of wind pressure on steep vault for 300kph wind speeds 117
Table 13: Basalt geogrid mechanical properties tested at the University of the Witwatersrand, South Africa (Surat, D (Personal communication)). 161
Table 14: Characteristic properties of earth bricks (Heuer, N (Personal communication)). 162
Table 15: Load combinations for FEA model. 167
Table 16: A visual illustration of load combinations (StaadPro V8i FEA model) for a traditional concentrically post-tensioned vault. 168

Table 17: Worst Case Scenario on Tendon force vs tensile stress and bending moment in section of traditional catenary vault in concentric post-tension configuration. 171
Table 18: Visual illustration of load combination (StaadPro V8i FEA model) for a five point contact post-tensioned vault. 179
Table 19: Tendon loads for different load combination of five point post-tension vault for no tension allowed in 300kph wind load condition. 182
Table 20: Tendon support loads for different load combination of five point post-tension vault for no tension allowed in 300kph wind load condition. 183
Table 21: Foundation loads for five point contact post-tensioned vault where no tension is allowed in 300kph wind load condition. 184
Table 22: Tendon loads for different load combination of five point post-tension vault for no tension allowed in service wind load condition - 22kN effective post-tensioning. 187
Table 23: Tendon support loads for different load combination of five point post-tension vault for no tension allowed in service wind load condition - 22kN effective post-tensioning. 189
Table 24: Foundation loads for five point contact post-tensioned vault where no tension is allowed for service wind load condition - 22kN effective post-tensioning. 190
Table 25: Tendon loads for different load combination of five point post-tension vault for no tension allowed in ultimate wind load condition - 22kN effective post-tensioning. 191
Table 26: Tendon support loads for different load combinations of five point post-tension vault for no tension allowed in ultimate wind load condition - 22kN effective post-tensioning. 192
Table 27: Foundation loads for five point contact post-tensioned vault where no tension is allowed for ultimate wind load condition - 22kN effective post-tensioning. 194

Table 28: Tendon loads for different load combination of five point load post-tension vault for no tension in 300kph wind load condition - - 22kN effective post-tensioning. 196
Table 29: Tendon support loads for different load combinations of five point post-tension vault for no tension in 300kph wind load condition - 22kN effective post-tensioning. 197
Table 30: Foundation loads for five point contact post-tensioned vault where no tension is allowed for 300kph wind load condition - 22kN effective post-tensioning. 198
Table 31: Tendon loads where no tension is allowed in service wind load condition with 13kN post-tension force. 201
Table 32: Tendon support loads where no tension allowed in service wind load condition with 13kN post-tension force. 202
Table 33: Foundation loads where no tension is allowed in service wind load condition with 13kN post-tension force. 203
Table 34: Tendon loads for 335mm vault at 13kN post-tension force. ... 204
Table 35: Tendon support loads for 335mm vault at 13kN post-tension force. 205
Table 36: Foundation loads for 335mm vault at 13kN post-tension force. 206
Table 37: Tendon loads for final vault configuration where no tension is allowed in hurricane wind load condition with 13kN post-tension force. 207
Table 38: Tendon support loads for final vault configuration for no tension allowed in hurricane wind load condition with 13kN post-tension force. 208
Table 39: Foundation loads for final vault configuration where no tension is allowed for hurricane wind load condition with 13kN post-tension force. 209
Table 40: Section capacity vs applied forces for 335mm effective shell thickness at 13kN post-tension force 211

Table 41: Summary of section capacity for different structural parameters. 212
Table 42: Tendon loads for 350mm vault with 25kN post-tension..... 215
Table 43: Tendon support loads for 350mm vault with 25kN post-tension..... 215
Table 44: Foundation loads for 350mm vault with 25kN post-tension.... 217
Table 45: Tendon loads for 350mm vault with 25kN post-tension in ultimate limit state condition. 218
Table 46: Tendon support loads for 350mm vault with 25kN post-tension in ultimate limit state condition. 219
Table 47: Foundation loads for 350mm vault with 25kN post-tension in ultimate limit state condition. 220
Table 48: Tendon loads for 350mm vault with 25kN post-tension in hurricane wind condition..... 222
Table 49: Tendon support loads for 350mm vault with 25kN post-tension in hurricane wind condition. 222
Table 50: Foundation loads for 350mm vault with 25kN post-tension in hurricane wind condition..... 224
Table 51: Critical buckling load factors for dominant load case of vault post-tensioned to pure compression for service loads. 229
Table 52: Critical buckling load factors for dominant load case of vault post-tensioned to pure compression for 300kph wind loads..... 233
Table 53: Critical buckling loads of 250mm and 335mm thick catenary vault..... 235
Table 54: Section capacity vs applied forces for 250mm effective shell thickness with 22kN post-tension force. 247
Table 55: Section capacity vs applied forces for 350mm effective shell thickness with 25kN post-tension force 249
Table 56: Tendon loads for 350mm vault with 33.5kN jacking force. 254
Table 57: Tendon support loads for 350mm vault with 33.5kN jacking force. 255
Table 58: Foundation loads for 350mm vault with 33.5kN jacking force. 255

Table 59: Section capacity vs applied forces for 350mm effective shell thickness with 31.25kN transfer post-tension force. 256

1. INTRODUCTION

1.1 GENERAL

The geometric definition of structures in resisting loads most optimally has been a topic of research for many centuries. The catenary arch and its evolved sister shape, the catenary vault, are known for its efficient utilization of the materials it is constructed of. As a result, these majestic structures require minimal materials to achieve significant spans, making them cost effective and efficient in solving structural problems.

As construction materials get increasingly more expensive, it is thought that the use of these structures will play a key role in future construction. By implementing these structures effectively in poor communities, governments of third world nations may be able to supply such structures in high volumes to underprivileged communities at reduced cost.

The Philippines is considered one of the countries which may benefit from such an initiative. Tropical storms are, however, found to be a challenging aspect in these regions, as these storms tend to result in extensive damage to property of the poor and wealthy communities. It is therefore thought that it would be beneficial if these housing initiatives take into account these adverse weather conditions, and supply the underprivileged with low cost, durable and safe structures.

Catenary vaults are, however, sensitive to non-uniform loading. As a result, a need arises to investigate whether catenary shaped vaults can be designed to feasibly resist loads it may be subjected to during a Category 5 tropical cyclone (Typhoon).

1.2 TYPHOONS AND THEIR EFFECTS ON THE PHILIPPIAN COMMUNITIES

1.2.1 Super Typhoon Haiyan

On Friday morning, the 8th of November 2013, Super Typhoon Haiyan made first landfall at the Philippian islands in the East (Mullen, 2013). With 25 million people in its path, the typhoon plowed through the islands of this third world nation, leaving only devastation in its wake (Mullen, 2013). Apart from flights being cancelled and casualties reported, over 100 000 people were forced to take shelter in evacuation centers (Mullen, 2013). For the most part, the typhoon destroyed their homes and everything they held dear (Mullen, 2013).

"With sustained winds of 315 kph (195 mph) and gusts as strong as 380 kph (235 mph), Haiyan was probably the strongest tropical cyclone to hit land anywhere in the world in recorded history." - (Mullen, 2013)

As the typhoon passed through the vulnerable tropical islands towards the West, it retained most of its strength and saw sustained wind speeds of 295kph, and gusts as strong as 360kph (Mullen, 2013). As a result, it was classified as a Category 5 typhoon according to the Saffir-Simpson Hurricane Scale (Rowlett & University of North Carolina, 2000).

The typhoon was visible from outer space as depicted in Figure 1.1[1], indicating the eye of the storm approaching the Archipelago. Figure 1.2 and Figure 1.3 depicts the devastating aftermath of Super Typhoon Haiyan, where over 10 000 souls were lost (Jaramillo, 2013).

[1] Images, figures and tables, not compiled or created by the author, but included in this report as reference, were copied in terms of "Fair Dealing" in Section 12 of the SA Copyright Act No. 98 of 1978 (as amended).

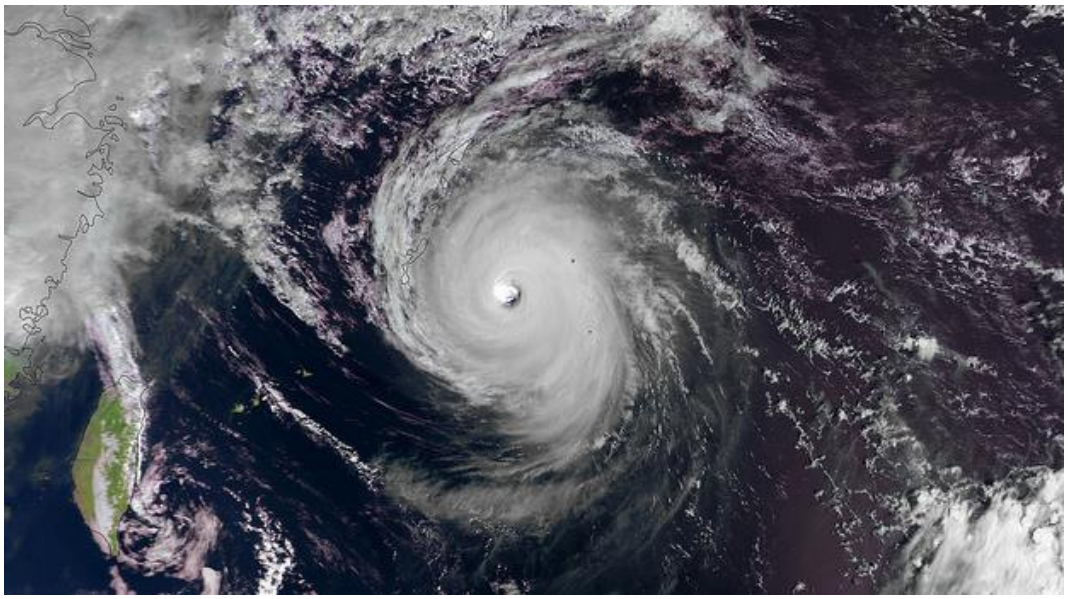


Figure 1.1: Super Typhoon Haiyan seen from outer space (Marsh, 2013).



Figure 1.2: Residents walking in the street after Super Typhoon Haiyan (Jaramillo, 2013).



Figure 1.3: Damaged house after Super Typhoon Haiyan (Jaramillo, 2013).

1.2.2 Typhoon Haima

Typhoons such as Haiyan are, however, not an isolated incident in these regions. On Wednesday evening, 19 October 2016, typhoon Haima made landfall on the North-eastern end of the Archipelago (Griffiths, Berlinger, Westcott & Alexander, 2016). It was the second typhoon to hit the Philippian islands in less than a week with torrential rain and raging winds (Griffiths *et al.*, 2016). At landfall, she was categorised as a Category 4 typhoon according to the Saffir-Simpson Hurricane Scale, with raging winds of 220kph (Rowlett & University of North Carolina, 2000; Griffiths *et al.*, 2016). At her peak, she packed winds of up to 315kph, raising her categorisation to a Category 5 typhoon (Griffiths *et al.*, 2016).

1.2.3 A History of Tropical Cyclones

Considering the tropical storm history of the Philippian archipelago of over 7100 islands, the islands are hit by an average of 20 typhoons or tropical storms each year (Padua, 2013). An increase in the amount of sever typhoons are recorded, as Super Typhoon Haiyan was the 24th tropical storm of the year, exceeding the annual average (Padua, 2013). This change is ascribed, among other reasons, to the controversial phenomenon of global warming (Padua, 2013). Scientists, however, deem it premature to make global warming the scapegoat for storms such as Haiyan in this era, as devastating storms have numerous times rocked the Philippian islands in the past (Padua, 2013).

Horrific tropical storms, recorded as early as 1951, are listed in Table 1, and reinforce the adverse weather conditions these regions are faced with frequently.

Table 1: 10 Deadliest typhoons in the Philippians till 2012 (Padua, 2013).

Name	Date	Casualties
Typhoon Thelma	15 Nov 1991	5100
Typhoon Bopha	3 Dec 2012	1900
Typhoon Ike	31 Aug 1984	1363
Typhoon Washi	16 Dec 2011	1080
Typhoon Trix	16 Oct 1952	995
Typhoon Amy	9 Dec 1951	991
Typhoon Nina	25 Nov 1987	979
Typhoon Fengshen	20 Jun 2008	938
Typhoon Angela	2 Nov 1995	936

Typhoon Agnes	5 Nov 1984	895

The majority of Philippian's live below the poverty line as will be discussed. As a result, they lack durable and safe housing and are therefore especially vulnerable to the weather conditions of this region.

1.3 POVERTY IN THE PHILIPPINES

1.3.1 Current Poverty Status

Poverty in the Philippines is an obstacle yet to be overcome. This is the view of the latest official statistics review on the poverty state in the Philippines, released by the Philippian Statistics Authority (PSA) in October 2016 (Perez, 2016). The statistics report reports on the poverty status of the Philippian community for the full year of 2015 (Perez, 2016).

According to this report, the poverty incidence among Filipinos in 2015 was estimated at 21.6% (Perez, 2016). Although this figure is an indication for great concern, a decline in the poverty levels since 2012 was observed, where the poverty incidence during the same period was estimated at 25.2% (Perez, 2016). In conjunction with this, PSA moreover estimated that 8.1 percent of Filipinos' income fall below the food threshold; 2.3% lower than estimated during the same period in 2012 (Perez, 2016).

It was estimated by PSA that, during 2015, a family of five people required an average of (Philippian Peso) PhP 6,329 per month in order to meet the family's basic food needs, while an average of PhP 9,064 per month covered the family's food and other needs (Perez, 2016). These values are set to be the monthly food and poverty thresholds and were determined as such by PSA for the year 2015 (Perez, 2016).

1.3.2 A History of Poverty

Poverty is, however, part of the Philippian history (Asian Development Bank, 2009). From 1985 to 2000, poverty was reduced at a slow rate of 0.7% per annum (Asian Development Bank, 2009). As recorded in Table 2, an average of 27,600,987 people were living in poverty from 1985 to 2000. Although this decrease was welcomed in the past, and seemingly still on the decline, it is clearly far from eradicated.

Table 2: Magnitude of poverty in the Philippines population, 1985 – 2000 (Asian Development Bank, 2009).

Year	Poor Population	% Increase(+) or Decrease (-) in Poverty Since Previous Year of Assessment
1985	26,674,645	-
1988	25,385,200	-4.83%
1991	28,554,247	12.48%
1994	27,372,971	-4.14%
1997	26,768,596	-2.21%
2000	30,850,262	15.25%
Avg.	**27,600,987**	**-**

1.3.3 Characteristics of the Poor

According to the Asian Development Bank (2009, p. 2), families classified as poor have the following characteristics:

1. The majority lives in rural areas and work in the agriculture sector, mostly as farmers or fishers.
2. In urban areas, such as Metro Manila, they are found in slums and the informal sector.
3. They have large families of six members or more.
4. In two thirds of poor families, the head of the household only has an elementary qualification or below.
5. They have few or no assets with minimal access to credit.

6. A major income source is from enterprise income (informal sector activities).
7. A significant segment of the families classified as poor are considered "chronically poor[2]".

1.3.4 Causes of Poverty in the Philippines

The main causes of poverty in these communities are related to (Asian Development Bank 2009, p. 2):

1. Low to moderate economic growth for the past 40 years.
2. Low growth elasticity of poverty reduction.
3. Weakness in employment generation and the quality of jobs generated.
4. Failure to fully develop the agriculture sector.
5. High inflation during crisis periods.
6. High levels of population growth.
7. High and persistent levels of inequality, which dampen the positive impacts of economic expansion.
8. Recurrent shocks and exposure to risks such as economic crisis, conflicts, natural disasters, and environmental poverty.

As poverty is till this day the struggle for many Filipinos, it is thought that many of them may benefit from effective and durable low cost housing solutions.

1.4 OBJECTIVES

The objective of this research is to find a possible low cost housing solution in extremely high wind regions. This investigation provides information on how high winds affect catenary vault shaped structures, and how these structures can be designed to resist these loads efficiently.

[2] The term "chronically poor" refers to people constantly living below the poverty threshold.

In order to ascertain the feasibility of such a solution, different design approaches and analysis techniques were utilised. Three fundamental structural solutions were explored. These three solutions are:

1. A flat catenary vault on elevated vertical walls.
2. A steep catenary vault with adequate rise to acquire sufficient head room as a practical living space.
3. A post-tensioned vault of adequate dimensions to obtain a practical living space.

Methods of providing the required post-tensioning force were investigated, and three post-tensioning techniques will be presented.

1.5 SCOPE

Section 2 of this document presents a review on previous work conducted on the optimisation of catenary structures. Methods in determining pressure forces resulting from wind were reviewed, while the design for tension in materials with low tensile resistance was investigated.

Section 3 presents a review on the method of optimizing a catenary vault to resist non-uniform loads in pure compression. Loading assumptions and the derivations of the magnitude of the design loads will be noted. Finite Element Analysis (FEA) programs were utilised in assessing the results of the geometric optimisation, while the characteristic mechanical properties of the material used will be discussed.

Section 4 presents the design of all structural elements of the proposed solution.

In Section 5 a visualization of the proposed solution will be presented. Means of post-tensioning were also evaluated and will be discussed in this section, while the conclusions and recommendations on the findings of this research are noted in Section 6.

2. LITERATURE REVIEW

In this chapter, the origin, design and practical application of the catenary barrel vault will be discussed. Form finding techniques, structural responses to applied loads, and efficient ways of designing the shell of the vault will be reviewed.

2.1 AN INTRODUCTION TO ARCHES

2.1.1 History of Arches

In the Netherlands, almost all historical buildings are largely made of masonry (Vermeltfoort, 2001). As a result of the poor tensile capacity masonry provides, the utilization of its compressive strength had to be optimised by our European ancestors (Vermeltfoort, 2001). In Europe, the arch was considered as one of the most efficient ways of bridging the gap of having a construction material with a high compressive resistance and almost no tensile capacity (Vermeltfoort, 2001). This was mainly due to being able to ensure that the line of thrust is contained within the section, ensuring no tensile stress development in the section under loading (Vermeltfoort, 2001).

The first arches made out of brick were corbelled arches (Vermeltfoort, 2001), (Cowan, 1977). These arches, as depicted in Figure 2.1, had horizontal bed joints which was perceived as an in-effective load path for resisting loads (Vermeltfoort, 2001), (Cowan, 1977). It was in later years observed that a more efficient way of constructing the arch was to align the bed joints to be perpendicular to the dominant line of thrust of the structure (Cowan, 1977). These arches, as seen in Figure 2.2, are considered true arches (Cowan, 1977).

In these traditional and non-sophisticated arches, the following variables were manipulated to minimize tension in the section:

1) Increased section depth to ensure that the line of thrust is contained within the kern of the section.
2) Ensuring that the loads applied to the structure did not induce a thrust line that fell outside the kern of the arch.

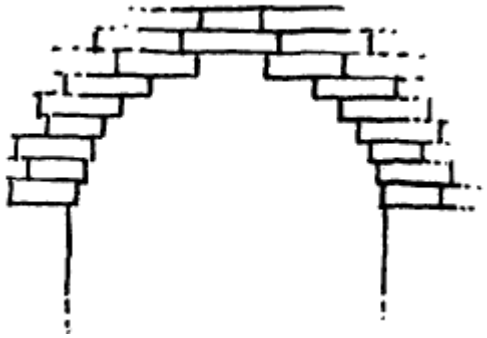


Figure 2.1: Corbelled arch (Cowan, 1977).

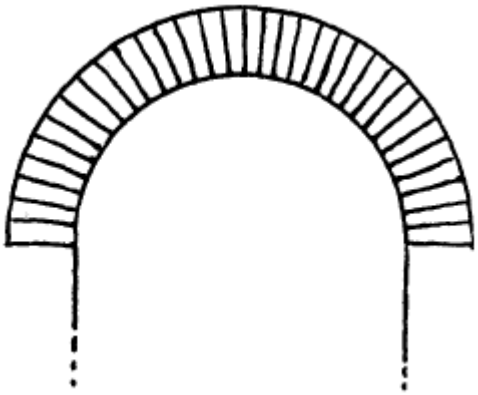


Figure 2.2: True arch (Cowan, 1977).

Although arches were historically constructed of material with a high compressive capacity (Vermeltfoort, 2001), these structures were still highly volatile to collapse when subjected to loads that resulted in the formation of four or more hinges (Huerta, 2001).

2.1.2 Collapse Mechanism of Arches

Fernandez (2001) suggests that when the line of thrust of an arch touches the limit of the masonry section it is constructed of, a hinge will form which

will allow rotation. In the presence of three hinges, an arch is statically determinate and stable, as a highly stable tri-pod configuration will be formed (Huerta, 2001). Increasing the amount of hinges above three, collapse of the structure will be inevitable (Huerta, 2001). The application of load to an arch, which will lead to the formation of four hinges, will lead to collapse of the structure without having the material fail in compression (Huerta, 2001). This phenomenon is adequately depicted in Figure 2.3, and indicates the failure mechanism of a four hinged thrust line, generated by a point load to a masonry arch.

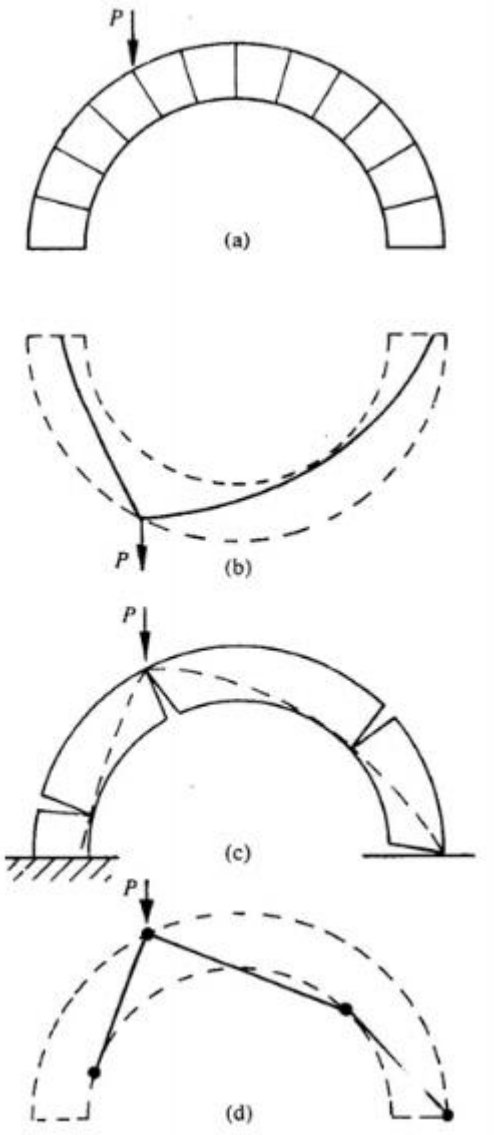


Figure 2.3: Collapse of a semi-circular masonry arch under a point load (Huerta, 2001).

2.1.3 Design of Arches

With the aid of computer technology, more sophisticated means of iterative calculation can be utilised to implement geometry optimisation of arches, vaults and domes. A highly efficient way of constructing these antique structures is by ensuring its geometry to be catenary (Allan, Zaleski & Boston Structures Group, 2010). Ensuring the geometry of these

majestic structures to be purely catenary requires highly accurate graphical, or other computational determinations.

The quest of finding the catenary curve started back in 1690 (Truesdell, 1983). Hooke stated in 1675 that *"as hangs the flexible line, so but inverted will stand the rigid arch"* (Truesdell, 1983). Since then, many mathematicians embarked on researching several approaches in the determination of the catenary arch curve (Truesdell, 1983). Traditional means of determining the catenary form, in the absence of computerised programs, was the application of force resolution methods (Allan *et al.*, 2010). These methods were used extensively by all engineers until about the 1960's, after which it died out with the dawn of the era of computers.

Stem element theory is a computational means based on element equilibrium. Although graphical approaches in the optimisation of structural forms have been around for quite some time, computerised models, based on theory such as that of stem elements, improves design accuracy and time requirements drastically (Gohnert & Bradley, 2016).

With the aim on constructing arches, vaults and domes with ever longer spans, and the use of less and cheaper building materials, catenary structures are considered as an ideal option due to its efficient resistance of forces (Allan *et al.*, 2010).

2.2 CATENARY STRUCTURES

2.2.1 The Funicular Form

A catenary structure is a funicular form which, when subjected to a pre-defined set of loads, resist them in a pure compression (Allan *et al.*, 2010). As a barrel vault is essentially an arch with a defined depth parameter, the catenary barrel vault is an extrusion of its ancestral catenary arch.

The geometry of a catenary arch can physically be determined by the hanging chain principle (Allan *et al.*, 2010). When a chain is suspended

between fixed supports, gravitational attraction will cause the flaccid chain to take a unique geometric shape. This particular shape will cause the cross section of the chain to be in pure tension. This unique profile of the hanging chain is known as its funicular form (Allan *et al.*, 2010).

Assuming the inverted chain with rigid chain links, it will resist its own weight in pure compression (Allan *et al.*, 2010). This phenomenon can be graphically represented by means of funicular and force polygons as depicted in Figure 2.4. Based on this theory, for each unique set of loads a structure is subjected to, there exists a unique geometric shape which will resist the applied loads in the absence of bending and shear stresses.

The basis of this research relies on the fact that each set of predefined loads has a funicular geometric shape. In turn, this informs the objective of the research, as structural elements act most efficiently in the absence of bending and shear stresses.

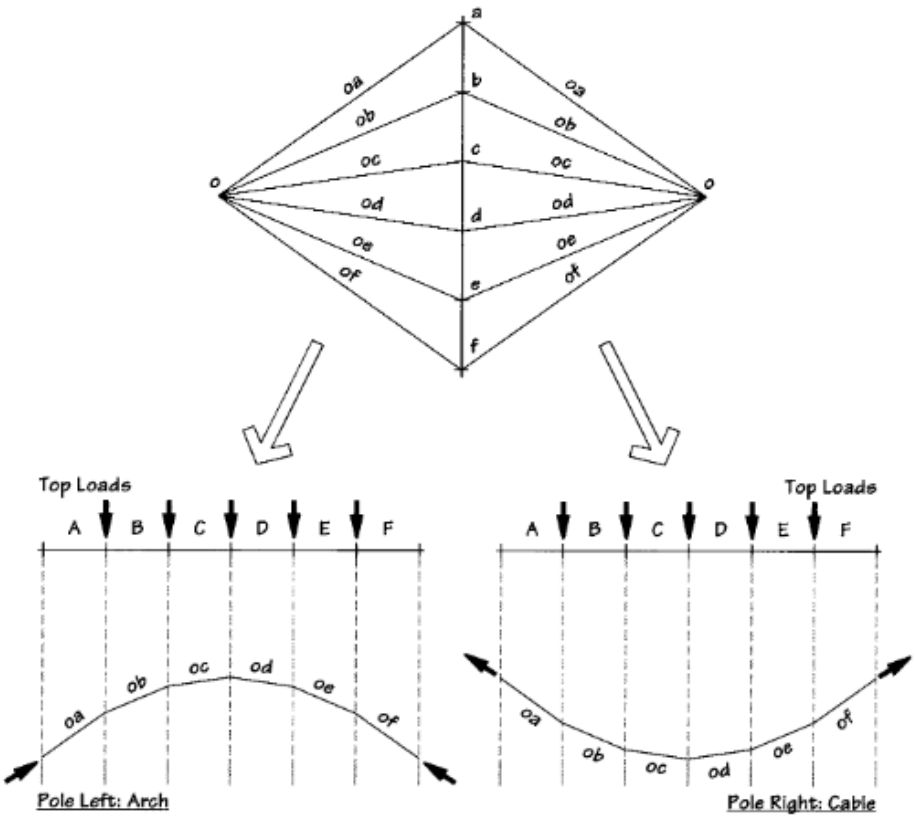


Figure 2.4: Graphical representation of a hanging chain and it's inverted catenary arch shape (Allan *et al.*, 2010).

2.2.2 The Catenary Arch

The traditional catenary arch resist its own-weight in the absence of bending and shear stresses, resulting in the effective utilisation of its construction material (Allan *et al.*, 2010). According to Gohnert and Bradley (2016), the traditional catenary equation can be described by the hyperbolic cosines equation:

$$y = \mathbf{a}\cosh\left(\frac{x}{a}\right) \qquad \textbf{(1)}$$

Where a = Arbitrary constant

x = Distance variable along the span of the vault

y = Height variable along the span of the vault

By manipulating equation (1), the traditional catenary arch equation can be mathematically represented as (Gohnert & Bradley, 2016):

$$y = H - \mathbf{acosh}\left(\frac{x}{a}\right) - a \qquad (2)$$

Where H = Maximum soffit height of arch.

L = Length between supports.

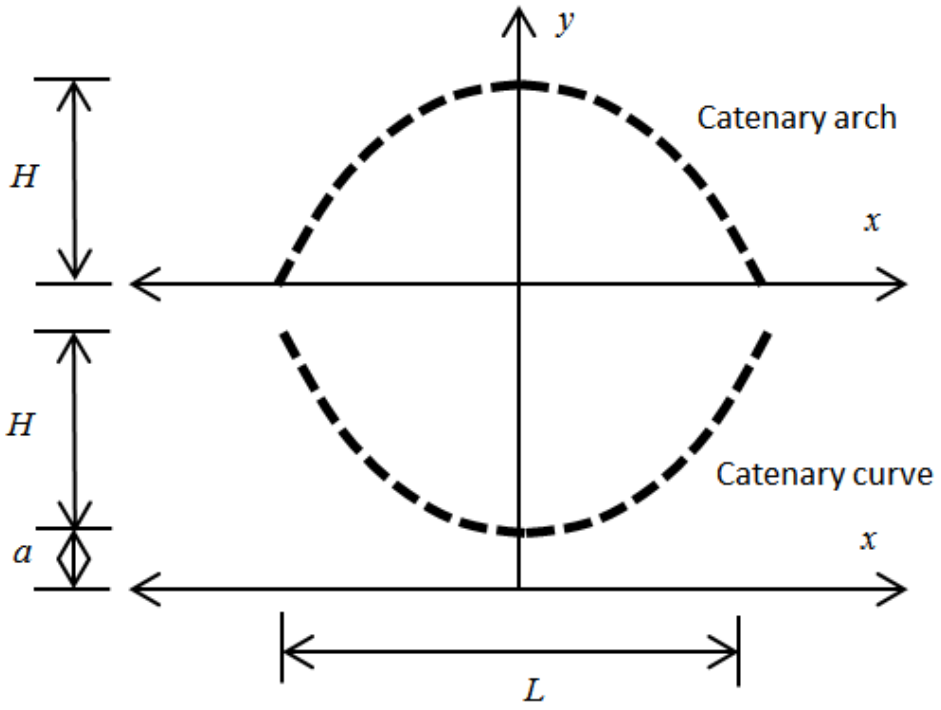


Figure 2.5: Catenary arch for uniform load (Gohnert & Bradley, 2016).

From equation (2), the traditional catenary arch, under uniform loading, can be drafted. The geometry is defined such by equation (2) that a section along the curve will be in pure compression as long as the load condition it was defined by remains unchanged (Gohnert & Bradley, 2016). Considering static equilibrium, the reactions at the base of the arch can be derived as depicted in Figure 2.6.

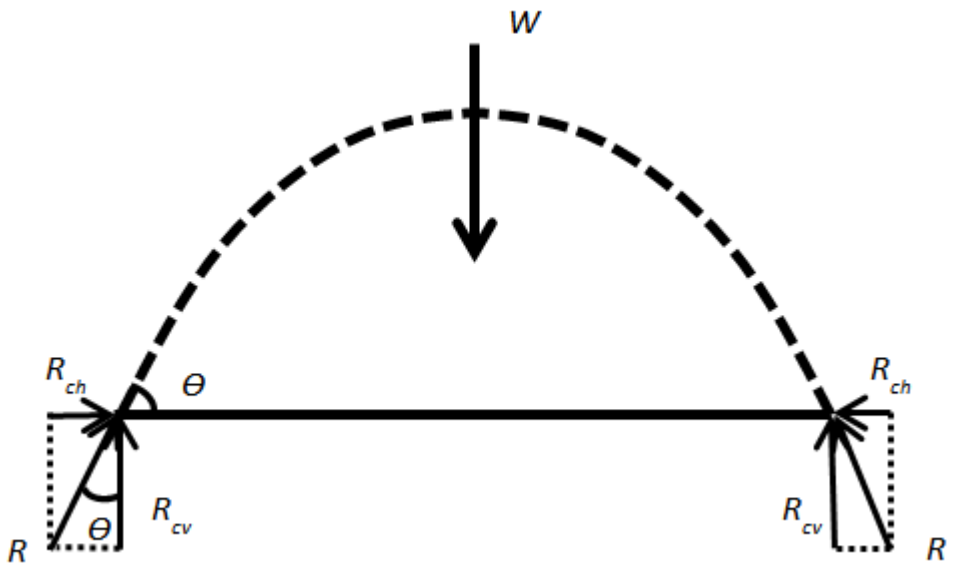


Figure 2.6: Reactions of a catenary arch subjected to self-weight (Gohnert & Bradley, 2016).

The base reactions can be mathematically represented by (Gohnert & Bradley, 2016):

$$\boldsymbol{R_{cv} = \frac{W}{2} = Rcos\theta} \quad \textbf{(3)}$$

$$\boldsymbol{R_{ch} = Rsin\theta} \quad \textbf{(4)}$$

With:

$$\boldsymbol{\theta = tan^{-1}\left[sinh\left(\frac{L}{2a}\right)\right]} \quad \textbf{(5)}$$

Where W = Total weight of vault

Stem Elements Gohnert and Bradley (2016) suggest that the original shape of the catenary arch can be modified to resist non-uniform loads by subdivision of the catenary curve, and cognisance of the fact that each segment should be in static equilibrium. Stem elements can therefore be considered as a mathematical approach to the traditional geometric determination of the funicular shape of a loaded structure.

Traditionally the funicular form of a loaded structure was determined by considering the discrete magnitude of each element of the subdivided structure. The force polygon, centred about an arbitrarily selected pole, as seen in Figure 2.4, becomes the geometric backbone to the funicular form. Each segment on the force polygon represents the natural direction of flow the applied forces prefers to follow during the load transfer process. By intersecting these segments with one another in a controlled manner, a funicular form is generated of which each segment is in static equilibrium (Allan *et al.*, 2010).

In a mathematical context, an isolated element's internal forces should be in static equilibrium. The structure is moreover to resist loads in the absence of bending moments while rotational degrees of freedom at the far ends of each element is not to be considered (Gohnert & Bradley, 2016). The equilibrium of these discrete elements is graphically represented by Gohnert and Bradley (2016) as depicted in Figure 2.7.

By starting at either one of the extreme ends of the structure, the progressive determination of the axial force and its corresponding orientation will yield the funicular form for the load condition under consideration (Gohnert & Bradley, 2016).

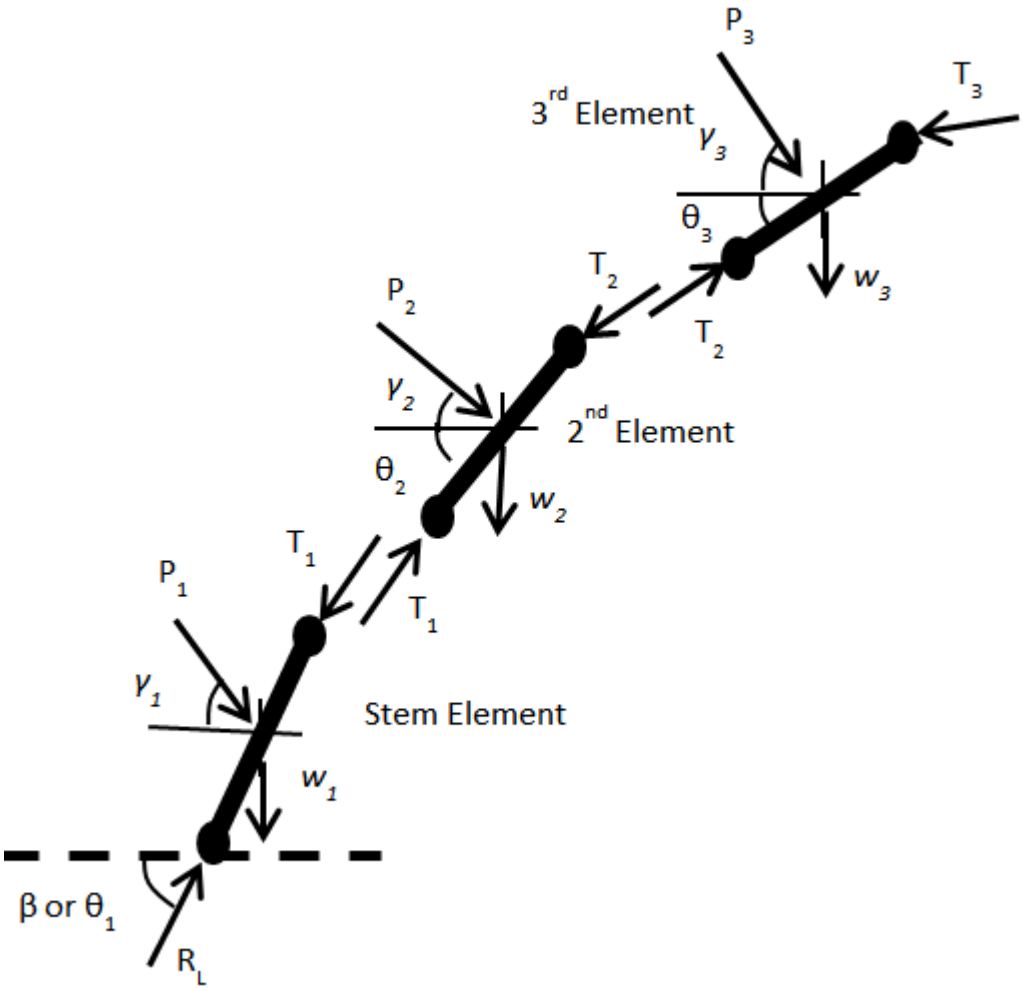


Figure 2.7: Growth of the funicular shape, starting with stem element (Gohnert & Bradley, 2016).

The stem element The stem element is defined by Gohnert and Bradley (2016) as the elements at the base of the funicular curve, programmed with intelligence, to form a pure compression structure. The orientation and magnitude of the T_i^{th} and T_{i+1}^{th} axial force is defined as the load-shape genetics of the element under consideration (Gohnert & Bradley, 2016).

As the stem element is defined as the first element on either of the two extreme ends of the funicular curve, it is intuitive that the reaction force at

the base of the curve will directly impact the shape thereof. This observation is utilised by Gohnert and Bradley (2016), by recognizing that a single concentrated load on a flaccid string will yield a funicular shape for resisting the applied load in pure tension. Inverting it will yield a form which will be able to resist the applied load in pure compression and is depicted in Figure 2.8 (Gohnert & Bradley, 2016).

Considering the fact that the resistance of this load yields a unique reaction at the base of the funicular curve, it can be assumed that the application of point loads to the original catenary curve will yield unique base reactions at the stem element (Gohnert & Bradley, 2016). As it has been proven that the stem element's axial load and orientation forms the foundation of the curve's geometry, one can expect to observe a change in the load shape genetics of the stem elements which is defined by the loads applied to the system as a whole (Gohnert & Bradley, 2016).

Load shape genetics The orientation and magnitude of the T_{i+1}^{th} force, as per Figure 2.7, is a function of the self-weight of the element under consideration as well as any additional load applied to the centre of it (Gohnert & Bradley, 2016). Considering static equilibrium of each element, the magnitude of the axial force and the direction thereof is determined (Gohnert & Bradley, 2016).

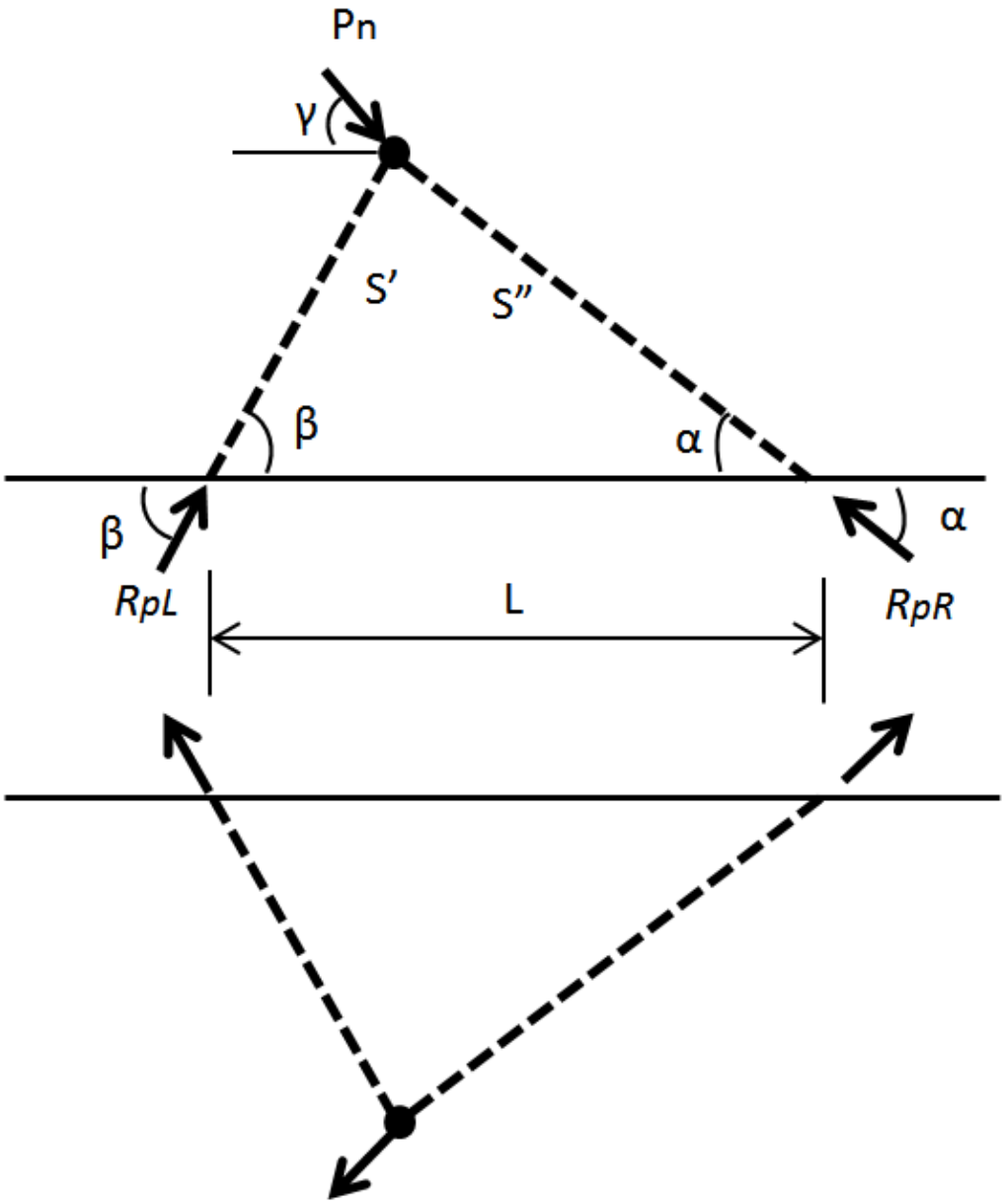


Figure 2.8: Triangular shape to support a point load in pure compression (Gohnert & Bradley, 2016).

Line of Thrust The natural response of each element to the applied load induces a progressive growth of the so called catenary shape. The shape will therefore, as a natural response, follow a path which represents the most efficient flow of forces (Allan *et al.*, 2010). This path, for the loads applied, is known as the structures line of thrust (Allan *et al.*, 2010). Should the centreline of the structure's geometry coincide with the line of thrust defined by the loads applied to it, the structure would be in pure compression and defined as a pure catenary shape (Allan *et al.*, 2010).

Should the same structure be subjected to a different set of loads, the thrust line of the structure will shift as seen in Figure 2.9. It is important to note that the thrust line is to start and end near the foundations of the vault, as the loads applied to it can only be transferred to the ground via the foundations. When the line of thrust shifts from its original position, as defined by the initial design loads, an eccentricity develops between the new thrust line and the original geometric centreline of the vault's shell. This results in an unfavourable force eccentricity which generates a force eccentricity moment.

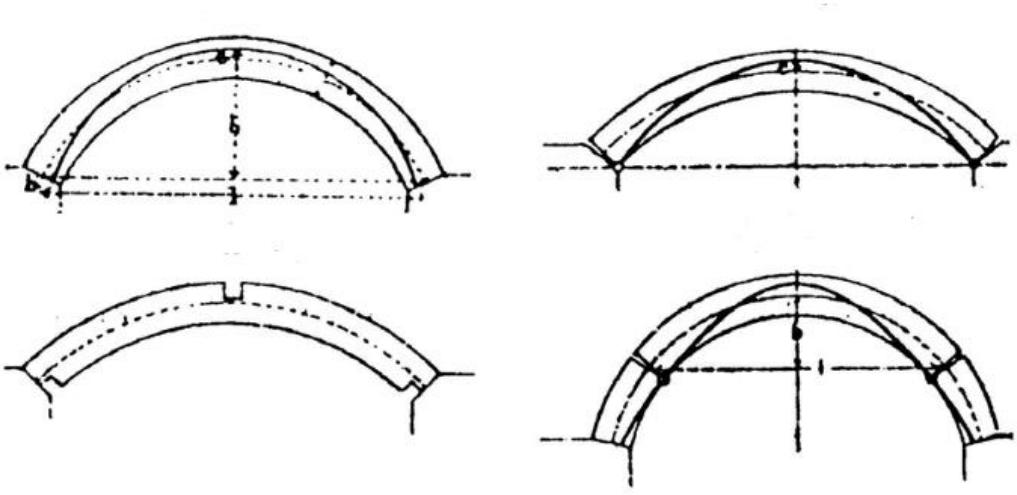


Figure 2.9: Shifting of the line of thrust of a masonry vault due to a change in support condition (Huerta, 2001).

When considering the development of the funicular form by means of stem element theory, the stem element selected as the origin of the curve is assumed to be fixed (Gohnert & Bradley, 2016). Depending on the loads applied, the load shape genetics will inform the growth of the funicular form. The funicular form of each load set can now be assumed to be the line of thrust for the load set under consideration.

The Kern The kern is a geometric property of a cross section, defined as the area in a cross section where, when the line of thrust falls within the set boundary of the kern, no tension is developed in the section (Marshall & Robberts, 2000). For a section subjected to bending moments and axial forces, the force eccentricity of the line of thrust for the load set can be defined as:

$$\boldsymbol{e = \frac{M}{P}} \qquad \textbf{(6)}$$

Where M = Bending moment in section

P = Axial force in section

The boundaries of the kern can be mathematically computed by taking cognisance of the fact that, when a section is eccentrically loaded under an axial compressive force, compression- and tension stress is generated in the section fibres (Marshall & Robberts, 2000). With the objective set as zero tension in the extreme fibres of the section (when loaded under compression), the following equation governs:

$$\boldsymbol{\frac{P}{A} + \frac{P \times k_i}{Z} \geq 0MPa} \qquad \textbf{(7)}$$

With A = Cross-sectional area

Z = Section modulus

k_i = As per Figure 2.10

**Negative values imply compression in the fibres*

Re-arranging the terms of equation (7), and making the eccentricity (k_i) the subject thereof, the dimension of the first boundary of the kern, as measured from the geometrical centroid of the cross-section, is obtained (Sengupta & Menon, n.d.). The area of the kern of a rectangular cross-section is depicted in Figure 2.10.

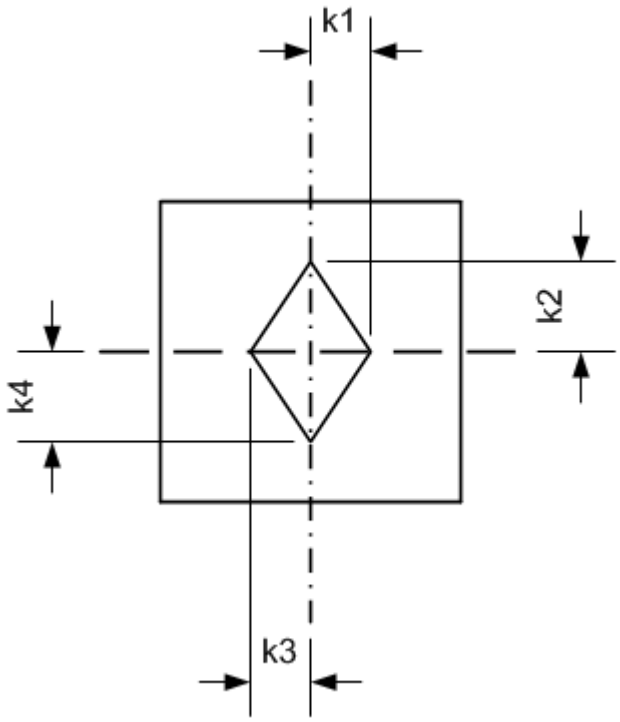


Figure 2.10: Kern points of rectangular cross section

Should the line of thrust fall outside the kern of the section, the total stress in the section is as depicted in Figure 2.11. It should be noted that the stresses at the extreme fibres of the section are not equal to one another. This is due to the fact that there is an eccentric bending moment residing within the compressed section which yields a reduced pressure on the one extreme end of the section with an increased pressure at the other. Should the stress conditions within the section be such that there is inadequate compressive stress within the section, a portion thereof may

be subjected to tension which will lead to the formation of cracks (Curtin, Shaw, Beck & Bray, 1995).

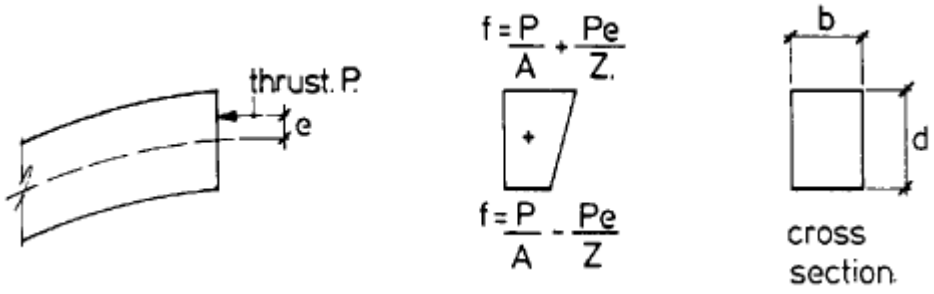


Figure 2.11: Stress condition in section of arch (Curtin *et al.*, 1995).

Buckling of Arches As arches are structural forms known for resisting loads primarily in axial compression, these structures are susceptible to collapse due to buckling just as any other compression element. The derivation of the critical buckling load of arches is extensively discussed by Timoshenko and Gere (1963). Jinsan and Yanlin (2002) suggest that the buckling behaviour of arches is much more complex than that of beams, columns or beam-column behaviour. This is a result of the high load-carrying capacity when subjected to a full span uniform load (Jinsan & Yanlin, 2002). Arches are however highly susceptible to geometric imperfections and perturbations, and therefore complex buckling shapes and loads are inevitable (Jinsan & Yanlin, 2002).

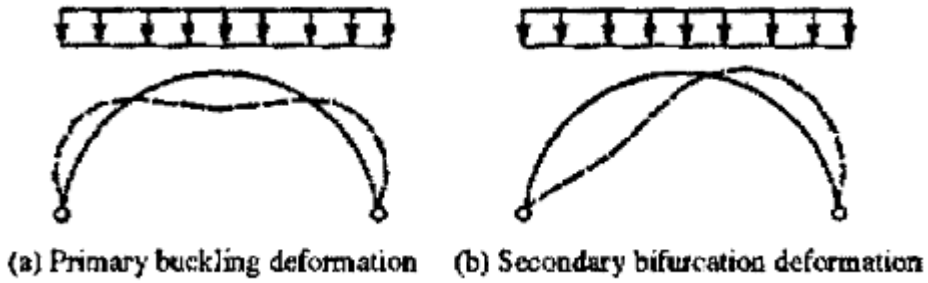


Figure 2.12 : Two buckling modes of a two hinged arch (Jinsan & Yanlin, 2002).

The effect of geometric imperfections and perturbations are seen in Figure 2.12, where a symmetrically loaded arch suddenly deflect from symmetric

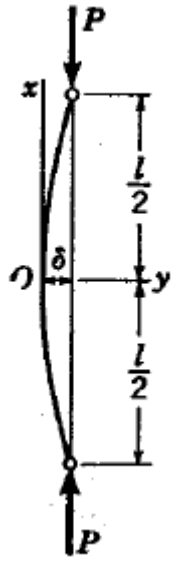
deformation in the primary buckling mode shape, to an asymmetric deformation of its secondary bifurcation mode (Jinsan & Yanlin, 2002).

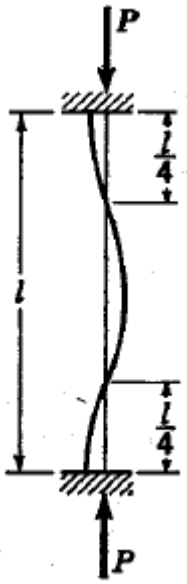
Euler buckling Leonard Euler was the first to recognise the fact that straight elements can buckle in the absence of any theoretical eccentrically applied axial load (Timoshenko & Gere, 1963). The renowned Euler buckling equations for axially loaded columns are used by mathematicians and engineers till this day.

The Euler buckling equation for axially loaded elements under compression were first documented by Leonard Euler in 1744 in his book *"Methodus inveniendi lineas curvas maximi minimive propreitate gaudentes"* (Timoshenko & Gere, 1963). These formulas are most commonly known as the critical buckling loads of compression elements, and are implemented by many design standards around the world. The most common variations of these formulas are tabulated in Table 3 (Timoshenko & Gere, 1963).

Timoshenko and Gere (1963) further suggests that the basis of these formulas could be utilised in determining the critical buckling loads of other, more complex structural forms. Extensive research was conducted by Timoshenko and Gere (1963) on the buckling of rings, curved bars and arches. The complex mathematical derivations used as basis for these formulas are thoroughly discussed by Timoshenko and Gere (1963). As the derivation of most of their work falls beyond the scope of this research, only their findings on the buckling of arches are discussed.

Table 3 : Common Euler buckling equations (Timoshenko & Gere, 1963)

End condition	Description	Critical buckling load
	The ends of the element are considered pinned. Translation in the axial direction is allowed while lateral translation is not permitted. The ends are free to rotate.	$P_{cr} = \frac{\pi^2 EI}{l^2}$ **(8)**

	The ends of the element are fixed against rotation and lateral translation. Axial translation is allowed.	$P_{cr} = \frac{4\pi^2 EI}{l^2}$ **(9)**

Buckling of a curved bar If a curved bar with hinged ends are subjected to a uniformly distributed load "q", as depicted in Figure 2.13, the buckling profile of the bar will be as suggested by the dashed line (Timoshenko & Gere, 1963).

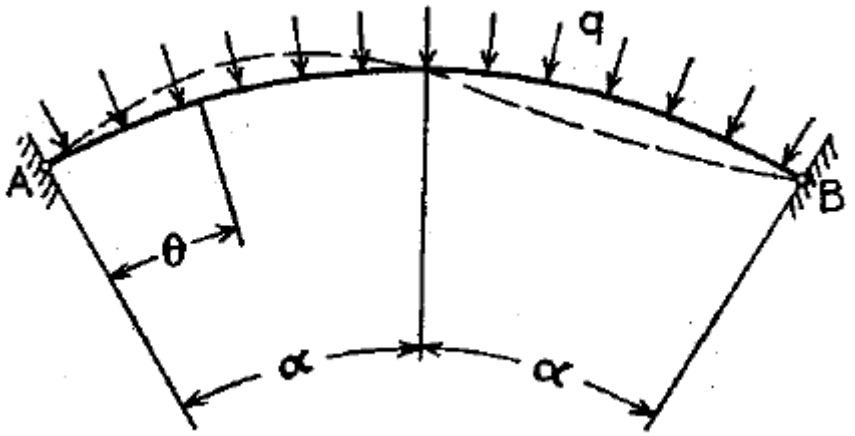


Figure 2.13 : Buckling profile of a uniformly compressed circular arch with hinged ends (Timoshenko & Gere, 1963).

The critical buckling load of the curved bar is described by the following differential equation (Timoshenko & Gere, 1963):

$$\frac{d^2w}{d\theta^2} + w = -\frac{R^2Sw}{EI} \qquad (10)$$

Where S = qR

q = Uniformly distributed load

w = Radial displacement towards the centre

R = Total length of curve

E = Modulus of elasticity

I = Moment of inertia of the section

θ = Variable length of curve

By manipulating the differential equation to determine a solution by means of calculus, the critical buckling load of a uniformly compressed circular arch is derived (Timoshenko & Gere, 1963).

$$q_{cr} = \frac{EI}{R^3}\left(\frac{\pi^2}{\alpha^2} - 1\right) \qquad (11)$$

In a similar fashion, Timoshenko and Gere (1963) determined the critical buckling load for a curved bar with fixed ends, as depicted in Figure 2.14.

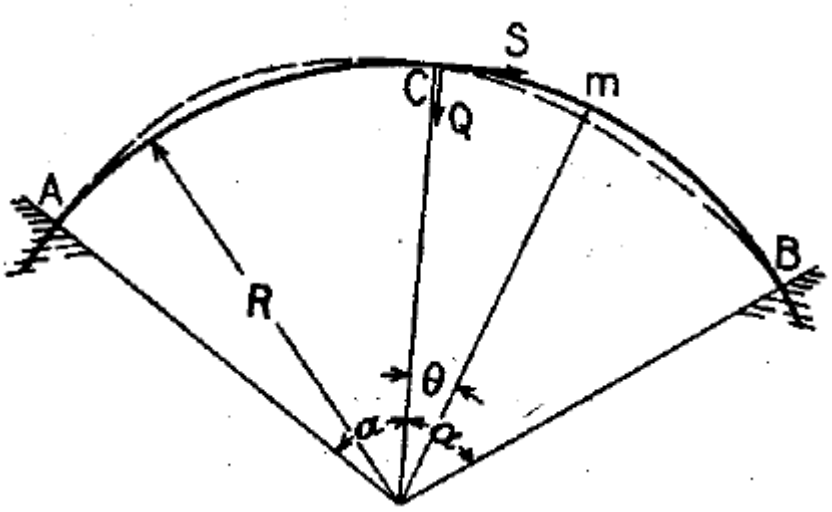


Figure 2.14 : Buckling profile of a uniformly compressed circular arch with fixed ends (Timoshenko & Gere, 1963).

For this condition, the differential equation defining the buckling curvature of the curved bar is described as (Timoshenko & Gere, 1963):

$$\frac{d^2w}{d\theta^2} + k^2w = \frac{QR^2 sin\theta}{EI} \quad (12)$$

Where the general solution is given as (Timoshenko & Gere, 1963):

$$w = Asin(k\theta) + Bcos(k\theta) + \frac{QR^2 sin\theta}{(k^2-1)EI} \quad (13)$$

Considering the boundary conditions, the constants (A) and (B) are determined and the equation for the determination of the critical value of the uniform pressure (q) is obtained (Timoshenko & Gere, 1963):

$$ktan\alpha \times \cot(k\alpha) = 1 \quad (14)$$

Timoshenko and Gere (1963) suggest that the arbitrary constant (k) and the value of the uniform pressure depend on the magnitude of the angle (α). For a set value of constant uniform load, the value of (k) can be determined for a variety of α-angles. Substituting the applicable values of the constant (k) into equation (15), the critical buckling load of a curved bar with fixed ends is determined (Timoshenko & Gere, 1963):

$$q_{cr} = \frac{EI}{R^3}(k^2 - 1) \quad (15)$$

The determination of the critical buckling load of any curved arch can alternatively be determined by applying an effective length factor (β) to the original Euler equation for pinned and fixed end conditions. The effective length factor (β) is defined as (German Building and Civil Engineering Standards Committee & German Committee for Structural Steelwork, 1990):

$$\beta = \frac{s_k}{s} \quad (16)$$

Where s_k = Effective length of the section considered for buckling

s = Half of the arc length

By the application of an effective length factor, the code simplifies the determination of the critical buckling load by increasing or decreasing the magnitude of the effective length considered by the Euler buckling equation. By increasing the effective length, the critical buckling load is reduced. A reduction of the effective length factor yields a more conservative critical buckling resistance of the section.

The critical buckling load of the arch at its end supports can be determined by (German Building and Civil Engineering Standards Committee & German Committee for Structural Steelwork, 1990: 18):

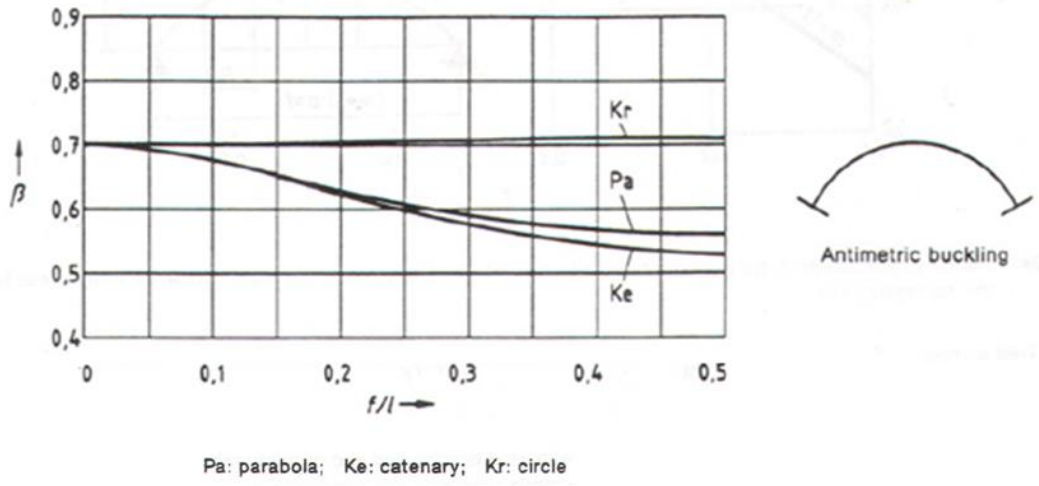
$$\boldsymbol{P_{cr} = \left(\frac{\pi}{\beta s}\right)^2 E I_y} \qquad \textbf{(17)}$$

Where β = Effective buckling length factor

E = Modulus of elasticity of the arch material

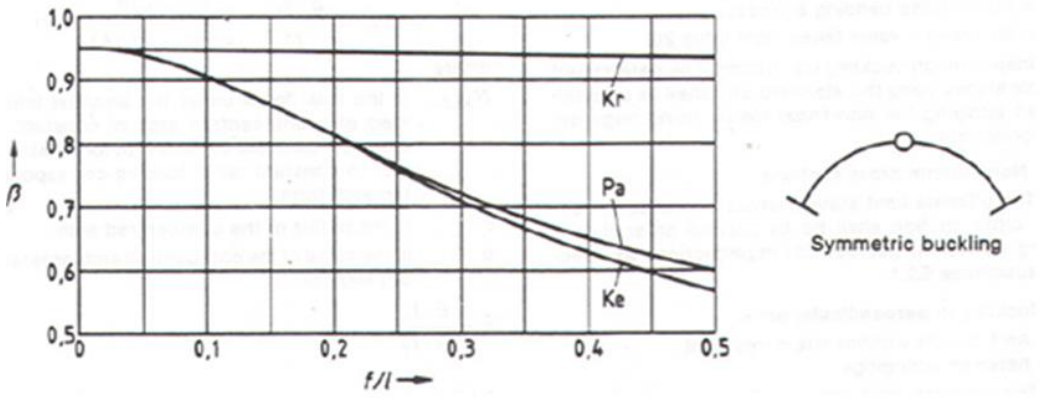
I_y = Second moment of inertia about the weak axis of section

Buckling coefficients are determined for arches with various types of end conditions and plotted for parabolic, catenary and circular arches respectively (German Building and Civil Engineering Standards Committee & German Committee for Structural Steelwork, 1990: 18). These graphs are listed from Figure 2.15 through Figure 2.18 and plot the buckling coefficient (β) on the vertical axes, against the rise to span ratio (f/l) of the arch (German Building and Civil Engineering Standards Committee & German Committee for Structural Steelwork, 1990).



Pa: parabola; Ke: catenary; Kr: circle

Figure 2.15: Buckling coefficient (β) for in-plane buckling of a monolithic arch system (German Building and Civil Engineering Standards Committee & German Committee for Structural Steelwork, 1990).



Pa: parabola; Ke: catenary; Kr: circle

Figure 2.16: Buckling coefficient (β) for in-plane buckling of an one hinged arch system (German Building and Civil Engineering Standards Committee & German Committee for Structural Steelwork, 1990).

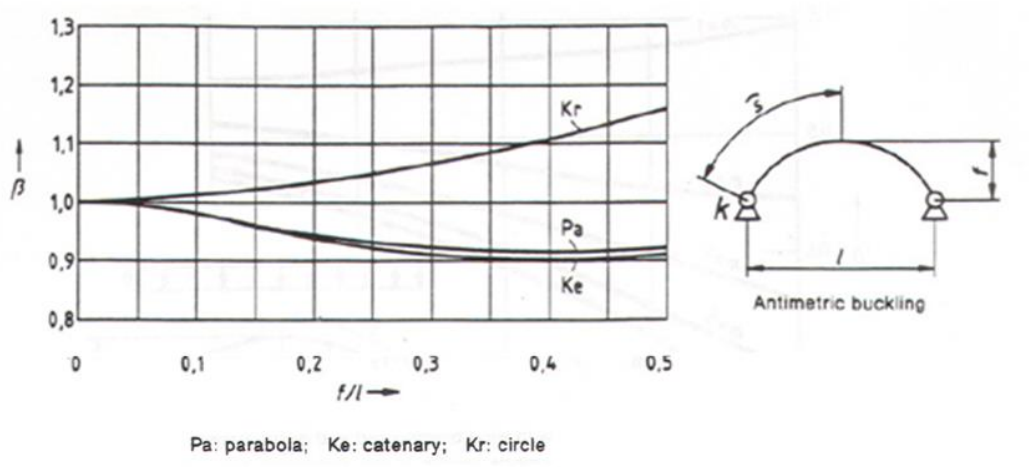


Figure 2.17: Buckling coefficient (β) for in-plane buckling of a two hinged arch system (German Building and Civil Engineering Standards Committee & German Committee for Structural Steelwork, 1990).

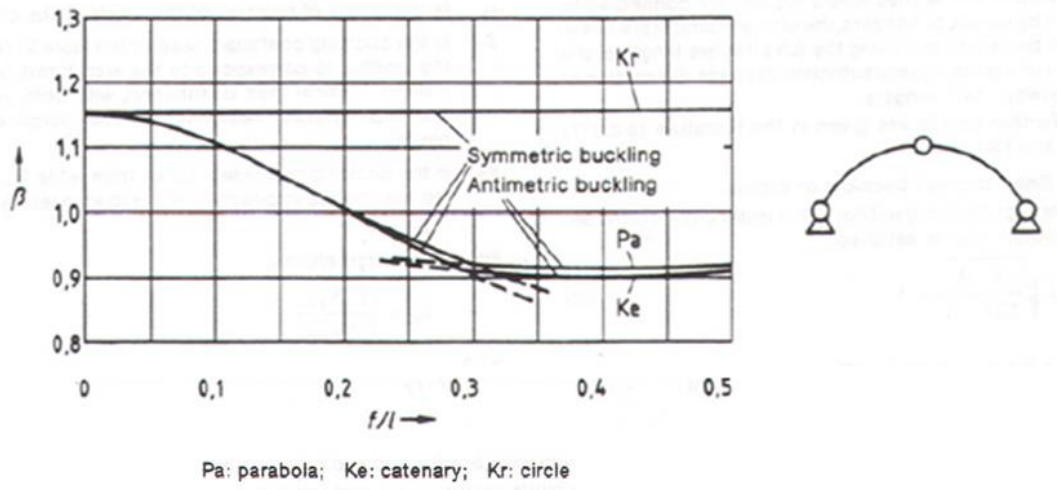


Figure 2.18: Buckling coefficient (β) for in-plane buckling of a three hinged arch system (German Building and Civil Engineering Standards Committee & German Committee for Structural Steelwork, 1990).

Buckling load of catenary arch With further manipulation and application of the previously discussed theory on the buckling of arches, the critical uniform pressure that can be resisted by a catenary arch was derived (Timoshenko & Gere, 1963):

$$q_{cr} = \gamma_4 \frac{EI}{R^3} \quad (18)$$

The values of the constant (γ_4) here is based on the amount of hinges within the curve as well as the rise to span ratio of the arch. This is displayed in Table 4.

As long as the axial load in the section is small in comparison to the critical buckling value, the influence of the axial load on bending and deformation can be neglected when designing arches (Timoshenko & Gere, 1963). Timoshenko and Gere (1963), however, do not state what defines a small relationship of the axial load to the critical buckling load of the section.

Table 4 : Values of the constant (γ_4) for catenary arches of constant cross section with load uniformly distributed along the arch's axis (Timoshenko & Gere, 1963).

h/l	No hinges	Two hinges
0.1	59.4	28.4
0.2	96.4	43.2
0.3	112	41.9
0.4	92.3	35.4
0.5	80.7	27.4
1.0	27.8	7.06

While the critical buckling load of the catenary arch is mathematically determined by Timoshenko and Gere (1963), a comparative result can be obtained by the determination of the critical buckling load according to the

DIN 18800 part 2:1990 structural design standards (German Building and Civil Engineering Standards Committee & German Committee for Structural Steelwork, 1990).

Pedreschi and Theodossopoulos (2007) suggest that the buckling mode of a catenary arch, subjected to its self-weight, is as illustrated in Figure 2.19. It is suggested that the critical buckling load can be expressed as (Pedreschi & Theodossopoulos, 2007):

$$\chi = \frac{q_{cr} l^3}{EI} \qquad (19)$$

Where χ = Variable based on a set of boundary conditions (Figure 2.20)

l = Half of the arc length

Eladio Dieste (1917-2000) evaluated values for χ for a finite set of vertical positions on a series of catenary arches (Pedreschi & Theodossopoulos, 2007). This procedure yielded a series of curves as illustrated in Figure 2.20.

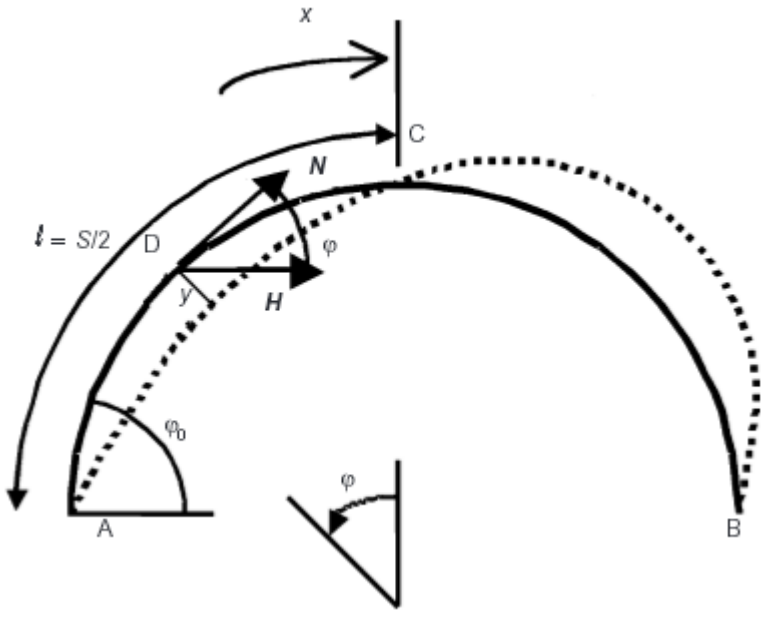


Figure 2.19: Buckling of a catenary arch under self-weight (Pedreschi & Theodossopoulos, 2007)

In order to utilise the design charts as depicted in Figure 2.20, the values of γ and υ should be determined (Pedreschi & Theodossopoulos, 2007):

$$\boldsymbol{\gamma = \frac{1}{tan\varphi_0}} \quad \textbf{(20)}$$

$$\boldsymbol{\upsilon = \frac{I_{crown}}{I_{support}}} \quad \textbf{(21)}$$

Where φ_0 = As per Figure 2.19

I_{crown} = Second moment of inertia of masonry section at the crown

$I_{support}$ = Second moment of inertia of masonry section at support

For a vault of constant cross section, the value of υ = 1.0.

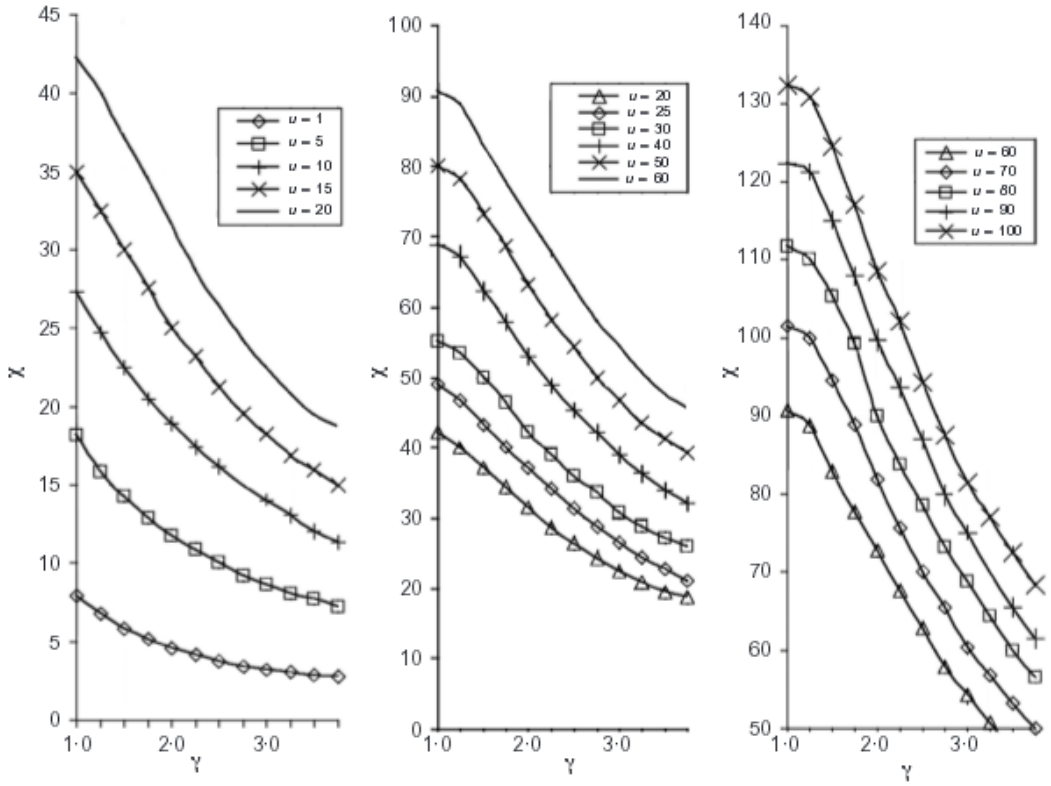


Figure 2.20: Design charts for the buckling of catenary arches (Pedreschi & Theodossopoulos, 2007).

Pre-stressing of Vaults The period from the late nineteenth through the twentieth century saw great innovation and experimentation with vaulted structures (Pedreschi, 2006). Eladio Dieste (1917-2000) is considered as one of the engineers that helped develop highly expressive vaults as economic solutions for the construction of industrial buildings (Pedreschi, 2006).



Figure 2.21: Double cantilever free-standing vault at Refresco del Norte, Uruguay (Pedreschi, 2006).

One of his most significant structural designs was the "*Double cantilever free-standing vault at refresco del Norte, Uruguay*" (Pedreschi, 2006). The large spans of the vault were achieved by means of pre-stressing, counter acting the stresses caused by hogging moments over the central columns (Pedreschi, 2006).

Most of the literature on the pre-stressing of vaults was developed and applied by Dieste. These techniques are illustrated in Figure 2.22 and are indicative of stress reduction in the length of the vault span (Pedreschi, 2006).

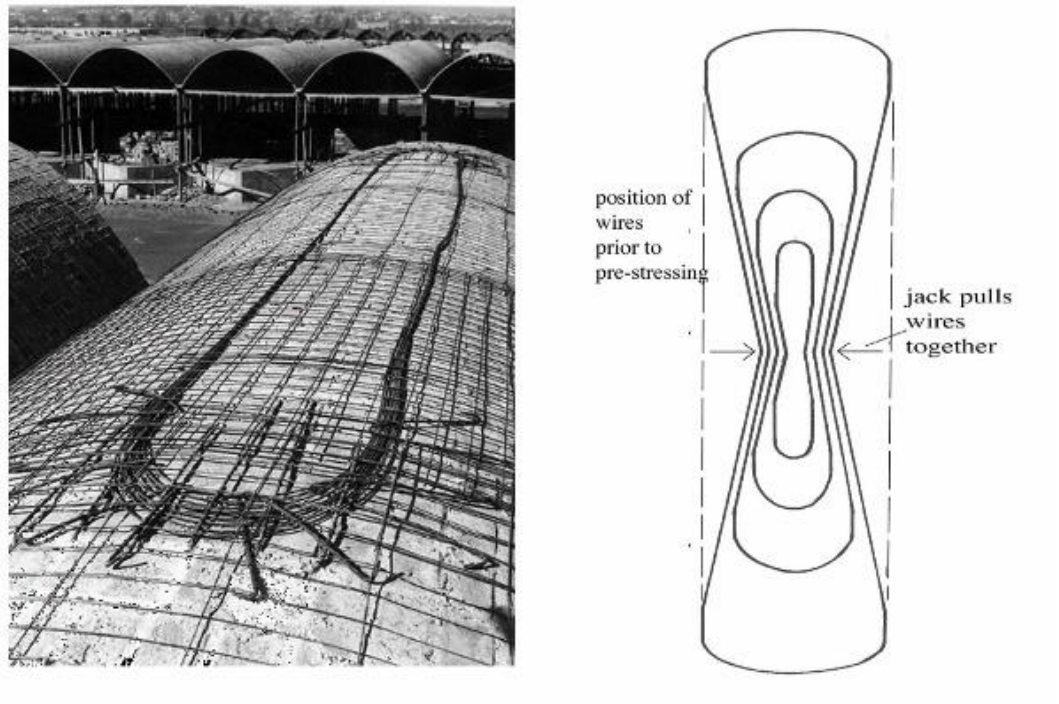


Figure 2.22: Looped pre-stressing steel in vault (Pedreschi, 2006).

2.3 WIND LOAD ON VAULTED STRUCTURES

2.3.1 Defining Wind Load

The load wind exerts on structures competes with seismic action as the dominant environmental load structures are designed to resist (Holmes, 2001). Over long periods of time, wind load have caused equal amounts of damage to structures than that as a result of seismic events (Holmes, 2001). It was furthermore recorded that the frequency of large catastrophic wind storms are noticeably higher than that of devastating earthquakes (Holmes, 2001).

From a meteorological aspects, wind can be defined as the movement of air relative to the surface of the earth (Holmes, 2001). Holmes (2001) suggests that the two most important forces acting on the upper level air in the "*free atmosphere*" is the pressure gradient and the Coriolis force. It is known, through the theory of fluid dynamics, that a resultant force per unit mass is generated in the presence of a pressure gradient (Holmes, 2001). This pressure gradient is defined as (Holmes, 2001):

$$\boldsymbol{Pressure\ gradient\ force\ per\ unit\ mass} = -\left(\frac{\mathbf{1}}{\boldsymbol{p_a}}\right)\frac{\boldsymbol{\partial p}}{\boldsymbol{\partial x}} \qquad \textbf{(22)}$$

Where p_a = Air density

∂p = Partial derivative of atmospheric pressure

∂x = Partial derivative of height above natural ground level

This pressure force acts from a high pressure region to a low pressure region (Holmes, 2001).

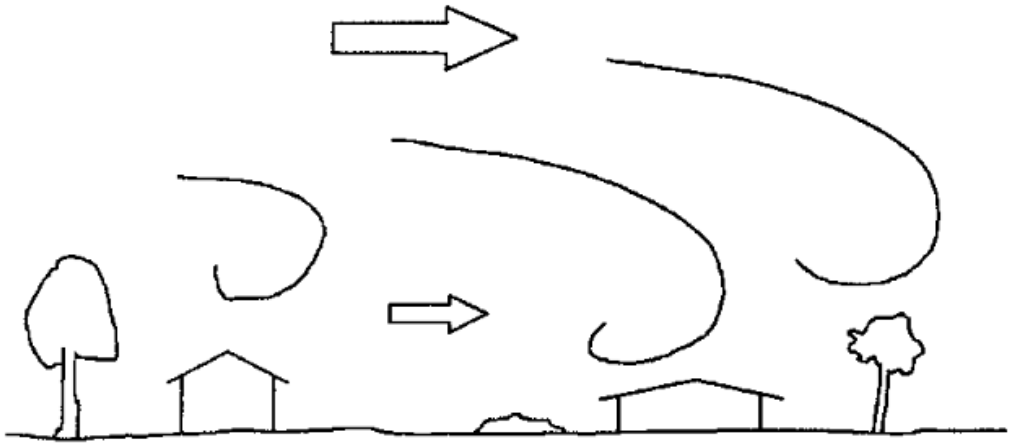


Figure 2.23: Wind flow near the boundary layer of the earth's surface (Holmes, 2001).

"*The Coriolis force is an apparent force due to the rotation of the earth*" (Holmes, 2001). Assuming that air intends to move in a straight line, the rotation of the earth will alter the original path of movement, curving it into the direction of rotation (Holmes, 2001). This influence, of the rotation of the earth on the direction of airflow, is also related to the boundary layer friction between the "*free atmosphere*" and that of the earth's surface and is depicted in Figure 2.24.

Considering the impact of the apparent Coriolis force on the pressure gradient, the basis for wind load can be established. This wind load is known as the geographic wind (Holmes, 2001):

$$\boldsymbol{U = -\left(\frac{1}{p_a f}\right)\frac{\partial p}{\partial x}} \qquad \textbf{(23)}$$

Where f = The Coriolis force factor on wind flow

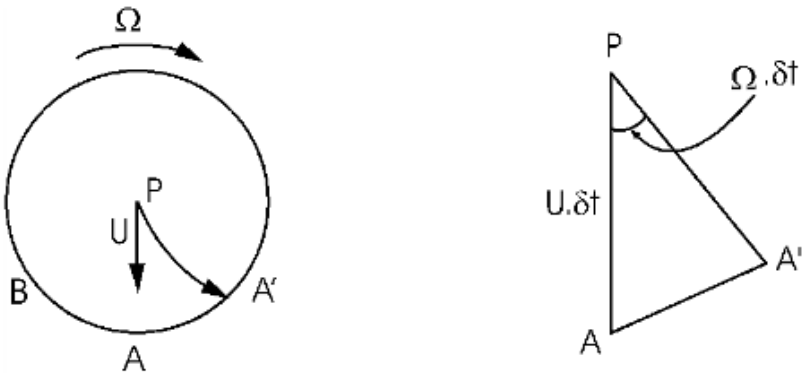


Figure 2.24: The apparent Coriolis force due to the earth's rotation (Holmes, 2001).

As the earth's surface is not flat and smooth, but rough and jagged, air flow is obstructed near the boundary layer. This obstruction causes friction between moving air in the "*free atmosphere*" and that at the boundary layer, causing wind speeds to be slower at the boundary layer than that of the "*free atmosphere*". This phenomenon is schematically depicted in Figure 2.23. The friction generated between the earth's surface and that of the moving air in the "*free atmosphere*" is dissipated by any and all obstructions in its path. This dissipation of energy results in it being transformed from being kinetic in nature, to forces in structural elements.

A combined effect of the pressure gradient and Coriolis force is termed the geostrophic wind force (Holmes, 2001). This force is represented in equation (23). The direction of the pressure gradient and the Coriolis force is depicted by Holmes (2001) in Figure 2.25. Here it is seen that the direction of flow is parallel to the lines of constant pressure (isobars) (Holmes, 2001). It can further be seen that, in the Northern hemisphere, the high pressure is to the right of an observer facing the flow direction while in the Southern hemisphere it is to the left (Holmes, 2001). In both hemispheres, rotation about a low pressure centre is known as a cyclone, while rotation about a high-pressure centre is known as an anti-cyclone

(Holmes, 2001). Cyclones are related to extreme wind speeds (Holmes, 2001).

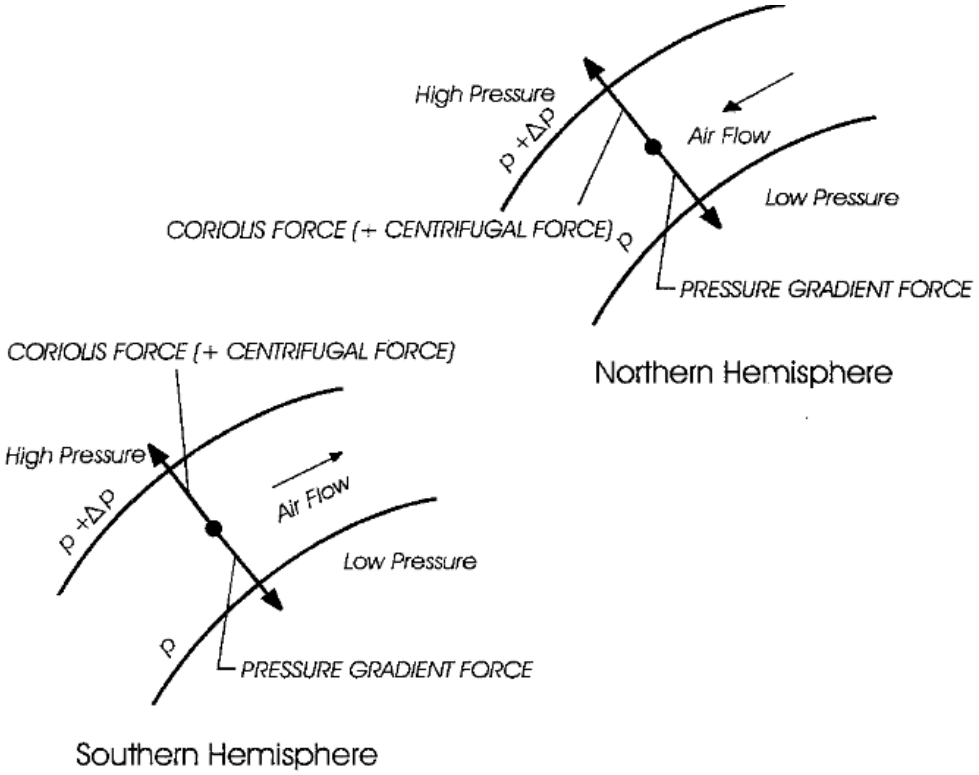


Figure 2.25: Balanced geostrophic flow in the Northern and Southern hemisphere (Holmes, 2001).

2.3.2 Tropical Cyclones

Holmes (2001) suggests that tropical cyclones are intense cyclonic storms which occur over and close to tropical oceans in late summer and autumn. "*They are driven by the latent heat of the oceans, and require a minimum sea temperature of about 26 degrees Celsius to sustain them; they rapidly degenerate when they move over land, or into cooler waters*" - (Holmes, 2001, p. 7).

The strongest types of cyclones have occurred in the Caribbean where they are known as hurricanes while the ones that occurred in the South China Sea are called typhoons (Holmes, 2001). Holmes (2001) suggests that a developed tropical cyclone has a three-dimensional vortex structure.

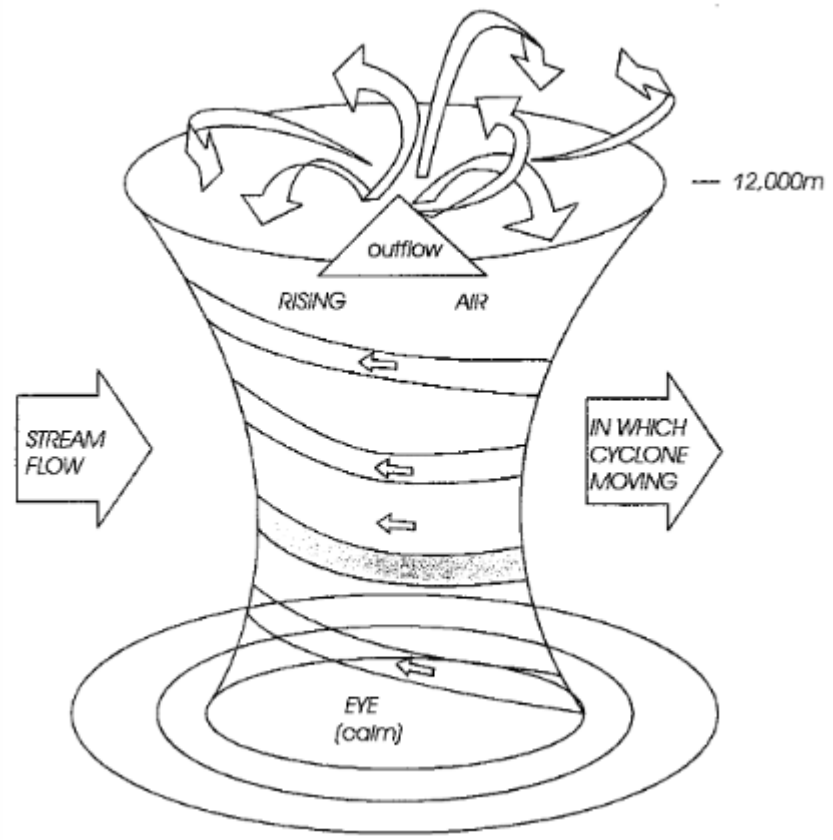


Figure 2.26: Three-dimensional vortex structure in a developed tropical cyclone (Holmes, 2001).

The circulation of wind flow is in a radial direction towards the "*eye*", which is defined by a region of relatively calm air, slowly sinking towards the surface of the earth (Holmes, 2001). On the outside of the "*eye*" there is a region of intense thermal convection where air currents spiral upwards (Holmes, 2001). The diameter of the "*eye*" can range between 8km and 80km (Holmes, 2001).

The gradient wind speed of a tropical cyclone can be determined by equation (24) (Holmes, 2001):

$$\boldsymbol{U} = -\frac{|f|r}{2} + \sqrt{\frac{f^2r^2}{4} + \frac{r}{\rho_a}\left|\frac{\partial p}{\partial r}\right|} \qquad \textbf{(24)}$$

Where f = Coriolis parameter

r = Radius from the storm centre

ρ_a = Air density

p = Atmospheric pressure

In 1974, Darwin in Australia was hit by the tropical cyclone "*Tracy*" (Holmes, 2001). The anemograph of the cyclone suggests that a peak wind speed of 180kph was recorded (Holmes, 2001). The gradient wind speed versus the radial distance from the centre of the cyclone suggested that a steep inclination of the wind speed was expected within a 5th of the radius as an observer moves outwards (Holmes, 2001). This is graphically represented in Figure 2.27.

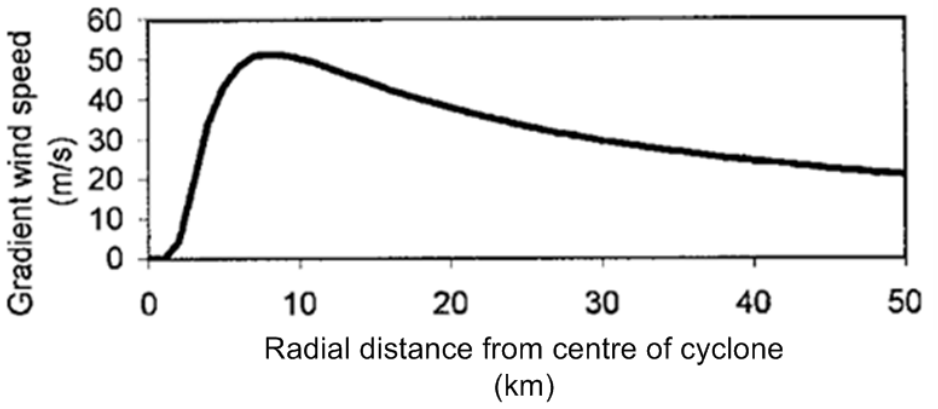


Figure 2.27: Gradient wind speed for Cyclone "Tracy" (Holmes, 2001).

The United State Government's National Hurricane Centre however classifies hurricanes according to the Saffir-Simpson Hurricane Wind Scale (Rowlett & University of North Carolina, 2000). This scale (as recorded in Table 5) rates the severity of a hurricane from a level one to five, where level one indicates the least severe storm and level five indicates the most severe storm (Rowlett & University of North Carolina, 2000).

Table 5: Saffir-Simpson hurricane wind scale (Rowlett & University of North Carolina, 2000).

Category	Sustained wind speed (km/h)	Types of damage expected
1	119-153	**Very dangerous winds will produce some damage:** Well-constructed frame homes could have damage to roof, shingles, vinyl siding and gutters. Large branches of trees will snap and shallowly rooted trees may be toppled. Extensive damage to power lines and poles likely will result in power outages that could last a few to several days.
2	154-177	**Extremely dangerous winds will cause extensive damage:** Well-constructed frame homes could sustain major roof and siding damage. Many shallowly rooted trees will be snapped or uprooted and block numerous roads. Near-total power loss is expected with outages that could last from several days to weeks.
3	178-208	**Devastating damage will occur:** Well-built framed homes may incur major damage or removal of roof decking and gable ends. Many trees will be snapped or uprooted, blocking numerous roads. Electricity and water will be unavailable for several days to weeks after the storm passes.
4	209-251	**Catastrophic damage will occur:** Well-built framed homes can sustain severe damage with loss of most of the roof structure and/or some exterior walls. Most trees will be snapped or

		uprooted and power poles downed. Fallen trees and power poles will isolate residential areas. Power outages will last weeks to possibly months. Most of the area will be uninhabitable for weeks or months.
5	252 or higher	**Catastrophic damage will occur:** A high percentage of framed homes will be destroyed, with total roof failure and wall collapse. Fallen trees and power poles will isolate residential areas. Power outages will last for weeks to possibly months. Most of the area will be uninhabitable for weeks or months.

2.3.3 Limit State Design Approach

The limit state design approach is a rational approach to the design of structures (Holmes, 2001). This approach assigns partial load factors and material factors to the applied loads and member resistances respectively (Holmes, 2001). Holmes (2001) further suggests that the application of this approach in itself is not probabilistic, but the derivation of the safety factors implemented is, however, derived by considering the probability of exceedance of the design element under consideration.

A typical ultimate limit state equation for a structural element, subjected to a dominant dead and wind load, is (Holmes, 2001):

$$\boldsymbol{\varphi R \geq \gamma_D D + \gamma_W W} \qquad \textbf{(25)}$$

Where φ = Material resistance factor

γ_D = Partial safety factor for dead load

γ_W = Partial safety factor for wind load

R = Nominal structural resistance of designed element

D = Nominal dead load structural element is subjected to

W = Nominal wind load structural element is subjected to

From equation (25), the application of safety factors is such that the material factor will reduce the nominal structural resistance of the element, underestimating its actual structural resistant capacity. Inversely, the application of a partial safety factor to the dead and wind loads will overestimate the actual applied loads to the structural element. It can therefore be stated that Equation (25) is an over-conservative approach to the design of the structural element (Holmes, 2001).

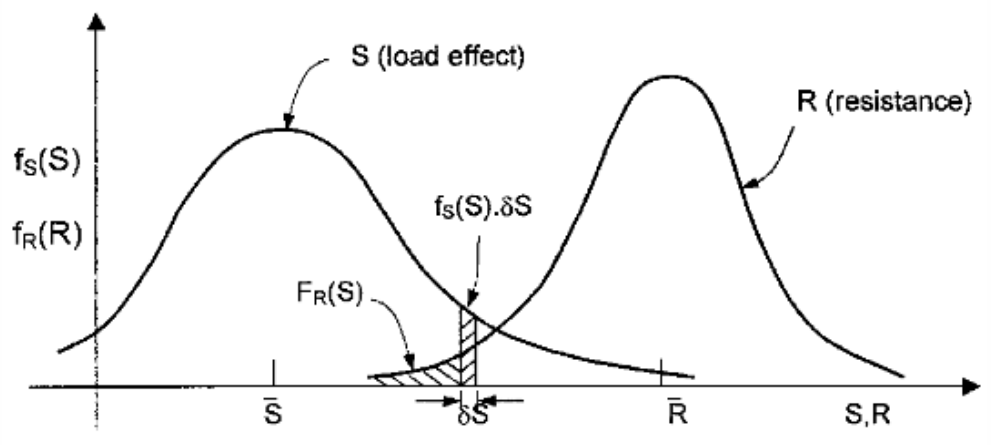


Figure 2.28: Probability densities for load effects and resistance (Holmes, 2001).

Holmes (2001) suggests that the quantity of measuring the safety of a structure is called its safety or reliability index. This method of calibration is used by many countries and implemented in most national standards for structural design (Holmes, 2001). The design process is based on the visual representation of the probability of exceedance in Figure 2.28 and the application of the basic ultimate limit state equation (25). It is suggested that the structural load effect "*S*", and the corresponding resistance "*R*" of the structural element, should overlap such that the probability of the load effect, exceeding the structural resistance of the element, is at a specified minimum (Holmes, 2001).

The determination of the safety index and the derivation of partial safety factors fall beyond the scope of this research. It should however be noted that these derivations form the basis of the ultimate limit state design approach. The South African National Standards as well as the British Standards for the design of structural steel, concrete and masonry are based on this theory.

2.3.4 Wind loads as per SANS 10160-3:2011

"*Wind action is represented by a simplified set of pressures or forces whose effects are equivalent to the extreme effects of turbulent wind"* - (SABS, 2011, p. 12). SANS 10160-3:2011 suggests that wind forces can be determined as a set of internal and external pressure loads. These loads are derived from the peak wind speed, which are factored by the applicable internal and external pressure coefficients in order to yield a resultant wind pressure on an architectural or structural face (SABS, 2011).

Peak Wind Speed The code suggests that the basic wind speed shall be determined by (SABS, 2011):

$$\boldsymbol{v_b = c_{prob} \times v_{b,0}} \qquad \textbf{(26)}$$

Where v_b = Basic wind speed at 10m above ground in terrain category B

$v_{b,0}$ = Fundamental value of the basic wind speed (Figure 2.29)

c_{prob} = Probability factor based on a "*x*" year return period

Once the basic wind speed is determined, it needs to be converted to a peak wind speed at the applicable height (z) where the pressure forces are to be determined (SABS, 2011). The peak wind speed is defined as (SABS, 2011):

$$\boldsymbol{v_p(z) = c_r(z) \times c_0(z) \times v_{b,peak}} \qquad \textbf{(27)}$$

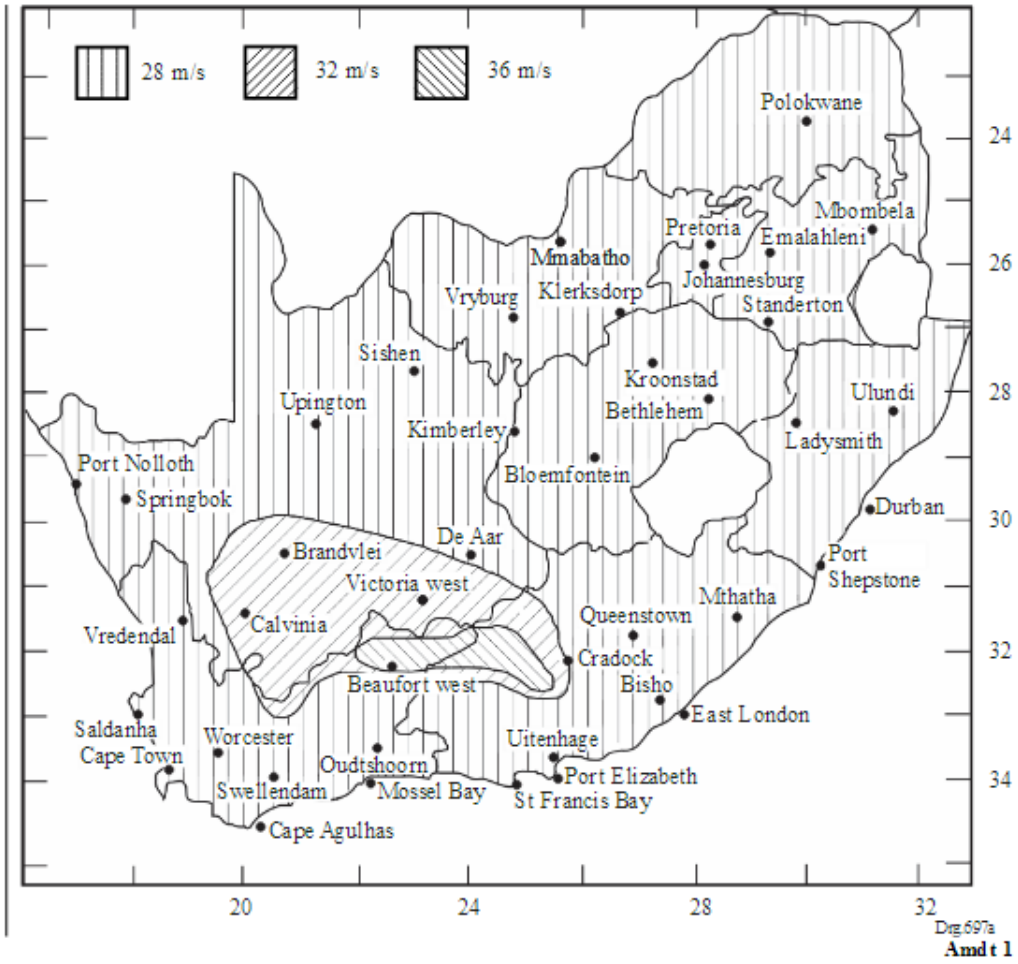
Where $v_{b,peak}$ = 1.4 x v_b

$c_r(z)$ = Roughness factor (Height (z) dependant)

$c_0(z)$ = Topography factor which should be taken as 1.0

It is suggested that the roughness factor is dependent on the profile of the earth's surface at the location under consideration. Therefore, depending

on whether it is open fields or densely populated urban areas, the roughness factor will take these factors into consideration (SABS, 2011).



NOTE For most areas of the country a basic fundamental wind speed of 28 m/s is stipulated. The South African climate (i.e. also the wind climate) is complex, in particular with regard to the dominance of frontal winds in coastal areas and intense thunderstorms inland. These two types of strong wind events cannot be fairly represented by a single value of mean wind speed in terms of 10 min averaging time. In order to overcome this problem an actual magnitude of wind speed of 28 m/s was obtained for coastal areas based on a conversion factor between hourly and 10 min mean wind speeds. For inland areas of the country an effective speed of 28 m/s was adopted.

Figure 2.29: Map of the fundamental value of the basic wind speed in South Africa (SABS, 2011).

Four terrain categories are distinguished by the code and are depicted in Figure 2.30. These categories and their dependant variables have an effect on the factorisation of the peak wind speed as suggested by equation (27). They are depicted in Figure 2.31.

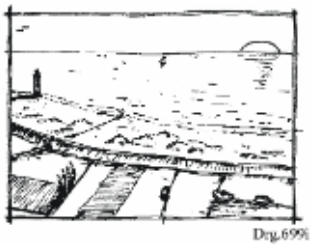
1	2	3
Category	**Description**	**Illustration**
A	Flat horizontal terrain with negligible vegetation and without any obstacles (for example coastal areas exposed to open sea or large lakes)	 Drg.699i
B	Area with low vegetation such as grass and isolated obstacles (for example trees and buildings) with separations of at least 20 obstacle heights	 Drg.699ia
C	Area with regular cover of vegetation or buildings or with isolated obstacles with separations of maximum 20 obstacle heights (such as villages, suburban terrain and permanent forest)	 Drg.699ib
D	Area in which at least 15 % of the surface is covered with buildings and their average height exceeds 15 m	 Drg.699ic
NOTE 1 A certain amount of a reduction in loading for category D can be obtained (see 7.3.5) by using a procedure described in A.5, which takes into account the vertical displacement of the peak wind pressure profile, within an environment with closely spaced obstructions.		

Figure 2.30: Terrain categories for the determination of the roughness factor (SABS, 2011).

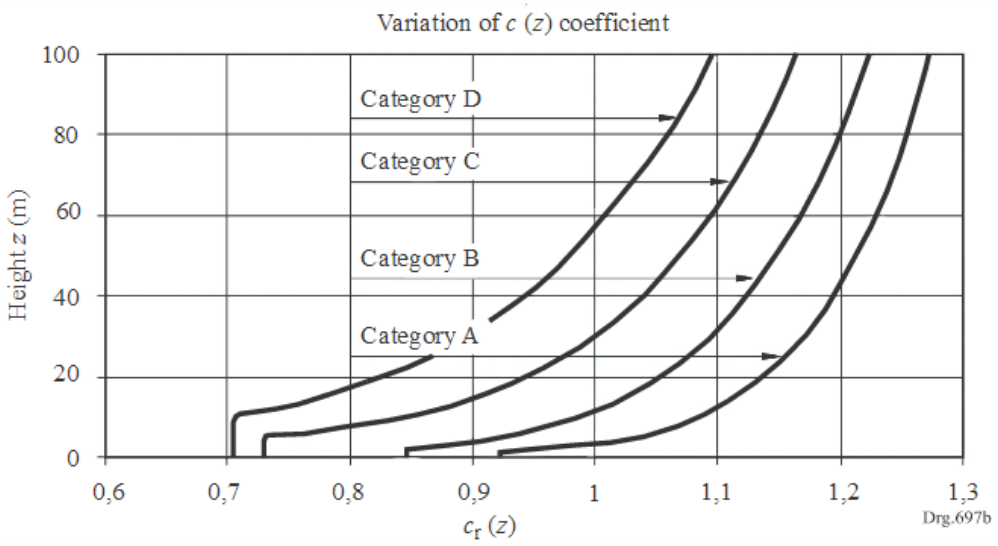


Figure 2.31: Variation of the roughness factor with height above ground level (SABS, 2011).

Peak Wind Speed Pressure Taking into consideration the air density at the altitude where the structure designed will be constructed, the peak wind speed pressure can be derived (SABS, 2011):

$$\boldsymbol{q_p(z) = \frac{1}{2} \times \rho \times v_p^2(z)} \qquad \textbf{(28)}$$

Where ρ = Air density in kg/m^3

The peak wind speed pressure is considered as the quadratic function of the peak wind speed under consideration. Should the designer wish to make use of a more stringent peak wind speed value, this value can be utilised in equation (28) to obtain the relevant peak wind speed pressure for the design purpose under consideration.

Design Wind Pressure The design wind pressure is a function of the peak wind speed pressure and the relevant internal and external pressure coefficients (SABS, 2011):

$$\boldsymbol{w = q_p(z) \times c_{p,R}} \qquad \textbf{(29)}$$

Where w = Design wind pressure

$q_p(z)$ = Peak wind speed pressure as per equation (28)

$c_{p,R}$ = Resultant pressure coefficient on the face considered

Pressure Coefficients As per Section 2.3.1, moving air will result in the generation of forces in structures subjected to it. By means of physical testing, wind pressures on structural and architectural faces have been determined over decades of research (Holmes, 2001). These pressure coefficients are readily available in most structural design codes of which SANS 10160-3:2011 is one. Architectural faces are subdivided into zones, where a specific pressure coefficient is identified to be applicable based on the geometry of the overall structure (SABS, 2011).

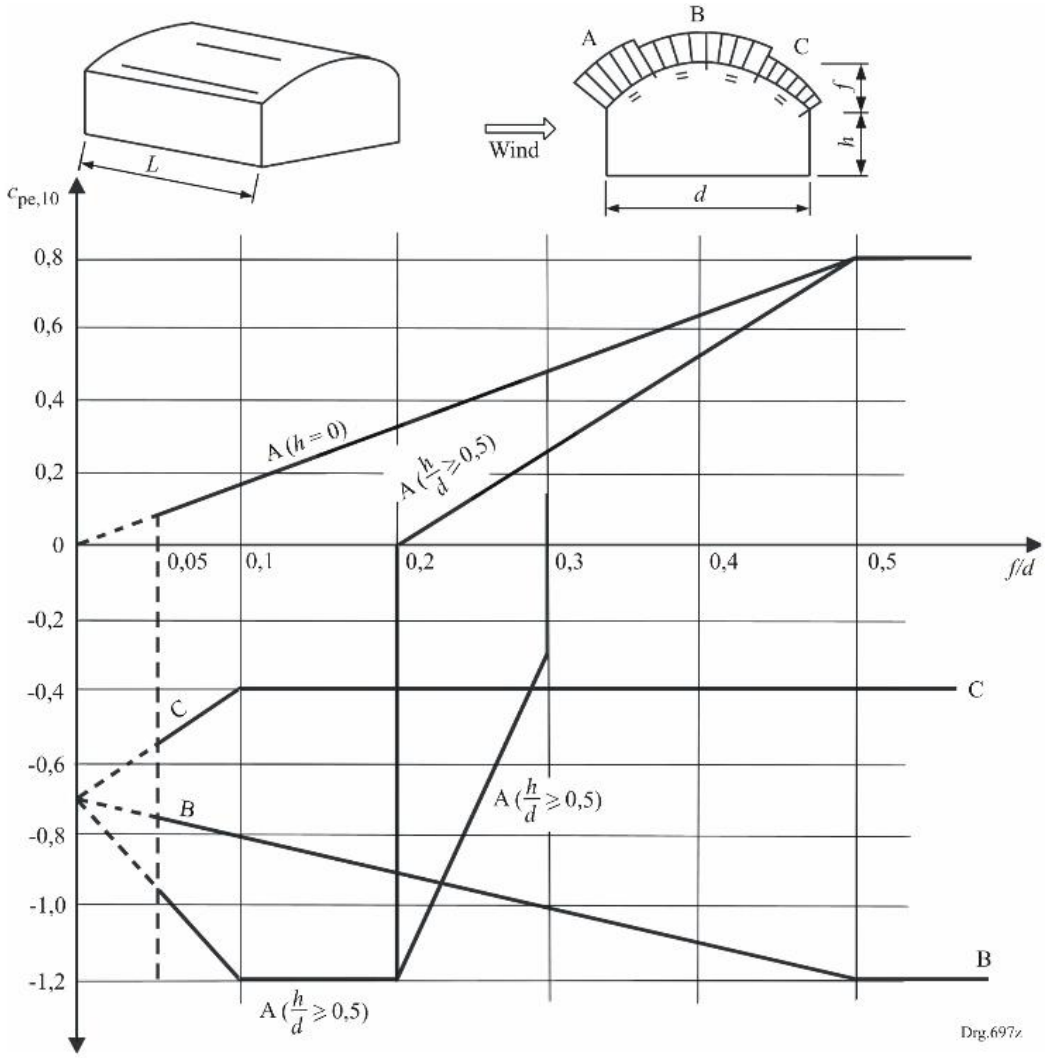
The resultant wind pressure force experienced by each zone will be a factor of the wind pressure, and the resultant coefficient between the internal and external pressure coefficients experienced by the zone under consideration.

Internal pressure coefficients Highly sophisticated means of determining the internal pressure coefficients of a structure is implemented by SANS 10160-3:2011. It is however suggested by the code that: "*where it's not possible, or deemed to be justified, the internal pressure coefficients of a structure can be taken as the most onerous of +0.2 or -0.3*" (SABS, 2011, p. 48).

External pressure coefficients SANS 10160-3:2011 does not cater for the determination of wind forces on catenary vaulted structures. It does, however, consider wind loads on circular vaults and domes. These loads, although not exactly similar to that of catenary vaults, are closely related to one another and considered as an adequate approximation for initial load calculations (Bradley, 2011).

The external pressure coefficients on circular vaulted roofs with rectangular bases can be determined by considering the span (d), vertical wall height (h) and rise of the vault (f) (SABS, 2011). For each zone (A, B

or C) external pressure coefficients can be determined from the applicable linear relationships as illustrated in Figure 2.32.



NOTE 1 For $0 < h/d < 0,5$, $c_{pe,10}$ is obtained by linear interpolation.

NOTE 2 For $0,2 \leq f/d \leq 0,3$ and $h/d \geq 0,5$, two values of $c_{pe,10}$ should be considered.

NOTE 3 The diagram is not applicable to flat roofs.

Figure 2.32: Recommended values of external pressure coefficients for vaulted roofs with rectangular bases (SABS, 2011).

The values of the external pressure coefficient, as determined by Figure 2.32, relates to values as determined for each zone by Bradley (2011) in Figure 2.33 through Figure 2.35. It should be noted that, for catenary vaults, a fourth pressure zone is identified (Bradley, 2011). It had been

found that, for the zone identified by a line perpendicular to the curve with an angle to the horizontal of between 45 degrees and 90 degrees, the force may switch from positive pressure to negative suction on the shell surface (Ryan Bradley, 2011).

Bradley (2011) does, however, not include the effect a vertical wall will have on the external pressure coefficients near a wall-to-shell intersection.

2.3.5 Wind Loads on Catenary Vaults

Bradley (2011) suggests that external pressure coefficients on catenary vaults can be determined from Figure 2.33 through Figure 2.35. These coefficients were determined by wind-tunnel testing at the CSIR laboratories in Pretoria East, South Africa (Bradley, 2011).

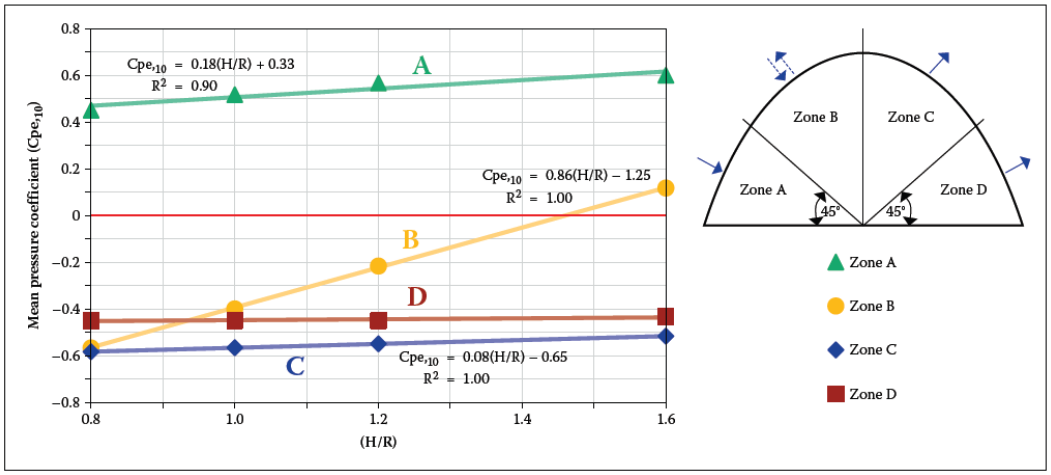


Figure 2.33: Wind azimuth direction 0/180 degrees (Bradley, Gohnert, Goliger & Mistry, 2016)

The magnitude and direction of the pressure coefficient is solely based on the geometry of the vault (Bradley, 2011). In other words, the magnitude of the wind speed assumed in the calculation of the design pressure force is not a variable in the external pressure coefficient determination. Instead, it is merely a constant by which each pressure coefficient (as determined by the geometry of the structure) is multiplied to obtain the design wind speed pressure applicable to each zone.

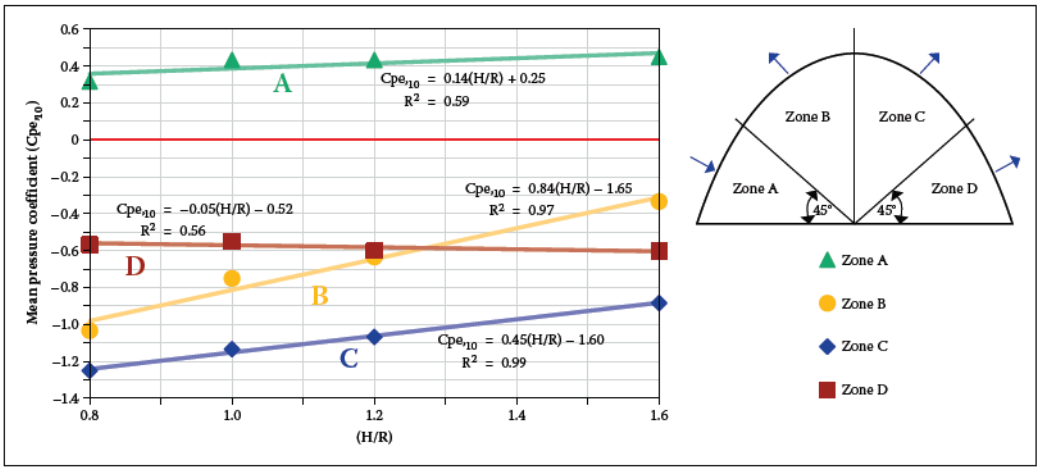


Figure 2.34: Wind azimuth direction 30/45 degrees (Bradley *et al.*, 2016)

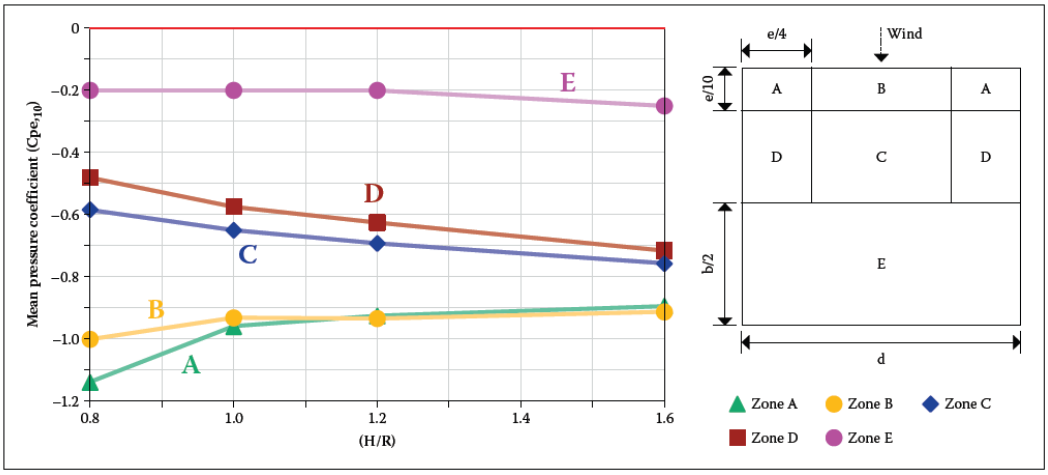


Figure 2.35: Wind azimuth direction 90/270 degrees (Bradley *et al.*, 2016)

2.4 DESIGN OF THE SHELL

By defining the geometry of a structure to be catenary, the structure will resist forces highly efficiently (Allan *et al.*, 2010). These structures require the minimum amount of construction materials to resist its intended loads safely (Allan *et al.*, 2010). It can therefore be assumed that for a catenary vault, the shell thickness of the vault will most likely be ultra-thin in comparison to the load it's designed to resist.

As catenary forms resist their applied loads in pure compression, it needs to be ensured that the shell of the structure can safely resist the compressive stresses it is subjected to. Under *Buckling of Arches* the buckling characteristics of a catenary shell will be discussed. In addition to buckling failure, the shell may be subjected to load conditions which unfavourably force the line of thrust outside of the kern of the section. This will result in the generation of flexural tension in the extreme fibres of the section, which needs to be accounted for in the design.

As a first step in the design process, the total stress in the section should be determined (Curtin *et al.*, 1995):

$$\boldsymbol{\sigma = \frac{P}{A} \pm \frac{Pe}{Z}} \qquad \textbf{(30)}$$

Where σ = Total stress in extreme fibre of section

P = Axial force in section

A = Area of section

e = Eccentricity of axial force to geometric centroid of section

Z = Section modulus

Should the outcome of equation (30) yield pure compression within the section fibres, it can be assumed that the line of thrust lies within the kern of the section and that no requirement for tensile reinforcement exists. Should equation (30) yield tension within the section fibres, the opposite is true, and the section should be adequately designed to accommodate the tensile stresses within it.

2.4.1 Dealing with Tensile Stresses

Although concrete and masonry are known for their effective compressive resistance, these materials do not provide significant resistance to any tension load (Robberts & Marshall, 2010) and (Cowan, 1977). As a result

of this deficiency, alternative means of ensuring structural reliability and durability need to be explored.

Tension in a masonry section is considered unfavourable, as masonry does not poses a high tensile resistance capacity (Curtin *et al.*, 1995). Should tension therefore be developed in a general masonry section, crack development is highly likely (Curtin *et al.*, 1995). There are basically three primary means of ensuring no tension in the section (Sengupta & Menon, n.d.):

1. Ensure that the structure will never be subjected to loads that will induce tensile forces in the section.
2. Provide tension reinforcement which is designed to resist the tension force developed in the section.
3. Pre-stress or Post-tension the section to a point where no load case will be able to generate tension stress within the section.

The selection of one of the above solutions may depend on its cost implications, structural efficiency and constructability of the design.

As suggested by Figure 2.36, there are a number of variables affecting the structural strength of a masonry element. These variables and their application will be discussed Section 2.4.2.

2.4.2 Design of the Masonry Section

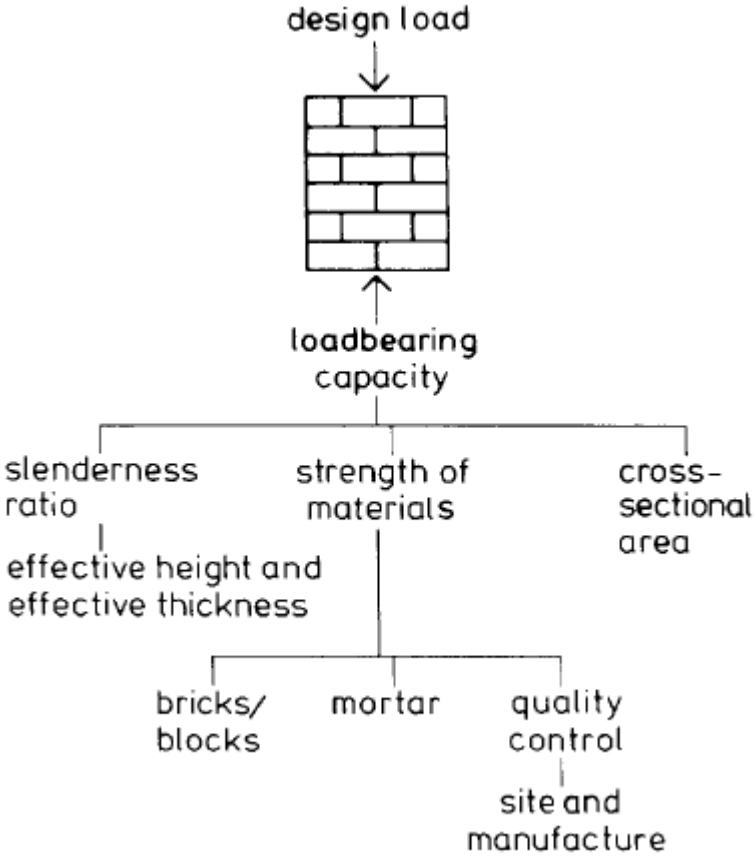


Figure 2.36: Factors affecting the compressive strength of masonry (Curtin *et al.*, 1995).

Ensuring No Tension Development By defining the geometry of a structure such that no axial or flexural tension develop under any of the load cases it is subjected to, no tension reinforcement will be required (Robberts & Marshall, 2010). Such a structure is said to be catenary in its nature of resisting loads (Allan *et al.*, 2010) and is discussed under section 2.2. Optimisation of the geometry, to accommodate loads in a pure compression fashion, will eliminate the need for any tension reinforcement or pre-stressing within the section.

In addition to not having a requirement for tension reinforcement, the design may require nominal reinforcement to ensure durability of the

structure (Curtin *et al.*, 1995). In areas where the shear stress approaches the shear capacity of the section, nominal reinforcement may be required to avoid crack formation (Curtin *et al.*, 1995). Should nominal reinforcement be required, it should be supplied in the form of links, and spaced at three quarters of the lever arm length (Curtin *et al.*, 1995).

Pure Compression The aim of the limit state design process, as adopted by most design codes, is to ensure that the factorized resistance of the structural section exceeds the factorized loads applied to it (Curtin *et al.*, 1995) and (Holmes, 2001). For the design of masonry structures, this interaction is mathematically expressed by (Curtin *et al.*, 1995):

$$\boldsymbol{f}\left(\frac{\boldsymbol{f_k}}{\boldsymbol{\gamma_m}}\right) \geq \boldsymbol{f}(\boldsymbol{\gamma_f F_k}) \qquad \textbf{(31)}$$

Where f_k = Characteristic strength of masonry

γ_m = Partial factor of safety for masonry

F_k = Characteristic loading

γ_f = Partial safety factor on loadings

f = Mathematical function involving the symbols in parentheses

Characteristic strength of bricks The characteristic strength of the masonry as a whole relies on many variables. One of these is the compressive strength of the brick or block units it is constructed of, while the other is the mortar used as bedding material (Curtin *et al.*, 1995). Figure 2.37 suggests the standard available masonry brick and block strengths available on the market (Curtin *et al.*, 1995).

	Compressive strength of unit (N/mm^2)		
	Bricks	Blocks	
Typically available values	5.0	2.8	Typical structural units
	10.0	3.5	
	15.0	5.0	
	20.0	7.0	
	27.5	10.0	
	35.0	15.0	Blocks of these strengths may not be readily available
	50.0	20.0	
	70.0	35.0	
	100.0		

Figure 2.37: Compressive strength of a variety of masonry units (Curtin *et al.*, 1995).

Empirical tests on different shapes and sizes of masonry bricks have proven to yield different compressive test results (Curtin *et al.*, 1995). It was found that the larger the masonry bricks used in construction, the higher the overall compressive resistance of the masonry (Curtin *et al.*, 1995). A shape factor was identified to more accurately represent the compressive resistance of masonry, comprising of different shapes of brick elements (Curtin *et al.*, 1995). An example on the determination of the shape factor (aspect ratio) of a masonry unit is seen in Figure 2.38.

The bond of a masonry structure is defined as the order in which the masonry units are placed (Curtin *et al.*, 1995). It was found, by means of experimental testing, that the bond also plays a significant role in the overall strength of the masonry (Curtin *et al.*, 1995). The characteristic compressive strength of masonry based on bond type is listed by various structural codes of practice (Curtin *et al.*, 1995).

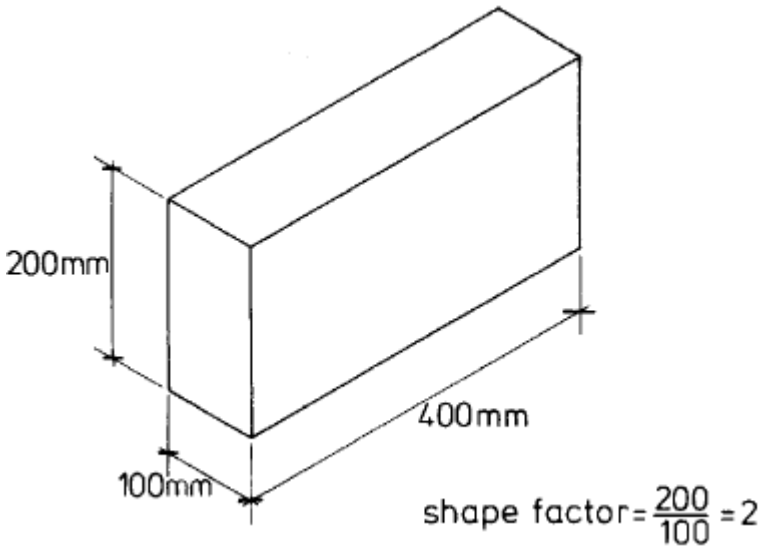


Figure 2.38: Determination of the shape factor of a masonry brick (Curtin *et al.*, 1995).

Mortar classification BS 5628 Part 1 classifies mortar into four distinct categories based on their mix ratios and 28 day mean compressive test results. The mortar class, as defined by Figure 2.39, in conjunction with the selected brick or block unit strength from Figure 2.37, will yield the characteristic design compressive strength of the masonry as a whole (Curtin *et al.*, 1995).

	Mortar designation	Type of mortar (proportion by volume)			Mean compressive strength at 28 days	
		Cement : lime : sand	Masonry cement : sand	Cement : sand with plasticizer	Preliminary (laboratory) tests	Site tests
↑ Increasing strength / Increasing ability to accommodate movement, e.g. due to settlement, temperature and moisture changes ↓					N/mm²	N/mm
	(i)	1 : 0 to ¼ : 3	–	–	16.0	11.0
	(ii)	1 : ½ : 4 to 4½	1 : 2½ to 3½	1 : 3 to 4	6.5	4.5
	(iii)	1 : 1 : 5 to 6	1 : 4 to 5	1 : 5 to 6	3.6	2.5
	(iv)	1 : 2 : 8 to 9	1 : 5½ to 6½	1 : 7 to 8	1.5	1.0
Direction of change in properties is shown by the arrows		Increasing resistance to frost attack during construction →				
		← Improvement in bond and consequent resistance to rain penetration				

Figure 2.39: Mortar requirements according to BS 5628 Part 1 (Curtin *et al.*, 1995).

The main structural role of the mortar in masonry is to provide a bedding in which the masonry elements can be placed (Curtin *et al.*, 1995). The mortar joint is considered the weakest link within the masonry, and thick joints have proven to reduce the compressive resistance of the masonry significantly (Curtin *et al.*, 1995). It is suggested that a mortar joint thickness of 10mm is used with an upper tolerance of 13mm (Curtin *et al.*, 1995).

Characteristic strength of masonry The characteristic compressive strength of masonry has been determined and recorded by means of empirical research for a variety of different masonry elements and mortar mixtures (Curtin *et al.*, 1995). It is therefore based on the mortar designation as per Figure 2.39, the unit compressive strength as per Figure 2.37 as well as other aspects such as the unit's aspect ratio as per Figure 2.38 (Curtin *et al.*, 1995). An example of these values is depicted in Figure 2.40 for masonry bricks having an aspect ratio of 2.0 and 4.0 (Curtin *et al.*, 1995).

Mortar designation	Compressive strength of unit (N/mm^2)							
	2.8	3.5	5.0	7.0	10	15	20	35 or greater
(i)	2.8	3.5	5.0	6.8	8.8	12.0	14.8	22.8
(ii)	2.8	3.5	5.0	6.4	8.4	10.6	12.8	18.8
(iii)	2.8	3.5	5.0	6.4	8.2	10.0	11.6	17.0
(iv)	2.8	3.5	4.4	5.6	7.0	8.8	10.4	14.6

Figure 2.40: Characteristic compressive strength of masonry (f_k) for solid bricks having a ratio of height to least horizontal dimension of between 2.0 and 4.0 as per BS 5628 - Table 2d (Curtin *et al.*, 1995).

Standard of workmanship The standard of workmanship is considered one of the most important factors pertaining to the structural strength of masonry (Curtin *et al.*, 1995). In order to account for poor construction techniques, a partial safety factor for materials is implemented (Curtin *et al.*, 1995). This factor reduces the characteristic compressive strength of masonry to a design strength as per equation (32) (Curtin *et al.*, 1995):

$$\boldsymbol{Design\ strength} = \frac{f_k}{\gamma_m} \qquad \textbf{(32)}$$

		Category of construction control	
		Special	Normal
Category of manufacturing control	Special	2.5	3.1
	Normal	2.8	3.5

Figure 2.41: Partial factors of safety on materials (Curtin *et al.*, 1995).

Figure 2.41 suggests four variables regarding quality control. These variables are listed and defined as (Curtin *et al.*, 1995):

1. Manufacturing control
    a. Normal – Supplier can meet the compressive strength requirements of the appropriate National Standard
    b. Special – Supplier can meet a specified strength limit more stringent than that said by the National Standard
2. Construction control
    a. Normal – The construction works complied with the workmanship recommendations given by the applicable National Standard

b. Special – The construction works complies with the normal condition as a minimum with additional quality control specifications

Compression resistance For pure compression resistance of the masonry section, the following equation governs (Curtin *et al.*, 1995):

$$N_d = \beta\left(\frac{f_k}{\gamma_m}\right) \times t \qquad (33)$$

Where N_d = Axial resistance of element in force per linear length

β = Capacity reduction factor as per Figure 2.42

t = Thickness of the element under consideration

Depending on the slenderness ratio (SR) of the compression element, the compressive resistance can be taken as the actual compressive resistance of the section, or a reduced design resistance as a result of possible construction imperfections (Curtin *et al.*, 1995):

$$SR = \frac{effective\ length}{effective\ thickness} \qquad (34)$$

The capacity reduction factor (β), as applied in equation (33), is implemented to govern the design axial resistance of the section based on its slenderness ratio.

By applying equation (30), the stress condition within the section can be determined. Should the section be in pure compression, and the compressive stress within it not exceeding the compressive resistance as per equation (33), it can be assumed that the section will be fit for purpose and that only nominal reinforcement may be required (Curtin *et al.*, 1995). Should this not be the case, alternative means of dealing with the tension generated in the section should be considered (Curtin *et al.*, 1995).

Slenderness ratio h_{ef}/t_{ef}	Eccentricity at top of wall, e_x			
	Up to $0.05t$ (see note 1)	$0.1t$	$0.2t$	$0.3t$
0	1.00	0.88	0.66	0.44
6	1.00	0.88	0.66	0.44
8	1.00	0.88	0.66	0.44
10	0.97	0.88	0.66	0.44
12	0.93	0.87	0.66	0.44
14	0.89	0.83	0.66	0.44
16	0.83	0.77	0.64	0.44
18	0.77	0.70	0.57	0.44
20	0.70	0.64	0.51	0.37
22	0.62	0.56	0.43	0.30
24	0.53	0.47	0.34	
26	0.45	0.38		
27	0.40	0.33		

Note 1. It is not necessary to consider the effects of eccentricities up to and including $0.05t$.
Note 2. Linear interpolation between eccentricities and slenderness ratios is permitted.
Note 3. The derivation of β is given in Appendix B of BS 5628.

Figure 2.42: Capacity reduction factor for load bearing masonry structures (Curtin *et al.*, 1995)

Tension Stress in Masonry Most structures are subjected to a wide variety of load conditions (Allan *et al.*, 2010). Many of these loads are resisted in flexure which yields flexural compression and tension stress within the section. When it comes to the use of masonry as a construction material, care should be taken in the way these tensile stresses are being resisted (Curtin *et al.*, 1995).

For a structural section subjected to compression, or a combination of compression and bending, the section can be considered and designed as a column (Curtin *et al.*, 1995).

Combined stress state Although it would be ideal to have structures resist load in pure compression, most structures need to be designed to resist some of the applied load in direct compression, tension, flexure or a combination of the previously stated. To determine whether a section will crack under a given set of loads depends on the combined stress state of the extreme fibres (Curtin *et al.*, 1995). Structural sections can be subjected to a combination of any of the four distinct stress conditions listed:

1. Uniform (Direct) compression
2. Uniform (Direct) tension
3. Uni-axial flexure (Bending)
4. Bi-axial flexure (Bending)

The phenomenon of the cracked section comes into play when tension develops within the section as a result of the combined stress conditions (Curtin *et al.*, 1995). When the eccentricity, as determined by equation (6), falls within the kern of the section, "*case 1*" as per Figure 2.43 will govern and no tension will develop within the section (Curtin *et al.*, 1995). Should the axial force be similar or small in relation to the applied external moment, the eccentricity of the applied loads may fall outside the kern and tension will develop within the section (Marshall & Robberts, 2000).

If it can be assumed that the masonry has some tensile capacity, and that the applied tensile stress does not exceed the design tensile capacity of the section, no cracking will occur and "*case 2*" will govern (Curtin *et al.*, 1995). Alternatively, in the event that it is assumed that the masonry does not possess any tensile capacity, the section will crack and *"case 3*" will govern (Curtin *et al.*, 1995).

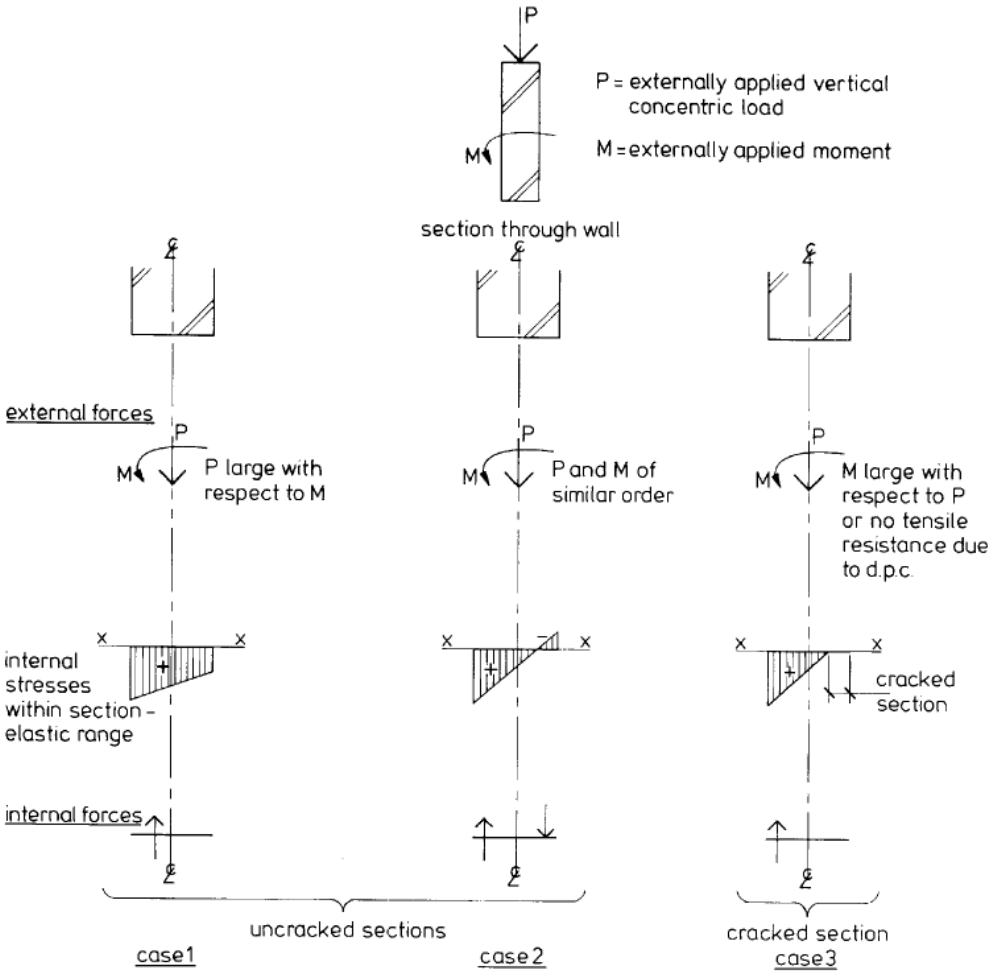


Figure 2.43: Un-cracked vs cracked masonry sections (Curtin *et al.*, 1995).

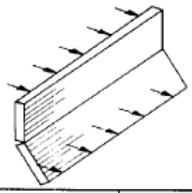
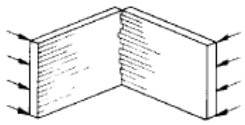
Direct tension Direct tension occurs when the tension force in a section is applied to the section's geometric centroid (Curtin *et al.*, 1995). The section will, as a result, be subjected to a uniform tension stress state. Curtin *et al*. (1995) suggests that there should be no reliance on the tension capacity of masonry structures. BS 5628 does however allow designers to consider masonry's tensile resistance capacity at their own discretion (Curtin *et al.*, 1995). Two cases are identified as acceptable (Curtin *et al.*, 1995):

1. In the design of sections for the resistance of suction forces due to wind loads. Nevertheless, some form of positive restraint is to be

implemented and can be achieved by the application of restraint straps.

2. The consideration of the probable effects of misuse or accidental damage to the structure.

When considering these cases, the code limits the tensile stress to half the values of the flexural tensile stresses as depicted in Figure 2.44. Under no circumstance should the combined stress in the section be allowed to exceed these values (Curtin *et al.*, 1995).

	Plane of failure parallel to bed joints			Plane of failure perpendicular to bed joints		
						
Mortar designation	(i)	(ii) and (iii)	(iv)	(i)	(ii) and (iii)	(iv)
Clay bricks having a water absorption						
less than 7%	0.7	0.5	0.4	2.0	1.5	1.2
between 7% and 12%	0.5	0.4	0.35	1.5	1.1	1.0
over 12%	0.4	0.3	0.25	1.1	0.9	0.8
Calcium silicate bricks	0.3		0.2	0.9		0.6
Concrete bricks	0.3		0.2	0.9		0.6
Concrete blocks (solid or hollow) of compressive strength in N/mm²:						
2.8, 3.5, 7.0 used in walls of thickness* up to 100 mm	0.25		0.2	0.40 0.45 0.60		0.4 0.4 0.5
2.8, 3.5, 7.0 used in walls of thickness* 250 mm	0.15		0.1	0.25 0.25 0.35		0.2 0.2 0.3
10.5, 14.0 and over used in walls of any thickness*	0.25		0.2	0.75 0.90†		0.6 0.7†

* The thickness should be taken to be the thickness of the wall, for a single-leaf wall, or the thickness of the leaf, for a cavity wall.

† When used with flexural strength in parallel direction, assume the orthogonal ratio $\mu = 0.3$.

Linear interpolation between entries in Table 6.1 is permitted for: (a) concrete block walls of thickness between 100 mm and 250 mm; (b) concrete blocks of compressive strength between 2.8 N/mm² and 7.0 N/mm² in a wall of given thickness.

Figure 2.44: Characteristic flexural strength of masonry (Curtin *et al.*, 1995).

Un-cracked sections Sections which are allowed to develop tension are termed un-cracked sections (Curtin *et al.*, 1995). For masonry elements subjected to pure bending, the moment of resistance can be expressed as (Curtin *et al.*, 1995):

$$\boldsymbol{M_r = \frac{f_{kx}}{\gamma_m} \times Z} \qquad \textbf{(35)}$$

Where f_{kx} = Characteristic flexural strength perpendicular to bed joints

Equation (35) is a pure flexure equation and no provision for the inclusion of additional uniform pressure is made. Curtin *et al* (1995) suggest that the inclusion of a uniform pressure in the section can be achieved by modifying equation (35) as follows:

$$\boldsymbol{M_r = \left(\frac{f_{kx}}{\gamma_m} + \sigma_n\right) \times Z} \qquad \textbf{(36)}$$

Where σ_n = Additional uniform pressure in section fibres

By increasing the uniform pressure in the section, a reduction in the force eccentricity is achieved (Curtin *et al.*, 1995). This results in a reduced eccentric bending moment in the section, which in turn yields reduced tension in the section (Curtin *et al.*, 1995).

Cracked sections At a section where no capacity to the resistance of tension stress is assumed, the section is termed a cracked section (Curtin *et al.*, 1995). The design moment of resistance of the section is therefore solely provided by the gravitational stability moment and any net load about the appropriate lever arm (Curtin *et al.*, 1995). This stability moment must, therefore, be sufficient to resist the applied overturning moment (Curtin *et al.*, 1995). This mechanism is illustrated in Figure 2.45.

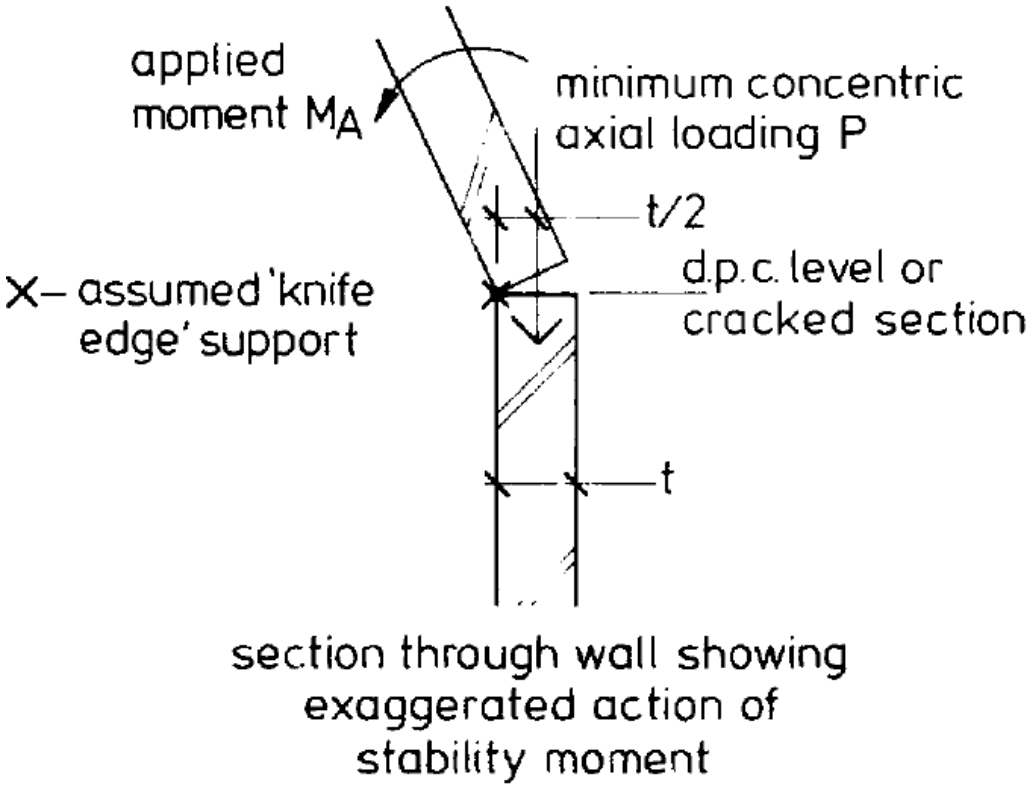


Figure 2.45: Exaggerated action of stability moment (Curtin *et al.*, 1995).

In Figure 2.45 it is assumed that the section is to overturn about a pivot point "*X*". This point is defined by Curtin *et al*. (1995) as the "*Knife edge support*". It seems intuitive that this pivot point is not practical, as the concentration of a load to an infinitely small area will yield infinitely large compressive stresses (Curtin *et al.*, 1995).

A more realistic approach would be to assume that some brittle failure of the material in this area will occur and that the "*Knife edge support*" will have a finite thickness (Curtin *et al.*, 1995).

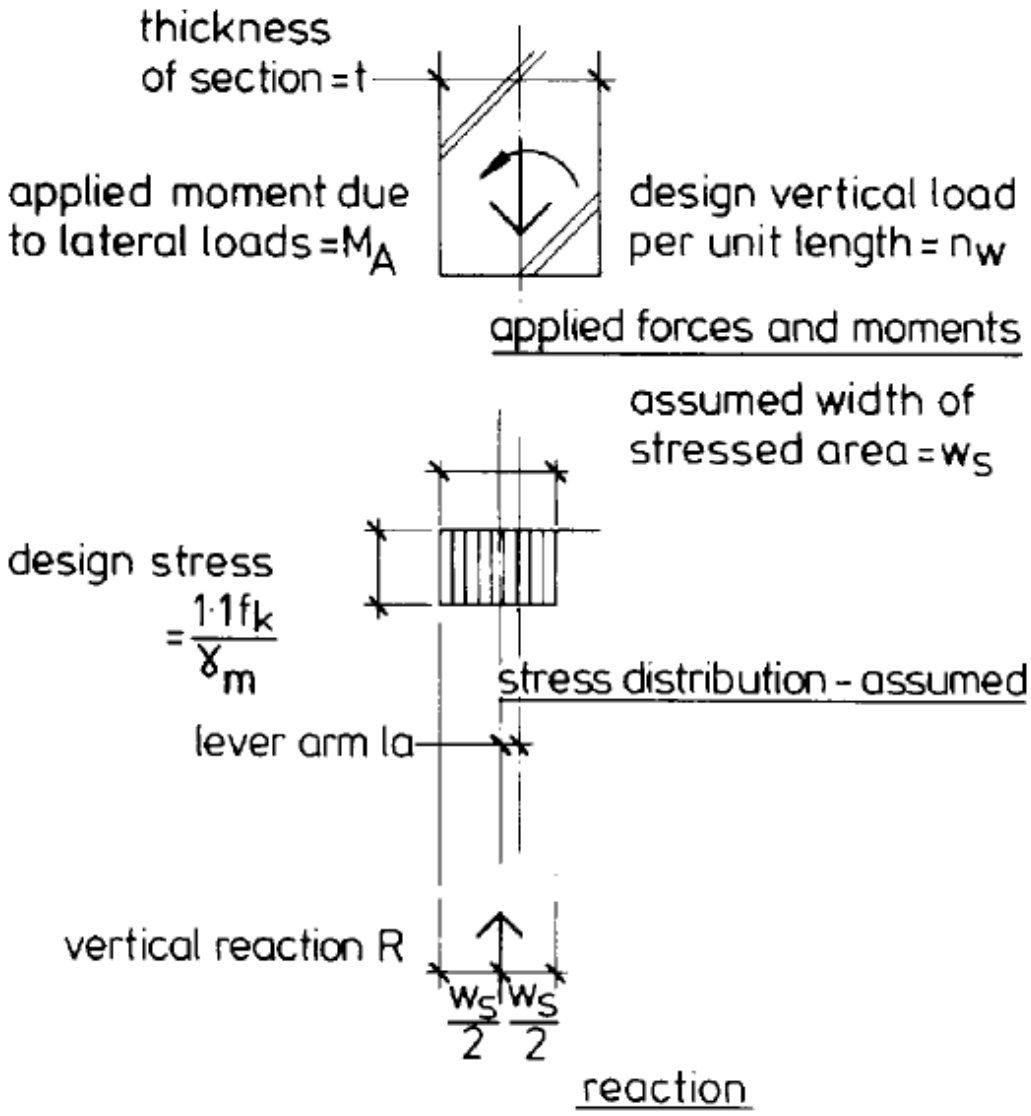


Figure 2.46: Assumed moment equilibrium in cracked masonry section (Curtin *et al.*, 1995)

BS 5628 suggests that the "*Knife edge support*" can be accurately represented by an equivalent stress block which is defined as (Curtin *et al.*, 1995):

$$C_{kes} = \frac{1.1f_k}{\gamma_m} \times t \times w_s \qquad (37)$$

Where C_{kes} = Compressive force countering overturning

$$w_s = \frac{n_w}{1.1 f_k t}$$

n_w = Total applied (factorised) external vertical load

By considering moment equilibrium in the section and re-arranging terms, the moment of resistance for a cracked masonry section is derived (Curtin *et al.*, 1995):

$$\boldsymbol{M_{r,crack} = \frac{n_w}{2}\left(t - \frac{n_w \gamma_m}{1.1 f_k}\right)} \qquad \textbf{(38)}$$

This resisting moment is always greater than the un-cracked moment resistance of the section.

Reinforced Masonry Curtin *et al*. (1995) suggests that masonry can be reinforced by two means:

1. By providing normal tension reinforcement
2. By introducing pre-stressing or post-tensioning to the masonry

The main differences in the two methods of reinforcement are illustrated in Figure 2.47. Here it can be seen that normal reinforcement is primarily applied at the location of tensile stress development in the section (Curtin *et al.*, 1995). Before the section starts to crack, the tension reinforcement is activated by means of strain development. This activation yields the resistance of tension stress by the reinforcement in the section.

On the other hand, post-tension tendons are loaded prior to putting the structure in service (Marshall & Robberts, 2000). As the tendon is loaded with tension force, the reaction of the section to this force is an opposite but equal compressive resistance. Should the tendon be placed at the geometric centroid of the section, the section will be placed under uniform compressive stress (Curtin *et al.*, 1995; Marshall & Robberts, 2000). Off-setting the tendon by an eccentricity (e) from the centroid, the section will

be subjected to a combination of uniform compression and flexure stress (Curtin *et al.*, 1995; Robberts & Marshall, 2010).

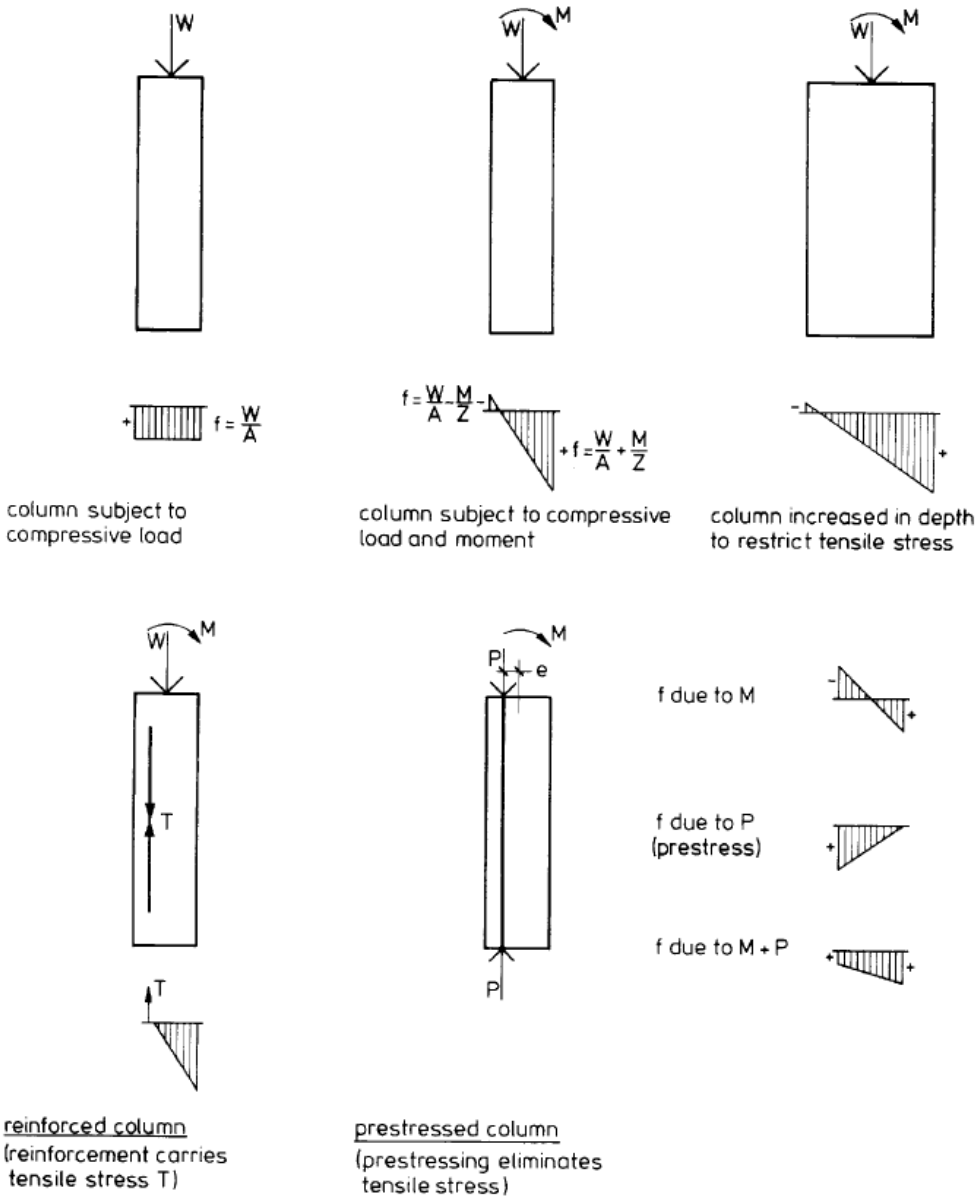


Figure 2.47: Illustration of the difference between normal reinforcement and pre-stressing (Curtin *et al.*, 1995).

This method of off-setting the pre-stressing tendon can be used to the advantage of the designer as an opposite eccentricity moment can be generated (Curtin *et al.*, 1995; Marshall & Robberts, 2000). The eccentricity moment can be carefully calculated to match the applied in

service moment, hence eliminating any tension in the section (Curtin *et al.*, 1995; Marshall & Robberts, 2000). This method of stress reduction is termed section decompression.

Normal reinforcement As with the design of reinforced concrete, the reinforced masonry section is designed such that the reinforcement will yield in tension prior to the masonry failing in compression (Curtin *et al.*, 1995). The following assumptions are valid (Curtin *et al.*, 1995):

1. Plane sections remain plane.
2. The tensile strength of masonry is ignored.
3. The compressive stress distribution is assumed to be rectangular over the compression zone

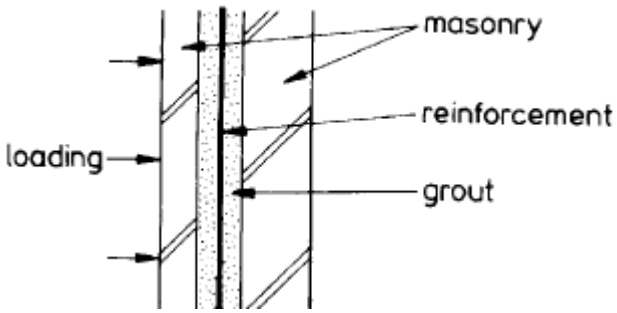


Figure 2.48: Section through a normally reinforced masonry section (Curtin *et al.*, 1995).

Considering flexure, a typical section through a normally reinforced masonry wall is illustrated in Figure 2.48. For a balanced section, the stress strain distribution within the reinforced section is as depicted in Figure 2.49.

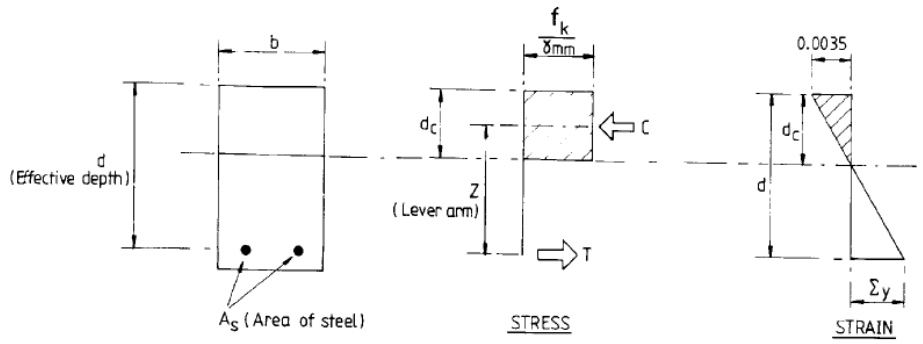


Figure 2.49: Stress strain relationship in a reinforced masonry section (Curtin *et al.*, 1995).

For normally reinforced masonry elements, the partial safety factors for materials are amended as per Figure 2.50 and Figure 2.51.

Category of manufacturing control of structural units	Value of γ_{mm}
Special	2.0
Normal	2.3

When considering accidental loading the above values may be halved.

Figure 2.50: Partial factor of safety for masonry in reinforced sections in ultimate limit state (Curtin *et al.*, 1995).

	Limit state	
	Ultimate	Accidental damage
Steel γ_{ms}	1.15	1.0
Bond between mortar/grout and steel γ_{mb}	1.5	1.0
Shear strength of masonry γ_{mv}	2.0	1.0

Figure 2.51: Partial factor of safety on materials – ultimate and accidental damage limit states (Curtin *et al.*, 1995).

From Figure 2.49 it can be determined that the compressive force exerted by the compression block and the tensile force exerted by the tension reinforcement are (Curtin *et al.*, 1995):

$$\boldsymbol{C = \frac{f_k}{\gamma_m} \times b \times d} \qquad \textbf{(39)}$$

$$\boldsymbol{T = \frac{A_s f_y z}{\gamma_s}} \qquad \textbf{(40)}$$

Where A_s = Area of tension reinforcement

γ_s = Partial safety factor for strength of steel

$z = \frac{d(1-0.5A_s f_y \gamma_m)}{bdf_k \gamma_s}$ (Internal lever arm)

f_y = Characteristic tensile strength of steel

From the strain diagram, as illustrated in Figure 2.49, the bending moment resistance of the section can be determined (Curtin *et al.*, 1995):

$$\boldsymbol{M_{r,nr} = 0.36 \frac{f_k b d^2}{\gamma_m}} \qquad \textbf{(41)}$$

Curtin *et al*. (1995) suggests that a more convenient way of representing the bending moment resistance of a masonry section is to introduce a moment of resistance factor (Q):

$$\boldsymbol{M_c = Qdb^2} \qquad \textbf{(42)}$$

Where $Q = \frac{2c(1-c)f_k}{\gamma_m}$

$c = \frac{z}{d}$

Structural codes for the design of reinforced masonry gives useful graphs based on the moment of resistance factor (Q) (Curtin *et al.*, 1995).

Considering the resistance of axial loads, the axial resistance of the section depends on the slenderness ratio of the section under discussion. Should the slenderness ratio not exceed 12, the axial resistance of a reinforced masonry section is simply the combination of its vertical axial strength, as determined for unreinforced masonry, plus the vertical axial strength of the reinforcement (Curtin *et al.*, 1995). Where the slenderness ratio exceeds 12, the element will be subjected to bending and reference to BS 5628: Part 2 or similar should be made (Curtin *et al.*, 1995). Thus, the design vertical axial strength of a normally reinforced masonry section is defined as (Curtin *et al.*, 1995):

$$\boldsymbol{N_{r,nr} = \beta\left(\frac{f_k A}{\gamma_m} + \frac{0.83 f_y A_s}{\gamma_s}\right)} \qquad \textbf{(43)}$$

Pre-stressing and post-tensioning When deemed feasible from a financial and practical perspective, pre-stressing of a structure may be considered viable (Raju, 2007). This method of section reinforcement applies a pre-load to the structural section in order to relieve the section from tension (Marshall & Robberts, 2000). More details on these methods and procedures are discussed under Section 2.5.

Pre-stressing refers to a tendon being loaded prior to the casting of concrete or laying or masonry, while post-tensioning refers to the

tensioning of the tendon post the casting of concrete or placement of the masonry.

2.5 PRE-STRESSING OF STRUCTURES

2.5.1 Mechanics of Pre-stressing

An alternative method to reinforcing concrete or masonry structures is by applying an initial pre-load to the structural section (Marshall & Robberts, 2000). Normal reinforcement is required in structural sections where tensile stresses are generated (Robberts & Marshall, 2010). This solution is mostly considered cost effective and viable under moderate tensile loads. It does however become expensive and sometimes impractical when tension stresses are excessively large (Raju, 2007).

Pre-stressing is a form of reinforcement where the structural section is pre-loaded in an attempt to reduce the generation of tensile stresses (Raju, 2007). Various means and methods of pre-stressing are available of which most of the details are beyond the scope of this report.

Between pre-stressing and post-tensioning of concrete members, the former has been most widely used in concrete construction (Curtin *et al.*, 1995). On the other hand, the post-tensioning of masonry members has proven to be the preferred pre-stressing method as it was found to be the most successful while being simplistic in execution (Curtin *et al.*, 1995).

A typical section through a post-tensioned masonry column is depicted in Figure 2.52. The procedure is briefly to anchor the rod to the foundation of the column. A cap-plate is placed over the end of the rod at the top of the column and a nut is supplied to fasten it. The nut is then turned to a predetermined angle of rotation. Fastening of the nut will yield tension in the rod which will transfer load as compression into the masonry.

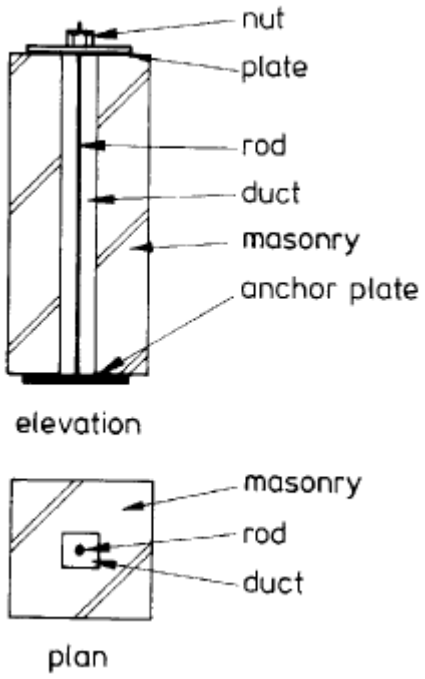


Figure 2.52: Section through a typical post-tensioned masonry column (Curtin *et al.*, 1995).

The basic idea of post-tensioning is quite simple, but gets more complex when other phenomena is considered which may decrease or increase the applied force (Curtin *et al.*, 1995). Some of these phenomena are listed in Table 6 (Curtin *et al.*, 1995).

Table 6: Factors that influence losses or gains in post-tension force (Curtin *et al.*, 1995)

No.	Factor description
1	Moisture movement in masonry
2	Relaxation of post-tensioning steel
3	Elastic deformation of masonry
4	Friction
5	Natural growth of clay brickwork

6	Creep of brickwork and blockwork
7	Thermal movement

For post-tensioned masonry sections (subjected to loads which may vary in direction and magnitude) it is recommended to place the post-tension tendon concentrically (Curtin *et al.*, 1995). This will result in a uniform increase in compressive stress over the section, reducing the amount of tension which will develop as a result of flexure (Curtin *et al.*, 1995). As depicted in Figure 2.53, the aim would be to have a state of zero stress at the extreme fibres on the side of the section where tension develops during service (Curtin *et al.*, 1995).

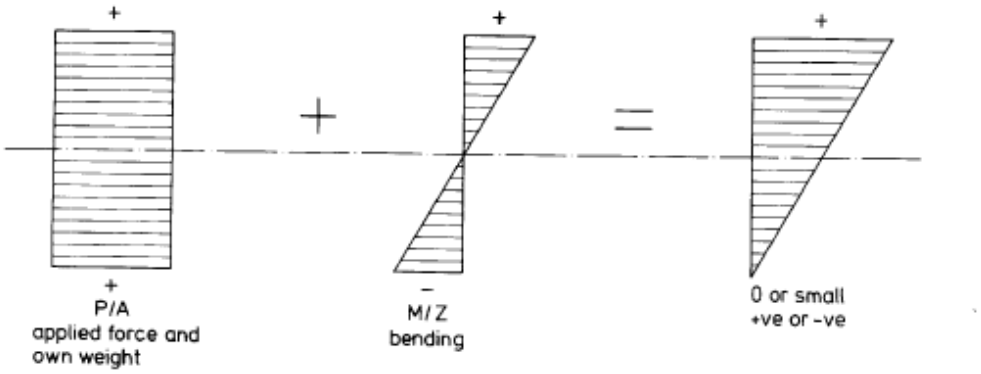


Figure 2.53: Stress state in a concentrically pre-stressed element (Curtin *et al.*, 1995).

Curtin *et al*. (1995) suggests that the three governing stress stages are as illustrated in Figure 2.54. The allowable stress in masonry at transfer is (Curtin *et al.*, 1995):

$$f_{trans} = \frac{1.2\beta f_k}{\gamma_m} \qquad (44)$$

When the structure is in service and all losses have realised, the maximum stress state is defined as (Curtin *et al.*, 1995):

$$f_{serv} = \frac{1.25 f_k}{\gamma_m} \quad (45)$$

While, after all losses realised, stress in the unloaded section should not exceed (Curtin *et al.*, 1995):

$$f_{unloaded} = \frac{\beta f_k}{\gamma_m} \quad (46)$$

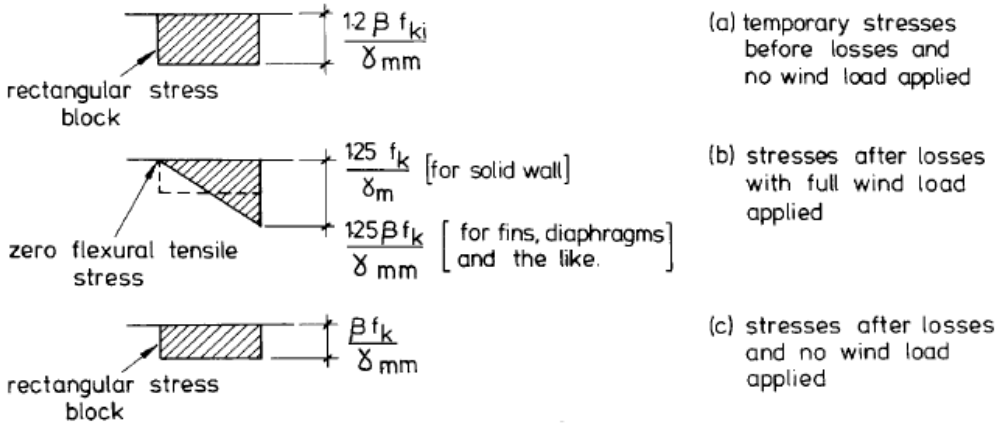


Figure 2.54: Stress state of a post-tensioned masonry section before, during and after wind load (Curtin *et al.*, 1995).

It is suggested that a limit on the allowable tendon stress at transfer is imposed. This is to account for the significant effect on the loss of post-tensioning force due to stress relaxation in the tendon (Curtin *et al.*, 1995). It is furthermore suggested that the maximum initials tendon stress should be limited to 70% of the normal applicable design strength of f_y/γ_s (Curtin *et al.*, 1995). Marshall and Roberts (2000) suggests that a maximum initial tendon stress of 75% may be assumed.

2.5.2 Traditional Pre-stressing Materials Pre-stressing tendons can be made of a variety of material known to resist tensile loads fairly well (Raju, 2007). Where high tensile strength steel is used, it generally consist of wires, bars or strands (Raju, 2007). The higher the tensile strength required, the more carbon content is added to the steel (Raju, 2007).

Raju (2007) further suggests that there are a variety of different types of material which can be used in pre-stressing systems. Figure 2.55 through Figure 2.58 indicates some of the traditional pre-stress tendon characteristic properties typically used in pre-stressing systems.

The 0.2% proof load is typically used as the resistant strength of a tendon in an ultimate limit state design (Raju, 2007).

Nominal diameter (mm)	*Tensile strength (minimum) (N/mm^2)*	*Elongation (per cent)*
2.50	2010	2.5
3.00	1865	2.5
4.00	1715	3.0
5.00	1570	4.0
7.00	1470	4.0
8.00	1375	4.0

Figure 2.55: Tensile strength and elongation characteristics of cold drawn stress relieved wires (Raju, 2007).

(a) Characteristic tensile strength (minimum)	980 N/mm^2
(b) Proof stress	Not less that 80 per cent of the minimum specified tensile strength
(c) Elongation at rupture on a gauge length of $5.65\sqrt{A}$ (minimum)	10 per cent

where, A = area of cross-section

Figure 2.56: Mechanical properties of high-tensile steel bars (Raju, 2007).

Nominal diameter (mm)	*Tensile strength (minimum) (N/mn^2)*	*Elongation (per cent)*
5.00	1570	4.00
4.00	1715	3.00
3.00	1865	2.50

Figure 2.57: Mechanical properties of high tensile indented wires (Raju, 2007).

Class	*Designation*	*Nominal Diameter of strand (mm)*	*Tolerances on the nominal diameter of strand*	*Nominal cross sectional area of strand (mm^2)*	*Breaking load minimum (N)*	*0.2 per cent proof load minimum (N)*
	2–ply 2mm	—	—	6.28	12,750	10.840
—	2–ply 3mm	—	—	14.14	25,500	21,670
	3–ply 3mm	—	—	21.21	38,250	32,460
1	6.3 mm 7–ply	6.3	±0.4	23.20	40,000	34,000
	7.9 mm 7–ply	7.9	±0.4	37.40	64,500	54,700
	9.5 mm 7–ply	9.5	±0.4	51.60	89,000	75,600
	11.1 mm 7–ply	11.1	±0.4	69.70	1,20,100	1,02,300
	12.7 mm 7–ply	12.7	±0.4	92.90	1,60,100	1,36,200
	15.2 mm 7–ply	15.2	±0.4	139.40	2,40,200	2,04,200
2	9.5 mm 7–ply	9.5	+0.66 –0.15	54.80	1,02,300	87,000
	11.1 mm 7-ply	11.1	+0.66 –0.15	74.20	1,37,900	1,17,200
	12.7 mm 7-ply	12.7	+0.66 –0.15	98.70	1,83,700	1,56,100
	15.2 mm 7-ply	15.2	+0.66 –0.15	140.00	2,60,700	2,21,500

Figure 2.58: Mechanical properties of uncoated stress-relieved strands (Raju, 2007).

A typical stress-strain curve for normal and pre-stress reinforcement is illustrated in Figure 2.59. This indicates the position of the 0.2% proof stress on the stress-strain curve for typical reinforcing materials. In a typical fashion, all these materials have a linear elastic region where stress increase linearly to the elongation of the member. At the end of the linear elastic region, yielding of the material is evident and a stress plateau

is reached; ultimately resulting in rupture of the material fibres. For each material, the amount of strain required, to reach a point of yielding or rupture, varies.

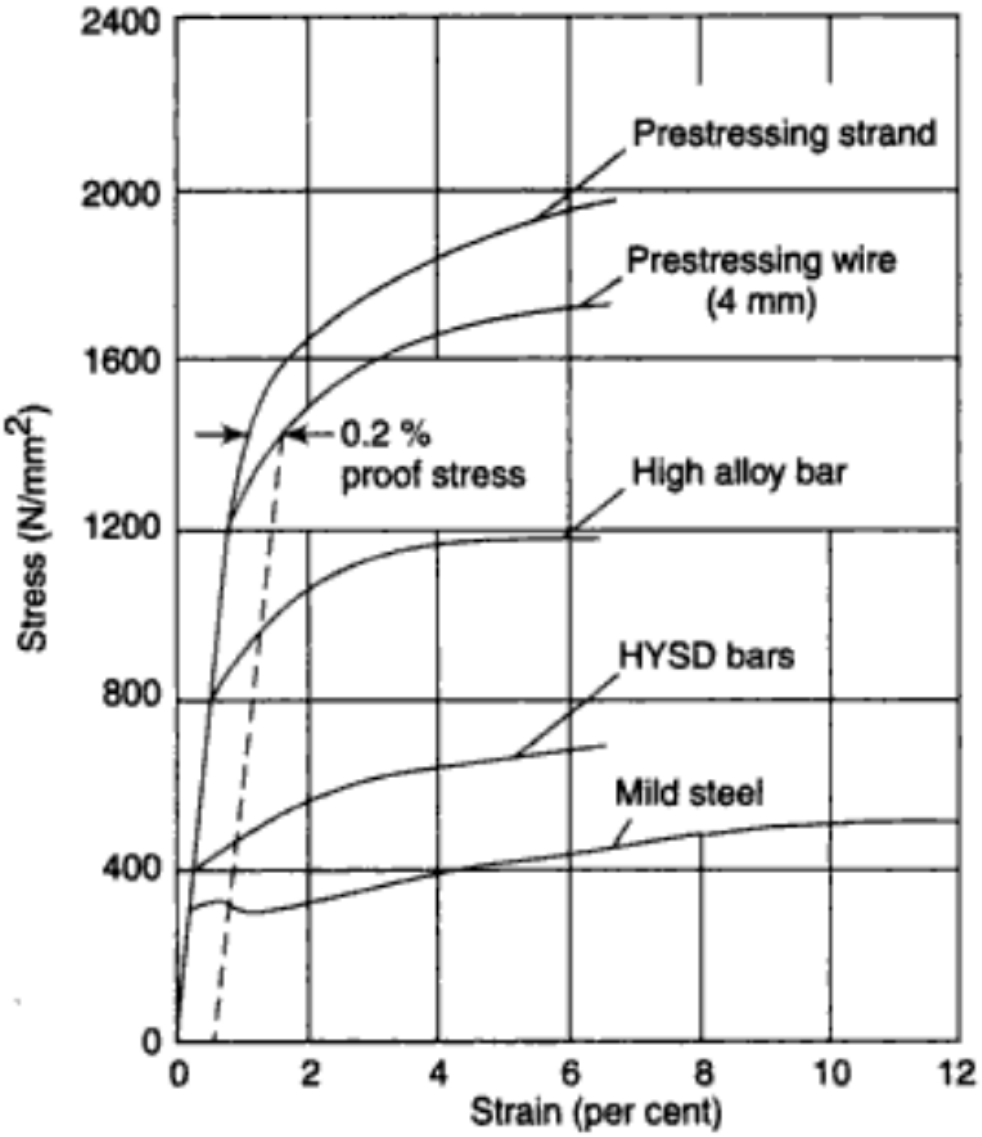


Figure 2.59: Stress-strain curves for reinforcing and pre-stress steel (Raju, 2007).

2.5.3 Basalt Geo-reinforcing Basalt geo-reinforcing is a material which yields exceptionally high tensile resistance for the area of reinforcing provided (Fiore, Scalici, Di Bella & Valenza, 2015). Most basalt material are 80% made up of Plagiocene and Pyroxene (Fiore *et al.*, 2015). Fiore *et al*. (2015) further suggests that Basalt materials are exceptional in resisting tensile forces at a relatively low cost.

Although reinforcement made up of basalt fibres seems promising regarding their high tensile resisting properties, caution should be taken when using this material (Sim, Park & Moon, 2005). This is mainly due to the high elongation potential of the fibres during stressing (Sim *et al.*, 2005). As a result of this, tensile reinforcement which depends on proper bondage between itself and the embedment material, usually results in reduced tensile resistance of the element (Sim *et al.*, 2005).

It is thought that this result is mainly ascribed to the fact that the basalt fibres pull away from the embedded material (Sim *et al.*, 2005). Elongation of the fibres yields a reduction in cross-sectional thickness due to the poisson effect (Sim *et al.*, 2005). This results in breaking of the bond between itself and the embedded material (Sim *et al.*, 2005).

Sim *et al*. (2005) further suggests a tensile capacity of 992.4MPa, elastic modulus of 7.6GPa and elongation potential of 2.56%. This contradicts the findings of Saravanan (2006), suggesting a modulus of elasticity of 89GPa with a tensile resistance capacity of 1200MPa to 4840MPa and elongation potential of 3.15%.

	Basalt	Carbon	Glass (S-glass)
Tensile strength (MPa)	992.4	3528.1	1798.3
Elastic modulus (MPa)	7600	–	–
Elongation at failure (%)	2.56	–	–

Figure 2.60: Mechanical properties of basalt fibres (Sim *et al.*, 2005).

Property	Value
Density, g/cc	1.95 - 2.75
Tensile Strength, Mpa	1200 - 4840
Compressive Strength, Mpa	420
Bending Strength, Mpa	800
Elastic Modulus, Gpa	89
Elongation at Break, %	3.15
Moisture at 65% RH, %	< 0.1
Max Application Temperature, °C	982
Sustained Operating Temperature, °C	820
Min Operating Temperature, °C	-260
Melting Point, °C	1450
Thermal Conductivity, W/m K	0.031 - 0.038
Glow Loss, %	1.9 - 2.0
Sound Absorption Coefficient	0.9 - 0.99
Loss Angle Tangent Frequency, MHz	0.005
Specific Volume Resistance, Ωm	1×10^{12}
Relative Dielectric Permeability, MHz	2.2

Figure 2.61: Characteristic properties of basalt fibres (Saravanan, 2006)

When comparing the results of the two sources as depicted in Figure 2.60 and Figure 2.61, it is evident that the mechanical properties of basalt fibres vary drastically. This is confirmed by consulting additional studies in this regard and may be a result of the way these fibres are bound together. Caution should therefore be taken in assuming values for this material's mechanical parameters.

From Figure 2.62 it is evident that basalt fibres can resist an exceptional amount of tensile stress before rupture occurs. It is furthermore important to note that the linear elastic zone of this material is significantly larger than that of conventional tensile materials illustrated in Figure 2.59. It should be noted that, as suggested by Figure 2.62, basalt fibres do not poses a significant yield region, and are therefore more likely to rupture at the end of its elastic stress-strain range than high tensile strength materials.

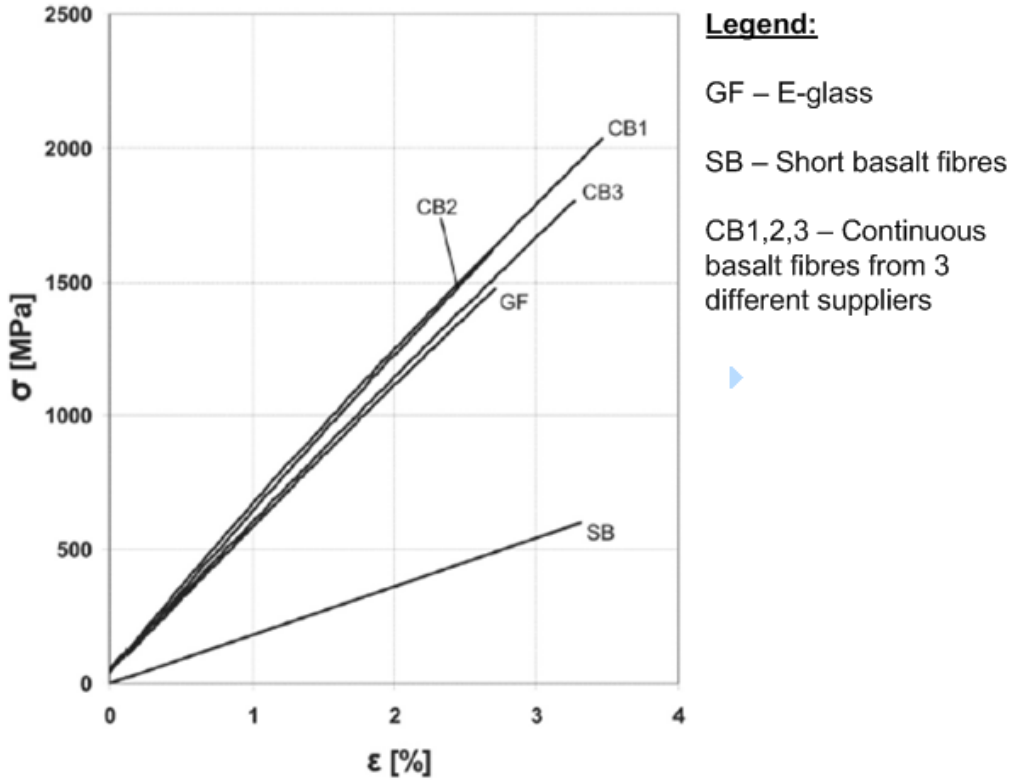


Figure 2.62: Typical stress-strain diagram of basalt fibres vs fibre glass (Fiore *et al.*, 2015).

All the materials in Figure 2.59 have a linear elastic region up until just below 2% elongation. This is in contrast with the majority of basalt fibre tests, as depicted in Figure 2.62, which suggest a linear elastic region up until an average strain of 3% elongation. This finding has an impact with regards to the pre-loading requirement of elements constituting of this material.

It can furthermore be derived that more strain of the structure will be required before the full tensile potential of the material is developed. As a result, the strain range of the surrounding masonry or concrete may be exceeded prior to the basalt fibres reaching its optimum tensile capacity. This may lead to cracking, exposing the reinforcement of concrete or masonry sections to chemical attack, reducing the durability and ultimately the lifespan of the structure (C&CI, 2009).

Alternative forms to tensile reinforcing bars are available. One such form is by weaving the material into a mesh or woven fabric (Saravanan, 2006).

2.5.4 Loss of Pre-stress

The initial pre-stress force in concrete undergoes a gradual reduction in magnitude over time (Raju, 2007). Raju (2007) suggests four pertinent causes for the loss of pre-stress in pre-stressing configurations and six in the case of post-tensioning. These causes are listed in Table 7. Highly sophisticated means and methods for quantifying the loss of pre-stress are available (Marshall & Robberts, 2000; Raju, 2007). The results of these methods can usually be combined into a single conservatively assumed percentage of the applied pre-stress force at transfer (Marshall & Robberts, 2000).

In post-tensioning systems, the loss is suggested to be taken as 20% of the transfer load (Marshall & Robberts, 2000). This value is assumed to account for all long-term post-tension losses of the system (Marshall & Robberts, 2000). A more accurate figure can only be determined by a programme of research into the various effects at play (Curtin *et al.*, 1995;

Marshall & Robberts, 2000). As previously mentioned, need for a more accurate figure is however debatable and should only be determined if deemed required (Curtin *et al.*, 1995; Marshall & Robberts, 2000).

Considering the use of basalt fibres as pre-stressing tendons, Pearson *et al* (2013) tested basalt fibre reinforced polymer bars in a pre-stressing configuration. The results of these tests proved that the long term pre-stress or post-tensioning losses were less or equal to that of generally used pre-loaded steel and cable elements (Pearson, Donchev & Salazar, 2013).

During application of the tension to a tendon, instantaneous losses are incurred (Raju, 2007). These losses are labelled as losses during jacking, and are an additional loss to the effective pre-stress that needs to be accounted for. Jacking losses can be estimated as 5-8% of the initial pre-stress force required at transfer (Marshall & Robberts, 2000). Considering the use of basalt fibres, initial observed losses were recorded to be in the order of 4% (Pearson *et al.*, 2013).

Table 7: Causes for the loss of pre-stress (Raju, 2007).

Pre-tensioning	**Post-tensioning**
Elastic deformation of concrete	No loss due to elastic deformation if all wires a simultaneously tensioned. If the wires are successively tensioned, loss due to elastic deformation will occur.
Relaxation of stress in steel	Relaxation of stress in steel
Concrete shrinkage	Concrete shrinkage
Concrete creep	Concrete creep
-	Friction losses
-	Anchorage slip

By taking pre-stress losses into consideration, the pre-stress force required as input into the system can be determined.

$$\boldsymbol{P_t = \frac{P_e}{\chi_{total}}} \qquad \textbf{(47)}$$

Where P_t = Pre-stress force required at transfer

P_e = Effective pre-stress force required

χ_{total} = Total estimated loss of pre-stress (%)

As a result of taking pre-stress losses into consideration, two pre-stress conditions are generally considered (Robberts & Marshall, 2010). These conditions are; pre-stressing force at transfer and pre-stressing force during service (Marshall & Robberts, 2000). For each loading conditions, different internal stresses are generated and needs to be accounted for. The structure to be pre-loaded should hence be validated to ensure that it has adequate capacity to resist the loads applied during transfer and service.

3. FORM FINDING TECHNIQUES

3.1 INTRODUCTION

3.1.1 Practical Living Space Definition

Catenary structures are renowned for being cost effective with respect to the utilisation of their construction materials. For this reason, it is envisaged that the use of catenary barrel vaults will be of high demand in 3rd world countries such as the Philippines. Here, typhoons and other tropical storms are frequently experienced. It is therefore thought that, should a catenary barrel vault be optimised to resist high wind loads in pure compression, these structures may be considered as a cost effective housing solution.

The housing needs of the underprivileged Philippian household are complaisant (Katayanagi Hiroshi, 2012). A reason for this is likely due to the fact that most underprivileged Philippians, also known as "*slum*", do not own any possessions and are therefore living from whatever they can find at the refuse and rural areas where they reside (Asian Development Bank, 2009). It was reported that the current huts, occupied by the typical "*slum*", do not have a kitchen, separation of rooms or a basic toilet (Katayanagi Hiroshi, 2012). The occupants do not have a requirement for any additional rooms as the huts are only used for sleeping. Sleeping arrangements are such that multiple people are crammed into one hut, where all occupants sleep on the floor or beds without matrasses (Katayanagi Hiroshi, 2012).

Based on this, the following criteria informed the design of the vault from a practical perspective:

1. The plan area of the vault should be such that it meets the needs of the average poor Philippian household. There is no need for room separation.

2. The soffit of the roof should be adequate to ensure it is a practical living space where people can easily move around.
3. The structure should be constructed of low cost material. Earth bricks with a compressive strength of 5MPa may be used.
4. Although costing of the structure falls beyond the scope of this report, the design should attempt to keep the material and construction costs at a minimum, by ensuring that the shell remains in pure compression under the dominant load condition.
5. When subjected to secondary load conditions, the structure should resist forces efficiently and safely in the absence of complex and expensive solutions and materials.

3.1.2 Design Objectives

The design objective is to ensure that the structure resists the loads applied to it most efficiently. It will therefore be considered first prize to have the structure in pure compression under all load conditions it is subjected to during its lifespan. Should this not be feasible, rationalisation of the design may be applied in an attempt to yield an effective flow of forces within the structure. The following cross-sectional stress conditions may be considered during the rationalisation process:

Table 8: Stress conditions considered for the design of the vault section.

No.	Load Condition	Solution Description
1	No tension allowed	The vault can be geometrically optimised to resist all load conditions in pure compression. This can be achieved by ensuring that the line of thrust remains inside the kern of the section.
2	No tension allowed	The vault can be post-tensioned to a point where all fibers in the cross section is

		subjected to pure compression, regardless of the load applied or the geometry defined.
3	Limited tension allowed	The vault can be post-tensioned to a point where the bulk of the flexural tension is relieved from the cross section. Normal tension reinforcement can then be designed to resist the residual tension in the section under the absolute load condition.
4	Tension allowed	The cross section can be reinforced with tension reinforcement which, is to be designed to resist the tension stresses induced by flexure.
5	Tension allowed	The vault can be designed to only resist complete failure under the absolute load condition. It can be assumed that the compressive materials do have some tension capacity and that the structure will yield and crack under the absolute load condition without catastrophically failing.

The design should moreover be easily constructible by relatively unskilled labourers. Complex construction techniques and equipment should be avoided as far as possible.

3.1.3 Alternative Designs

A number of different vault configurations were considered to determine the most feasible, and possibly the most cost effective solution to the design. The cost effectiveness of the designs should, however, be verified by future research on the topic.

Elevated Flat Vault As illustrated in Figure 3.1, the first type of vault considered was a flat vault with a rise of 1000mm over a span of 4000mm. In order to achieve a practical head clearance, the flat-vaulted roof required to be elevated on vertical walls. This configuration had an impact on pressure coefficients at the wall-to-vault interface.

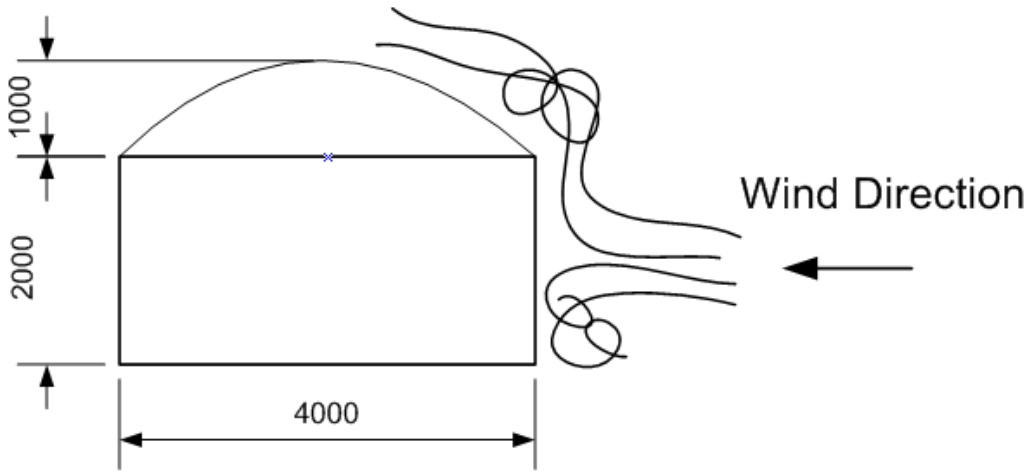


Figure 3.1: Elevated flat vault on vertical walls subjected to wind flow.

This configuration was considered feasible, as it was thought that such a configuration will possibly lead to lower moments at the base of the structure. The higher the vault, the more exposed it will be to wind drag. Drag forces will tend to push the structure in the direction of wind flow, resulting in it to rotate about the base. This rotation may lead to the generation of bending moments, and the longer the legs of the vault, the more subjected the structure will be to high bending moments in its shell.

Steep Vault A steep vault with a 4000mm span and 3000mm rise will also be adequate from a spatial perspective. This configuration is considered favourable as it will yield adequate living space. It will however be more exposed to wind drag, which may lead to undesirably high bending moments in the shell. An example of this configuration is depicted in Figure 3.2. The dashed line in Figure 3.2 illustrates that the structure will tend to deflect when it is subjected to wind load. It is therefore intuitive to assume that bending moments may be generated when the structure is subjected to high wind loads in this configuration.

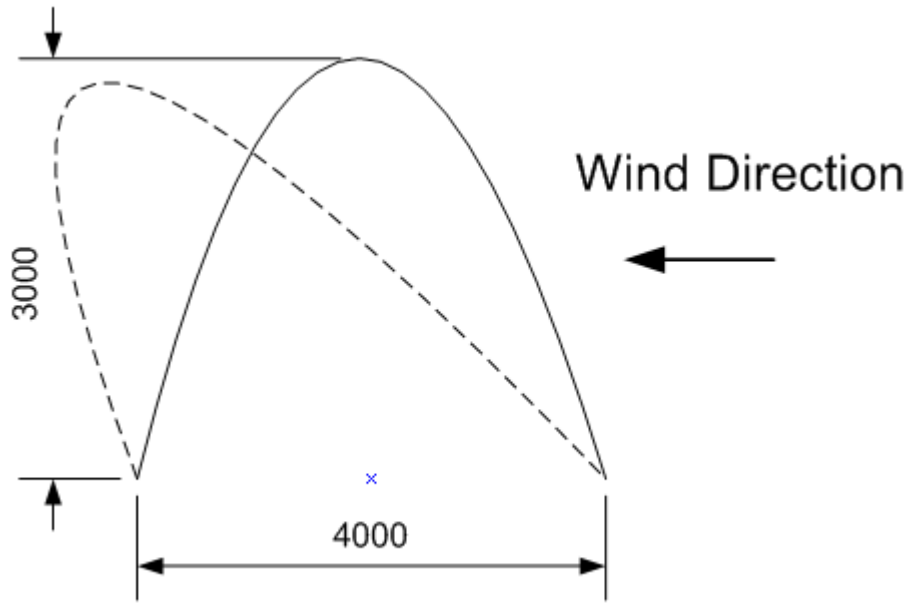


Figure 3.2: Steep vault subjected to wind load.

This structural configuration was considered as it provides ample space as a comfortable living environment. The shape is furthermore structurally highly efficient, which will lead to optimisation of its construction materials and considered key for a possible low-cost solution.

Traditionally Shaped Post-tensioned Vault A more advanced alternative may be to post-tension the vault. The traditionally shaped catenary vault, as illustrated in Figure 3.3, may be considered to function as a post-tensioned member, post-loaded along its geometric centroid. This configuration will result in a structure which will be subjected to bending moments during service and other loading conditions. The flexural tensile stresses will, however, be overcome by the design decompression stress induced by the post-tensioned tendon.

Should the vault be post-tensioned along its geometric centreline, no eccentric bending moments will be generated in the section. As a result, the tendon configuration in conjunction with the funicular shape of the structure will merely result in an increased uniform compression stress in the section. This result can be ascribed to the fact that the post-tensioned tendon is placed all along the dominant line of thrust of the structure. As the dominant line of thrust is the entity that informed the geometry definition of the catenary vault, the force exerted by the tendon will be resisted in pure compression.

A post-tensioned configuration, as illustrated in Figure 3.3, was considered to determine the level of post-tensioning required to relieve the section from tension in the event of a hurricane. This solution was considered viable, as a tendon can be placed along the centreline with relative ease (should hollow blocks be used). It was moreover considered a smart solution in artificially increasing the compressive force in the section, leading to a reduction in the force eccentricity which directly influences the magnitude of flexural stress in the section.

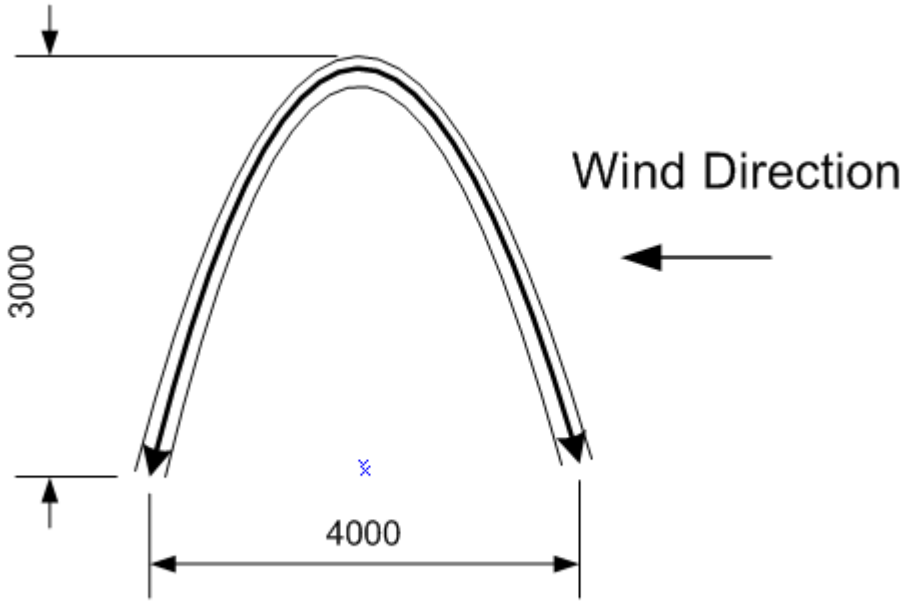


Figure 3.3: Traditionally shaped catenary vault - post-tensioned along geometric centroid.

Catenary Vault Draped in Post-tensioned Tendon Another alternative to post-tension the vault is to drape the structure in a net of post-tensioned tendons. This can be achieved by placing the tendon over the outer skin of the structure, after which it will be post-tensioned.

A typical configuration of such a case is depicted in Figure 3.4. Here, various assumptions may be made regarding the interface between the vault's shell and tendon interface. It may be assumed that the tendon is supported all along its length and that friction between the tendon and shell is present. Alternatively, it may be assumed that the tendon is supported along its entire length, but that a frictionless support is provided between itself and the shell. Finally, the design may possibly require the tendon to be only supported at identified positions of which these supports may provide friction or negate such depending on the requirement.

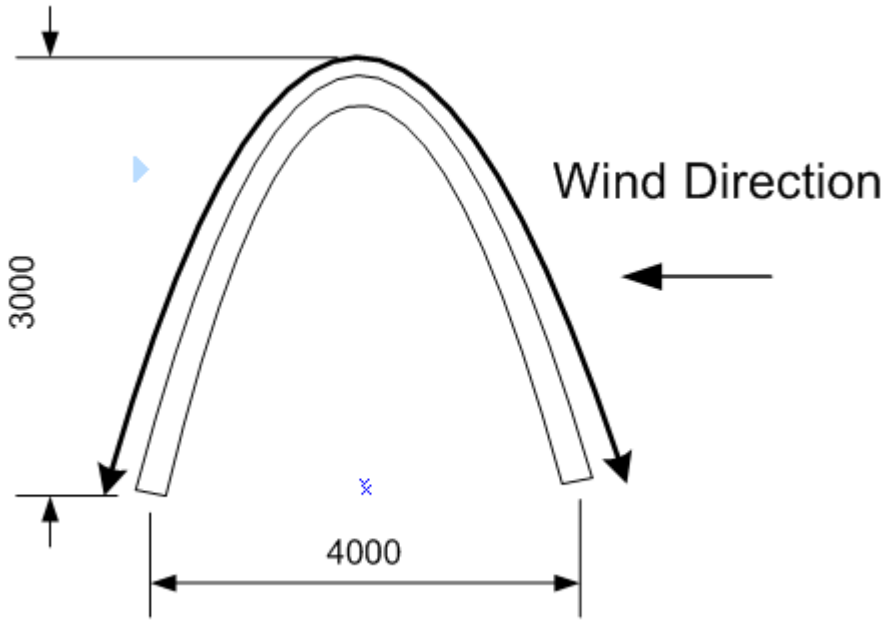


Figure 3.4: Optimised catenary vault - post-tensioned by externally placed tendon.

This solution may be beneficial considering the practicality of post-tensioning the structure, while the use of a post-tensioned mesh will reduce stresses at the mesh to shell interface. It was furthermore thought that, by draping the structure in a post-tensioned mesh, it will be pulled towards its foundations. This will assist in preventing foundation uplift.

3.1.4 Initial Geometry Definition

The funicular shape of a structure is informed by a combination of the self-weight of the structure and the loads applied to it (Allan *et al.*, 2010). As a result, the geometry of the structure needs to be defined first. An analysis should then be conducted in order to evaluate the effect of the applied loads on the funicular curve. This procedure is usually iterative and will most likely yield changes to the section thickness, span and rise of the vault.

Initial Vault Geometry The initial geometry of the vault, as informed by the spatial considerations, is listed in Table 9.

Table 9: Basic Vault Dimensions

Requirement	Value	Unit
Length (span)	4000	mm
Width	4000	mm
Rise	3000	mm
Section thickness	250	mm

In this research, alternative section thicknesses were considered. This was to ascertain the effect of self-weight on the geometry as well as the structural strength of the section.

Initial Material Properties of Section The vault's shell should be constructed of a relatively strong and inexpensive material. The selected material for this research is called earth bricks. That is, as the name suggests; bricks, blocks or tiles made of a mixture of earth soil and cement. The recommended mixture of cement to earth soil is 1:8 for a ±10MPa after 28 days (Heuer, N (Personal communication)). Alternatively, a 1:12 mixture may be used to obtain a final 28 day strength of ±5-7MPa (Heuer, N (Personal communication)).

Table 14 list the characteristic material properties of Earth Brick for a 28 day strength of ±5-7MPa.

3.2 DESIGN LOAD CONSIDERATIONS

The structure needs to be designed such that it can resist the loads it will be subjected to during its lifespan. Durability and safety were considered key. The primary loads identified were:

1. Self-weight
2. Wind load

Other loads considered as beyond the scope of this research were:

1. Maintenance loads.
2. Equipment load such as; solar panels, satellite television dishes etc.
3. Installation loads.

3.2.1 Self-weight

The self-weight of the structure was, as for conventional catenary vaulted structures, considered as the dominant load condition (Allan *et al.*, 2010). For post-tensioned vaults, the combination of the self-weight and effective post-tensioning force was considered the dominant load condition.

The self-weight of a vault can be assumed as a uniformly distribute line load in the vertical direction, determined along the perimeter of the arch (Allan *et al.*, 2010). It is as a result of this uniform load that catenary vaults, arches and domes have its distinctive funicular curvature (Allan *et al.*, 2010).

Shell Load

The uniform line load which represents the self-weight of any vault of uniform section thickness is defined by equation (48).

$$\boldsymbol{w = \rho t b} \qquad \textbf{(48)}$$

Where w = Self-weight of structure in force per unit length

ρ = Density of material

t = Effective thickness of the section

b = Width of section under consideration

Other Loads

Depending on the design and architecture of the vault, other loads may be associated with the self-weight of the structure. For the purpose of this research, no self-weight due to architectural finishes was considered. This is due to the fact that the design of the vault pertains to low cost housing. As a result, it was assumed that there will be no unnecessary trimmings and architectural features which will impact the self-weight of the structure.

Other loads which may be associated with the self-weight of the structure may be loads which results from structural elements required as per the design. These elements will only be applicable should the design shy away from its traditional catenary barrel vault shape. An example of such a case will be the event that post-tensioning of the structure is required, and that the loads of the post-tensioning tendon and ancillary items are deemed to be significant in relation to the self-weight of the shell.

Where post-tensioning of the vault was considered, it was assumed that the additional load, as a result of the self-weight of the post-tensioning tendon and its ancillary items, were negligible.

3.2.2 Wind Load

For the purpose of this investigation, wind load effects over the surfaces of catenary and circular barrel vaults were considered. The utilisation of wind load effects over circular barrel vaults were only considered during the preliminary stages of the investigation. This was primarily due to the fact that SANS 10160-3:2011 also considered wind pressure effects on the vault's shell as a result of it being elevated on vertical walls as depicted in Figure 3.1.

Wind Load on Elevated Flat Vaults The wind load on an elevated flat vault was determined as per the recommendation set by SANS 10160-3:2011. Internal pressure coefficients of +0.2 pressure and -0.3 suction was assumed. As a result, two load conditions were assessed for each set of external pressure coefficients.

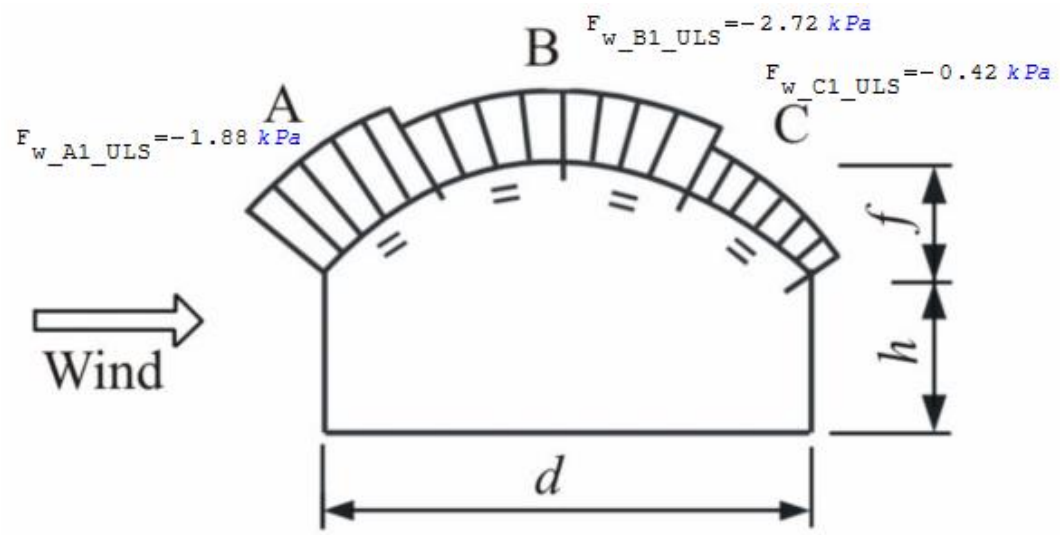


Figure 3.5: Resultant pressure force on elevated flat vault - load case 1 .

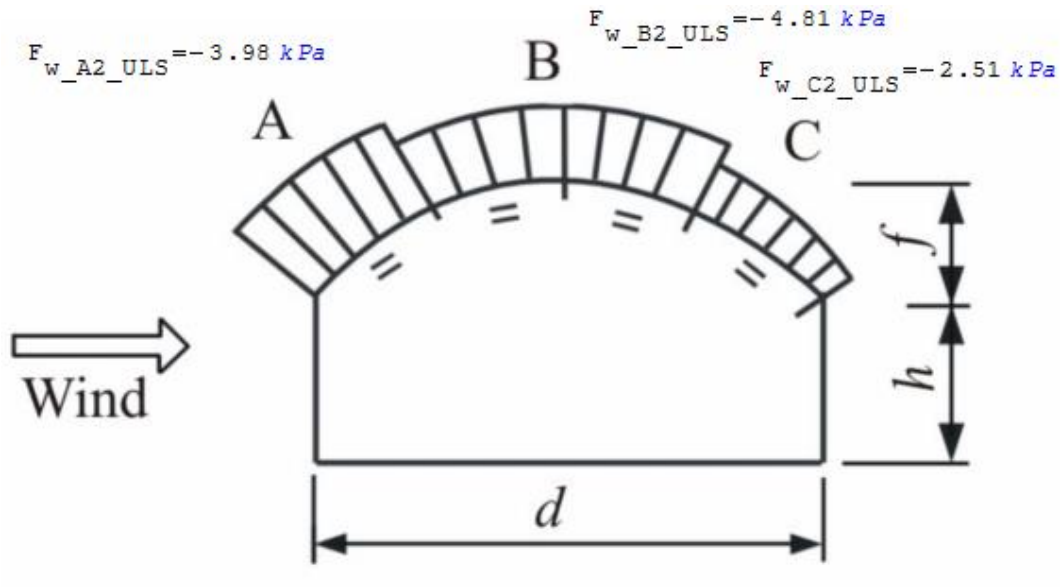


Figure 3.6: Resultant pressure force on elevated flat vault - load case 2.

Table 10: Summary of wind pressures on elevated flat vaults.

Symbol	Applicable zone	Internal pressure coefficient	External pressure coefficient	Resultant pressure (kPa)
Load combination 1 (LC1)				
$F_{w_A1_ULS}$	A	-0.3	-0.45	-1.88
$F_{w_B1_ULS}$	B	-0.3	-0.65	-2.72
$F_{w_C1_ULS}$	C	-0.3	-0.1	-0.42
Load combination 2 (LC2)				
$F_{w_A2_ULS}$	A	+0.2	-0.95	-3.98
$F_{w_B2_ULS}$	B	+0.2	-1.15	-4.81
$F_{w_C2_ULS}$	C	+0.2	-0.6	-2.51

Notes:

1. *A wind speed of 300kph was assumed.*
2. *Terrain category "A" was assumed as it was assumed that these vaults may be constructed on open coastal planes.*
3. *A coastal air density of 1.225kg/m^3 was assumed.*

Wind Load on Steep Vaults The wind load to be resisted by a steep catenary vault was determined as per the recommendation of Bradley (2016). The internal pressure coefficients of -0.3 suction and +0.2 pressure (as suggested by SANS 10160-3:2011) were used. This resulted in two load cases per wind load condition investigated. Two dominant azimuth wind directions, known to yield the most conservative results, were considered. These are the 0/180 degree and 45/225 degree wind directions (Ryan Bradley, 2011).

A case of zero internal pressure was not considered critical. The reason for this was due to the fact that a condition of either positive or negative internal pressure will ensure a destabilizing effect on the structure, resulting in a conservative loading condition at all times. In other words, should a certain external wind pressure configuration be benefited by an internal pressure of +0.2C_{pi}, the case of -0.3C_{pi} negative internal pressure will worsen this loading state and vice versa.

As discussed under section 2.3.5, external pressure coefficients are derived based on the geometry of the structure. Reversal of the pressure loads on the shell is evident in zone B for certain instances. As a result, six load conditions were identified as illustrated by Figure 3.7 through Figure 3.12.

Wind pressures for normal wind speeds as well as hurricane wind speeds were investigated.

Normal wind speeds [3] Normal wind speeds were determined in accordance with the provisions set by SANS 10160-3:2011, while the wind pressures resulting from these wind speeds were derived as suggested by Bradley *et al* (2016). The derivation of the wind pressures are illustrated in this section and summarized in Table 11.

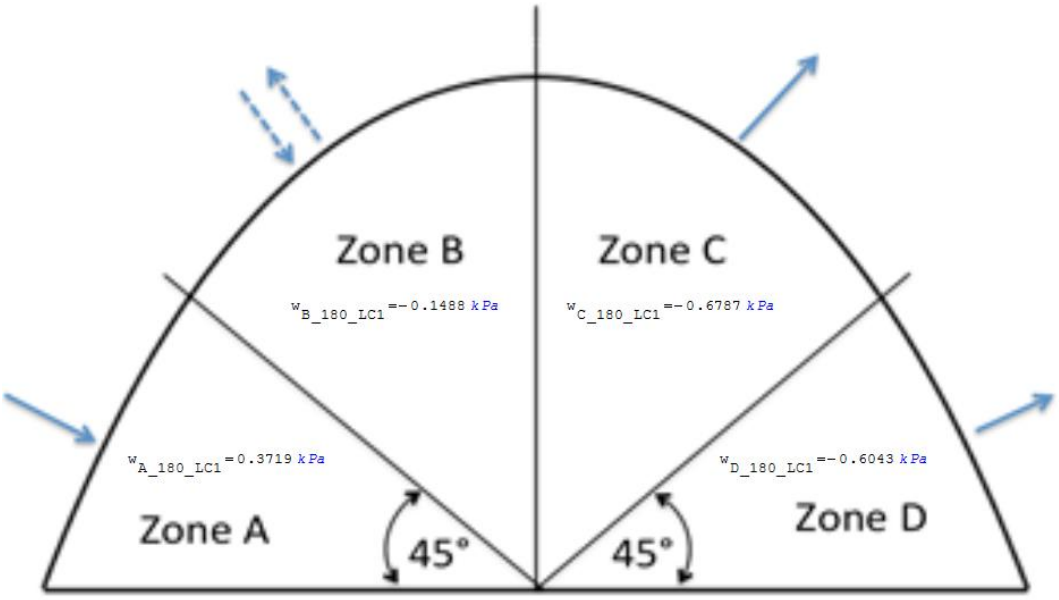


Figure 3.7: Resultant pressure force on steep vault for normal wind speeds - load case 1 (Bradley *et al.*, 2016).

[3] The term "normal wind speeds" refers to South African typical wind speeds. It was therefore determined on the basis of a 3 second gust, and based on a category "A" terrain, basic wind speed of 28m/s and coastal air density of 1.225kg/m^3.

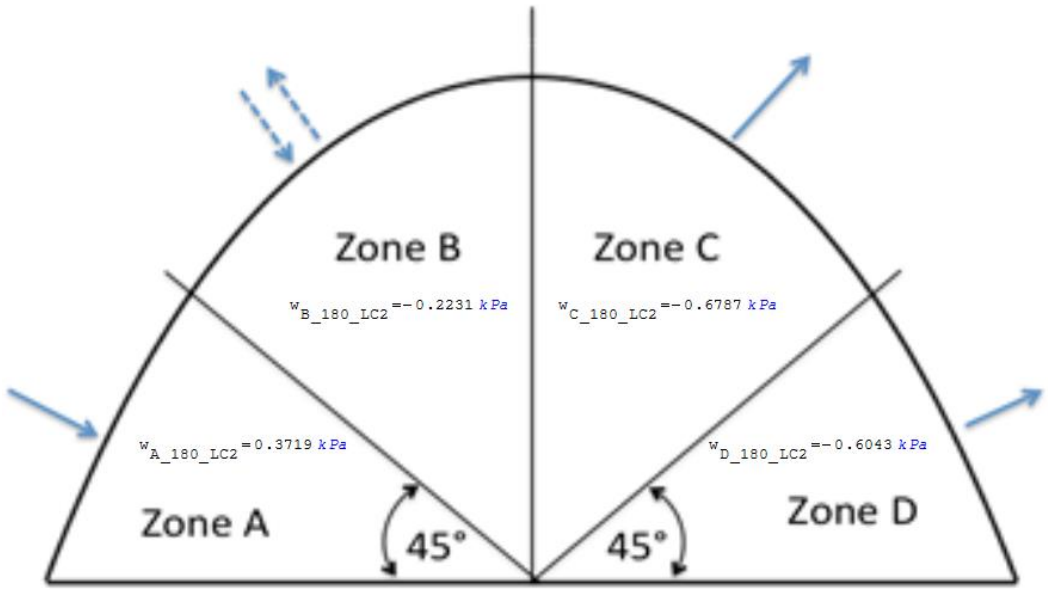


Figure 3.8: Resultant pressure force on steep vault for normal wind speeds - load case 2 (Bradley *et al.*, 2016).

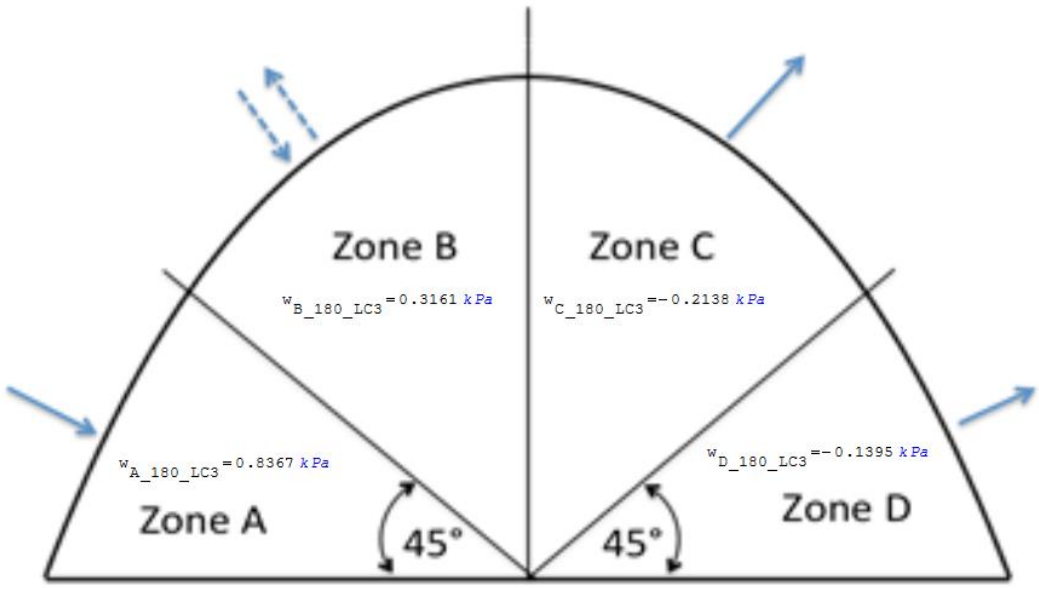


Figure 3.9: Resultant pressure force on steep vault for normal wind speeds - load case 3 (Bradley *et al.*, 2016).

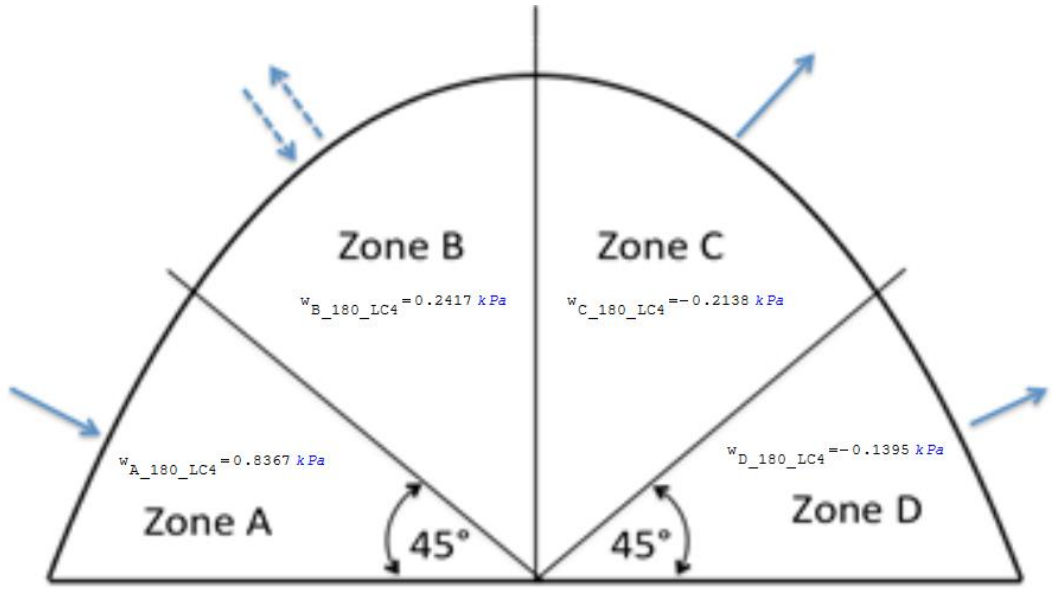


Figure 3.10: Resultant pressure force on steep vault for normal wind speeds - load case 4 (Bradley *et al.*, 2016).

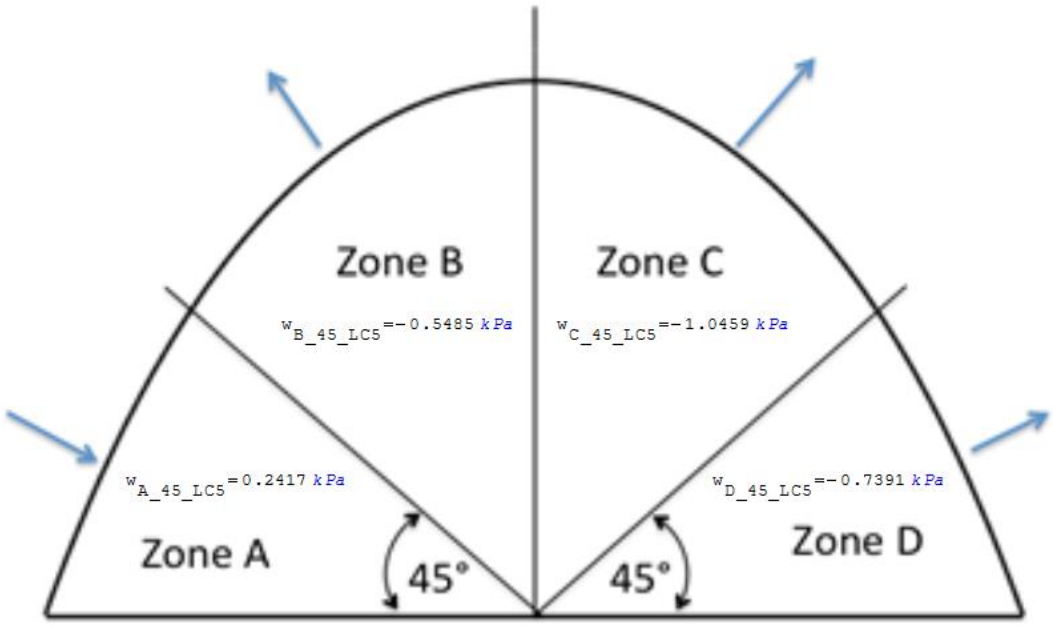


Figure 3.11: Resultant pressure force on steep vault for normal wind speeds - load case 5 (Bradley *et al.*, 2016).

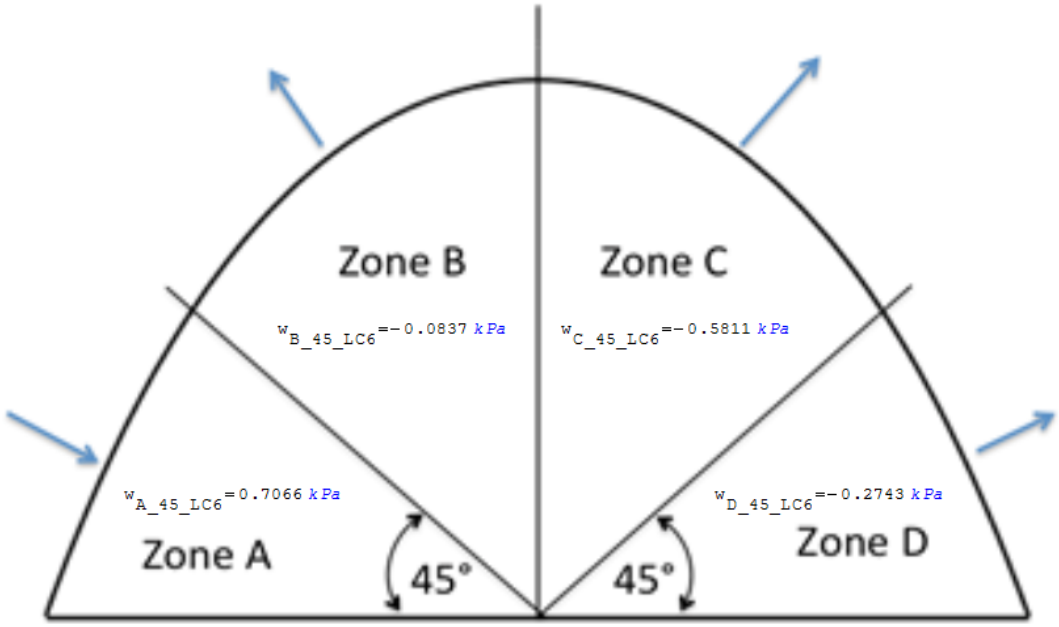


Figure 3.12: Resultant pressure force on steep vault for normal wind speeds - load case 6 (Bradley *et al.*, 2016).

Table 11: Summary of wind pressure on steep vault for normal wind speeds.

Symbol	Applicable zone	Internal pressure coefficient	External pressure coefficient	Resultant pressure (kPa)
Load combination 1 (LC1)				
$w_{A_180_LC1}$	A	+0.20	+0.6	0.37
$w_{B_180_LC1}$	B	+0.20	+0.04	-0.15
$w_{C_180_LC1}$	C	+0.20	-0.53	-0.68
$w_{D_180_LC1}$	D	+0.20	-0.45	-0.60
Load combination 2 (LC2)				
$w_{A_180_LC2}$	A	+0.20	+0.6	0.37
$w_{B_180_LC2}$	B	+0.20	-0.04	-0.22
$w_{C_180_LC2}$	C	+0.20	-0.53	-0.68
$w_{D_180_LC2}$	D	+0.20	-0.45	-0.60
Load combination 3 (LC3)				
$w_{A_180_LC3}$	A	-0.30	+0.6	0.84
$w_{B_180_LC3}$	B	-0.30	+0.04	0.32
$w_{C_180_LC3}$	C	-0.30	-0.53	-0.21
$w_{D_180_LC3}$	D	-0.30	-0.45	-0.14
Load combination 4 (LC4)				
$w_{A_180_LC4}$	A	-0.30	+0.6	0.84

$w_{B_180_LC4}$	B	-0.30	-0.04	0.24
$w_{C_180_LC4}$	C	-0.30	-0.53	-0.21
$w_{D_180_LC4}$	D	-0.30	-0.45	-0.14
Load combination 5 (LC5)				
$w_{A_45_LC5}$	A	+0.20	+0.46	0.24
$w_{B_45_LC5}$	B	+0.20	-0.39	0.55
$w_{C_45_LC5}$	C	+0.20	-0.92	-1.05
$w_{D_45_LC5}$	D	+0.20	-0.60	-0.74
Load combination 6 (LC6)				
$w_{A_45_LC6}$	A	-0.30	+0.46	0.71
$w_{B_45_LC6}$	B	-0.30	-0.39	-0.08
$w_{C_45_LC6}$	C	-0.30	-0.92	-0.58
$w_{D_45_LC6}$	D	-0.30	-0.60	-0.27

Hurricane wind speeds Hurricane wind speeds were derived by assuming a peak wind speed, in the form of a 3 sec gust, at 300kph. This wind speed was selected, as on the 8th of November 2013, typhoon Haiyan made landfall on the Philippian coast (Mullen, 2013). As typhoon Haiyan is the strongest typhoon in recorded history, its sustained wind speed was deemed a safe baseline for design purposes. The determination of the peak wind speed pressure was done in accordance with SANS 10160-3:2011, while the resultant wind pressures on the shell were derived as recommended by Bradley (2016).

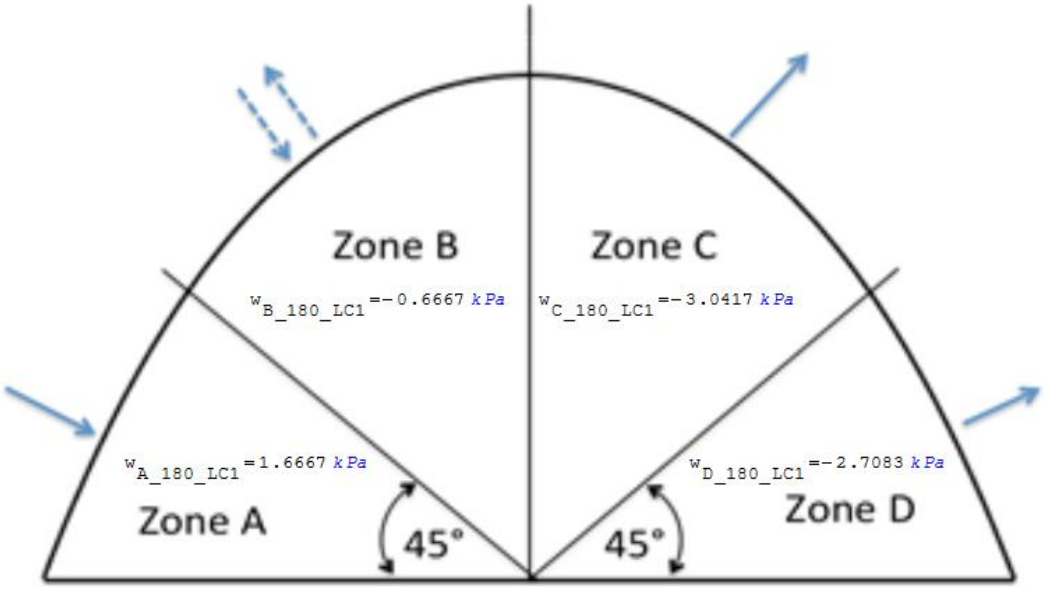


Figure 3.13: Resultant pressure force on steep vault for 300kph wind speed - load case 1 (Bradley *et al.*, 2016).

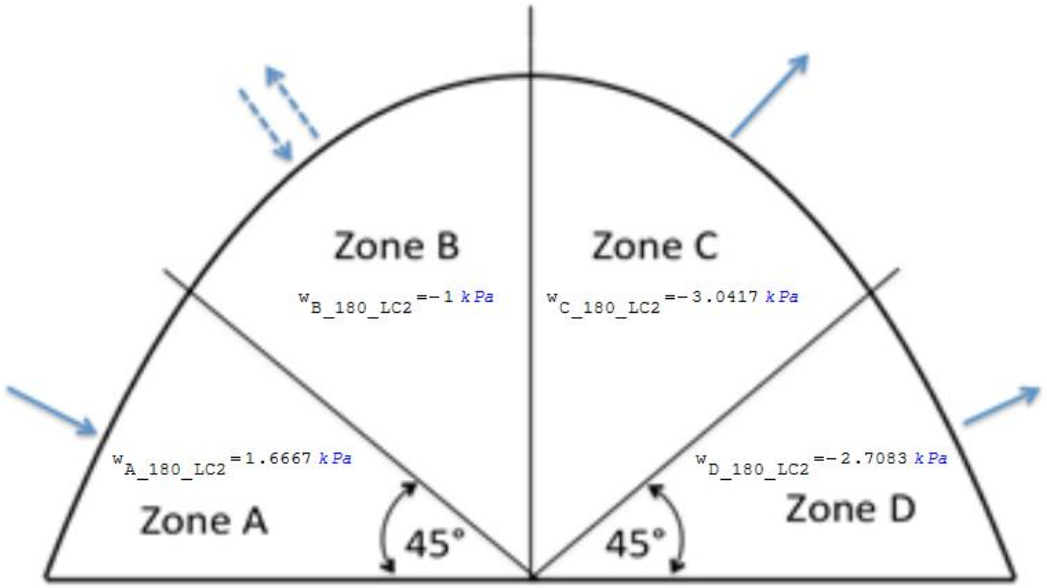


Figure 3.14: Resultant pressure force on steep vault for 300kph wind speed - load case 2 (Bradley *et al.*, 2016).

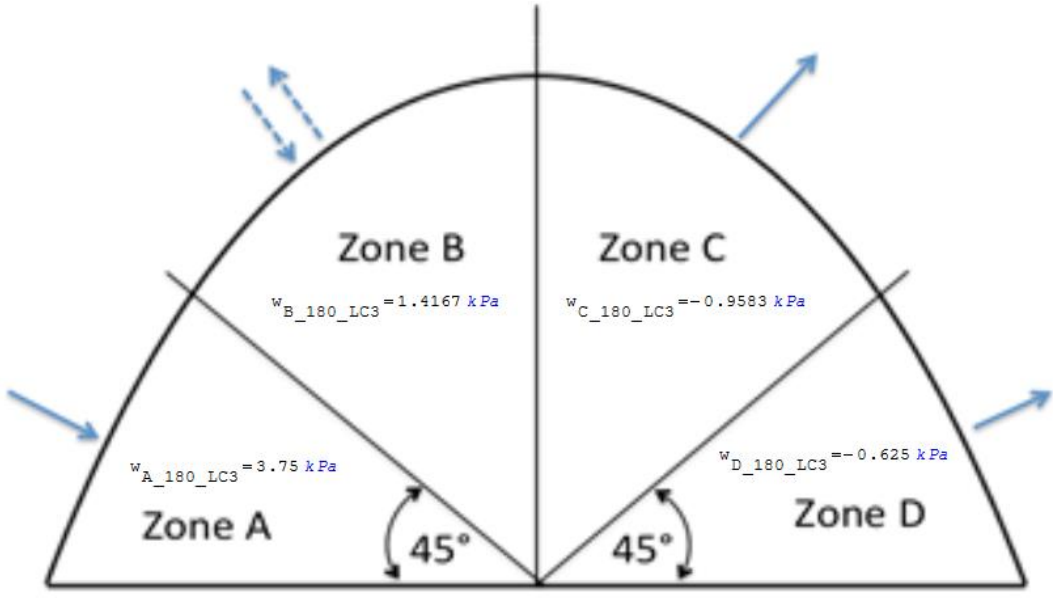


Figure 3.15: Resultant pressure force on steep vault for 300kph wind speed - load case 3 (Bradley *et al.*, 2016).

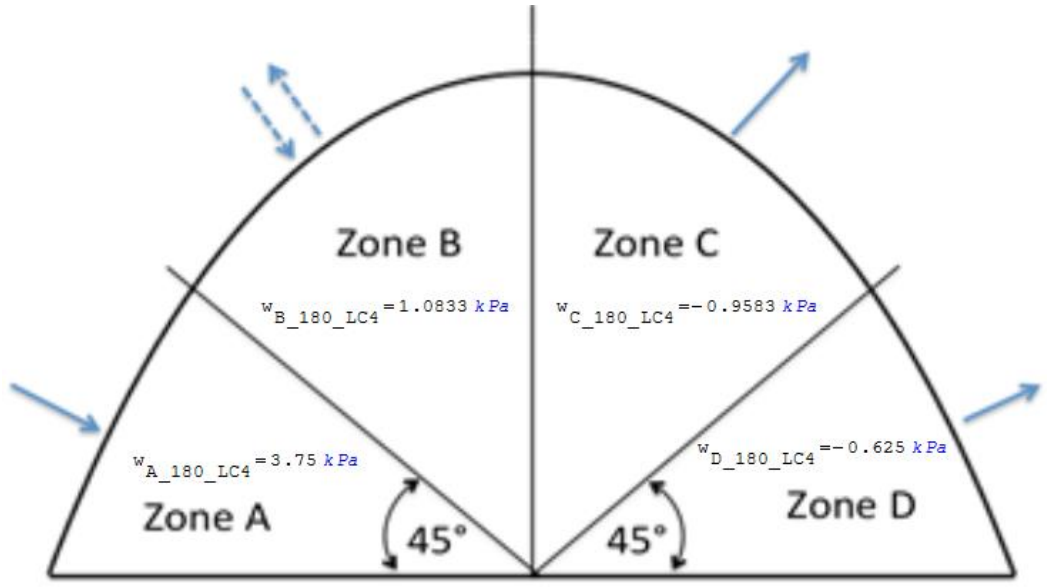


Figure 3.16: Resultant pressure force on steep vault for 300kph wind speed - load case 4 (Bradley *et al.*, 2016).

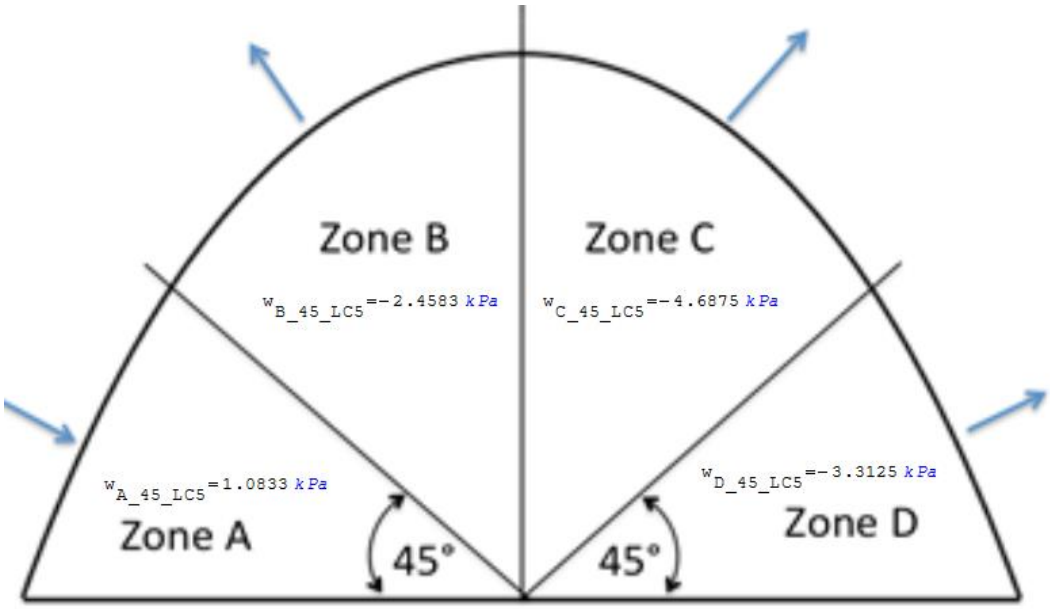


Figure 3.17: Resultant pressure force on steep vault for 300kph wind speed - load case 5 (Bradley *et al.*, 2016).

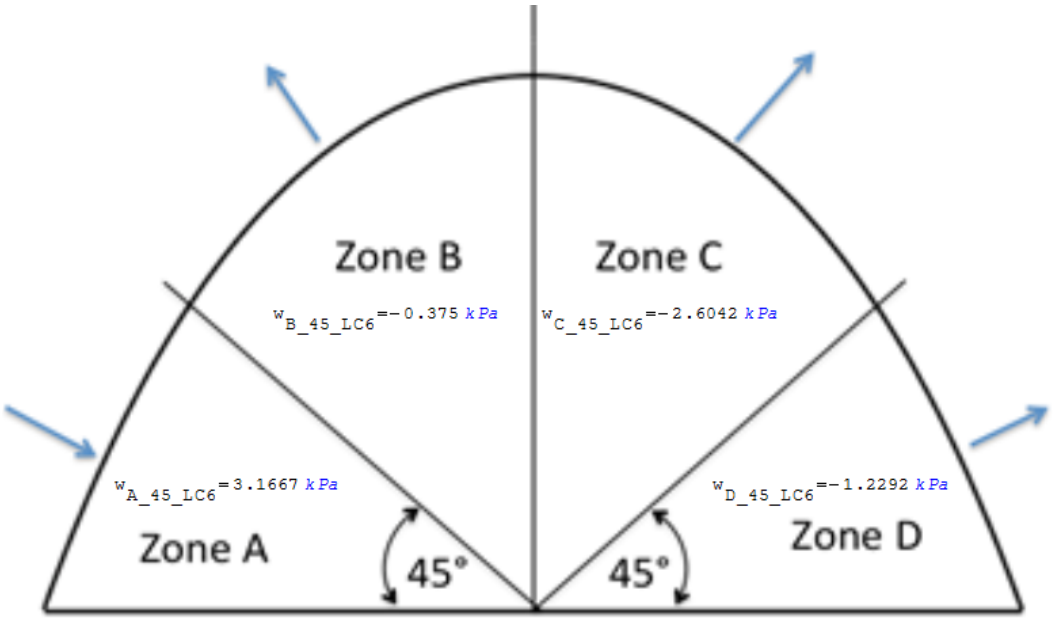


Figure 3.18: Resultant pressure force on steep vault for 300kph wind speed - load case 6 (Bradley *et al.*, 2016).

Table 12: Summary of wind pressure on steep vault for 300kph wind speeds.

Symbol	Applicable zone	Internal pressure coefficient	External pressure coefficient	Resultant pressure (kPa)
Load combination 1 (LC1)				
$w_{A_180_LC1}$	A	+0.20	+0.60	1.67
$w_{B_180_LC1}$	B	+0.20	+0.04	-0.67
$w_{C_180_LC1}$	C	+0.20	-0.53	-3.04
$w_{D_180_LC1}$	D	+0.20	-0.45	-2.71
Load combination 2 (LC2)				
$w_{A_180_LC2}$	A	+0.20	+0.6	1.67
$w_{B_180_LC2}$	B	+0.20	-0.04	-1.00
$w_{C_180_LC2}$	C	+0.20	-0.53	-3.04
$w_{D_180_LC2}$	D	+0.20	-0.45	-2.71
Load combination 3 (LC3)				
$w_{A_180_LC3}$	A	-0.30	+0.60	3.75
$w_{B_180_LC3}$	B	-0.30	+0.04	1.42
$w_{C_180_LC3}$	C	-0.30	-0.53	-0.96
$w_{D_180_LC3}$	D	-0.30	-0.45	-0.63
Load combination 4 (LC4)				
$w_{A_180_LC4}$	A	-0.30	+0.60	3.75

$w_{B_180_LC4}$	B	-0.30	-0.04	1.08
$w_{C_180_LC4}$	C	-0.30	-0.53	-0.96
$w_{D_180_LC4}$	D	-0.30	-0.45	-0.63
Load combination 5 (LC5)				
$w_{A_45_LC5}$	A	+0.20	+0.46	1.08
$w_{B_45_LC5}$	B	+0.20	-0.39	-2.46
$w_{C_45_LC5}$	C	+0.20	-0.92	-4.69
$w_{D_45_LC5}$	D	+0.20	-0.60	-3.31
Load combination 6 (LC6)				
$w_{A_45_LC6}$	A	-0.30	+0.46	3.17
$w_{B_45_LC6}$	B	-0.30	-0.39	-0.38
$w_{C_45_LC6}$	C	-0.30	-0.92	-2.60
$w_{D_45_LC6}$	D	-0.30	-0.60	-1.23

3.3 FINDING THE MOST EFFICIENT SHAPE

The determination of the most efficient structural shape is considered one of the key aspects of this research. It is therefore considered first prize to find a geometric shape, which will be under pure compression during a 300kph hurricane event, as well as under its dominant load condition. This can be achieved by ensuring that the geometry is defined such that the section of the vault always remains in pure compression, which was extensively discussed under section 2.2 (Allan *et al.*, 2010).

As discussed under Section 2.2.2, *Stem Elements*, Gohnert and Bradley (2016) suggests that the catenary shape of a loaded structure can be determined by defining a stem element. Determining the load shape genetics of each consecutive element in the arch chain, the funicular form of the structure is generated for the given load condition (Gohnert & Bradley, 2016).

An excel programme, implementing stem element theory, was utilised in this research (Gohnert, 2016). Manipulation of the programme was required to simulate the effect of non-uniform loads exerted by wind load on the structure. The original program allowed the user to assign point loads to selected nodal points along the funicular curve.

The effects of these loads on the thrust line were assessed, and a new curve was drawn. An example on how the original program determined the funicular shape of a catenary arch subjected to a 5kN point load is depicted in Figure 3.19.

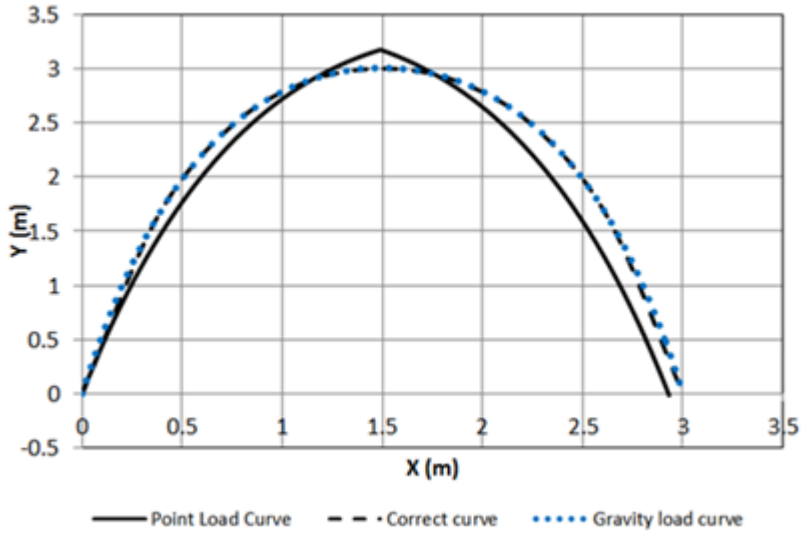


Figure 3.19: Catenary arch subjected to a 5kN point load at its centreline (Gohnert, 2016).

The program was modified to assign the uniform pressure per identified zone to the original curve and is illustrated in Figure 2.33 through Figure 2.35. This was achieved by converting the uniform pressure load to point loads on the funicular curve. It is important to note that wind pressure will always act normal to the surface of the vault. As the geometry of the vault change due to the changes in the global force applied to it, the direction of the applied force at a nodal level should remain normal to the curve.

The change in the line of action of the wind force was implemented by VBA code in an iterative manner. By iterating through the load direction and geometry definition, the position of the funicular arch converges. The point of convergence is an indication of the funicular curve based on the applied loads. This phenomenon is illustrated in Figure 3.20.

For the purpose of investigating the possibility, of finding a universal shape which will accommodate all load cases the structure will be subjected to in pure compression, a 250mm and 1000mm shell thickness were respectively selected. These section thicknesses were mathematically selected to represent a condition of little and excessive self-weight

respectively, and does not take into consideration practicality of the solution. Constructability and fabrication consideration, if possible to take into consideration, was considered after the final geometry was defined.

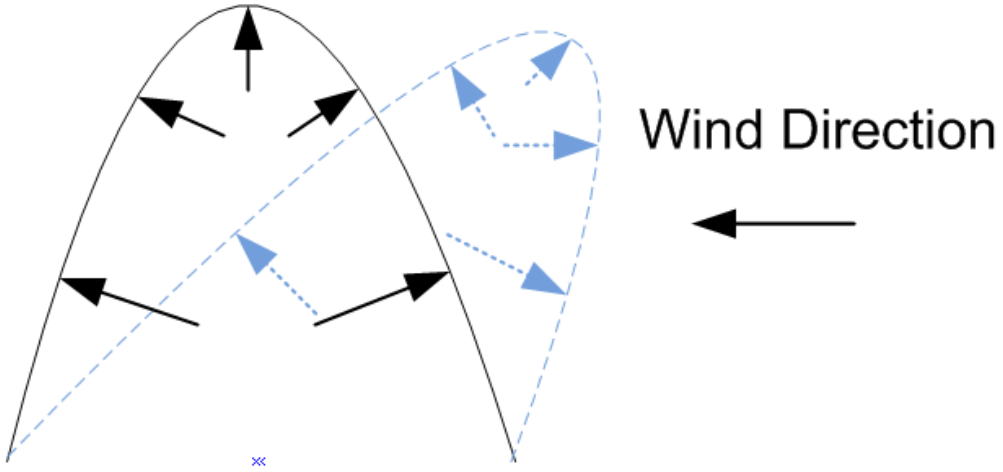


Figure 3.20: Convergence of the funicular curve based on normal pressure load assignments to the curve.

3.3.1 Graph Interpretation Three typical curves are produced by the Excel programme as developed by Gohnert (2016). These curves are illustrated in Figure 3.21.

Funicular line for pure compression (FLPC) The solid black lined curve suggests the required funicular shape the structure needs to assume in order for the loads to be resisted in pure compression. This line is considered key in the determination of an optimised geometric shape of a structure.

It can be assumed that the solid black line is the line of thrust for a structure defined by this particular curve and set of loading. Should the loading on the structure (whose geometry is defined by the curve) change, the solid black line will shift. It will then assume a new position which defines the line of thrust for a different geometry definition and new set of loads.

It is prudent to note that the solid black line does not represent the traditional line of thrust as defined by literature. For the purpose of this research, this line will instead be called the Funicular Line for Pure Compression (FLPC). Traditional literature assumes that the line of thrust of a structure starts and ends at fixed locations. It will be shown that in applying Stem Element theory, the FLPC has a fixed position to the left of the curve, while the other end point is free to move depending on the loads applied. In other words, the programme will locate the correct foundation point to the right of the curve to ensure pure compression of the arch for the given set of loads.

For a curve subjected to gravity load only, the FLPC will coincide with the gravity load curve.

Gravity curve The dotted blue line represents the curve developed by means of Stem Element theory (considering gravity loads only). This curve should, for all practical purposes, coincide with the mathematically calculated catenary arch curve as defined by equation (1). Small deviations of the gravity curve in relation to the mathematical version may be noticed under intense scrutiny. These differences are attributed to imperfection in the curve as a result of elements not being truly collinear. The more refined the curve, the more accurate the expected result. It was assumed that an 800 node curve provided sufficient reliability.

Mathematical curve The mathematical curve represents the true catenary curve and results from applying a purely mathematical formula as defined by equation (1). The application of this formula yields the pure catenary form based on the self-weight of the structure.

3.3.2 Funicular Curve for Elevated Flat Vaults As depicted in Figure 3.1, a flat vault will have to be elevated on vertical walls in order to be considered as a practical living space. These vertical walls will have an impact on the determination of the wind pressures at the wall-to-vault interface. The dimensions of the assumed vault were taken as per Table 9, with the exception to the rise which is set at 1000mm. The characteristic material properties of the shell were taken as per Table 14, while wind loads applied to the structure were as discussed under Section 3.2.2, *Wind Load on Elevated Flat Vault.*

FLPC for elevated vault (LC1) It is illustrated by Figure 3.21 that the FLPC, for the given load conditions and section thickness considered, did not yield a practical solution. It is important to note that, although this curve seems rather unusual, it will yield a pure compressive resistance in the structural section for the loads in its current configuration.

This is true, as Stem Element theory is based on static equilibrium on a miniscule level for each element the curve is constructed of (Gohnert & Bradley, 2016). As illustrated in Figure 2.7, the direction of the force (T_{i+1}) is considered a variable of the equilibrium equation for each element. The self-weight (w_i), applied load (P_i), and force exerted by the preceding element (T_i), is known.

From the theory of static equilibrium, the prediction of the traditional catenary curve becomes fairly easy. By assuming no additional load applied to the curve, and that each element has equal weight, the angle at which the balancing force (T_{i+1}) should be applied will be forced to reduce at each equilibrium iteration performed. This phenomenon is what leads to the traditional catenary structure to have its distinctive shape.

By applying this theory to the condition of low self-weight and high non-uniform loads, an unusual curve is expected. As the applied loads are significantly larger than the stabilizing self-weight of each element, the balancing force's orientation and magnitude needs to adjust such that the

system (on a minuscule level) remains in equilibrium. This rotation of the balancing force leads to unusual curves for non-uniform loads of high magnitude as illustrated in Figure 3.21.

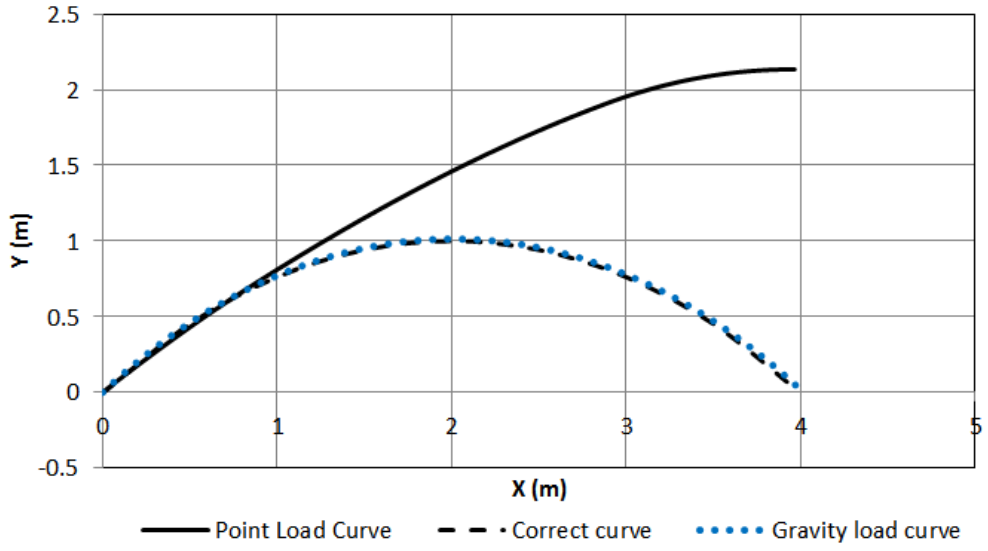


Figure 3.21: FLPC for elevated flat vault of 250mm thickness subjected to gravity and wind loads as per Table 10 (LC1).

It should, moreover, be noted that the FLPC is generated by iteration. Loads were therefore applied normal to the original gravity load curve and remained normal to the new FLPC in each iteration until convergence of the curve were observed.

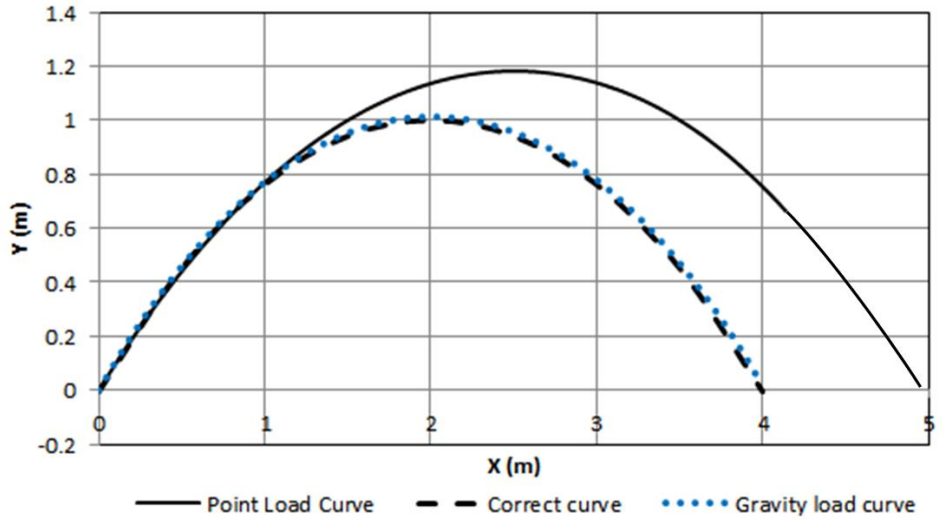


Figure 3.22: FLPC for elevated flat vault of 1000mm thickness subjected to gravity and wind loads as per Table 10 (LC1).

A more realistic funicular shape for the elevated vault was obtained by increasing the self-weight of the vault. As noted, a catenary vault, subjected to uniform gravity load only, yielded a curved shape as defined by the catenary equation (1). An increase in the downward load, overcoming the uplift forces as a result of wind flow, will therefore intuitively result in the curve trending more towards a traditional catenary shape.

This assumption is verified in Figure 3.22 by increasing the vault's section thickness to 1000mm, despite it being impractical. Comparing the FLPC obtained in Figure 3.21 and Figure 3.22, and taking cognisance of the fact that the applied loads remained unchanged in the two scenarios, it became clear that the higher the gravity loads, the more traditionally shaped the catenary arch will be.

FLPC for elevated vault (LC2) In a similar fashion, the FLPC for the second load condition (LC2) as per Table 10 was assessed. The result of this analysis is illustrated in Figure 3.23 and Figure 3.24.

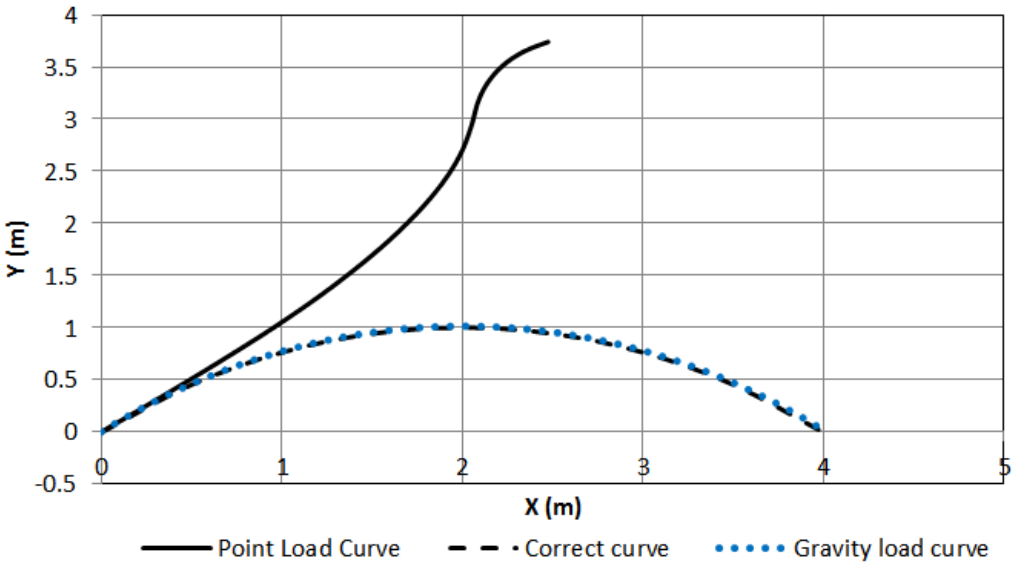


Figure 3.23: FLPC for elevated flat vault of 250mm thickness subjected to gravity and wind loads as per Table 10 (LC2).

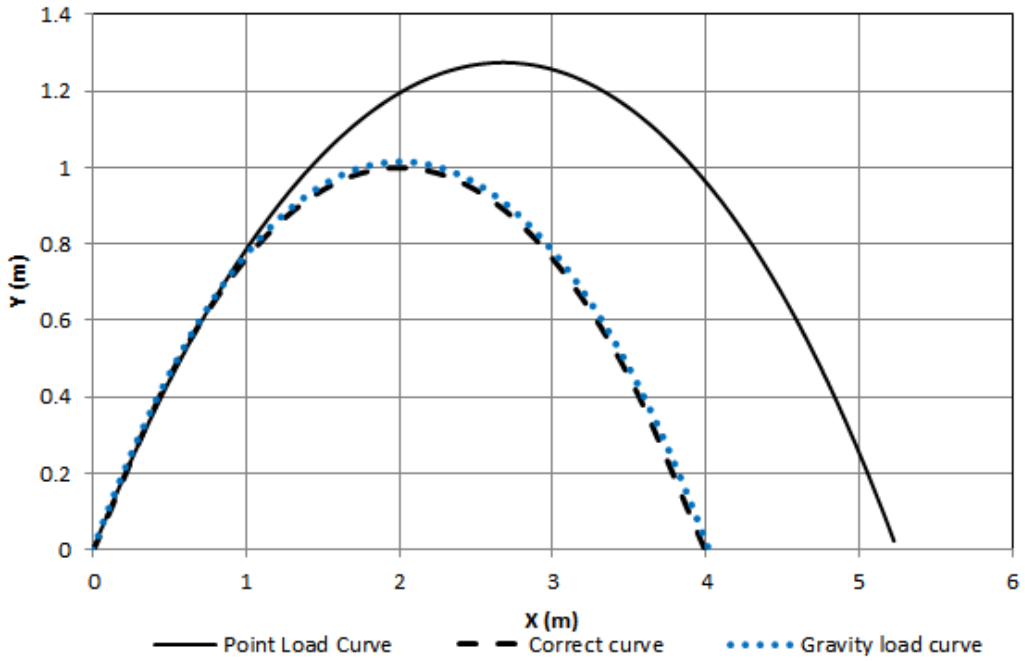


Figure 3.24: FLPC for elevated flat vault of 1000mm thickness subjected to gravity and wind loads as per Table 10 (LC2).

Conclusion From the above investigation it was found that, by applying non-uniform loads of high magnitude, the predicted shape of the structure does not converge to a useable form. In order to therefore have the curve in pure compression under loads generated by a 300kph hurricane wind load, the funicular curve is deemed unpractical. Wind load reversal requires that the section should furthermore be such that a reversal of the FLPC should fall within the kern of the section. The FLPC obtained in these instances are a-symmetric to such an extent that it is not deemed practical.

It was, however, concluded that, by increasing the gravity load of the vault, a practical geometric shape can be obtained.

3.3.3 Funicular Curve for Steep Vault In a similar fashion as discussed under *Funicular Curve for Elevated Flat Vault*, the FLPC was determined for a steep vault subjected to its self-weight and wind loads as per Table 11 and Table 12. The geometry definition of the vault was taken as per Table 9, while the characteristic material properties of the assumed shell were taken as per Table 14.

FLPC for steep vault under normal wind speed For service wind loads as determined and recorded in Table 11, the FLPC was determined and illustrated in Figure 3.25 through Figure 3.30.

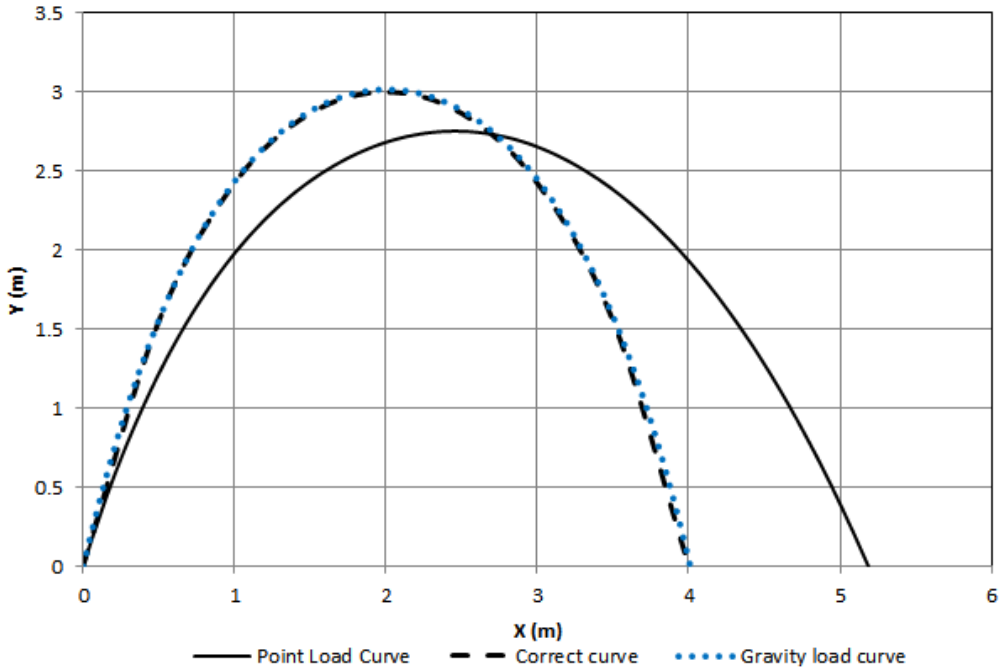


Figure 3.25: FLPC for steep vault of 250mm thickness subjected to gravity and wind loads (LC1) as per Table 11.

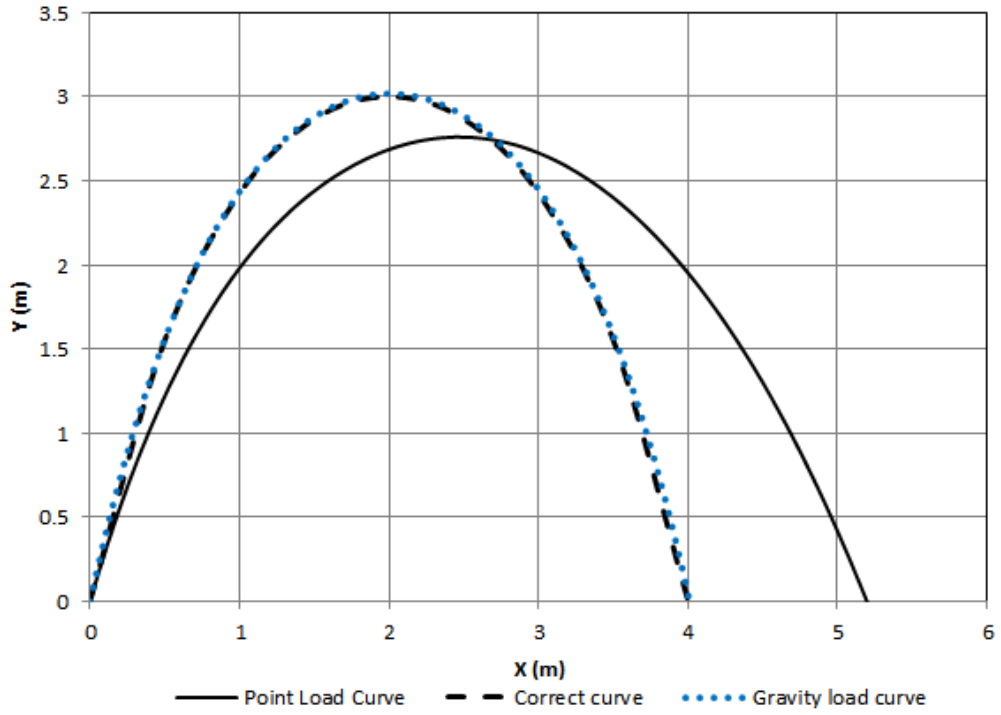


Figure 3.26: FLPC for steep vault of 250mm thickness subjected to gravity and wind loads (LC2) as per Table 11.

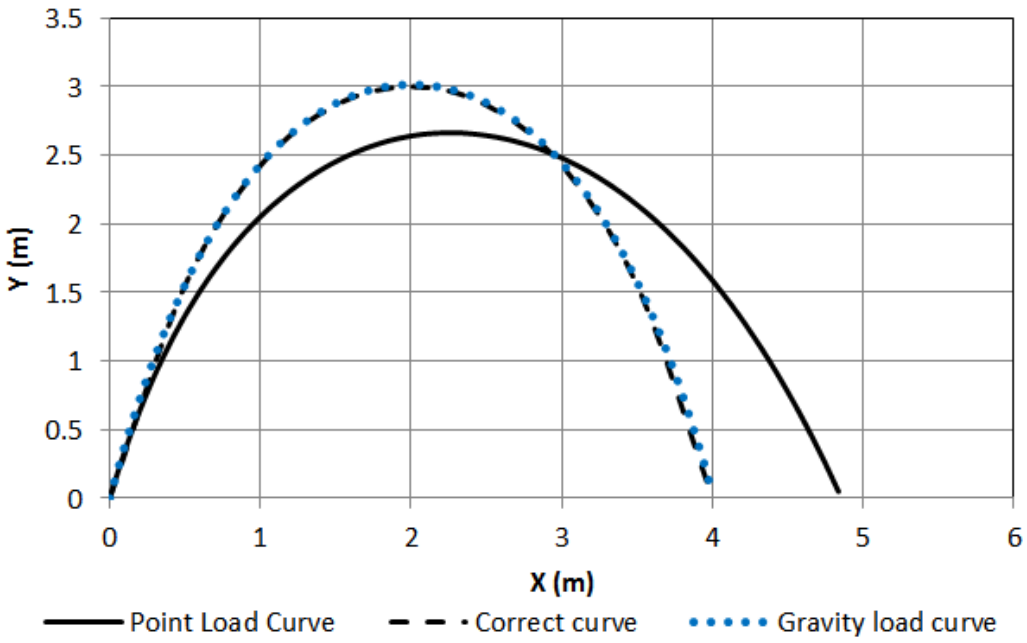


Figure 3.27: FLPC for steep vault of 250mm thickness subjected to gravity and wind loads (LC3) as per Table 11.

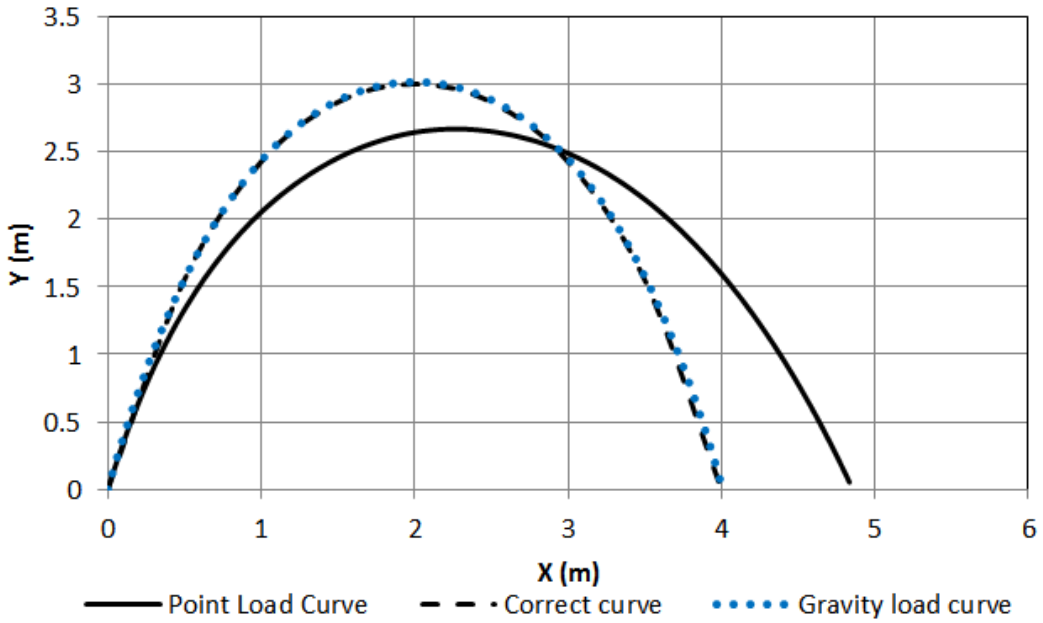


Figure 3.28: FLPC for steep vault of 250mm thickness subjected to gravity and wind loads (LC4) as per Table 11.

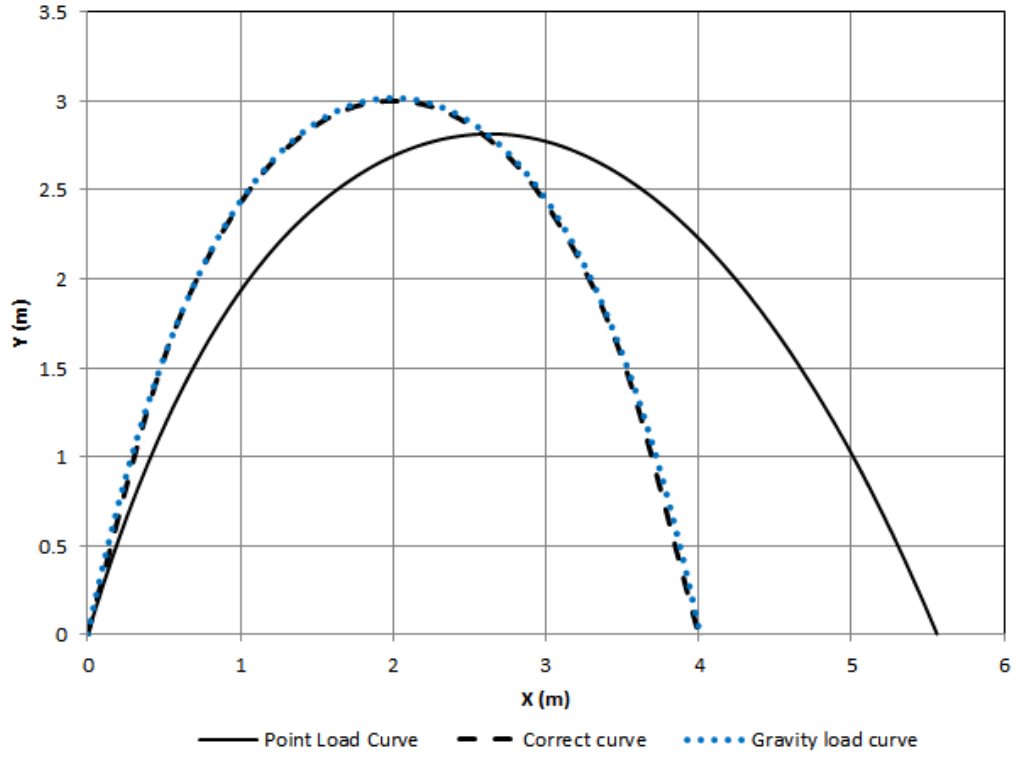


Figure 3.29: FLPC for steep vault of 250mm thickness subjected to gravity and wind loads (LC5) as per Table 11.

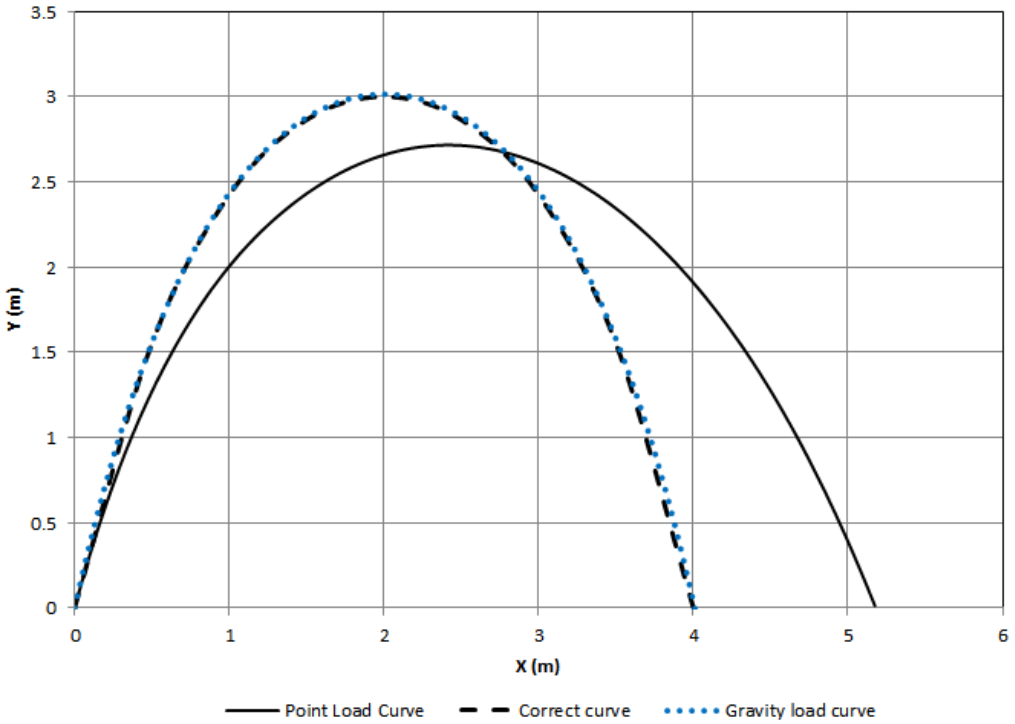


Figure 3.30: FLPC for steep vault of 250mm thickness subjected to gravity and wind loads (LC6) as per Table 11.

Figure 3.25 through Figure 3.30 suggests that, for a 250mm thick shell it may be possible to find a shape that will be able to accommodate the applied loads with minimal tensile stress development. Such a vault may typically have a rise of ±3000mm while the span should be in the order of ±5000mm. By changing the thickness of the shell, it may be possible to manipulate the geometry such, that for all load conditions, the line of thrust remains within the kern of the section.

FLPC for steep vault subjected to 300kph wind loads For hurricane wind speeds as determined and recorded in Table 12, the FLPC was determined. The vault geometry was taken as recorded in Table 9 while the material characteristic properties were taken as recorded in Table 14. The results of the FLPC for these load applications are illustrated in Figure 3.31 through Figure 3.36.

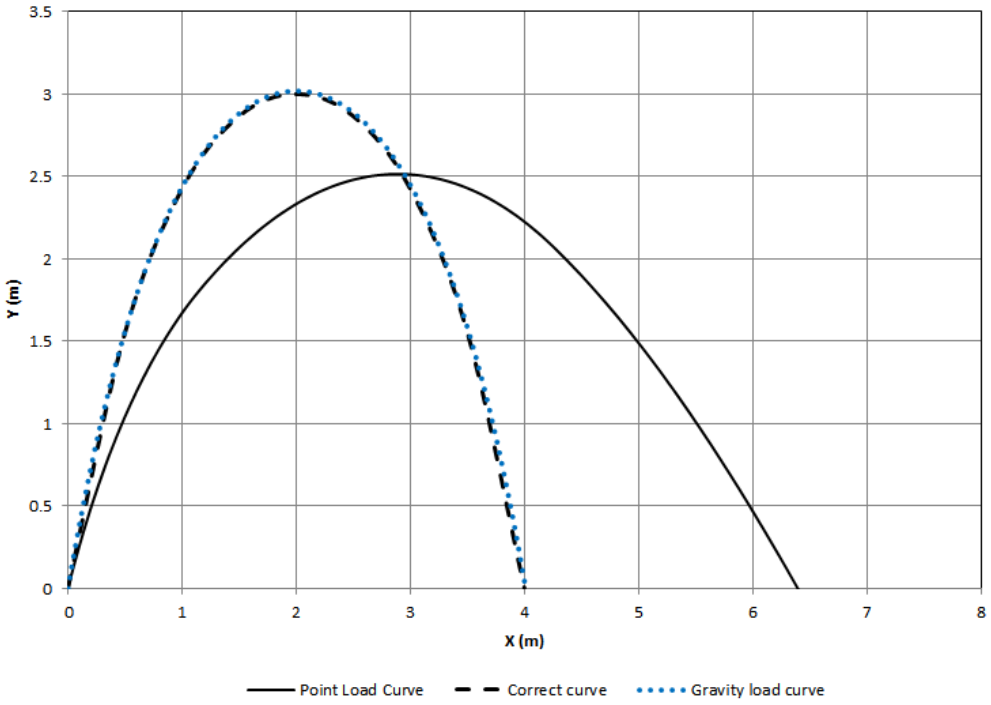


Figure 3.31: FLPC for steep vault of 250mm thickness subjected to gravity and wind loads (LC1) as per Table 12.

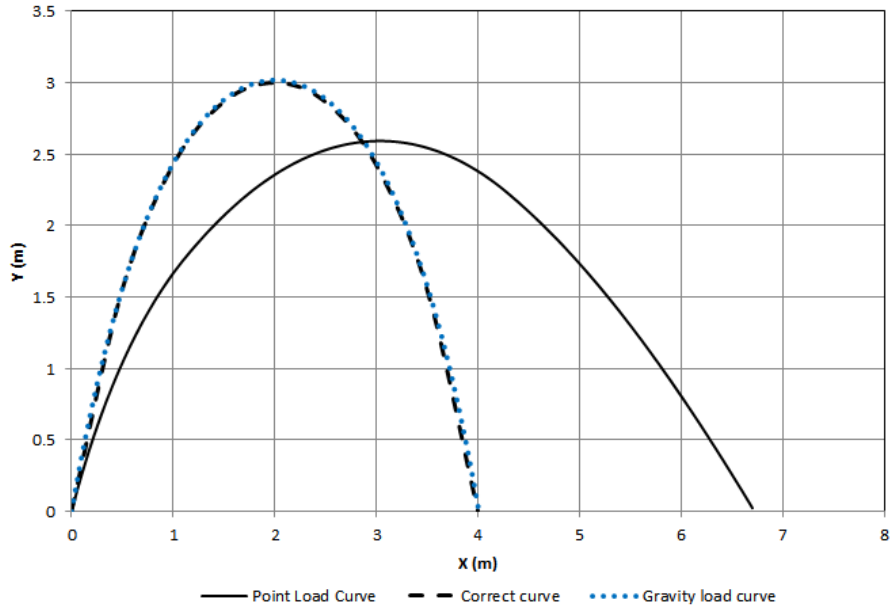


Figure 3.32: FLPC for steep vault of 250mm thickness subjected to gravity and wind loads (LC2) as per Table 12.

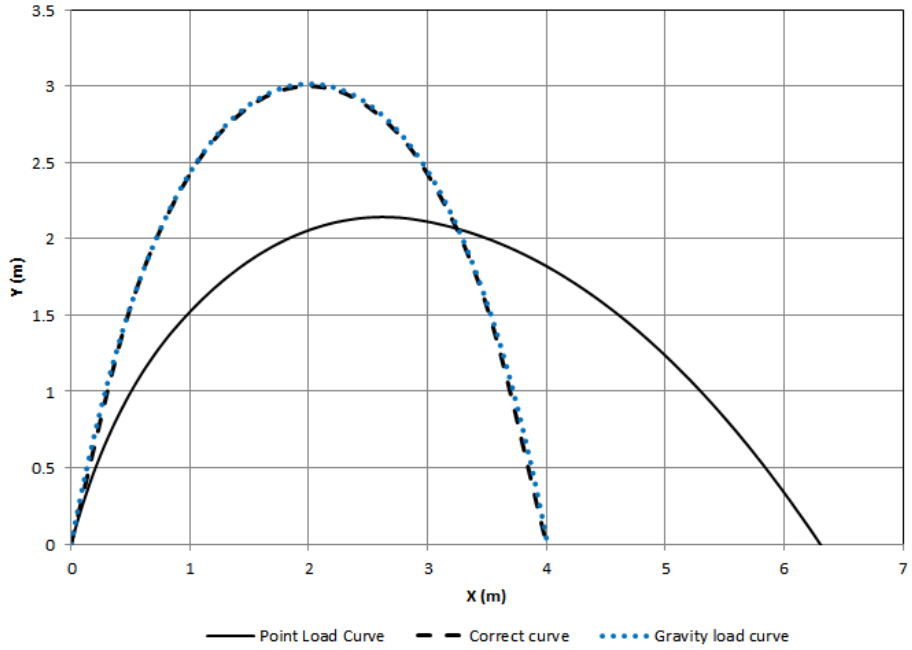


Figure 3.33: FLPC for steep vault of 250mm thickness subjected to gravity and wind loads (LC3) as per Table 12.

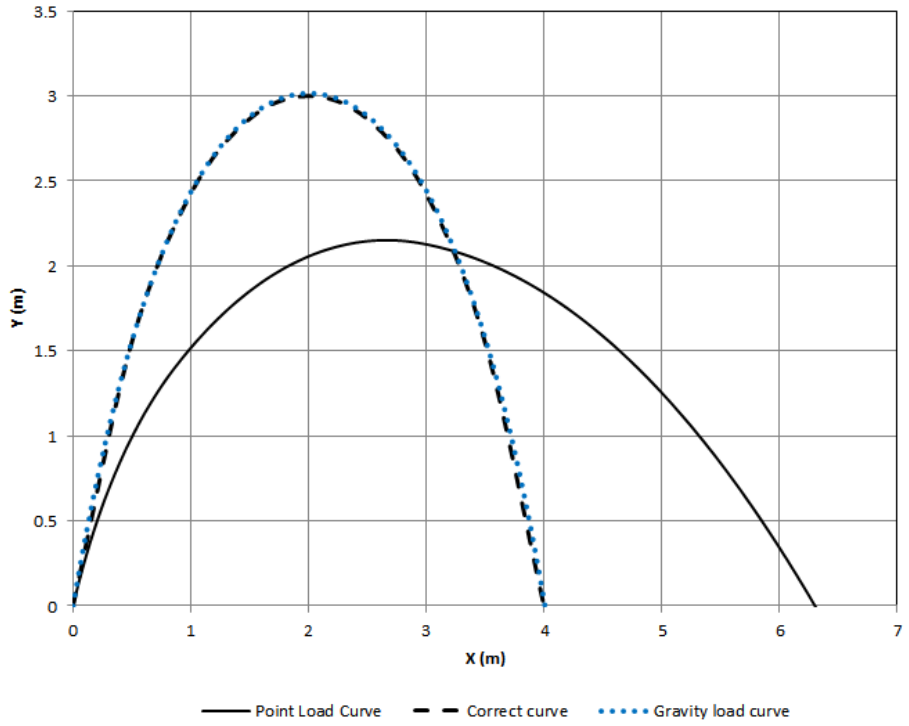


Figure 3.34: FLPC for steep vault of 250mm thickness subjected to gravity and wind loads (LC4) as per Table 12.

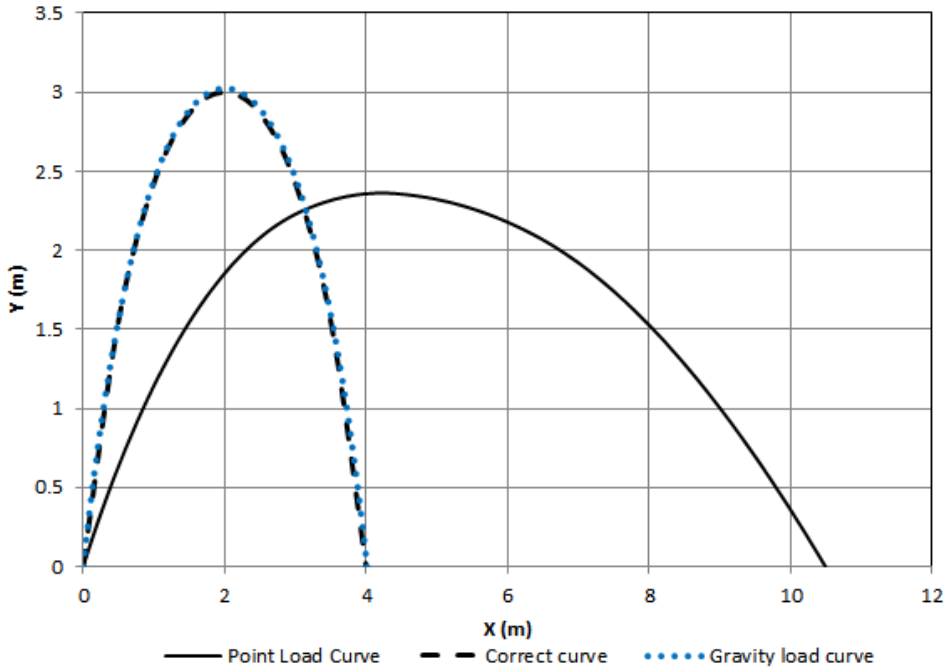


Figure 3.35: FLPC for steep vault of 250mm thickness subjected to gravity and wind loads (LC5) as per Table 12.

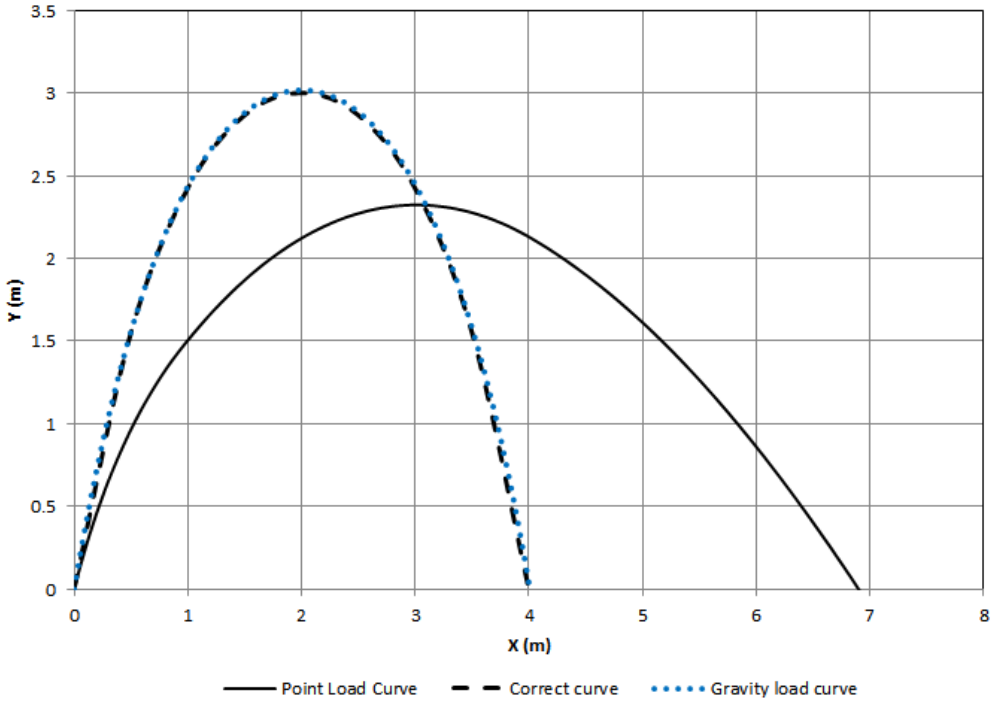


Figure 3.36: FLPC for steep vault of 250mm thickness subjected to gravity and wind loads (LC6) as per Table 12.

From Figure 3.31 through Figure 3.36, it is seen that the plotting of an FLPC for a 250mm shell vault, subjected to loads as recorded in Table 12, does not yield a practical solution to the problem. This statement is validated by noting that the FLPC for each load case yields a plot path which is not geometrically related to one another. In order to arrive at a practical solution, the FLPC for each load case should fall within, or close to, the defined kern of the section. For the given load conditions, this can only be achieved by either increasing the section to an un-practical thickness, or by implementing alternative means of forcing the force eccentricity to within the kern.

It can furthermore be noted that the plot path of the FLPC for these loads are even less related to the plot path of the dominant load condition. A universal solution for all the load conditions applicable could therefore not be obtained without increasing the shell to an unpractical thickness.

In order to counter the effect of uplift during high winds, it was envisaged that a thicker section may contribute to finding a pure compression solution to the problem. The same load cases were therefore applied to a vault of similar dimensions, but a shell thickness of 1000mm was assumed. The FLPC for each load case is plotted in Figure 3.37 through Figure 3.42.

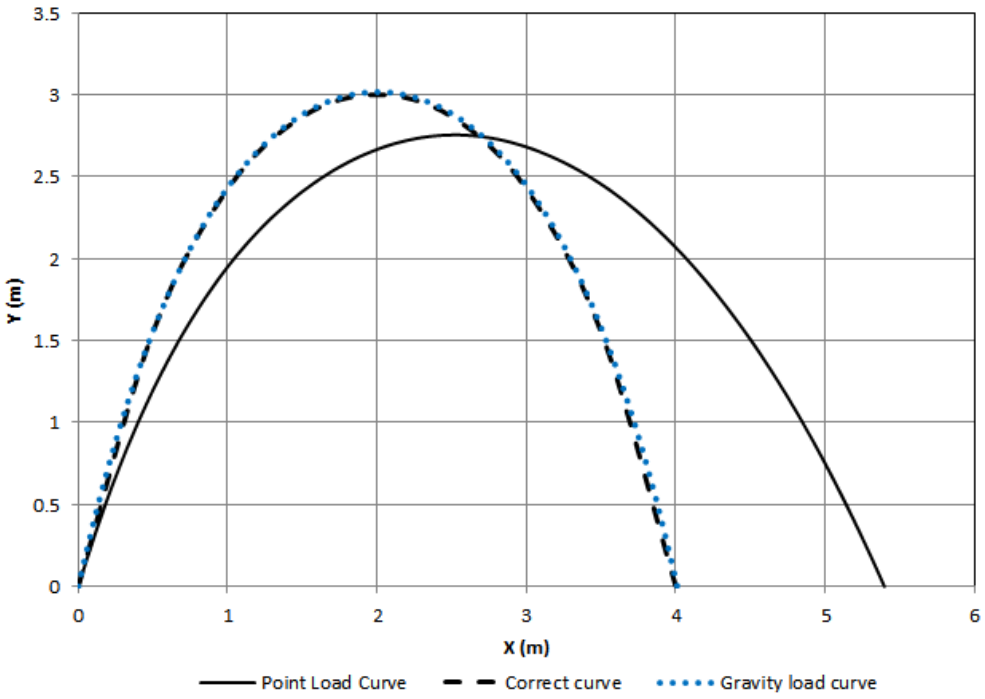


Figure 3.37: FLPC for steep vault of 1000mm thickness subjected to gravity and wind loads (LC1) as per Table 12.

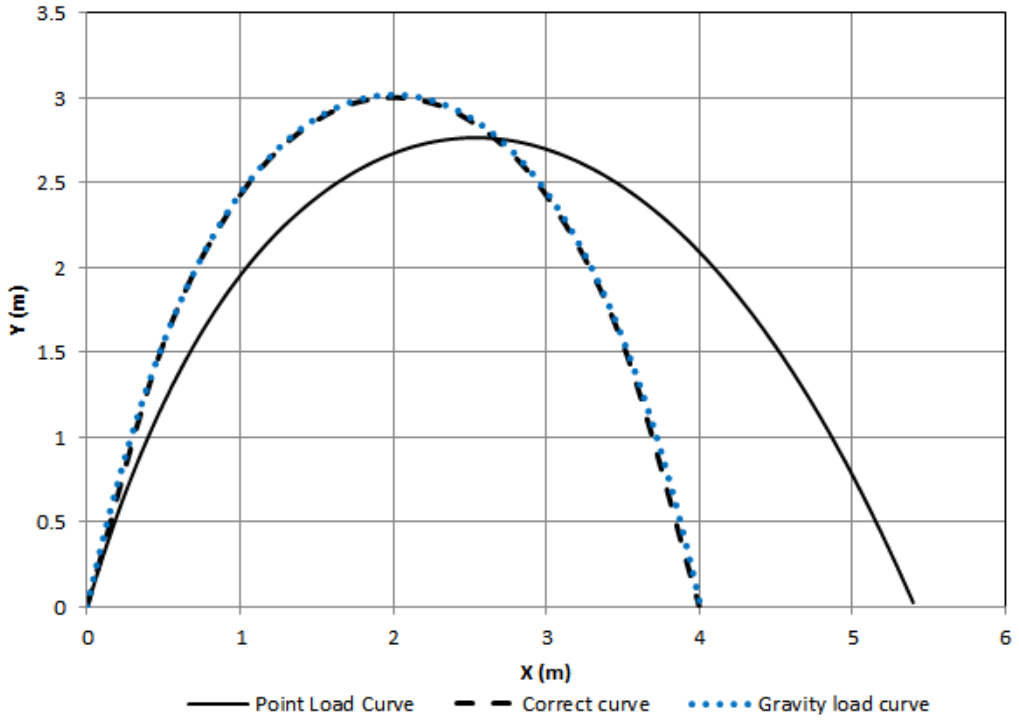


Figure 3.38: FLPC for steep vault of 1000mm thickness subjected to gravity and wind loads (LC2) as per Table 12.

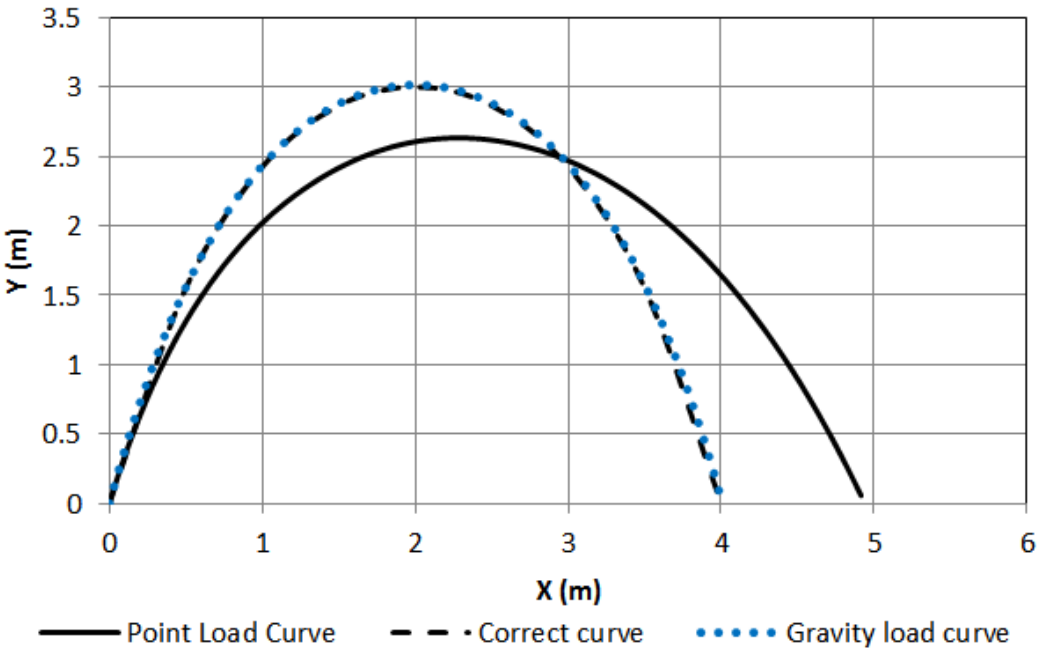


Figure 3.39: FLPC for steep vault of 1000mm thickness subjected to gravity and wind loads (LC3) as per Table 12.

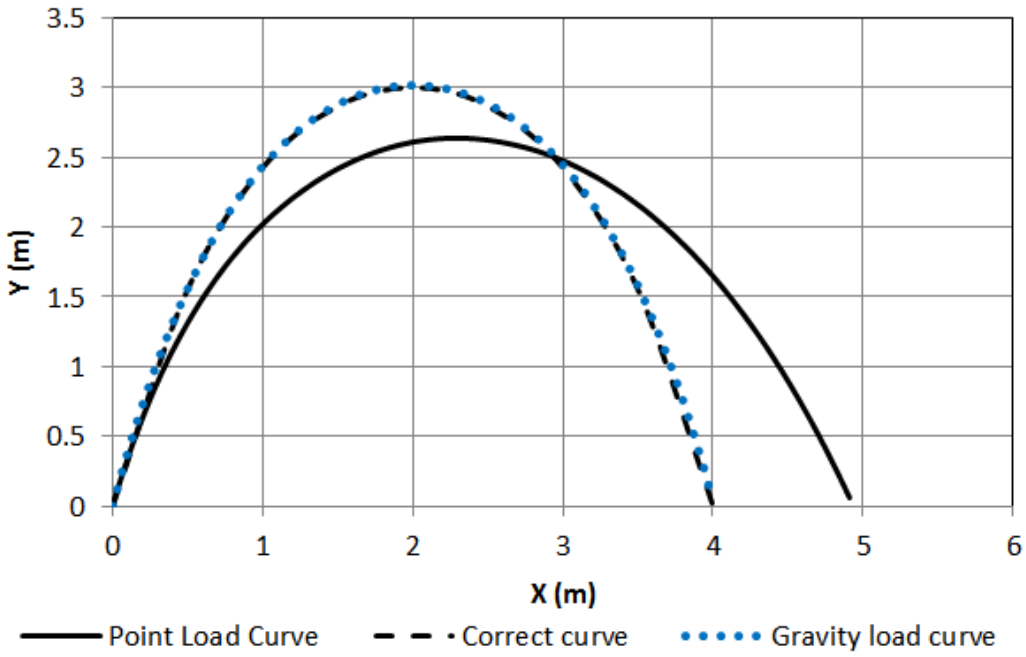


Figure 3.40: FLPC for steep vault of 1000mm thickness subjected to gravity and wind loads (LC4) as per Table 12.

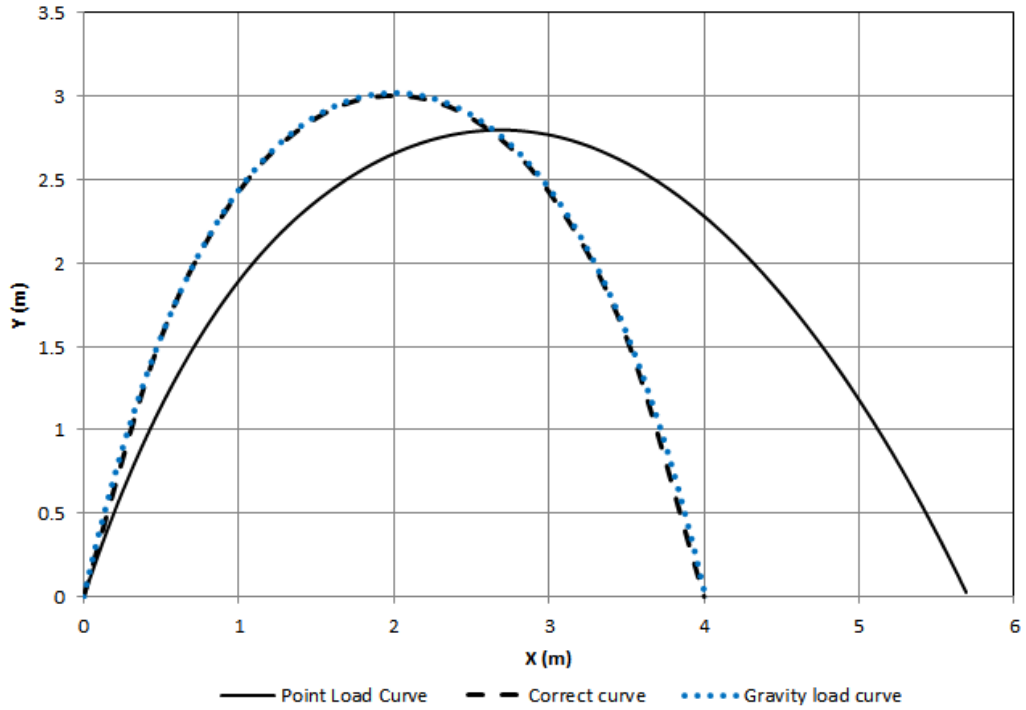


Figure 3.41: FLPC for steep vault of 1000mm thickness subjected to gravity and wind loads (LC5) as per Table 12.

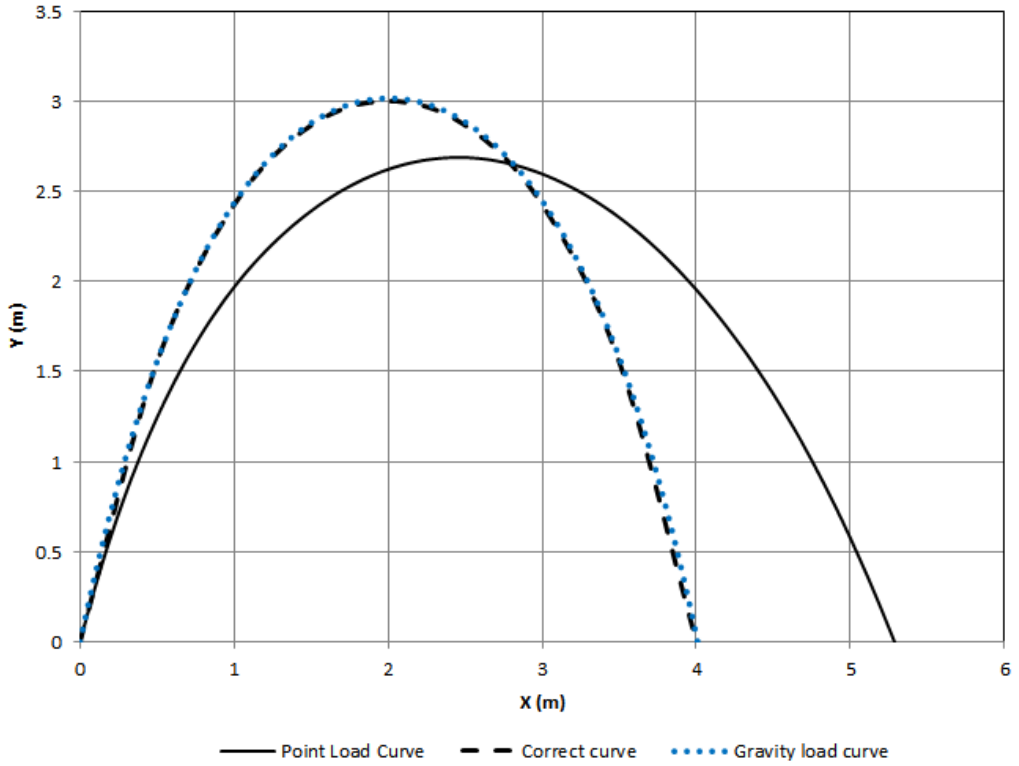


Figure 3.42: FLPC for steep vault of 1000mm thickness subjected to gravity and wind loads (LC6) as per Table 12.

Figure 3.37 through Figure 3.42 suggests that should the vault's shell thickness be increased to 1000mm, it may be possible to achieve a vault geometry which will resist loads with minimal tensile stress development.

Conclusion In the preceding discussion it was assumed that the vault will be subjected to normal as well as hurricane wind loads. It was found that for cases where normal wind speeds prevailed, a geometric shape may be obtained which will resist loads in pure compression. This shape will resist loads in such a fashion for all load conditions the vault may experience during its lifespan.

On the other hand, it is apparent that for the same vault configuration, no practical solution is expected when the vault is subjected to hurricane wind loads. During these load conditions, the uplift force was evidently overpowering the gravitational load induced by the structures self-weight.

This does not necessarily lead to foundation uplift and was easily verified by calculation, but does force the structure to resist the applied loads in tension and bending. The FLPC for each load case under consideration was far removed from one another. It was therefore deemed impossible to find a universal shape which will accommodate all load cases in the absence of tensile stress development.

It was moreover determined that an excessive increase in the shell's thickness may lead to convergence of a possible FPLC for all load cases the structure may be subjected to during its lifespan. An excessively thick shell was, however, considered unpractical and as a result, increasing the shell's thickness excessively was not considered a practical solution to the problem.

The next phase of this research was informed by considering the fact that it was determined that high vertical loads may lead to a feasible solution to the problem. By implementing post-tensioning to the vault, it may be possible to artificially induce excessive downward force onto the structure. This force may be designed such that it will ensure a converged FLPC for all load cases considered.

3.3.4 Post-tensioned Vaults

As discussed under section 3.3.3, the addition of a downward vertical force may result in convergence of the FLPC for a variety of load cases the structure might be subjected to. This can be assessed by considering two distinctly different methods of post-tensioning. These methods are presented in Section 3.3.4, *Traditionally Shaped Post-tensioned Vault* and *Catenary Vault Draped in Post-tensioned Tendon* respectively.

For the following discussions pertaining to this section, the shell thickness was assumed to be 250mm while its characteristic material properties were as recorded in Table 14.

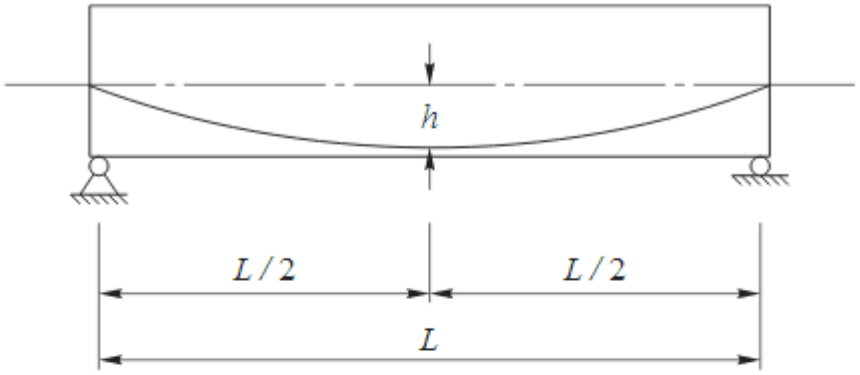
Traditionally Shaped Post-tensioned Vaults The first consideration was to post-tension the vault along its line of thrust defined by the self-weight condition. Here the geometry of the vault was defined as depicted in Figure 3.59. In such a case, the tendon will be placed concentrically to the FLPC of the catenary structure. This will result in all of the applied post-tension force to be transformed into pure compression stress under loading.

The geometry of the vault was defined by its gravity load and hence it was considered a traditional catenary vault. Determination of the structure's behaviour by manual means proved to be cumbersome. As a result, a finite element analysis (FEA) model was created to analyse the structure's behaviour to the applied loads and post-tension force. This procedure and the results thereof will be discussed under section 3.5.2.

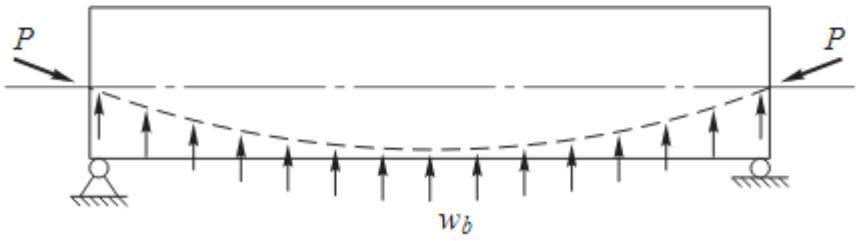
Catenary Vault Draped in Post-tensioned Tendon An alternative method of post-tensioning the vault is to drape it in a post-tensioned tendon mesh. This can be achieved by various means. The method assumed in this research was by draping the vault in a basalt geogrid mesh. A typical section through such a vault configuration is depicted in Figure 3.4. As discussed under Section 2.5.3, the mechanical properties of the material vary quite significantly from research to research.

Post-tensioned tendon supported at ±800mm c/c By anchoring an externally draped tendon at 800mm c/c along the vault's arch, it was found that the geometry of the structure may be optimised. Applying a post-tensioning force to the tendon, load was transferred by the tendon supports to the vault's shell. These loads are seen by the programme as point loads and the application of these loads influenced the FLPC of the structure. Should the post-tensioning force be high enough, the FLPC may be forced inside the kern of the section for all load conditions considered.

The theory of parabolic post-tensioned tendons was considered as illustrated in Figure 3.43. By post-tensioning a tendon that is draped to have a parabolic profile in a straight beam element, the tendon will have a tendency to straighten under load. This mechanism will result in the tendon to exert a uniform line load along the element, which will be opposite to the direction of draping. Assuming a defined set of nodes along the beam axis, the uniform line load can be converted to an equivalent point load at each node. Inverting this problem, the resemblance to the scenario, where a vault is draped in a post-tensioned tendon, becomes noticeable.



(a) Parabolic tendon profile



(b) Tendon forces acting on the concrete

Figure 3.43: Simply supported beam with parabolic tendon (Marshall & Robberts, 2000).

Assuming a case where the tendon is allowed to freely slide along the surface of the tendon support, the force exerted by it will remain normal to the vault's shell. By reconfiguring the Stem Element programme developed by Gohnert (2016), the normal force generated at the tendon to vault's interface was determined and applied to the structure as an equivalent force. The magnitude of the point force exerted by the tendon through the tendon supports was at this stage unknown, but based on the parabolic post-tensioned tendon scenario assumed to be uniform to one another. As the effect of point loads along the perimeter of the vault's arch was ,however, of concern, an arbitrary value was selected for these loads.

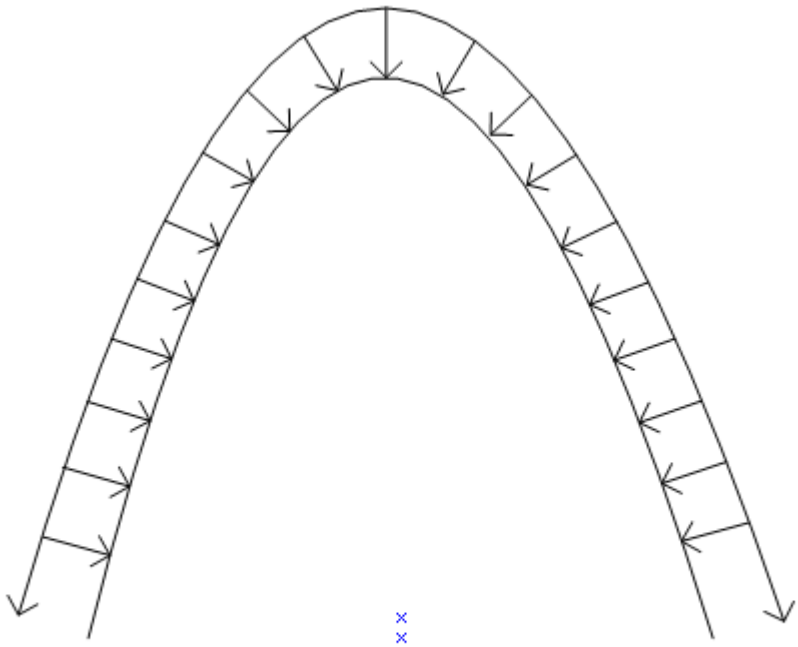


Figure 3.44: Schematic of vault draped in post-tension tendon and supported at 800mm increments.

Figure 3.45 illustrates the effect of this load configuration to the vault when subjected to this configuration. A significant reduction in rise and increases in span was noticed. The magnitude of the load exerted by the tendon to the external surface of the shell was assumed to be uniform at 10kN per tendon support.

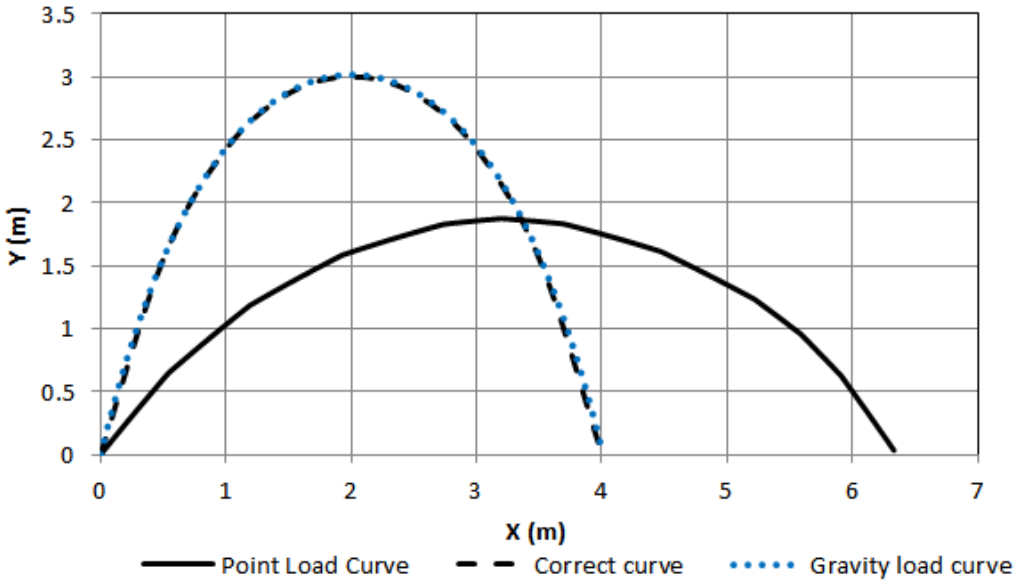


Figure 3.45: Optimised catenary geometry for externally draped post-tensioned tendon, supported along the vault's arch, and exerting a 10kN point loads along vault surface.

This load was only used as an assumption to determine the reaction of the FLPC to uniformly distributed point loads along the curve. It will be shown by the FEA analysis conducted that the support loads for the tendon were in the same order of magnitude. The differences recorded in the support loads were therefore considered negligible in finding the most suitable shape of the proposed structure.

By artificially decreasing the induced tendon support load, it was found that the gravity of the structure started to govern the curvature of the FLPC. This effect is adequately depicted in Figure 3.46 and shows that the FLPC tend to look more like the gravity load curve for the structure. By increasing the applied loads to 1000kN per support, a convergence was observed in the position of the FLPC. This convergence was indicative of the true FLPC for the assumed tendon support loads applied to the structure.

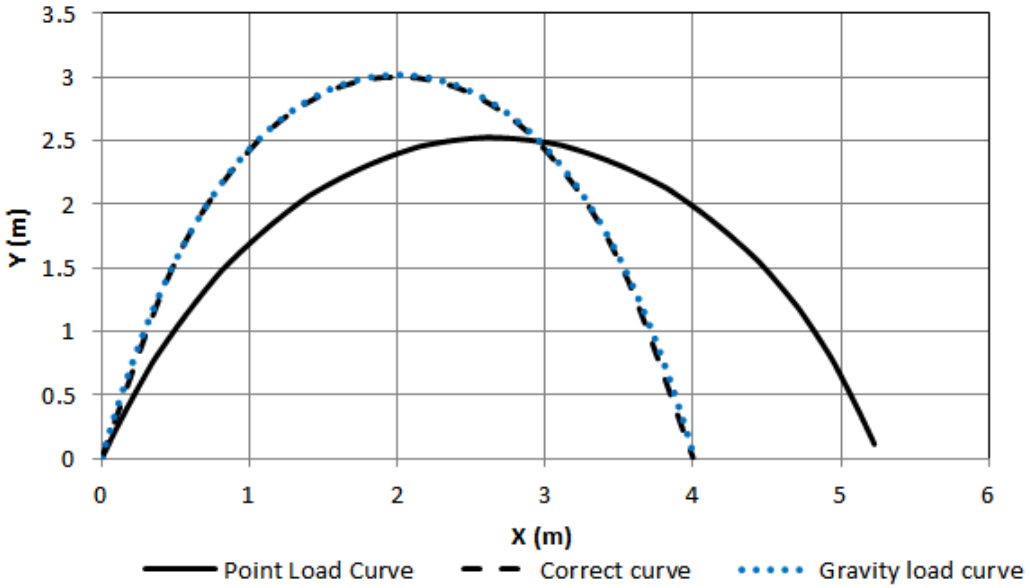


Figure 3.46: Optimised catenary geometry for externally draped post-tensioned tendon, supported along the vault's arch, and exerting a uniform 1kN load on vault surface.

These forces proved to suppress the effect of gravity on the FLPC and yielded the true funicular line for pure compression for the post-tensioned vault configuration under discussion (In the absence of self-weight). This effect is illustrated in Figure 3.47 and suggests a significant reduction in rise and increase in span required to resist the forces in pure compression.

Further investigation into the reaction of the FLPC to the applied loads revealed that, by having the tendon supported near the foundation of the vault, excessive spans and decreased rise are expected.

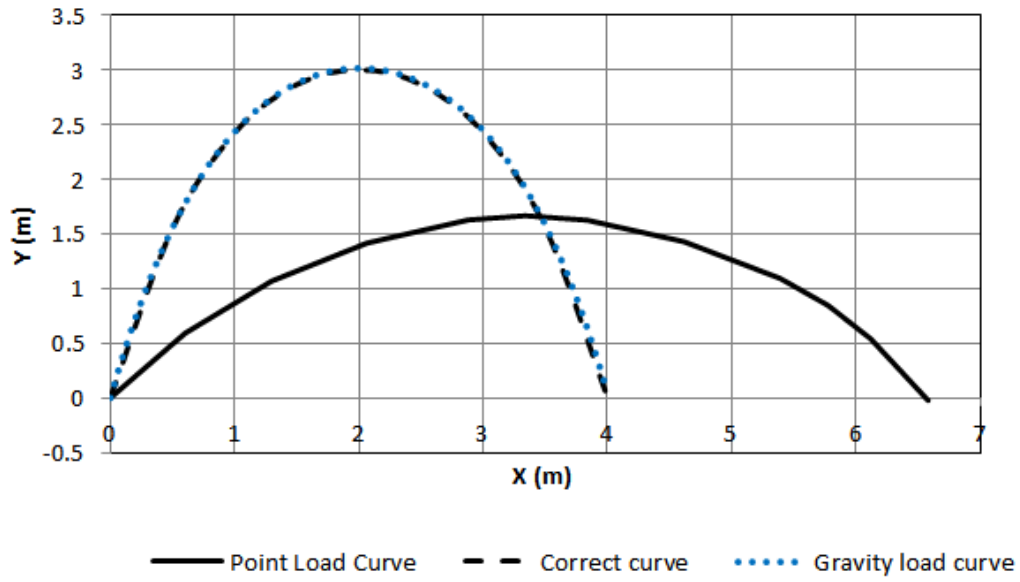


Figure 3.47: Optimised catenary geometry for externally draped post-tensioned tendon, supported along the vault's arch, and exerting a uniform 1000kN load on vault surface.

In order to ensure that the structure remained feasible from an economic perspective, it was deemed important to avoid having a solution with excessive spans. In addition to this, the solution should furthermore have sufficient rise to ensure adequate living space. Supporting the tendon near the foundations of the vault proved to counter these objectives, as it was found that tendon loads near the foundations resulted in an increase in span and decrease in rise.

Post-tensioned tendon supported over 1000mm of crown An alternative solution, as discussed under *Post-tensioned tendon supported at ±800mm c/c,* is to consider the tendon as being supported only at the vault's crown. As the tendon will be draped over the structure, it was intuitive to assume that the configuration can be manipulated such that the tendon can be supported uniformly at the crown. A 1000mm perimeter length of contact was assumed as illustrated in Figure 3.48.

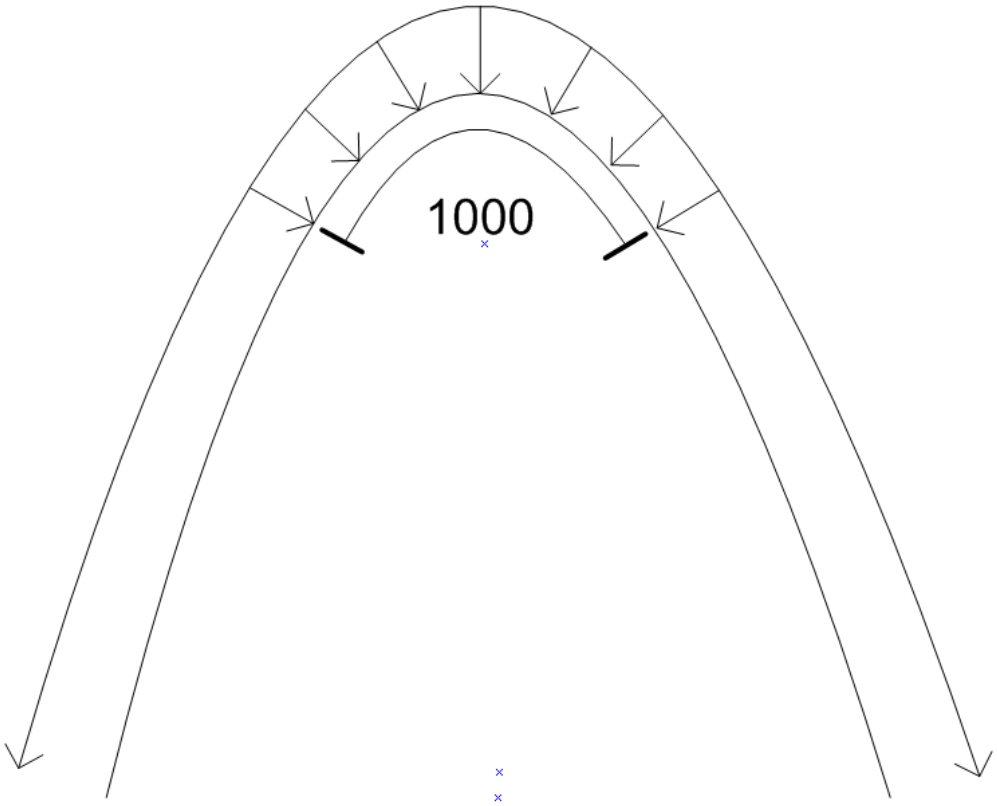


Figure 3.48: Schematic of vault draped in post-tension tendon and supported along 1000mm of crown.

The effect of the loads exerted by the tendon via the tendon supports were evaluated as discussed under *Post-tensioned tendon supported at ±800mm c/c.* The structure was effectively subdivided into two components namely; the crown and the legs. The crown was, for the purpose of this discussion, defined as the shell section supporting the tendon, while the legs are the shell section distributing the forces to the

foundations. It was expected to see a decrease in the leg curvature with an increase in tendon pull force. The reason for this expectation was mainly due to the fact that the axial compressive force in the shell will suppress the gravity loads responsible for the outwards curvature of the legs.

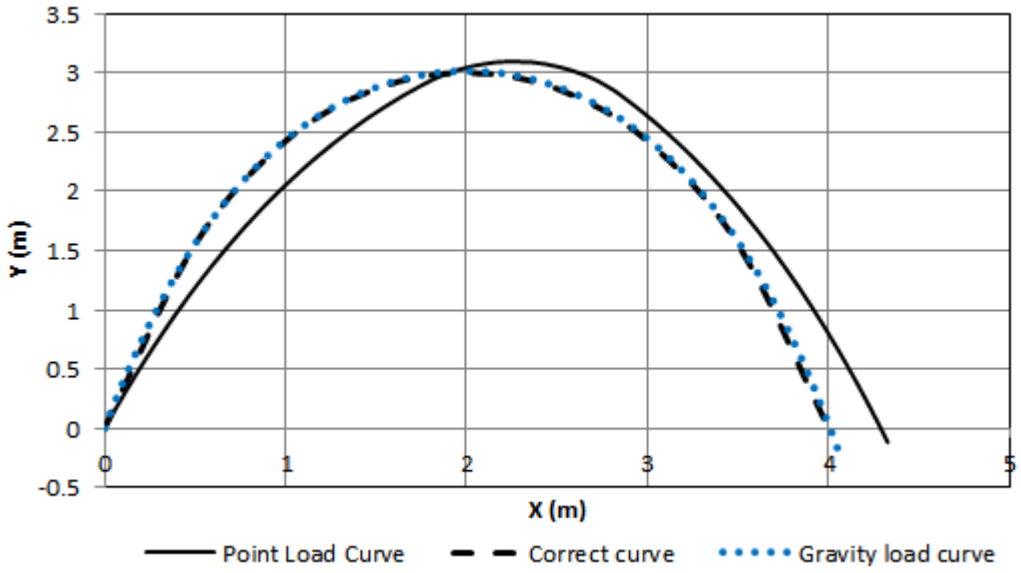


Figure 3.49: Optimised catenary geometry for externally draped post-tensioned tendon, supported along the vault's crown, and exerting a uniform 1kN load on vault surface.

From Figure 3.49, a straightening effect of the vault legs can be observed. Here the assumed force, exerted by the tendons onto the vault's shell, was a mere 1kN per node along the crown perimeter, and represented a constant line of support along the tendon. By increasing this force to an over-exaggerated 1000kN, the gravity effects were far less dominant and the FLPC of the load was plotted as depicted in Figure 3.51. Straightening of the legs were observed from more or less 10kN per node along the crown perimeter with the same assumptions made as previously discussed.

The effect of the load magnitude on the shape of the curve is ascribed to the "*hanging chain principle*" as illustrated in Figure 3.50 (Gohnert &

Bradley, 2016). Considering a flaccid chain, supported between two pinned supports as per ”A” in Figure 3.50 , a concentrated load at the centre of the span will result in the chain assuming two straight lines. The self-weight of chains is inherently dominant, and when supported between two pinned supports, it will yield a curved line as illustrated in “B” of Figure 3.50. Combining the two conditions as per C below, it can be seen that both these deflection conditions will influence the final shape of the structure.

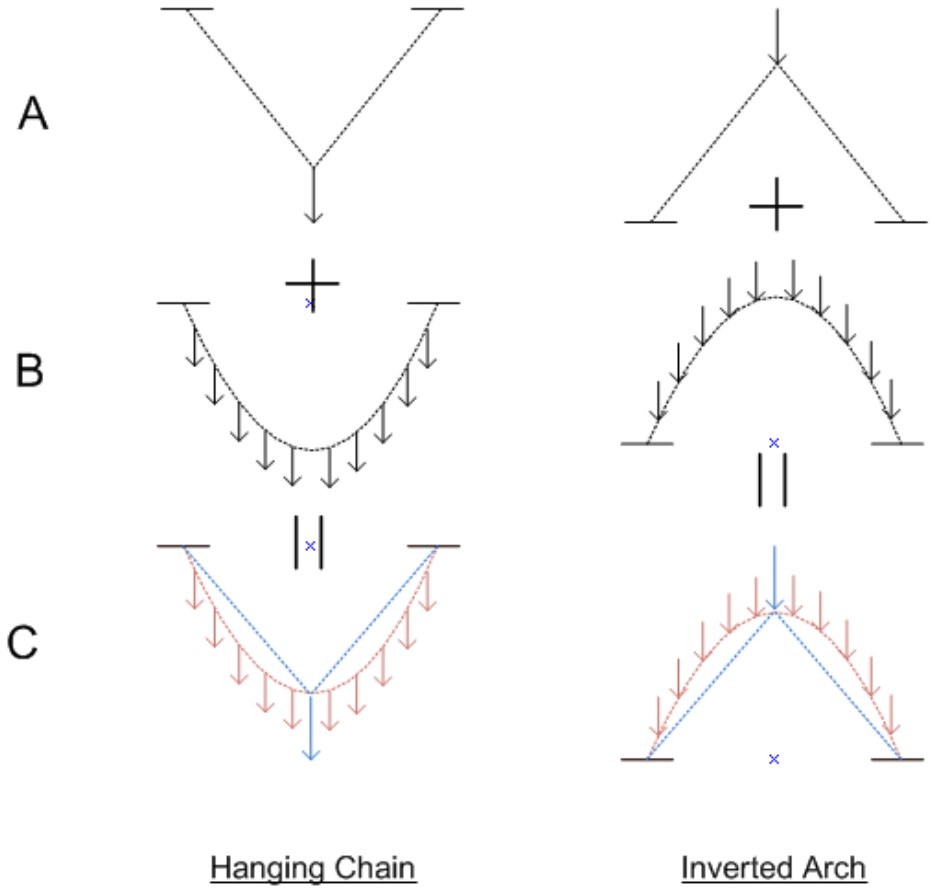


Figure 3.50: Hanging chain principle and the effect of uniform and concentrated loads on the chain and inverted arch.

The solution illustrated here is considered a possible viable solution to the problem. The reduction of the overall rise of the vault is fairly insignificant while an increase in the span length is moderate.

It is thought that this method may, however, cause possible complications during construction, as the geometry may require propping until the full effective post-tension force is applied. Moreover, it was also thought that straight legs will be more exposed to high bending moments as a result of wind pressure normal to the vault shell. These moments will have a profound effect on the generation of tensile forces and will yield a requirement for an even higher post-tension force to eliminate these stresses in the section. An increased leg length may furthermore result in a low critical buckling load of the shell, which may be of concern when high post-tension loads are applicable.

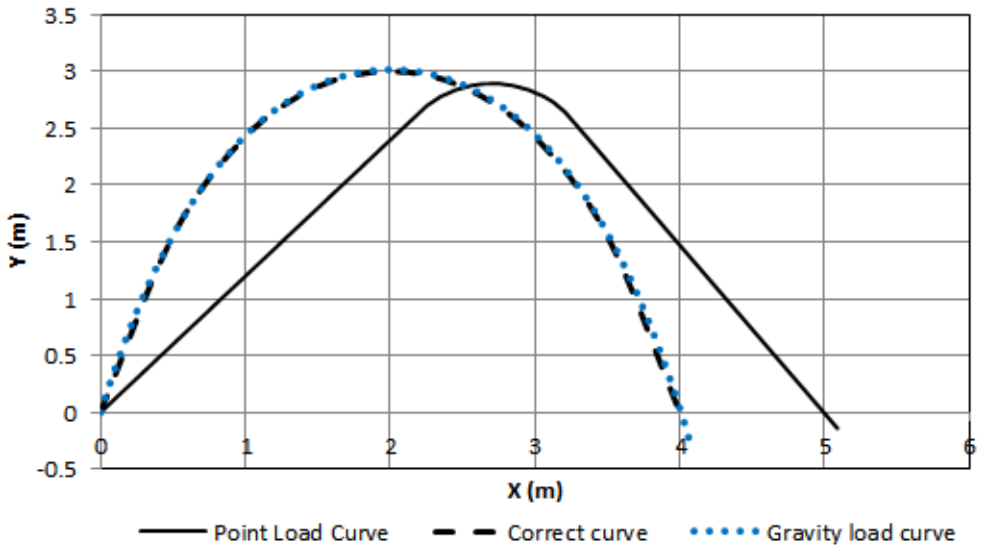


Figure 3.51: Optimised catenary geometry for externally draped post-tensioned tendon, supported along the vault's crown, and exerting a uniform 1000kN load on vault surface.

Three point contact tendon support From the discussions under *Post-tensioned tendon supported at ±800mm c/c* and *Post-tensioned tendon supported over 1000mm of crown*, it is evident that a combined approach regarding the distribution of tendon support loads should be considered. It may therefore be favourable to support the tendon such that the forces are distributed over the span of the vault while concentrated at specific locations. Such a possible configuration is illustrated in Figure 3.52.

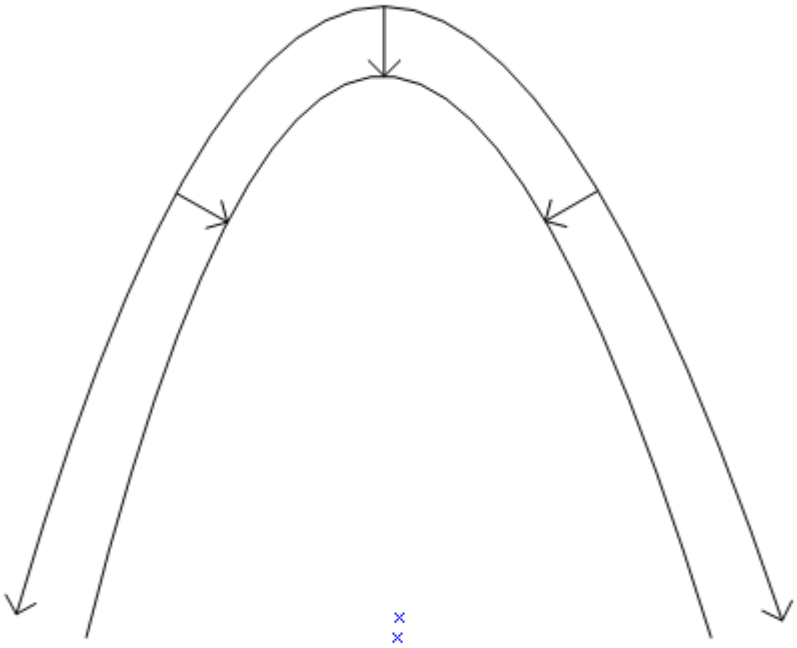


Figure 3.52: Schematic of vault draped in post-tension tendon and supported at three definitive locations.

By placing point loads nearer to the supports, the required span of the FLPC decreased with a decreased reduction in the vault rise. Convergence of the FLPC was only observed by applying point loads in excess of 1000kN normal to the curve. This is indicative that the self-weight of the structure plays a significant role in the shape of the FLPC for the load exerted by the tendon in this configuration.

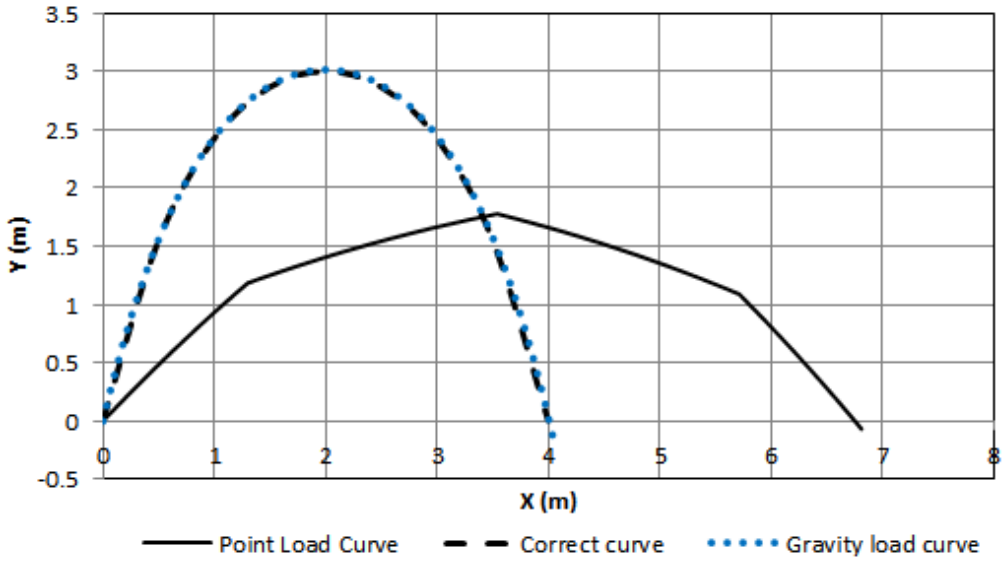


Figure 3.53: Optimised catenary geometry for externally draped post-tensioned tendon, supported at three pertinent positions, and exerting a 30kN point load.

An important observation of this configuration is that the direction of the force exerted by the tendon supports should remain at a fixed angle. By configuring the Stem Element programme such that the applied forces rotate to ensure normal contact to the shell at all times, the span of the section increased while the rise decreased drastically. This is ascribed to the FLPC's attempt to accommodate the loads applied to it in pure compression.

The solution as presented in this section was therefore considered viable. It should however be noted that, for a 30kN applied load at each tendon support, the vault will have a span of almost 7000mm with a maximum rise of only 1800mm. It was therefore deemed an un-practical shape for the purposes of this research, as it was considered favourable to keep the solution to the initial design objectives of a 3000mm rise at and 4000mm span.

Five point contact tendon support By applying the knowledge gained from the previous discussions, the following configuration was defined:

1. The tendon should be supported at five positions; occupying more or less a third of the vault's perimeter.
2. The tendon supports should be constructed such that it allows a theoretical frictionless bearing between the tendon and the tendon supports.
3. The tendon should exert a force at fixed angles to the tendon supports.

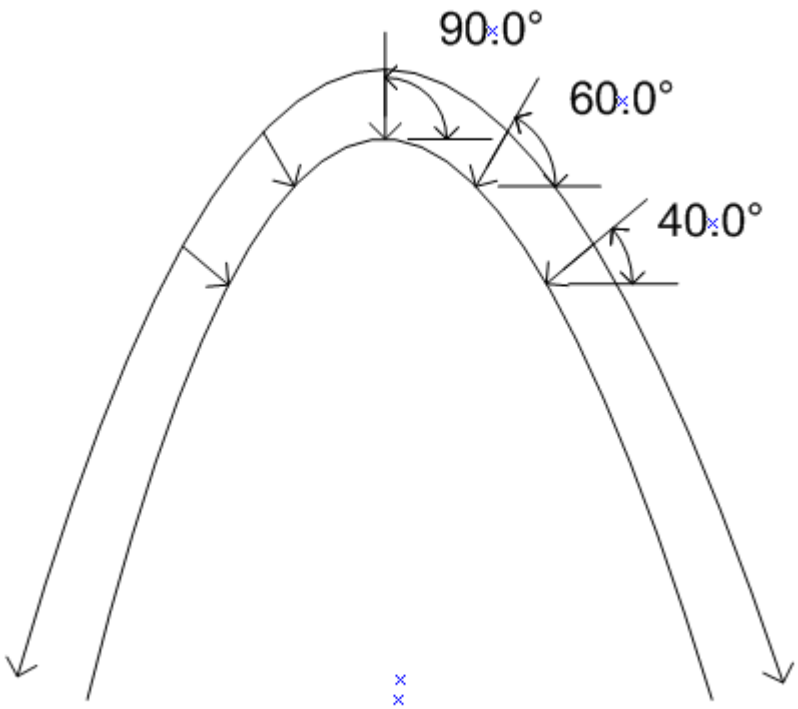


Figure 3.54: Schematic of vault draped in post-tension tendon and supported at five definitive locations.

By considering the configuration as illustrated in Figure 3.54, post-tensioning of the vault will result in an increase in span and decrease in rise. The tension forces in the tendon are transferred by means of tendon supports placed on the vault's shell. These support bearings should be

designed such that they ensure a point of contact with the tendon at an angle to the horizontal as suggested by Figure 3.54.

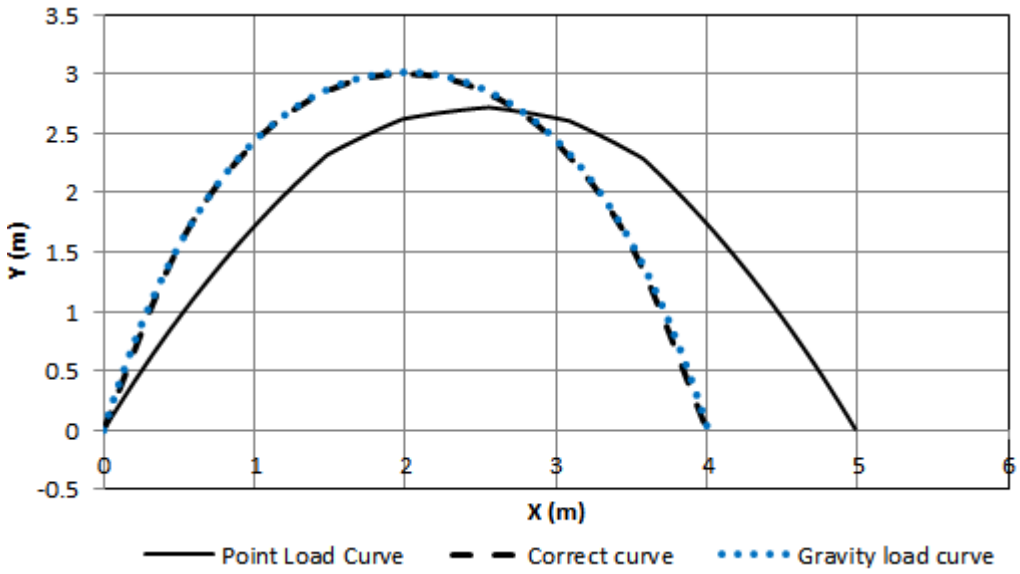


Figure 3.55: Optimised catenary geometry for externally draped post-tensioned tendon, supported at five pertinent positions, and exerting a 5kN point load.

By applying a mean force of 5kN at each of the five positions, a highly practical living space was obtained. By applying more post-tension force, the practicality of the solution did seem to deteriorate with a drop in rise and increase in span as depicted in Figure 3.56. From a 50kN point load per support position, the shape started to converge with a fairly practical solution even at an over-exaggerated 1000kN point force applied at all five locations.

This solution resulted in a practical living space as well as proved to be robust with regards to the magnitude of the post-tensioning force applied to it. Based on these findings, this specific solution was considered most viable to the problem statement.

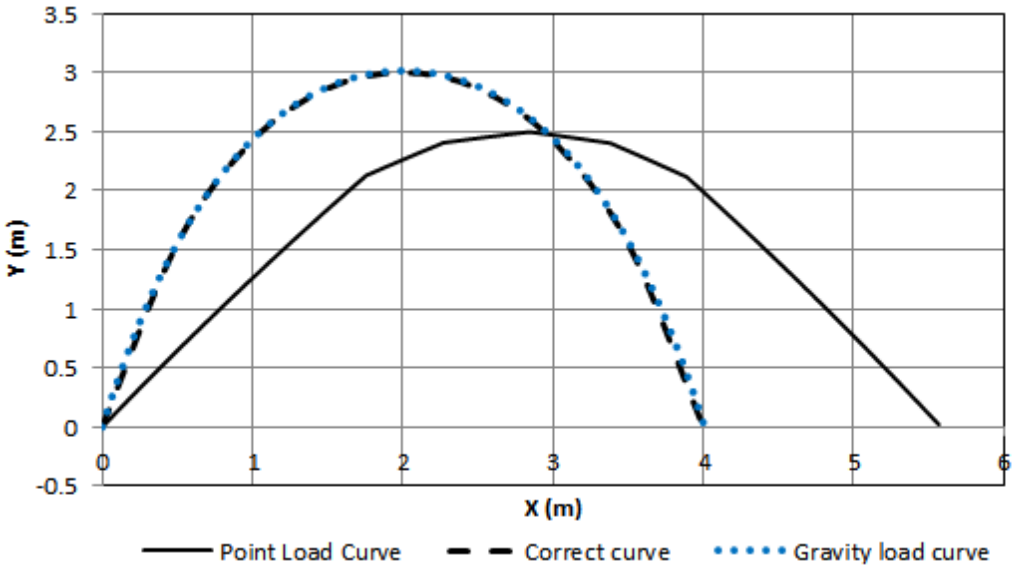


Figure 3.56: Optimised catenary geometry for externally draped post-tensioned tendon, supported at five pertinent positions, and exerting a 30kN point load.

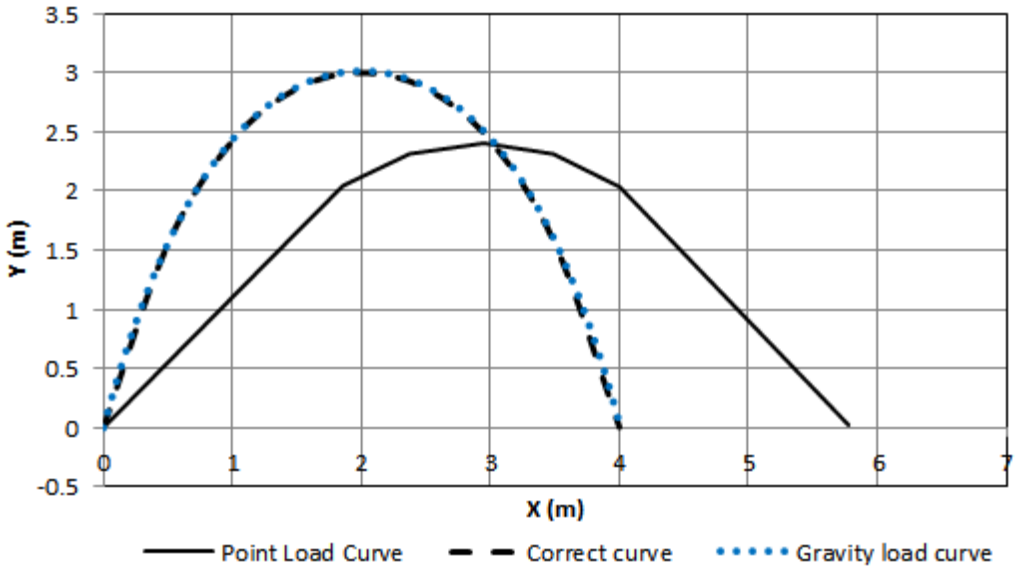


Figure 3.57: Optimised catenary geometry for externally draped post-tensioned tendon, supported at five pertinent positions, and exerting a 1000kN point load.

Conclusion Four different solutions, where the structure was draped in a post-tensioned tendon, were explored. The aim of this was to obtaining a practical FLPC for the dominant load condition. Although it may seem practical and fairly easy to drape a traditionally shaped catenary vault under a post-tensioned tendon, the reaction of the structure to this configuration was found not to be forgiving. Excessive spans with a low rise resulted in an un-practical structure and were therefore considered inadequate for the intended purpose.

By supporting the tendon over the vault's crown, a fairly practical solution was obtained. This solution is, however, expected to have constructability issues as a result of its geometry. It was moreover a concern that the long leg lengths of the vault may yield counter-productive bending moments under loading.

A configuration supporting the tendon at three distinct locations, however, yielded promising results. This configuration was, however, highly sensitive to the magnitude of the applied post-tension force, but did contribute to the understanding of the vault's reaction to concentrated loads at the locations of the tendon supports. It was observed that an increase in the support locations yielded more satisfying results.

As a result, a five point support system was selected. This post-tension solution yielded a practical living space as well as a robust solution with regards to excessive post-tension forces in the tendon. The latter was important as the amount of post-tension force required to relieve the section from tension stress was still unknown. It was moreover proven that this variable played a significant role in the liveable potential of the final solution.

For this solution, forces should be distributed from the tendon to the vault's shell at pre-defined angles. This can be achieved by means of applying frictionless bearing pads at these intersections.

Five point contact post-tensioned vault optimised for wind loads As seen in the preceding discussions regarding geometry optimisation, the shape of the vault changed depending on the post-tension configuration implemented. It is important to note that the original design objectives regarding the vault's rise and span were marginally different to that of the selected solution.

Wind load The selected solution's geometry looks fairly similar to that of a traditional catenary vault. As a result, it was assumed that the wind pressures as determined and recorded in Table 11 and Table 12, will accurately reflect the wind load conditions on the newly shaped vault. These loads were therefore considered applicable to the rest of this investigation and were used in the FEA analysis to be discussed under Section 3.5. Future research on this topic should, however, confirm this assumption by means of wind-tunnel testing on the final geometry.

Geometry optimisation for wind loads The selected solution resisted the load of its dominant load condition in pure compression. This load condition comprised of the structure's self-weight and post-tension force. It was considered favourable to attempt to optimise the vault's geometry such that it resisted all load conditions in pure compression. In order to determine if this may be a possibility, the optimised vault for post-tensioning was subjected to the wind loads previously calculated.

From a preliminary finite element analysis, it was determined that the force exerted by the tendon supports were in the order of 30kN for a ±80kN tendon load. The effects of the self-weight, post-tension force and wind loads could then be evaluated. These loads were implemented in the Stem Element programme as previously utilised. An FLPC for each load condition was plotted as per the load conditions considered in Table 15.

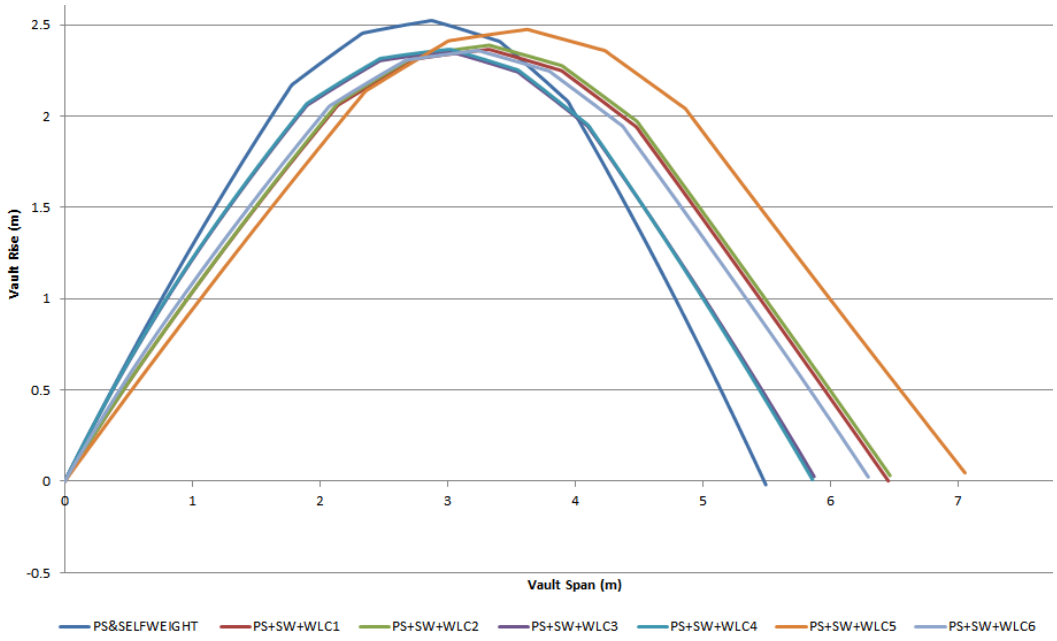


Figure 3.58: FLPC for five point post-tensioned vault, subjected to all load conditions.

As illustrated by the FLPCs in Figure 3.58, the vault's rise seems to be relatively un-effected by the application of a combination of loads. The span, however, varied significantly in order to accommodate the applied loads in pure compression. A variation in the span of up to 1600mm was noticed.

As a result of a significant variation in the position of the FLPC for each load condition, a practical solution did not seem viable considering geometry optimisation to resist these loads in the absence of bending. In order to find a practical solution, the vault's section needed to vary in thickness such that each load condition's FLPC falls within the kern of the section. This needed to be true at each position along the vault's perimeter. As a result, an un-practically thick section was required, which defeated the purpose of designing a structure that will require a minimal amount of construction materials.

3.4 TESTED MATERIALS

Physical test results were obtained for the material to be used in constructing the vault's shell and post-tension mechanism. Earth bricks were considered above the use of concrete blocks and clay bricks, as the objective of this research include the use of low cost material. As the name suggests, the major component in earth bricks is common soil. This will result in a mix with minimal cement content and no construction sand, yielding a low cost brick.

Regarding post-tension solutions, basalt fibres were considered above the use of normal post-tensioning steel. Basalt fibres are a modern, eco-friendly and highly durable solution as a tension resisting element (De Fazio, 2011). It is also known to be highly durable due to its low corrosion potential (De Fazio, 2011). This was considered beneficial, as some of the post-tensioning systems investigated, required the post-tensioned material to be exposed to the elements.

The product is available in a woven mesh, which allows the draping thereof over objects fairly simply, while also being known for its high tensile resistance capacity (De Fazio, 2011). Post-tensioning a mesh instead of a cable will moreover result in reduced local stresses at the bearing interface between the tendon and in-situ material.

3.4.1 Basalt Geogrid Mechanical Properties The mechanical properties of a basalt mesh were taken from laboratory tests conducted at the heavy structures laboratory at the University of the Witwatersrand in Johannesburg, South Africa. The results of these tests are listed in Table 13. From the results, a 95% confidence interval was determined. No testing was conducted on the thermal properties of this particular batch of basalt fibres. Consequently, it is recommended that future studies into this subject should investigate the effects of creep, thermal expansion and thermal contraction of the basalt fibres on the structure being investigated.

Table 13: Basalt geogrid mechanical properties tested at the University of the Witwatersrand, South Africa (Surat, D (Personal communication)).

Test No.	FAILURE STRESS (MPA)	YOUNG'S MODULUS (GPA)
1	753.40	73.00
2	690.61	62.78
3	753.40	58.13
4	690.61	62.78
5	878.96	87.20
6	778.51	71.34
7	816.18	57.08
8	652.94	73.00
DETERINATION OF THE 95% CONFIDENCE INTERVAL		
Standard Deviation	74	10
Average	752	68
sample size	8	8
Confidence coeff (95%)	2	3
Margin of Error	51	10
Upper Bound	803	79
Lower Bound	701	58
max	879	87
min	653	57

Range	226	30

A rupture stress of 701MPa and modulus of elasticity of 58GPa were consequently assumed in the design. From the eight tests conducted, it was furthermore found that the potential for elongation was 7.8%. This potential was important when it came to the design of the post-tension force required at jacking.

3.4.2 Earth Bricks Mechanical Properties

The mechanical properties of this material are listed in Table 14. The reader should note that the range for water absorption (between 4-6%), as noted in Table 14, is associated with a particular block made of a particular soil. This range is by no means true for all earth bricks; which can have a wide variety of mechanical properties depending on the soil used during manufacturing (Morton & Bennetts, 2008). It is therefore recommended that testing be conducted on the particular block to be used for construction, and that calculations are based on those values.

Table 14: Characteristic properties of earth bricks (Heuer, N (Personal communication)).

PROPERTIES	UNIT	CLASS A
28 day dry compressive strength (+20% after 1 year)	MPa	5 -7
28 day wet compressive strength (after 24 hours immersion)	MPa	2 - 3
28 day dry tensile strength (on a core)	MPa	1 - 2
28 day dry bending strength	MPa	1 - 2
28 day dry shear strength	MPa	1 - 2

Poisson's ratio	-	0.15 - 0.35
Young's Modulus	MPa	700 - 1000
Apparent bulk density	Kg/m^3	1900-2200
Coefficient of thermal expansion	mm/m^oC	0.010-0.015
Swell after saturation (24 hours immersion)	mm/m	0.5 - 1
Shrinkage (due to natural air drying)	mm/m	0.2 - 1
Permeability	mm/sec	1.10^{-5}
Total water absorption	% weight	4 - 6
Specific heat	KJ/Kg	~ 0.85
Coefficient of conductivity	W/m^oC	0.46 – 0.81
Damping coefficient	%	5 - 10
Lag time (for 40 cm thick wall)	h	10 - 12
Coefficient of acoustic attenuation (for 40 cm thick wall at 500 Hz)	dB	50
Fire resistance	-	Excellent
Flammability	-	Poor

3.5 FEA ANALYSIS

3.5.1 Introduction

In section 3.3, optimisation of the FLPC to accommodate post-tensioning and self-weight in pure compression was investigated. A practical FLPC was determined and selected, and a typical representation of the solution is presented in Figure 3.56.

Two post-tension solutions were considered as viable solutions to the problem statement. These two solutions were post-tensioning of a traditionally shaped catenary vault and a geometrically optimised five point contact post-tensioned vault. In this section, both of these solutions will be discussed in detail.

In all of the following discussions, unless specifically stated otherwise, the effective section thickness was assumed to be 250mm. The material the shell comprised of was earth brick masonry, of which the characteristic properties were as listed in Table 14.

3.5.2 Traditionally Shaped Post-tensioned Vault Considering the geometry of the traditional catenary vault, it was assumed that the vault had the material properties as listed in Table 9 and Table 14. As mentioned under Section 2.2.2, *Pre-stressing of Vaults*, vaults are traditionally not post-tensioned along the arch's circumference. In this research, the feasibility of post-tensioning a vault along its arch's circumference was, however, investigated.

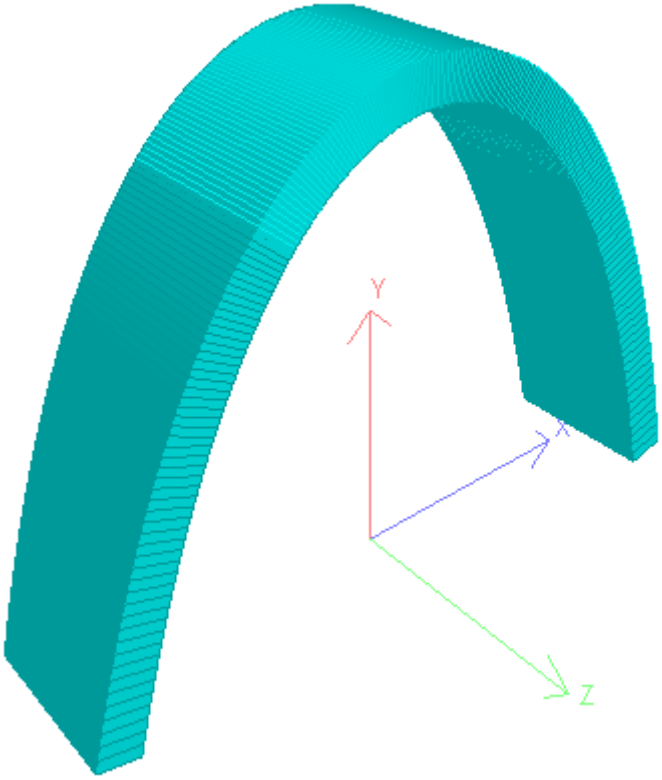


Figure 3.59: Isometric view (StaadPro V8i FEA model) of traditional catenary vault with concentrically placed post-tension tendon.

Modelling Considerations Due to the fact that wind loads are reversible, post-tensioning of the vault section was only considered along the shell's geometric centroid (Raju, 2007). The reason for this configuration was to prevent the generation of eccentricity moments in the section. This may worsen the tensile state of the section in a reversible wind load condition and should be avoided.

A solution to improve the tensile state in the section was to place the tendon along the section's geometric centroid. This post-compressed the section uniformly and led to a reduction, and possible elimination of the tensile flexure stress induced in the extreme fibres of the section during bending. This mechanism is best illustrates in Figure 2.53 and indicates the effect of post-compression on the stress state of a section subjected to bending. The vault post-tensioned in this discussion had the same dimension as defined under Section 3.1.3, *Steep Vault*.

For hurricane wind speeds, wind pressures as listed in Table 12 were assumed. The geometry of the vault was informed by its self-weight only; therefore a traditional catenary arch was expected in section. With the geometry and wind loads defined, the only unknown was the post-tensioning force required to eliminate the generation of tension stress in the section.

The tendon force required to decompress the section was determined by ensuring that no tension developed in the section under a combined loading condition. Placing the tendon concentrically with the vault's shell was a fairly easy way of determining a ball park figure for the required tendon force which will eliminate tension in the section.

FEA Modelling Details In order to determine the post-tension force required, an FEA model was constructed. StaadPro V8i is a finite element analysis program that allows fairly quick and easy manipulation of large amounts of modelling data. It additionally possesses the function of considering post-tensioning in beam elements. The finite element model considered a 1000mm section of vault, analysed in a linear static solver.

For the sake of simplicity, the model was defined by applying the traditional catenary equation for 801 horizontal coordinate positions. The nodes were then connected by 800 two node beam elements, each of which was assigned a section of 250mm thick and 1000mm wide.

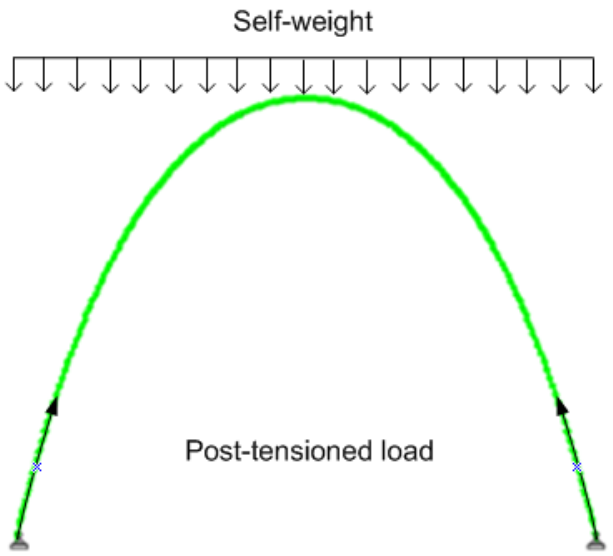
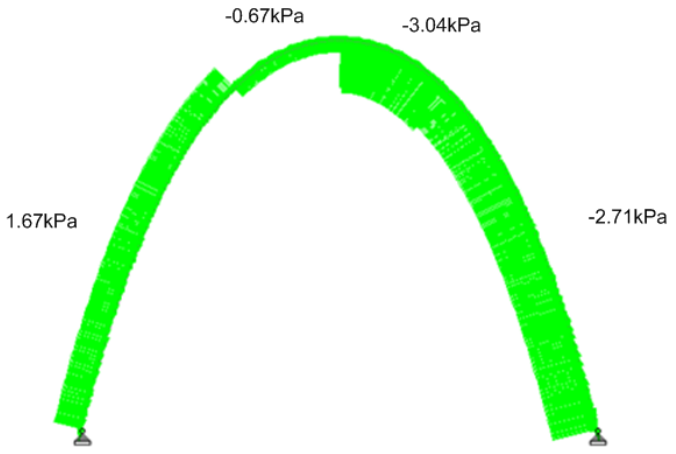
Load Combinations The load combinations considered were as listed in Table 15. The post-tension load was increased gradually until the section yielded pure compression in all load cases considered.

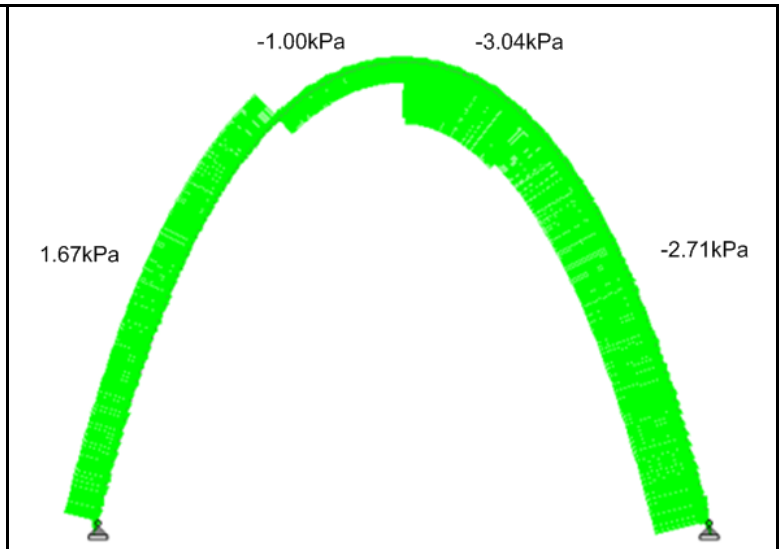
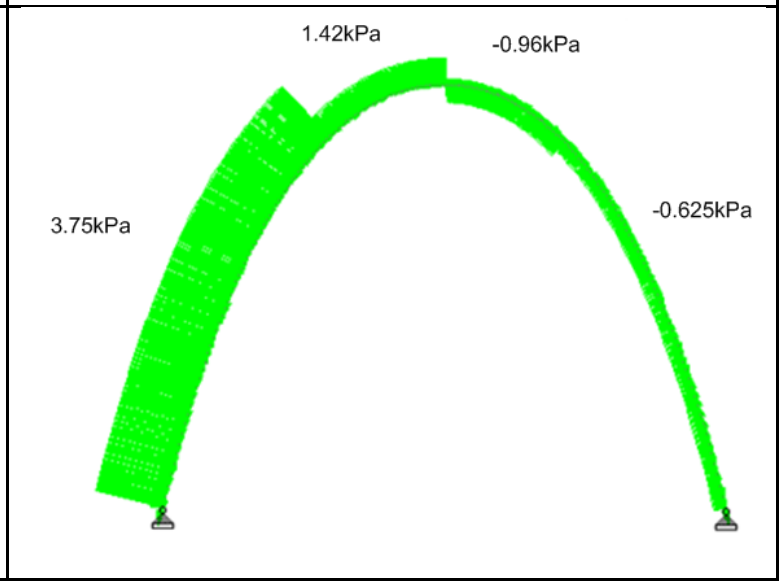
Table 15: Load combinations for FEA model.

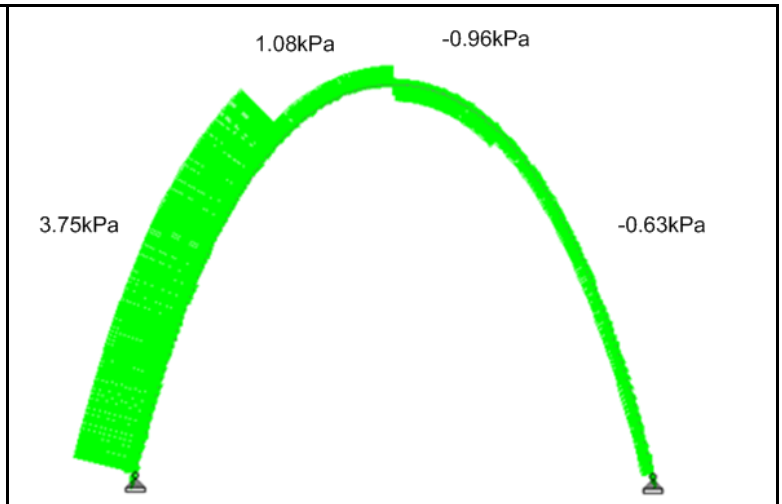
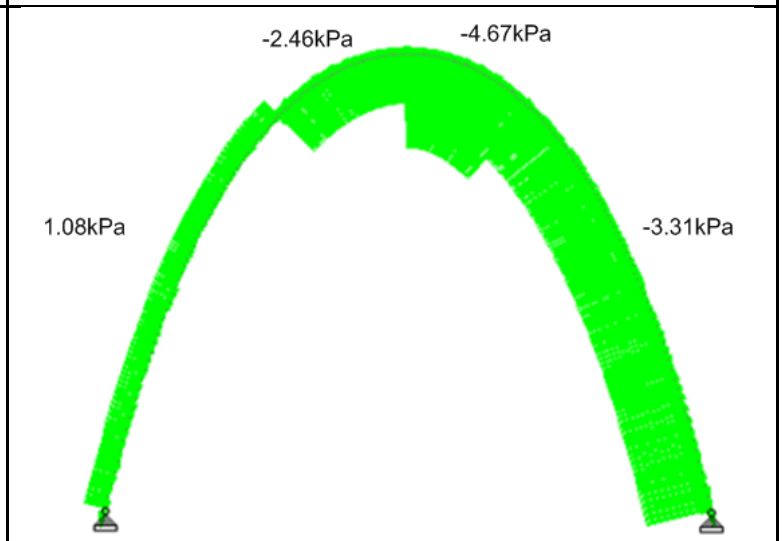
ID	Load combination
1	Self-weight + Post-tension
2	Self-weight + Post-tension + Wind Load Table 12 (LC1)
3	Self-weight + Post-tension + Wind Load Table 12 (LC2)
4	Self-weight + Post-tension + Wind Load Table 12 (LC3)
5	Self-weight + Post-tension + Wind Load Table 12 (LC4)
6	Self-weight + Post-tension + Wind Load Table 12 (LC5)
7	Self-weight + Post-tension + Wind Load Table 12 (LC6)

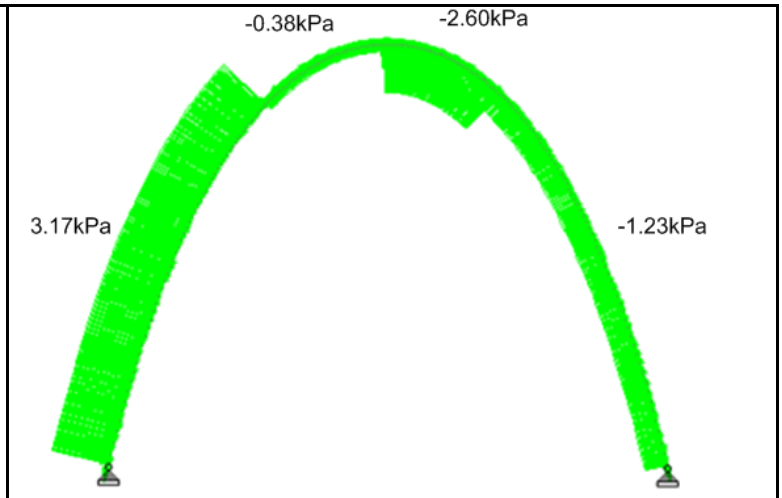
The application of the load combination is best illustrated visually as seen in Table 16**.**

Table 16: A visual illustration of load combinations (StaadPro V8i FEA model) for a traditional concentrically post-tensioned vault.

Load Combination	Model view of applied loads
LC1	
LC2	

LC3	-1.00kPa -3.04kPa 1.67kPa -2.71kPa
LC4	1.42kPa -0.96kPa 3.75kPa -0.625kPa

LC5	1.08kPa -0.96kPa 3.75kPa -0.63kPa
LC6	-2.46kPa -4.67kPa 1.08kPa -3.31kPa

LC7	

Results Interpretation The results from the linear static analysis are listed in Table 17. As expected, an increase in the concentric post-tension force along the centreline of the vault's arch yielded a linear reduction in the maximum tensile stress in the extreme fibres. It was additionally illustrated that an increase in the tendon stress not only yielded a decrease in the maximum bending moment, but also a decrease in the minimum bending moment in the section. This observation is illustrated in Figure 3.60 and Figure 3.61, and was not considered ideal.

Table 17: Worst Case Scenario on Tendon force vs tensile stress and bending moment in section of traditional catenary vault in concentric post-tension configuration.

Effective post-tension force per meter of vault (kN)	Max bending moment (kNm/m)	Min bending moment (kNm/m)	Tensile stress (MPa)
0	5.843	-6.715	0.613
50	5.780	-6.775	0.419
100	5.718	-6.836	0.225

150	5.655	-6.897	0.031
161	5.642	-6.910	0.000

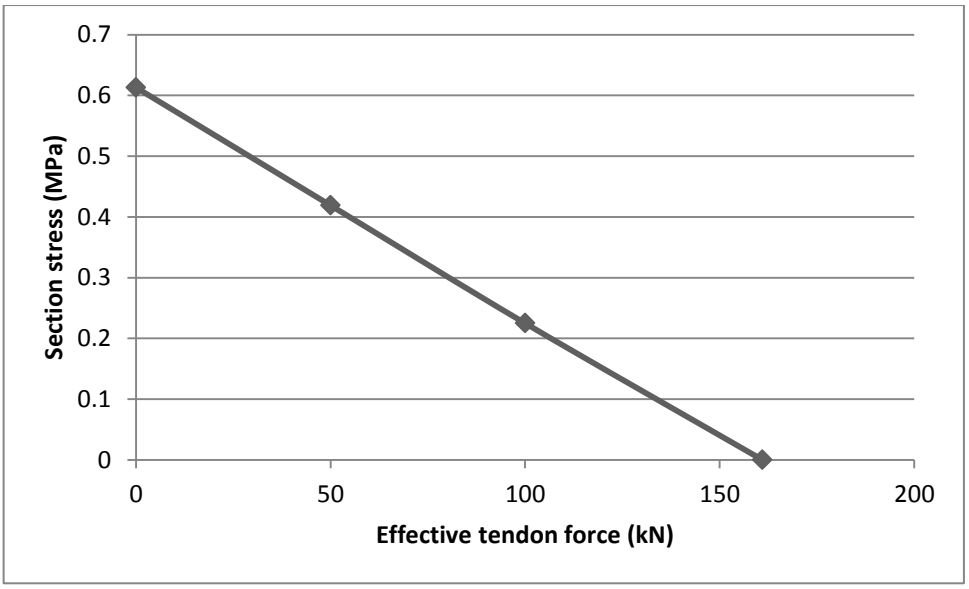


Figure 3.60: Graphical representation of stress reduction vs tendon force increase for data as per Table 17.

The reason for this behaviour of the structure can be ascribed to the fact that the structure deflected under the applied loads. Small changes in the geometry led to the post-tension force, originally applied to the FLPC, to shift. As a result, the structure no longer resisted the artificially induced compressive force in the absence of bending, but rather generated a secondary bending moment as a result of the increase in force eccentricity. This moment worsened the tension state of the section and led to an increased effective post-tension force required to decompress the section. As a result, it was considered as counterproductive and inefficient.

From Table 17 it can be seen that the section was subjected to a relatively high bending moment, but that no tension stress was developed in the section when a 161kN post-tension force was applied. This is ascribed to

the fact that the post-tension force compressed the section uniformly, relieving all flexural tensile stress developed during bending.

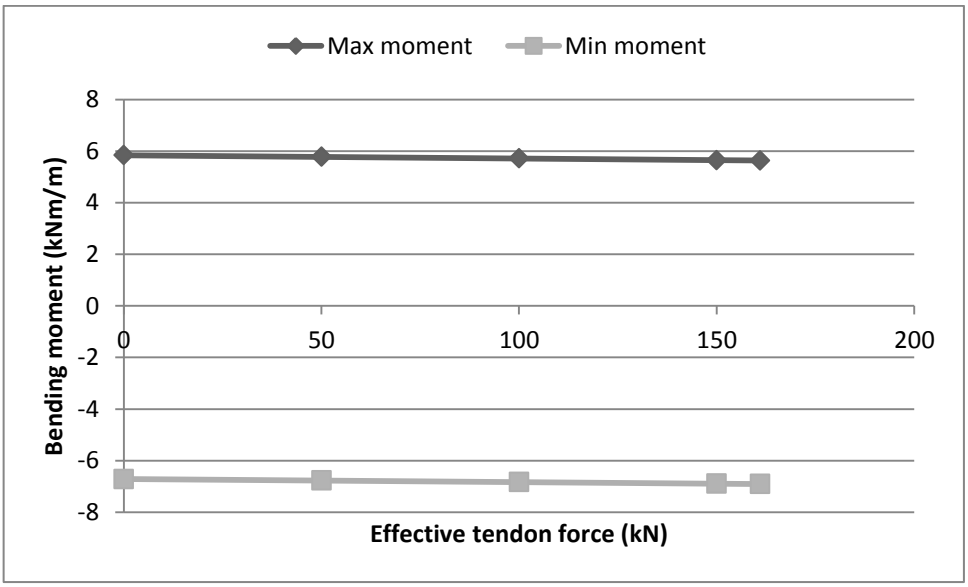


Figure 3.61: Graphical representation of bending moment reduction vs tendon force increase for data presented in Table 17.

Conclusion Post-tensioning the vault concentrically along its arch's perimeter was considered as a viable solution. It should, however, be noted that geometric changes, as a result of loads applied to the structure, generated unfavourable secondary bending moments. These moments increased the absolute moment in the section and yielded higher tensile stresses that had to be overcome by the post-tension force.

The post-tension force required to fully alleviate the structure from tension was significant. It was therefore not only considered as possibly defeating the purpose of having a low cost design, but also resulted in additional design verifications that will have to be conducted as a result of the high load. One of this key verification will be to ensure that the bearing resistance of the material, where the tendon is supported, can adequately resist the high bearing force at the tendon to shell interface.

Construction aspects may also be problematic, as jacking of the tendon at foundation level may be complicated to achieve in this particular

configuration. The design of the foundations is moreover expected to yield complications, as the high tensile stresses at the tendon foundation may interfere with the base reaction of the vault shell. This interference may lead to changes to the Stem Element of the FLPC, which will result in undesirable eccentricity moments in the shell.

The FEA model suggested that the required post-tension force to obtain pure compression in the section is an excessive 161kN.

3.5.3 Five Point Contact Post-tensioned Vault Solutions The optimised geometry for the self-weight and post-tension condition of this solution is presented in Figure 3.56. From the Stem Element analysis conducted, it was evident that the structural shape accommodated the loads in pure compression. It is, however, recommended that these findings are supported by an FEA analysis. Furthermore to proving the findings as reliable, the structure had to be subjected to service, ultimate and hurricane wind loads to determine the stress field in the section under these load conditions.

Three effective section thicknesses were analysed and discussed. Each of these investigations contributed to the final shell thickness, effective post-tension force and geometry definition selected. As an initial analysis, the previously assumed configuration of a 250mm shell thickness was selected. A structural design, as discussed under Section 4.4.1, proved this shell thickness as inferior. Further investigation suggested that a 335mm shell, at a lower post-tension force, yielded a suitable solution. This configuration, however, once again proved to be insufficient during a structural design verification, which led to a final section thickness of 350mm.

In order to achieve a section thickness of 350mm will require a custom made brick, specifically formed for mass production of these vaults.

Modelling Considerations In this analysis, a 1000mm section of vault was considered with an effective section thickness of 250mm. The magnitude of the effective post-tension force was reduced, or increased as required. The wind load conditions investigated were normal wind speeds as per SANS 10160-3:2011; factored to the serviceability and ultimate limit state, as well as hurricane wind conditions with an absolute wind speed of 300kph.

Depending on the combined stress requirement of the section and wind load condition applicable, the effective post-tension requirement varied. This resulted in changes to the magnitude of the tendon support loads, which in turn affected the FLPC of the structure. Geometry modifications, based on the new tendon support loads acquired from the model, were implemented in order to ensure pure compression of the section under the dominant and service load condition.

The magnitude of the effective post-tension force was determined based on the boundary conditions of the design. The following two design scenarios were identified:

1. The elimination of all tensile stress in the section for wind pressures as a result of an absolute wind speed of 300kph.
2. The elimination of all tensile stress in the section for wind pressures as a result of service loads, while the cracked moment capacity of the section should resist the applied moments induced by ultimate limit state loads. The structure may furthermore crack, but not collapse when subjected to a hurricane wind load conditions.

Geometry Refinement In evaluating the structural response of the model, StaadPro V8i was used. Here the vault was modelled in a non-linear analysis engine, as the model implemented beam and cable elements. Cable elements are considered as non-linear modelling elements by StaadPro V8i. The beam elements were utilised to represent a 1000mm section of the shell of the vault, while the cable elements represented the post-tensioned basalt geogrid mesh. The model configuration is depicted in Figure 3.62 and an 85kN effective post-tension force was assumed as the most un-favourable post-tension force requirement.

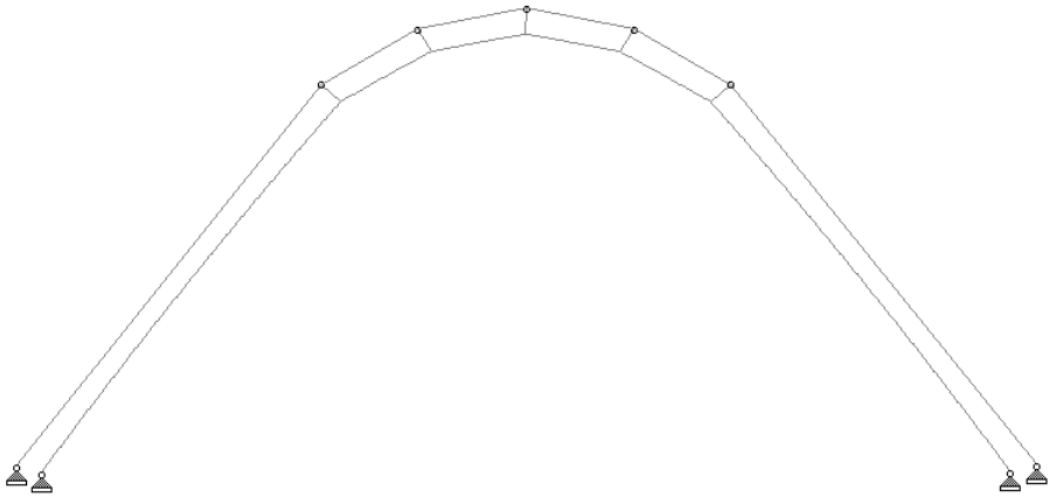


Figure 3.62: Five point contact post-tensioned vault (StaadPro V8i model) for no tension allowed in 300kph wind load condition.

A key consideration was the magnitude of the load exerted by the tendon supports to the vault's shell. The FLPC for the vault was determined by an initial estimation of the exerted force by each tendon support. In reality, the magnitude of the force in each tendon support may vary from one another. This needed to be taken into consideration to determine a true funicular shape for the structure.

In an initial attempt, the geometry was defined as illustrated in Figure 3.56. Here, the FLPC was based on a uniform 30kN estimated tendon support load. By running a non-linear solver on the model, the actual tendon support load at each support was determined. This load was extracted from the model and implemented in the Stem Element programme where the FLPC was defined.

As previously discussed, the FLPC was determined by considering the self-weight and post-tension loads applied to the structure. As a result, the FLPC shifted with a change in the magnitude of the tendon support loads. By applying the change in load magnitude, new geometry for the structure was defined and implemented in the FEA model. By iterating through this process, the geometry and tendon support magnitude changed until convergence was observed.

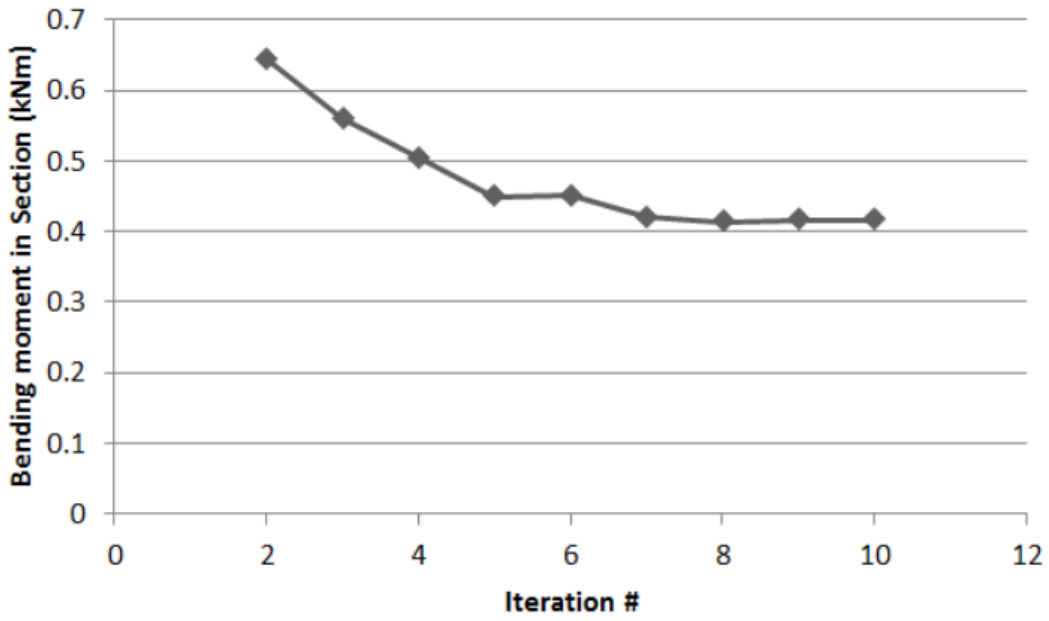


Figure 3.63: Convergence of FLPC based on bending moment in section of five point contact optimised vault.

Initial Geometry and Load Configuration At the first iteration, bending moments were observed in the vault's section for the dominant load condition. This result was expected, as the tendon support loads were assumed to be uniform at 30kN per support. The initial absolute maximum bending moment observed was 0.64kNm/m. Ten iterations were conducted until convergence of the bending moment in the section was obtained.

As illustrated by Figure 3.63, the bending moment started converging at the eighth iteration at an absolute magnitude of 0.42kNm/m and an effective post-tension load of 85kN. The fact that the bending moment did not reduce to 0kNm/m was ascribed to the structural imperfection of the model as previously discussed. Although this was considered an adequate level of fineness, the curve was still imperfect, as the beam elements remain straight and not curved as assumed by the Stem Element programme.

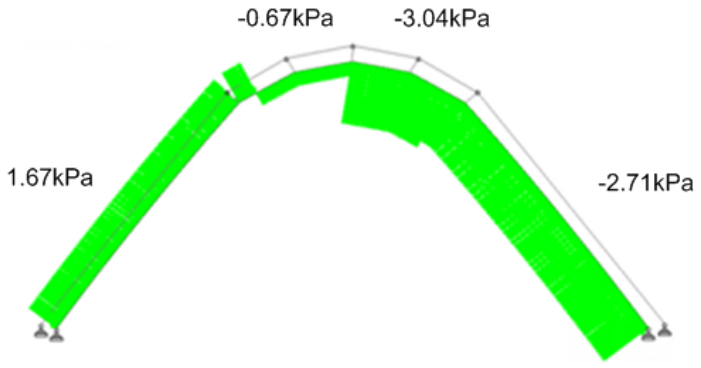
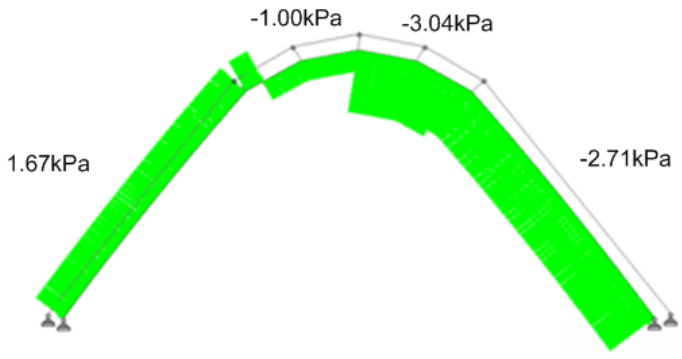
The axial force in the section was determined to be 100.40kN/m. Considering this magnitude of compressive force in the section, a 0.42kNm/m bending moment resulted in a mere 4.13mm eccentricity. Based on this, the geometry as defined was deemed at an acceptable level of accuracy for the purpose of this investigation.

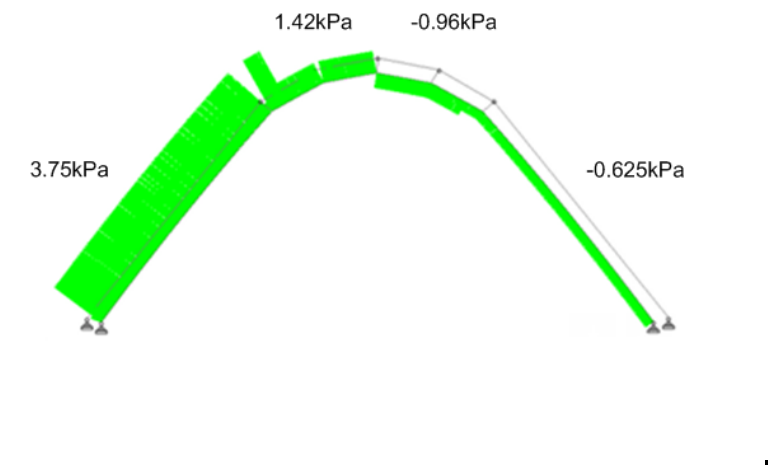
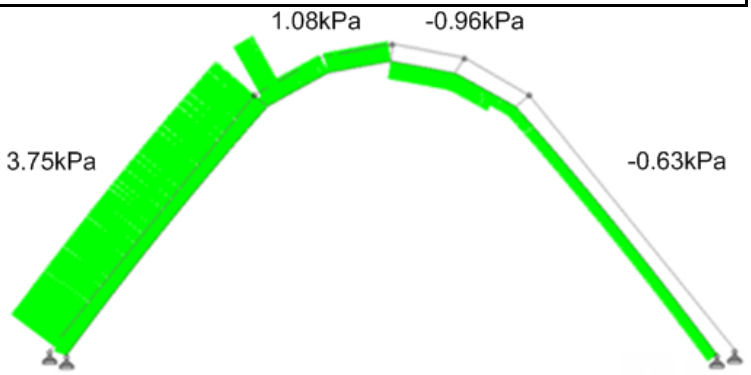
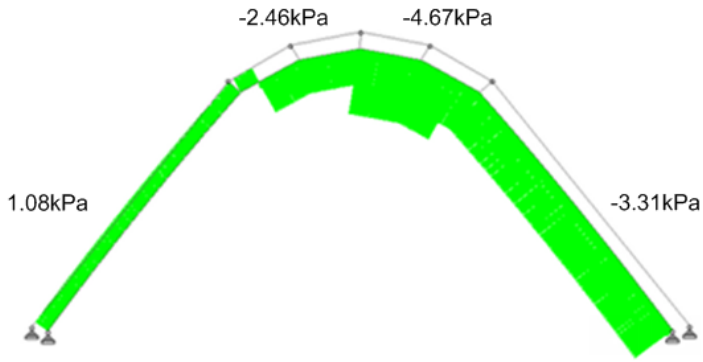
A decrease in the force eccentricity with a decrease in the tendon stress was expected. A reason for this forecast was because of the fact that imperfections of the model was found to be more visible with excessive post-tension load applications.

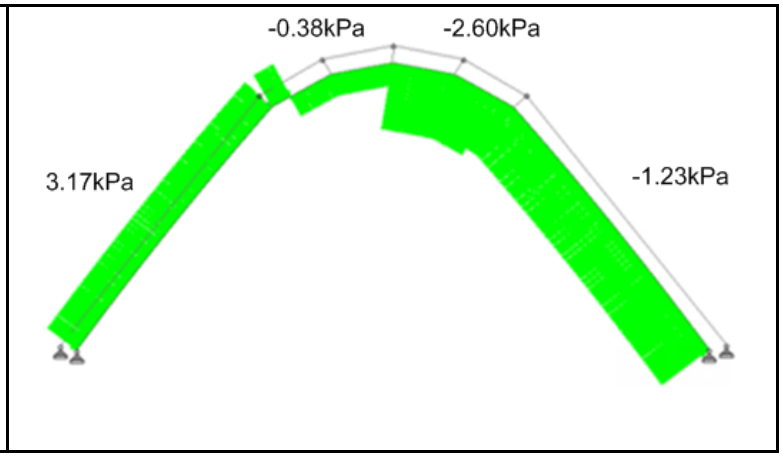
Complete Post-tensioning A drastic post-tension solution would be to design the effective post-tension force to be of a high enough magnitude to eliminate all tension in the section. Theoretically this may be a viable solution, but secondary considerations such as; buckling of the section, bearing resistance of the tendon supports and the cost of post-tensioning will come into play. If one or more of these secondary considerations becomes cumbersome, the design was not considered practical.

Wind load considerations The wind loads applied to the structure was as recorded in Table 12 and the effective post-tension force assumed in the analysis was 85kN. These loads are visually represented in Table 18.

Table 18: Visual illustration of load combination (StaadPro V8i FEA model) for a five point contact post-tensioned vault.

Load Combination	Model view of applied loads
LC1	
LC2	

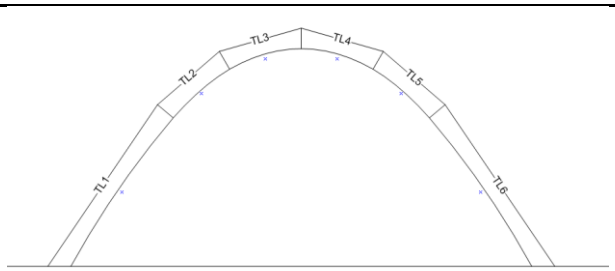
LC3	1.42kPa -0.96kPa 3.75kPa -0.625kPa
LC4	1.08kPa -0.96kPa 3.75kPa -0.63kPa
LC5	-2.46kPa -4.67kPa 1.08kPa -3.31kPa

LC6	

Results interpretation The tendon support loads for an initially applied 85kN post-tension force in the dominant load condition is illustrated in Figure 3.64. The effective tendon forces are recorded in Table 19 for all relevant load combinations.

It was evident that the tendon support loads were indeed relatively close to one another at ± 30kN, as previously assumed. The tendon support loads, however, varied marginally for each load combination considered. These changes are recorded in Table 20 and insignificantly small. The small tendon support forces suggested that very little structural deformation was present. This was confirmed by viewing the displacement of the structure for all the considered load conditions. Small deformation of the structure was considered highly favourable, as the FLPC should preferably remain within the kern of the section. The smallest movement of the FLPC or geometry resulted in the generation of unfavourable secondary bending moments.

Table 19: Tendon loads for different load combination of five point post-tension vault for no tension allowed in 300kph wind load condition.

Load combination	 Tendon load (kN)					
Tendon No	**TL1**	**TL2**	**TL3**	**TL4**	**TL5**	**TL6**
Dominant	79.85	85.04	90.02	89.11	84.20	79.28
LC1	79.85	85.04	90.02	89.11	84.20	79.28
LC2	79.85	85.04	90.02	89.11	84.20	79.28
LC3	79.85	85.04	90.02	89.11	84.20	79.28
LC4	79.85	85.04	90.02	89.11	84.20	79.28
LC5	79.85	85.04	90.02	89.11	84.20	79.28
LC6	79.85	85.04	90.02	89.11	84.20	79.28

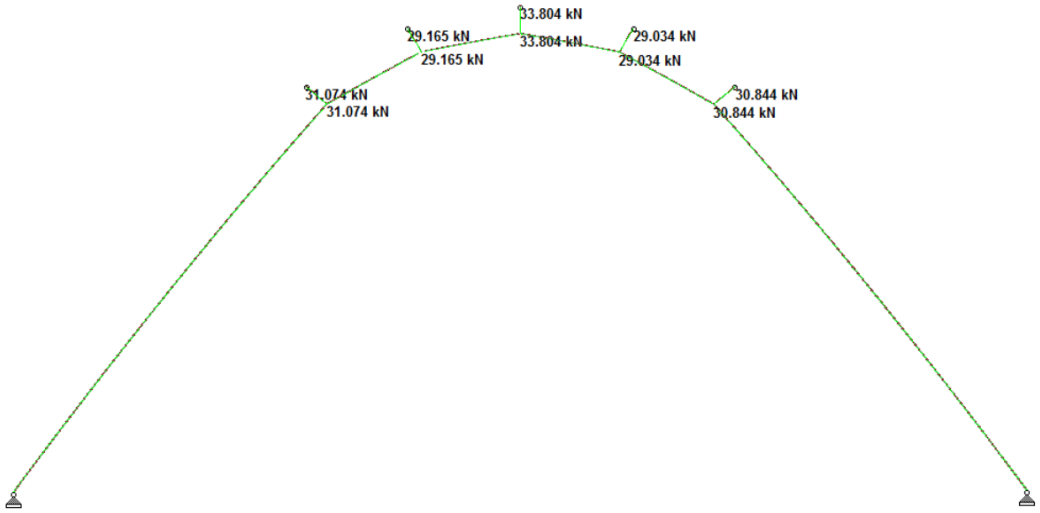
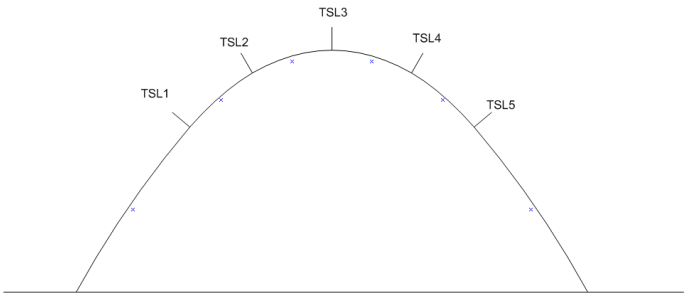


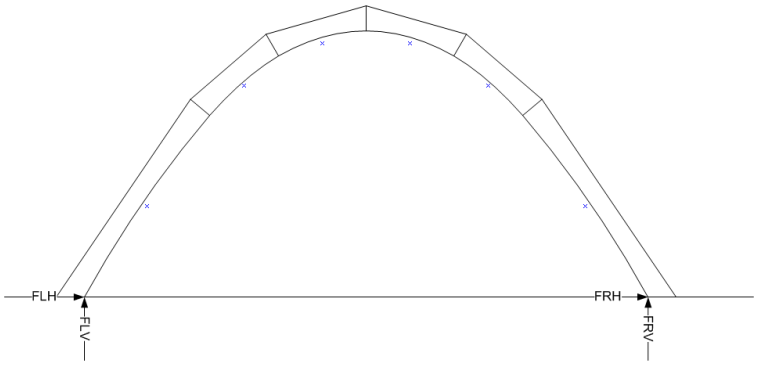
Figure 3.64: Five point contact post-tensioned vault (StaadPro V8i model) tendon support loads for no tension allowed in 300kph wind load condition.

Table 20: Tendon support loads for different load combination of five point post-tension vault for no tension allowed in 300kph wind load condition.

Load combination	 Tendon support load (kN)				
Tendon support No	**TSL1**	**TSL2**	**TSL3**	**TSL4**	**TSL5**
Dominant	31.07	29.17	33.80	29.03	30.84
LC1	31.08	29.17	33.80	29.04	30.85
LC2	31.08	29.17	33.80	29.04	30.85
LC3	31.07	29.17	33.80	29.03	30.84
LC4	31.07	29.17	33.80	29.03	30.84
LC5	31.08	29.17	33.81	29.04	30.85
LC6	31.07	29.17	33.80	29.04	30.85

The foundation reactions were, as expected, relatively high. The supports in the model were defined such that only translational fixity was applicable, hence only vertical and horizontal reactions were recorded for each load combination considered. The changes in the foundation loads were marginal as a result of the high post-tension force. It should furthermore be noted that no foundation uplift is expected during a hurricane load condition based on these results.

Table 21: Foundation loads for five point contact post-tensioned vault where no tension is allowed in 300kph wind load condition.

Load combination				
	FLH (→)	**FLV (↑)**	**FRH (→)**	**FRV (↑)**
Dominant	59.77	80.64	-59.54	80.14
LC1	59.71	80.62	-59.58	80.10
LC2	59.71	80.62	-59.58	80.10
LC3	59.72	80.68	-59.59	80.16
LC4	59.72	80.67	-59.59	80.16
LC5	59.70	80.60	-59.57	80.08
LC6	59.71	80.65	-59.58	80.13

Conclusions For an average post-tension force of 85kN, no tension developed in the section under any of the load combinations considered. It was found that the maximum compressive stress in the section was 0.402MPa and for this structural configuration equal to 100.4kN/m compressive force. The required effective tendon force was, however, deemed excessive and required more investigation.

Partial Post-tensioning of 250mm Shell Section As a second consideration, a partial post-tension configuration of the vault was adopted.

Modelling Considerations The model, as defined under *Complete Post-tensioning,* was used to determine a ball park figure of the magnitude for the required effective post-tension force. By iterating through the geometry modifications, informed by changes in the tendon support loads, the magnitude of the required effective post-tension force was determined. Convergence of the bending moment in the dominant load condition was observed from the 8th iteration at 0.09kNm/m with a maximum compressive force of 40.07kN/m. This configuration yielded a force eccentricity of 2.2mm from the geometric centroid of the section and was deemed negligible.

The structure was subjected to the following load conditions in order to evaluate the critical forces and stresses within its structural elements:

1. Service wind loads.
2. Wind loads factored to SANS 10160-1:2011 ($\gamma_w = 1.3$ & $\gamma_{sw} = 0.9$).
3. 300kph wind loads.

The section should resist bending moments, resulting from service and ultimate limit state load conditions, in the absence of crack development. Cracking of the section was allowed under hurricane wind load conditions, but catastrophic failure was considered unacceptable.

Service wind load conditions Figure 3.65 depicts the configuration of the vault under discussion. It should be noted that the vault's legs were curvier than that of the post-tensioned vault configured to resist a 300kph wind load in pure compression as depicted in Figure 3.62. This observation was due to a lesser requirement for post-tension force. As a result, gravity played a bigger role in defining the catenary geometry of the vault and the curvature tended to look more like that of a traditional catenary vault.

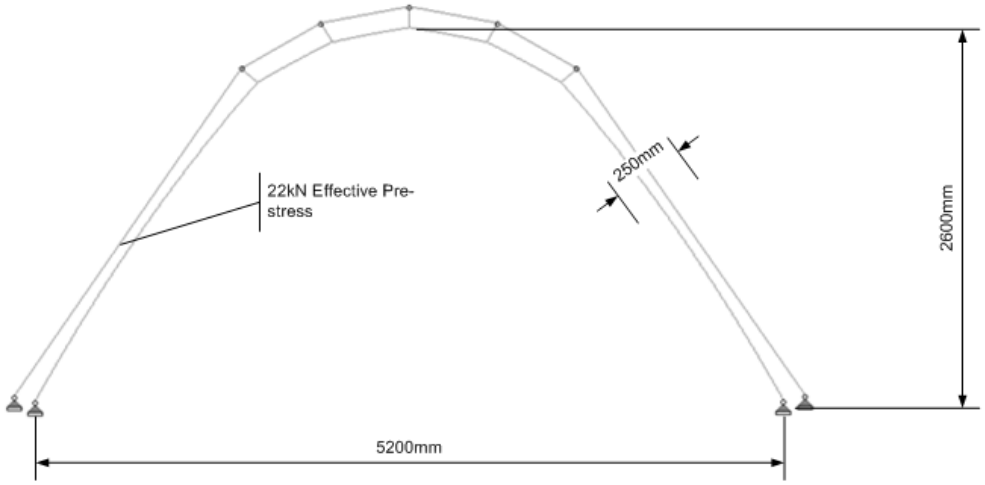


Figure 3.65: 250mm thick vault post-tensioned to 22kN effective post-tensioning.

From Table 22, it was evident that the variation of the force in the different tendon sections was higher than that recorded in Table 19. This was an expected result, as the tendon force required to decompress the section as discussed here, was significantly lower than the post-tension force required to completely decompress the section for all load conditions considered. An effective post-tension force of 22kN was required in this configuration.

The tendon support loads resulting from this configuration are recorded in Table 23

Table 22: Tendon loads for different load combination of five point post-tension vault for no tension allowed in service wind load condition - 22kN effective post-tensioning.

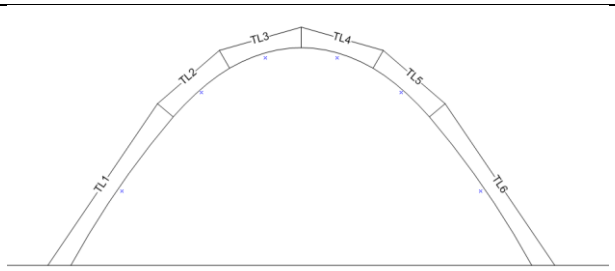
Load combination	 Tendon load (kN)					
Tendon No	**TL1**	**TL2**	**TL3**	**TL4**	**TL5**	**TL6**
Dominant	20.17	21.41	22.85	22.39	21.41	20.22
LC1	20.18	21.43	22.87	22.41	21.42	20.24
LC2	20.19	21.43	22.87	22.41	21.42	20.24
LC3	20.20	21.44	22.88	22.42	21.43	20.25
LC4	20.20	21.44	22.88	22.42	21.44	20.25
LC5	20.19	21.44	22.88	22.42	21.43	20.24
LC6	20.21	21.45	22.89	22.43	21.44	20.26
Max	**20.21**	**21.45**	**22.89**	**22.43**	**21.44**	**20.26**

Figure 3.66 is a graphical representation of the location of the tendon support loads on the vault's shell. The data obtained from Figure 3.66 coincides with the support loads in the dominant load case as captured in Table 23. This indicates that the forces listed in the table reads from the left-to-right tendon support in the figure.

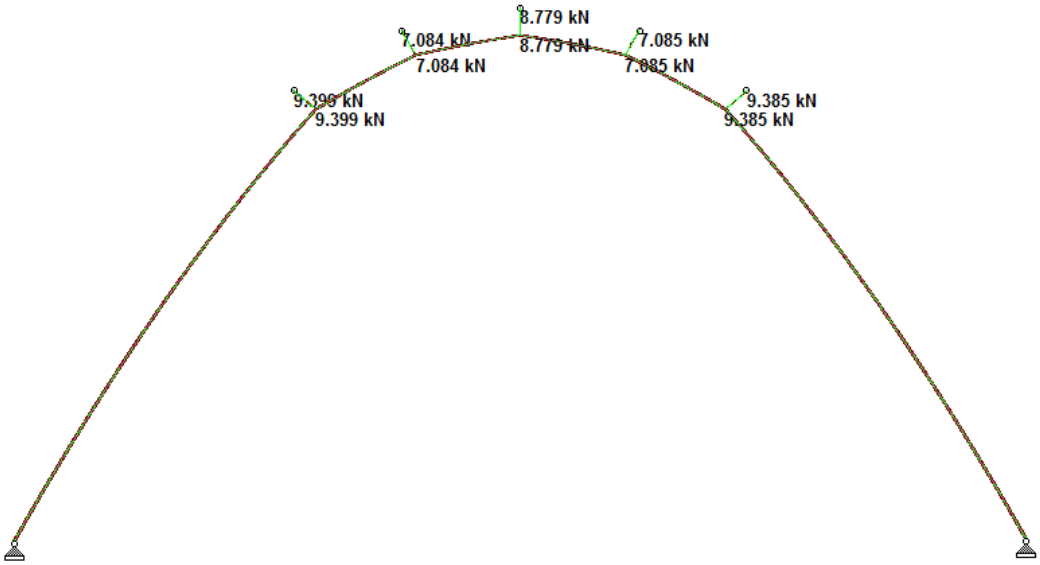


Figure 3.66: Five point contact post-tensioned vault (StaadPro V8i model) tendon support loads for no tension allowed in service wind load condition - 22kN effective post-tensioning.

The foundation support loads as recorded in Table 24 suggested that no uplift of the structure was evident under an un-factored wind load condition. These support loads were also more manageable than that recorded in Table 21.

Table 23: Tendon support loads for different load combination of five point post-tension vault for no tension allowed in service wind load condition - 22kN effective post-tensioning.

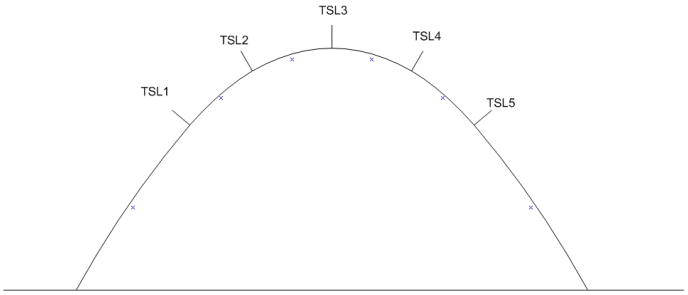
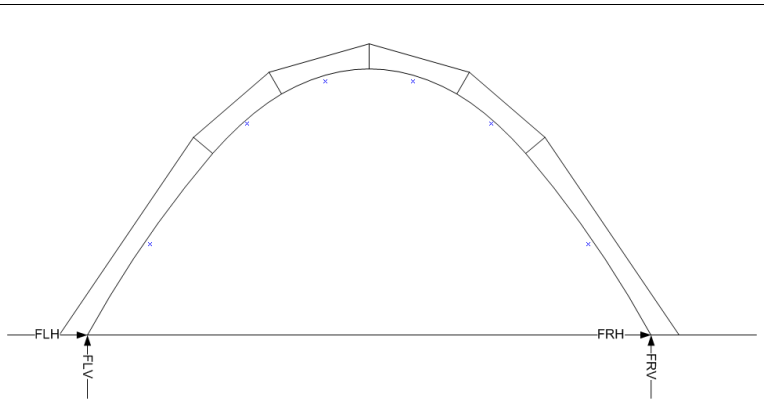
Load combination	 Tendon support load (kN)				
Tendon support No	**TSL1**	**TSL2**	**TSL3**	**TSL4**	**TSL5**
Dominant	9.40	7.08	8.78	7.09	9.39
LC1	9.40	7.09	8.78	7.09	9.39
LC2	9.41	7.09	8.79	7.09	9.39
LC3	9.41	7.09	8.79	7.09	9.40
LC4	9.41	7.09	8.79	7.09	9.40
LC5	9.41	7.09	8.79	7.09	9.40
LC6	9.41	7.10	8.79	7.10	9.40
Max	**9.41**	**7.10**	**8.79**	**7.10**	**9.40**

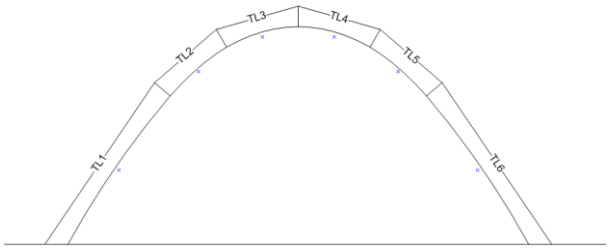
Table 24: Foundation loads for five point contact post-tensioned vault where no tension is allowed for service wind load condition - 22kN effective post-tensioning.

Load combination				
	FLH (→)	**FLV (↑)**	**FRH (→)**	**FRV (↑)**
Dominant	19.62	34.94	-19.63	34.87
LC1	18.20	34.41	-20.61	34.28
LC2	18.19	34.38	-20.58	34.25
LC3	18.32	35.63	-20.74	35.50
LC4	18.31	35.60	-20.70	35.47
LC5	18.01	33.85	-20.42	33.72
LC6	18.13	35.07	-20.54	34.94
Max	**19.62**	**35.63**	**-20.74**	**35.50**

The maximum bending moment in the section was 1.37kNm/m at a maximum axial force of 32.84kN/m. This resulted in a force eccentricity of 41.69mm, a maximum compressive stress of 0.23MPa and a maximum tensile stress of 0.00MPa. An absolute maximum compressive force of 40.07kN/m was recorded in the dominant load condition.

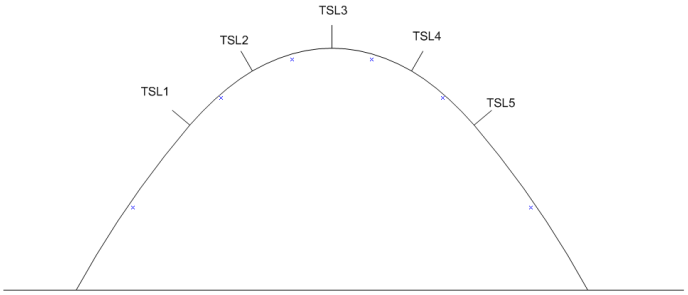
Ultimate limit state wind load conditions In the preceding discussion it was proven that a 22kN effective post-tension force resulted in no tension in the vault's section when subjected to service wind load conditions, as recorded in Table 11. It was of interest to determine the forces and stresses in the structure when these wind loads were factored by a partial load factor for wind and self-weight of 1.3 and 0.9 respectively. The structure may then be designed to resist these forces in the ultimate limit state and ensure that no cracking of the shell is expected.

Table 25: Tendon loads for different load combination of five point post-tension vault for no tension allowed in ultimate wind load condition - 22kN effective post-tensioning.

Load combination	 **Tendon load (kN)**					
Tendon No	**TL1**	**TL2**	**TL3**	**TL4**	**TL5**	**TL6**
Dominant	20.17	21.41	22.85	22.39	21.41	20.22
LC1	20.21	21.45	22.89	22.43	21.45	20.26
LC2	20.21	21.45	22.89	22.44	21.45	20.26
LC3	20.22	21.47	22.91	22.45	21.46	20.27
LC4	20.22	21.47	22.91	22.45	21.46	20.28
LC5	20.22	21.46	22.90	22.45	21.46	20.27
LC6	20.22	21.46	22.90	22.44	21.45	20.27
Max	**20.22**	**21.47**	**22.91**	**22.45**	**21.46**	**20.28**

Marginal differences in the tendon force over the different load combinations were noticeable and recorded in Table 25. The tendon support loads, as recorded in Table 26, suggested that marginal deflection of the structure was present. This observation was considered favourable, as vaults are sensitive to structural deformation (Allan *et al.*, 2010).

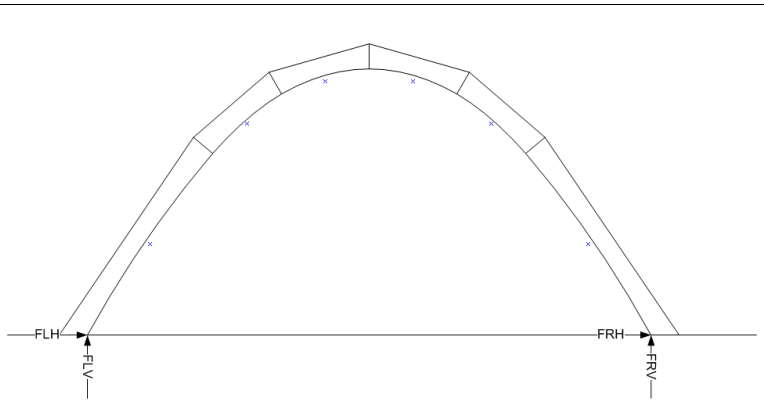
Table 26: Tendon support loads for different load combinations of five point post-tension vault for no tension allowed in ultimate wind load condition - 22kN effective post-tensioning.

Load combination	 **Tendon support load (kN)**				
Tendon support No	**TSL1**	**TSL2**	**TSL3**	**TSL4**	**TSL5**
Dominant	9.40	7.08	8.78	7.09	9.39
LC1	9.41	7.10	8.79	7.10	9.40
LC2	9.42	7.10	8.80	7.10	9.40
LC3	9.42	7.10	8.80	7.10	9.41
LC4	9.42	7.10	8.80	7.10	9.41
LC5	9.42	7.10	8.80	7.10	9.41
LC6	9.42	7.10	8.80	7.10	9.41
Max	**9.42**	**7.10**	**8.80**	**7.10**	**9.41**

By interpreting the foundation loads, it was found that no foundation uplift was applicable. A noticeable difference in the Cartesian components of

the foundation loads were, however, observed as recorded in Table 27. The maximum bending moment in the shell was 1.70kNm/m at a maximum compressive force of 31.86kN/m. This resulted in a 53.20mm eccentricity, a maximum compressive stress of 0.27MPa and a maximum tensile stress of 0.04MPa in the section. It was furthermore important to note that the tension stress in the section was a result of flexure and not uniform axial tension.

Table 27: Foundation loads for five point contact post-tensioned vault where no tension is allowed for ultimate wind load condition - 22kN effective post-tensioning.

Load combination				
	FLH (→)	**FLV (↑)**	**FRH (→)**	**FRV (↑)**
Dominant	19.62	34.94	-19.63	34.87
LC1	16.96	32.43	-20.09	32.29
LC2	16.94	32.40	-20.04	32.24
LC3	17.11	34.02	-20.25	33.87
LC4	17.09	33.98	-20.20	33.83
LC5	16.71	31.70	-19.84	31.55
LC6	17.68	35.11	-20.82	34.96
Max	**19.62**	**35.11**	**-20.82**	**34.96**

Hurricane wind load conditions It was previously proven that the vault under discussion will resist dominant and service loads in pure compression. It was furthermore proven that, under the ultimate limit state condition, the section was not over stressed, but that bending moments do occur. In this section, the structure was subjected to hurricane wind load parameters.

From the analysis, it was found that significant bending moments were generated in the vault's shell. The tendon and tendon support loads showed marginal changes in magnitude over the different load combinations. These results are recorded in Table 28 and Table 29.

The foundation loads, as recorded in Table 30, suggested marginal changes which are not deemed of concern.

Table 28: Tendon loads for different load combination of five point load post-tension vault for no tension in 300kph wind load condition -- 22kN effective post-tensioning.

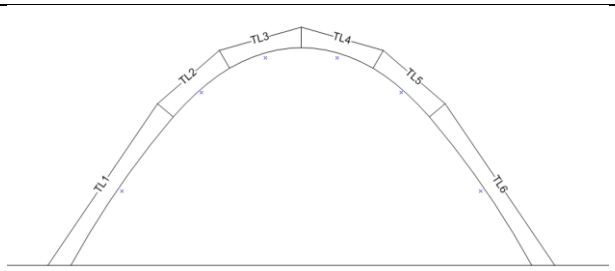
Load combination	 Tendon load (kN)					
Tendon No	**TL1**	**TL2**	**TL3**	**TL4**	**TL5**	**TL6**
Dominant	20.17	21.41	22.85	22.39	21.41	20.22
LC1	20.23	21.47	22.91	22.45	21.46	20.28
LC2	20.24	21.48	22.92	22.46	21.47	20.28
LC3	20.28	21.53	22.98	22.52	21.52	20.33
LC4	20.29	21.54	22.99	22.53	21.53	20.34
LC5	20.27	21.51	22.96	22.50	21.51	20.31
LC6	20.32	21.57	23.02	22.56	21.56	20.37
Max	**20.32**	**21.57**	**23.02**	**22.56**	**21.56**	**20.37**

Table 29: Tendon support loads for different load combinations of five point post-tension vault for no tension in 300kph wind load condition - 22kN effective post-tensioning.

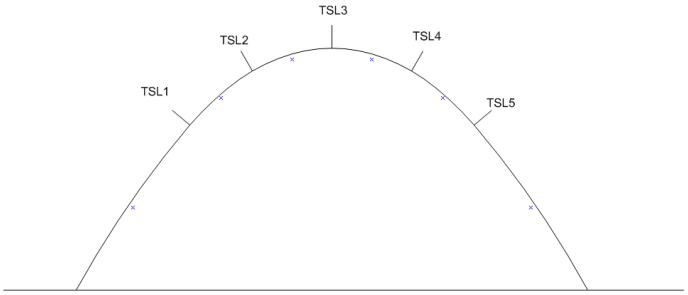
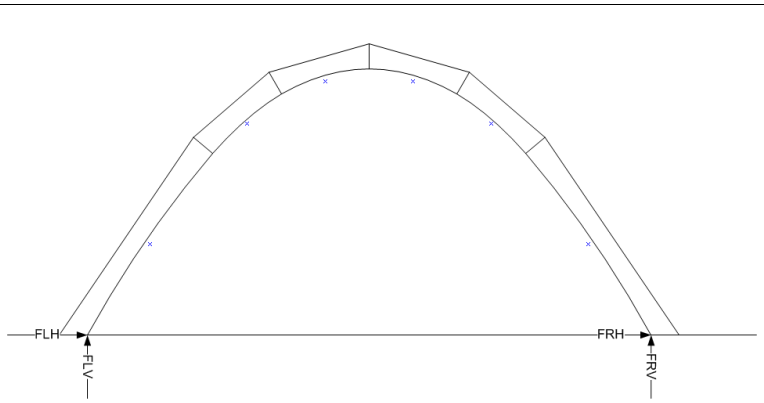
Load combination	 Tendon support load (kN)				
Tendon support No	**TSL1**	**TSL2**	**TSL3**	**TSL4**	**TSL5**
Dominant	9.40	7.08	8.78	7.09	9.39
LC1	9.42	7.10	8.80	7.10	9.41
LC2	9.43	7.11	8.81	7.11	9.42
LC3	9.45	7.12	8.83	7.12	9.44
LC4	9.45	7.13	8.83	7.13	9.44
LC5	9.44	7.12	8.82	7.12	9.43
LC6	9.46	7.14	8.84	7.14	9.46
Max	**9.46**	**7.14**	**8.84**	**7.14**	**9.46**

Table 30: Foundation loads for five point contact post-tensioned vault where no tension is allowed for 300kph wind load condition - 22kN effective post-tensioning.

Load combination				
	FLH (→)	**FLV (↑)**	**FRH (→)**	**FRV (↑)**
Dominant	19.62	34.94	-19.63	34.87
LC1	13.55	32.41	-24.02	32.22
LC2	13.21	32.45	-23.88	32.06
LC3	13.80	38.04	-24.58	37.69
LC4	13.74	37.92	-24.43	37.53
LC5	12.41	30.06	-23.17	29.70
LC6	12.94	35.53	-23.72	35.16
Max	**19.62**	**38.04**	**-24.58**	**35.16**

Under hurricane loads, the absolute bending moment in the section was determined as 5.84kNm/m with a maximum compressive force of 32.49kN/m. This yielded a force eccentricity of 179.78mm which was considered significant. The stress state of the section suggested a maximum compressive stress of 0.60MPa and a maximum tensile stress of 0.43MPa.

Conclusion This analysis proved that a 250mm thick vault can be optimised to resists its self-weight and service wind loads in pure compression at a practical 22kN post-tension force. Under the ultimate limit state, forces and stress distribution in the structure seemed manageable. Significant bending moments were generated when the structure was subjected to hurricane wind loads.

Under Section 4.4.1, a structural design on the shell will be discussed. It will be proven there that the selected shell thickness in this section resulted in adequate moment and axial capacity for the service and ultimate limit state, but failed to provide adequate resistance under hurricane wind load conditions.

Partial Post-tensioning of 335mm Shell Section As a 250mm section proved to fail during a limit state structural design, the section thickness and post-tension force previously assumed was revised. As a start, it was deemed intuitive to increase the shell thickness of the vault in order to increase the internal lever arm of the section. This resulted in an increased cracking moment resistance.

The analysis suggested that a vault of 335mm shell thickness can withstand the dominant and service load condition in pure compression at a mere 13kN of post-tension force. The effects of this configuration under the ultimate and hurricane load conditions had to be investigated. This discussion can be read in conjunction with the discussion on the structural design of the section in Section 4.4.2.

Geometry refinement The geometry of the vault was refined by the same procedure as discussed in section 3.5.2 under *Geometry Refinement,* and is depicted in Figure 3.67. At the 7^{th} iteration, convergence of the bending moment in the dominant load case was observed. The modifications that were implemented are:

1. An increase of the shell thickness from 250mm to 335mm.

2. A decrease of the post-tension force to 13kN.

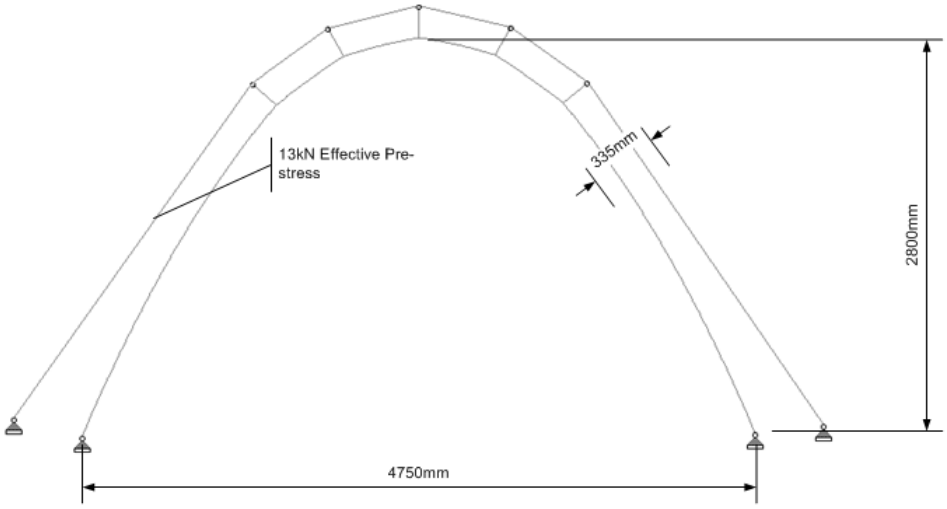


Figure 3.67: 335mm thick vault post-tensioned to 13kN effective post-tensioning.

By iteration, it was determined that a minimum effective post-tension of 13kN yielded pure compression in the vault's shell under the dominant and service load condition. It should be noted that the bending moment's magnitude did still suggest a marginal decline at the 7th iteration, but was however deemed insignificantly small. As a result, it was decided that a 0.12kNm/m bending moment in the dominant load condition resulted in adequate reliability of the model.

At an axial compressive force of 21.26kN/m in the dominant load condition, the force eccentricity was determined at 5.5mm. This was found to be well within the boundary of the kern of 55.83mm and suggested pure compression in the section.

Serviceability limit state loads As discussed under *Partial Post-tensioning of 250mm Shell Section,* no tension was allowed to develop under the service wind load conditions. The average tendon force, tendon support loads and foundation loads for this configuration are listed in Table 31, Table 32 and Table 33 respectively.

The maximum bending moment in the section was determined as 1.43kNm/m at an axial compressive force of 27.12kN/m. This resulted in a force eccentricity of 52.76mm which fell within the boundary of the kern. The maximum compressive stress in the section was 0.14MPa while the minimum compressive stress was determined to be 0.00MPa.

Table 31: Tendon loads where no tension is allowed in service wind load condition with 13kN post-tension force.

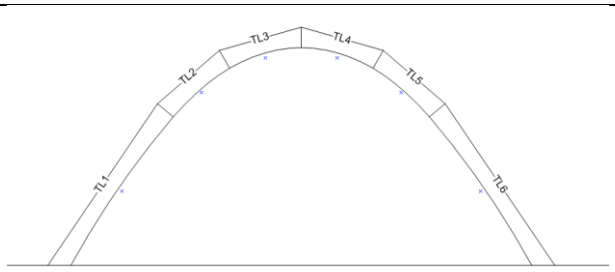
Load combination	 **Tendon load (kN)**					
Tendon No	**TL1**	**TL2**	**TL3**	**TL4**	**TL5**	**TL6**
Dominant	12.25	12.43	12.96	12.82	12.73	12.14
LC1	12.27	12.44	12.98	12.84	12.75	12.15
LC2	12.27	12.44	12.98	12.84	12.75	12.15
LC3	12.28	12.45	12.99	12.85	12.76	12.16
LC4	12.28	12.45	12.99	12.85	12.76	12.16
LC5	12.28	12.45	12.98	12.85	12.75	12.16
LC6	12.29	12.46	12.99	12.86	12.76	12.17
Max	**12.29**	**12.46**	**12.99**	**12.86**	**12.76**	**12.17**

Table 32: Tendon support loads where no tension allowed in service wind load condition with 13kN post-tension force.

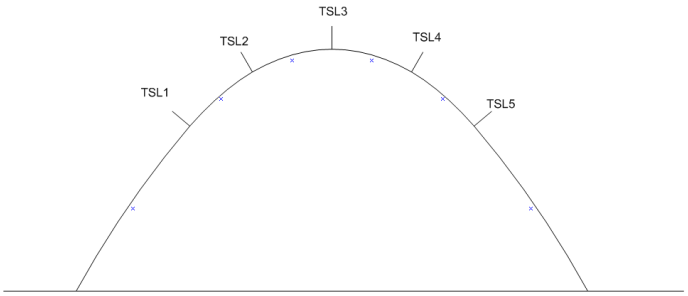
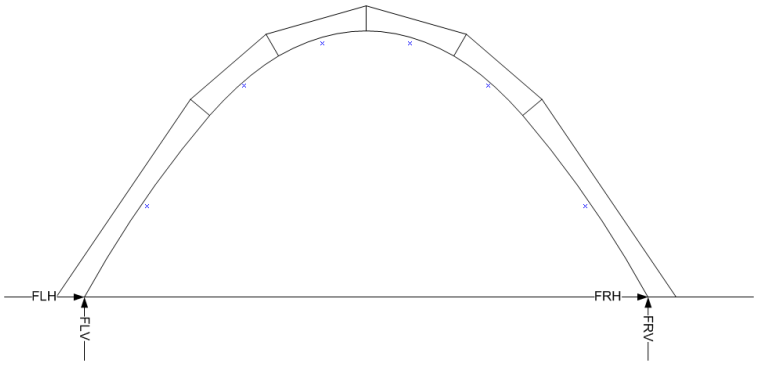
Load combination	 Tendon support load (kN)				
Tendon support No	**TSL1**	**TSL2**	**TSL3**	**TSL4**	**TSL5**
Dominant	3.97	4.97	6.07	4.97	4.26
LC1	3.98	4.98	6.08	4.98	4.27
LC2	3.98	4.98	6.08	4.98	4.27
LC3	3.98	4.98	6.08	4.99	4.27
LC4	3.98	4.98	6.08	4.99	4.27
LC5	3.98	4.98	6.08	4.98	4.27
LC6	3.98	4.98	6.08	4.99	4.27
Max	**3.98**	**4.98**	**6.08**	**4.99**	**4.27**

Table 33: Foundation loads where no tension is allowed in service wind load condition with 13kN post-tension force.

Load combination				
	FLH (→)	**FLV (↑)**	**FRH (→)**	**FRV (↑)**
Dominant	14.79	34.68	-14.56	34.45
LC1	13.37	33.99	-15.71	34.10
LC2	13.37	33.97	-15.68	34.06
LC3	13.31	35.10	-15.65	35.21
LC4	13.30	35.08	-15.62	35.17
LC5	13.30	33.47	-15.60	33.57
LC6	13.20	34.58	-15.54	34.68
Max	**14.79**	**35.10**	**-15.71**	**35.21**

Ultimate limit state loads The forces in the tendons, tendon supports and foundations are listed under Table 37, Table 38 and Table 39 respectively. The maximum bending moment in the shell was recorded as 1.77kNm/m at a maximum axial compressive force of 26.05kN/m. This yielded a force eccentricity of 68mm, which fell outside the perimeter defining the kern of the section. As a result, tension development was observed. The maximum compressive stress in the section was determined as 0.16MPa with a maximum tensile stress of 0.02MPa.

Table 34: Tendon loads for 335mm vault at 13kN post-tension force.

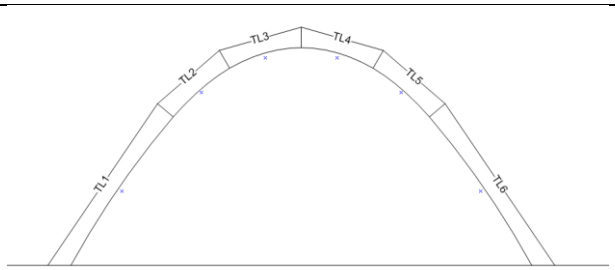
Load combination	 **Tendon load (kN)**					
Tendon No	**TL1**	**TL2**	**TL3**	**TL4**	**TL5**	**TL6**
Dominant	12.25	12.43	12.96	12.82	12.73	12.14
LC1	12.30	12.47	13.01	12.87	12.77	12.18
LC2	12.30	12.47	13.01	12.87	12.78	12.18
LC3	12.31	12.48	13.02	12.88	12.79	12.19
LC4	12.31	12.48	13.02	12.88	12.79	12.19
LC5	12.31	12.48	13.01	12.88	12.78	12.19
LC6	12.30	12.47	13.00	12.87	12.77	12.18
Max	**12.31**	**12.48**	**13.02**	**12.88**	**12.79**	**12.19**

Table 35: Tendon support loads for 335mm vault at 13kN post-tension force.

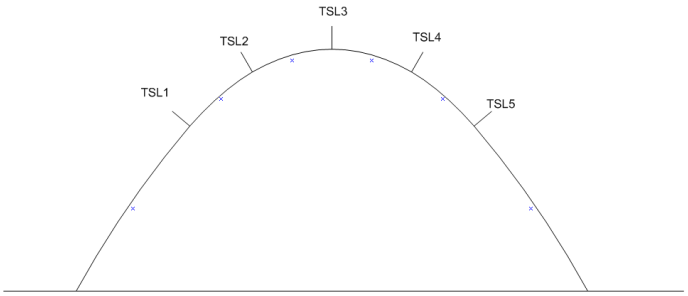
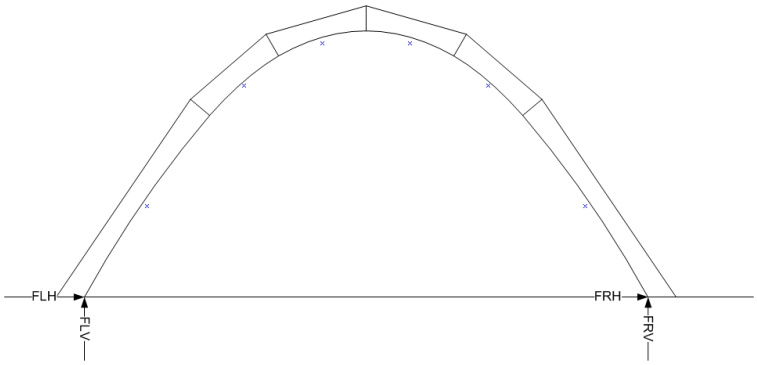
Load combination	 Tendon support load (kN)				
Tendon support No	**TSL1**	**TSL2**	**TSL3**	**TSL4**	**TSL5**
Dominant	3.97	4.97	6.07	4.97	4.26
LC1	3.99	4.99	6.09	4.99	4.28
LC2	3.99	4.99	6.09	4.99	4.28
LC3	3.99	4.99	6.09	5.00	4.28
LC4	3.99	4.99	6.10	5.00	4.28
LC5	3.99	4.99	6.09	5.00	4.28
LC6	3.99	4.99	6.09	4.99	4.28
Max	**3.99**	**4.99**	**6.10**	**5.00**	**4.28**

Table 36: Foundation loads for 335mm vault at 13kN post-tension force.

Load combination				
	FLH (→)	**FLV (↑)**	**FRH (→)**	**FRV (↑)**
Dominant	14.79	34.68	-14.56	34.45
LC1	12.06	31.34	-15.16	31.56
LC2	12.05	31.32	-15.12	31.51
LC3	11.98	32.79	-15.09	33.00
LC4	11.97	32.76	-15.05	32.95
LC5	11.92	30.67	-15.02	30.87
LC6	12.73	34.55	-15.83	34.75
Max	**14.79**	**34.68**	**-15.83**	**34.75**

Hurricane load condition The shell forces for hurricane wind conditions are listed in Table 37, Table 38 and Table 39. With a maximum bending moment of 6.16kNm/m at a maximum axial compressive force of 26.21kN/m, a force eccentricity of 234.8mm was determined. This eccentricity fell outside the boundaries of the kern and suggested relatively high tensile stresses in the section. The maximum compressive stress was determined as 0.36MPa with a maximum tensile stress of 0.25MPa.

Table 37: Tendon loads for final vault configuration where no tension is allowed in hurricane wind load condition with 13kN post-tension force.

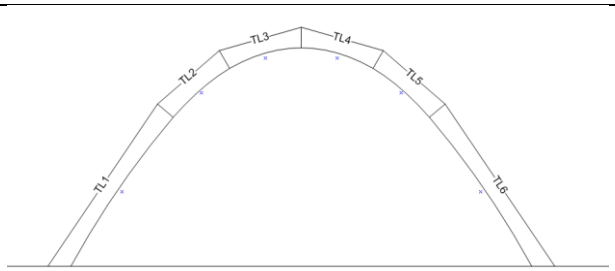
Load combination	 **Tendon load (kN)**					
Tendon No	**TL1**	**TL2**	**TL3**	**TL4**	**TL5**	**TL6**
Dominant	12.25	12.43	12.96	12.82	12.73	12.14
LC1	12.33	12.50	13.04	12.90	12.80	12.21
LC2	12.33	12.51	13.05	12.91	12.81	12.21
LC3	12.37	12.55	13.08	12.95	12.85	12.25
LC4	12.38	12.55	13.09	12.95	12.85	12.25
LC5	12.35	12.53	13.07	12.93	12.83	12.23
LC6	12.40	12.57	13.11	12.97	12.87	12.27
Max	**12.40**	**12.57**	**13.11**	**12.97**	**12.87**	**12.27**

Table 38: Tendon support loads for final vault configuration for no tension allowed in hurricane wind load condition with 13kN post-tension force.

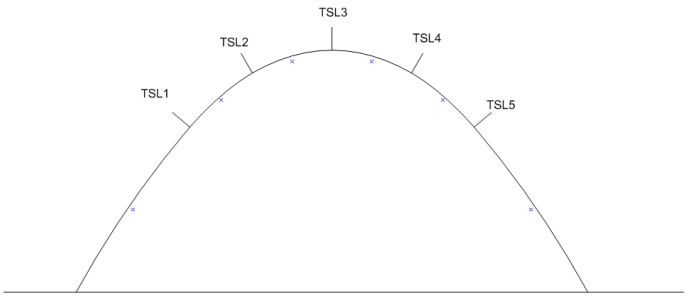
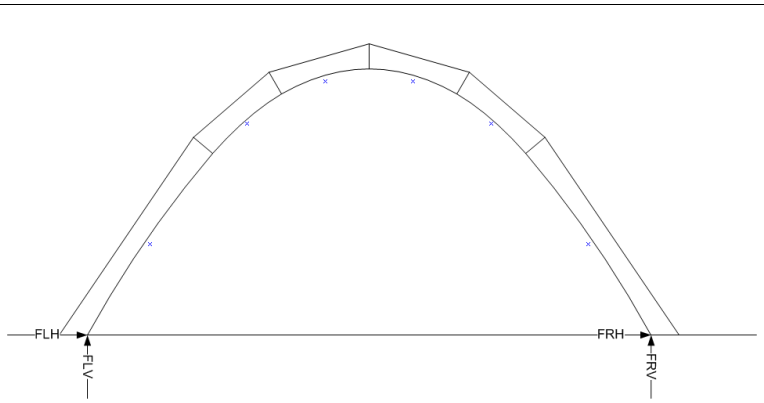
Load combination	 **Tendon support load (kN)**				
Tendon support No	**TSL1**	**TSL2**	**TSL3**	**TSL4**	**TSL5**
Dominant	3.97	4.97	6.07	4.97	4.26
LC1	4.00	5.00	6.10	5.00	4.29
LC2	4.00	5.00	6.11	5.01	4.29
LC3	4.01	5.02	6.12	5.02	4.30
LC4	4.01	5.02	6.13	5.02	4.31
LC5	4.00	5.01	6.12	5.01	4.30
LC6	4.02	5.03	6.14	5.03	4.31
Max	**4.02**	**5.03**	**6.14**	**5.03**	**4.31**

Table 39: Foundation loads for final vault configuration where no tension is allowed for hurricane wind load condition with 13kN post-tension force.

Load combination				
	FLH (→)	**FLV (↑)**	**FRH (→)**	**FRV (↑)**
Dominant	14.79	34.68	-14.56	34.45
LC1	8.75	31.47	-19.69	32.87
LC2	8.43	31.50	-19.56	32.70
LC3	8.16	36.57	-19.45	37.86
LC4	8.13	36.47	-19.30	37.68
LC5	7.98	29.26	-19.20	30.50
LC6	7.68	34.23	-18.94	35.47
Max	**14.79**	**36.57**	**-19.69**	**37.86**

Conclusion The simultaneous effect of increasing the shell thickness to 335mm and decreasing the effective post-tension force to 13kN was investigated. By manual calculation it was found that this configuration yielded an inadequate cracked moment capacity of the section. The reader may refer to Appendix B.2 for the full set of manual calculations and Section 4.4.2 for a discussion on the result of the structural design.

The results of the analysis are listed in Table 40. It was noted that a reduction in the section capacity was observed compared to the same section subjected to a 22kN post-tension force. A comparison of the section capacity, based on section thickness and post-tension force, is listed in Table 41.

A significant increase in the axial compressive resistance capacity, un-cracked bending moment capacity and cracked bending moment capacity was observed for a 335mm section post-tensioned to an effective post-tension force of 22kN. By reducing the post-tension force to 13kN, a reduction of the moment resisting parameters was observed, which yielded a failure of the section in the hurricane wind load condition.

The effect of the post-tension force on the section's moment capacity was however expected, as an increase in the post-tension force resulted in a reduction of the force eccentricity. The section was therefore able to adequately resist service loads in pure compression, and ultimate loads in the absence of cracking, but catastrophically failed under hurricane wind load conditions. It was found that, should the structure be optimised to a section thickness of 335mm at a post-tension force of 13kN, pure compression in the service load condition will prevail while catastrophic failure is expected to occur during a hurricane.

Table 40: Section capacity vs applied forces for 335mm effective shell thickness at 13kN post-tension force.

SECTION CAPACITY		SERVICE FORCES		ULTIMATE FORCES		ABSOLUTE FORCES	
Force description	**Magnitude**	**Force description**	**Magnitude**	**Force description**	**Magnitude**	**Force description**	**Magnitude**
Design compressive resistance	**421.14kN/m**	Absolute axial compression	**42.44kN/m**	Absolute axial compression	**42.44kN/m**	Absolute axial compression	**42.44kN/m**
Un-cracked moment capacity parallel to bed joints	**2.58kNm/m**	Service moment	**1.43kNm/m**	Ultimate moment	**1.77kNm/m**	Absolute Moment	**6.15kNm/m**
Un-cracked moment capacity perpendicular to bed joints	**4.72kNm/m**	Service moment	**1.43kNm/m**	Ultimate moment	**1.77kNm/m**	Absolute Moment	**6.15kNm/m**
Cracked moment	**4.14kNm/m**	Service moment	**1.43kNm/m**	Ultimate	**1.77kNm/m**	Absolute	**6.15kNm/m**

capacity				moment		Moment	

Table 41: Summary of section capacity for different structural parameters.

Section Capacity	**250mm section with 22kN post-tension force**	**335mm section with 22kN post-tension force**	**335mm section with 13kN post-tension force**
Design compressive resistance	314.3kN/m	421kN/m	421kN/m
Un-cracked moment capacity parallel to bed joints	1.96kNm/m	3.25kNm/m	2.58kNm/m
Un-cracked moment capacity perpendicular to bed joints	3.15kNm/m	5.39kNm/m	4.72kNm/m
Cracked moment capacity	3.68kNm/m	5.94kNm/m	4.14kNm/m

Partial Post-tensioning of 350mm Shell Section After trial and error, it was found that a shell thickness of 350mm in conjunction with an effective post-tension force of 25kN will result in a suitable solution. It is important to note that both the shell thickness and post-tension force played a significant role in the section's force resistance capacity. It was therefore possible to have a combination of a low post-tension force and a thick shell section, which resulted in a section that complied with the design requirements. On the other hand, a thinner shell section may have been utilised with a higher post-tension force and similar results may have been obtained.

Finding a balance between the two parameters was however considered key. It was therefore important to ensure that neither of the two parameters became excessively large. In other words, it had to be ensured to have a practical shell thickness at a practical tendon post-tension force. An example of such a configuration is illustrated in Figure 3.68.

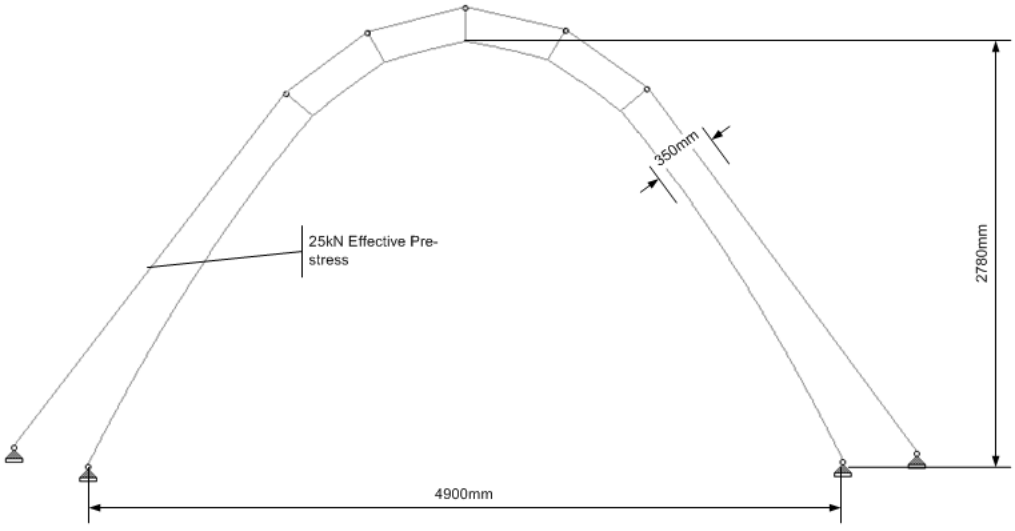


Figure 3.68: 350mm thick vault post-tensioned to 25kN effective post-tensioning.

Serviceability limit state loads For service wind load conditions, the tendon, tendon supports and foundation loads are listed in Table 42 through Table 44. A maximum bending moment of 1.46kNm/m was determined at an axial compressive force of 39.40kN/m. This yielded a force eccentricity of 37mm which fell within the boundary of the kern of 58.33mm. The section was therefore found to be in pure compression.

The maximum compressive stress in the shell was 0.2MPa with a minimum compressive stress of 0.02MPa.

Table 42: Tendon loads for 350mm vault with 25kN post-tension.

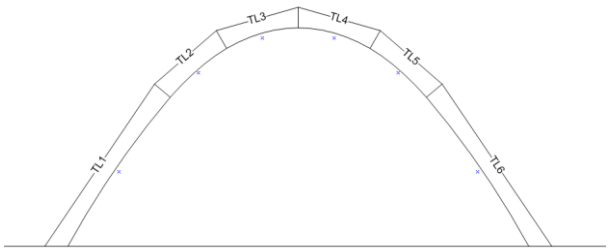
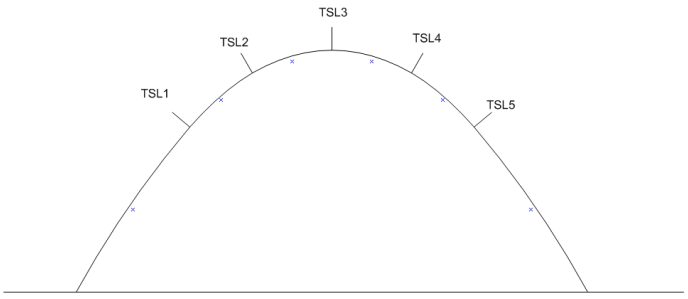
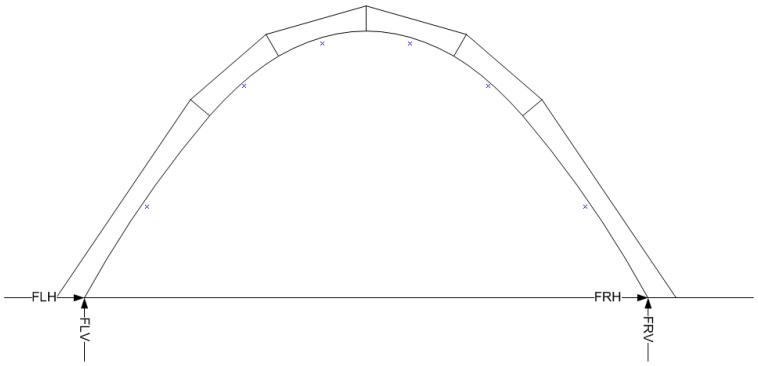
Load combination	 Tendon load (kN)					
Tendon No	**TL1**	**TL2**	**TL3**	**TL4**	**TL5**	**TL6**
Dominant	23.91	24.37	25.35	25.14	24.21	23.38
LC1	23.93	24.39	25.37	25.16	24.22	23.40
LC2	23.93	24.39	25.37	25.16	24.22	23.40
LC3	23.93	24.39	25.37	25.16	24.22	23.40
LC4	23.93	24.39	25.37	25.16	24.22	23.40
LC5	23.93	24.39	25.37	25.17	24.23	23.40
LC6	23.94	24.39	25.38	25.17	24.23	23.40
Max	**23.94**	**24.39**	**25.38**	**25.17**	**24.23**	**23.40**

Table 43: Tendon support loads for 350mm vault with 25kN post-tension.

Load combination	 Tendon support load (kN)				
Tendon support No	**TSL1**	**TSL2**	**TSL3**	**TSL4**	**TSL5**

Dominant	6.49	9.74	11.97	9.72	7.35
LC1	6.50	9.75	11.98	9.72	7.36
LC2	6.50	9.75	11.98	9.72	7.36
LC3	6.50	9.75	11.98	9.72	7.36
LC4	6.50	9.75	11.98	9.72	7.36
LC5	6.50	9.75	11.98	9.73	7.36
LC6	6.50	9.75	11.99	9.73	7.36
Max	**6.50**	**9.75**	**11.99**	**9.73**	**7.36**

Table 44: Foundation loads for 350mm vault with 25kN post-tension.

Load combination				
	FLH (→)	**FLV (↑)**	**FRH (→)**	**FRV (↑)**
Dominant	22.65	44.86	-22.00	44.24
LC1	21.23	44.23	-23.09	43.80
LC2	21.22	44.21	-23.05	43.76
LC3	21.23	45.38	-23.10	44.94
LC4	21.22	45.36	-23.07	44.90
LC5	21.10	43.70	-22.94	43.25
LC6	21.09	44.85	-22.95	44.40
Max	**22.65**	**45.38**	**-23.10**	**44.94**

Ultimate limit state wind load conditions In the ultimate limit state condition, the maximum bending moment in the shell was found to be 1.77kNm/m. At a maximum compressive force of 38.47kN/m, the force eccentricity was determined to be 46.06mm. This fell within the kern of the section, hence no tension stress developed. The tendon forces, tendon support loads and foundation loads are listed in Table 45 through Table 47 for this load condition. The compressive stress in the section was determined to be 0.18MPa with a minimum value of 0.02MPa.

Table 45: Tendon loads for 350mm vault with 25kN post-tension in ultimate limit state condition.

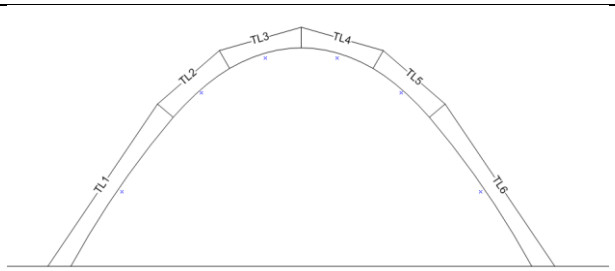
Load combination	 Tendon load (kN)					
Tendon No	**TL1**	**TL2**	**TL3**	**TL4**	**TL5**	**TL6**
Dominant	23.91	24.37	25.35	25.14	24.21	23.38
LC1	23.95	24.41	25.39	25.19	24.25	23.42
LC2	23.96	24.41	25.39	25.19	24.25	23.42
LC3	23.96	24.42	25.40	25.19	24.25	23.42
LC4	23.96	24.42	25.40	25.19	24.25	23.42
LC5	23.96	24.42	25.40	25.19	24.25	23.43
LC6	23.94	24.40	25.38	25.18	24.24	23.41
Max	**23.96**	**24.42**	**25.40**	**25.19**	**24.25**	**23.43**

Table 46: Tendon support loads for 350mm vault with 25kN post-tension in ultimate limit state condition.

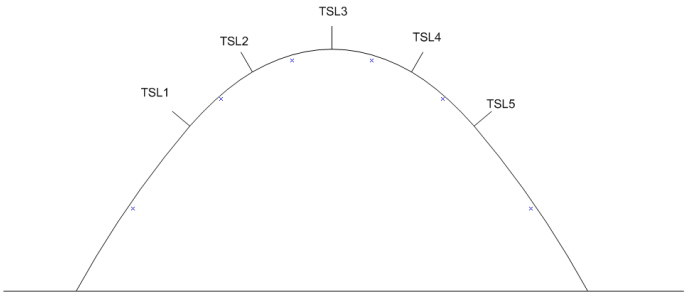
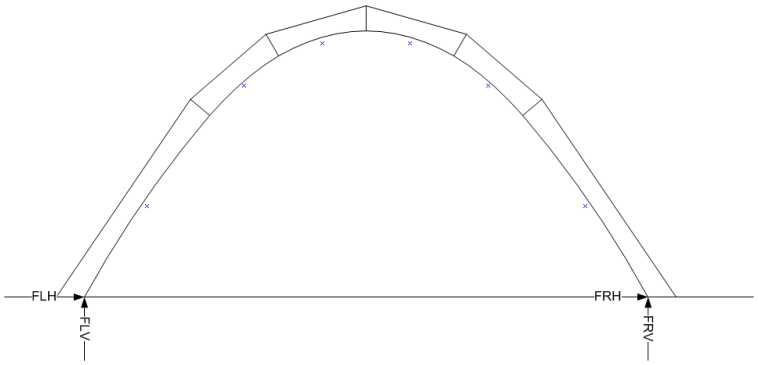
Load combination	 Tendon support load (kN)				
Tendon support No	**TSL1**	**TSL2**	**TSL3**	**TSL4**	**TSL5**
Dominant	6.49	9.74	11.97	9.72	7.35
LC1	6.50	9.76	11.99	9.73	7.37
LC2	6.50	9.76	11.99	9.73	7.37
LC3	6.50	9.76	12.00	9.73	7.37
LC4	6.50	9.76	12.00	9.74	7.37
LC5	6.51	9.76	12.00	9.74	7.37
LC6	6.50	9.76	11.99	9.73	7.36
Max	**6.51**	**9.76**	**12.00**	**9.74**	**7.37**

Table 47: Foundation loads for 350mm vault with 25kN post-tension in ultimate limit state condition.

Load combination				
	FLH (→)	**FLV (↑)**	**FRH (→)**	**FRV (↑)**
Dominant	22.65	44.86	-22.00	44.24
LC1	19.77	41.49	-22.38	41.11
LC2	19.76	41.46	-22.34	41.06
LC3	19.77	42.98	-22.40	42.61
LC4	19.76	42.96	-22.35	42.56
LC5	19.60	40.80	-22.19	40.41
LC6	20.63	44.85	-23.24	44.45
Max	**22.65**	**44.86**	**-23.24**	**44.45**

Hurricane wind load condition The absolute bending moment in the section for this load condition was found to be 6.08kNm/m, at a compressive force of 38.79kN/m. This resulted in a force eccentricity of 156.8mm which fell beyond the boundary of the kern. Tensile stress developed in the section and was at a maximum value of 0.19MPa, while the maximum compressive stress in the section was determined to be 0.36MPa. The tendon forces, tendon support loads and foundation loads are listed in Table 48 through Table 50.

Table 48: Tendon loads for 350mm vault with 25kN post-tension in hurricane wind condition.

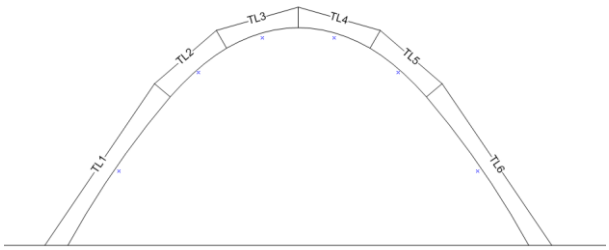
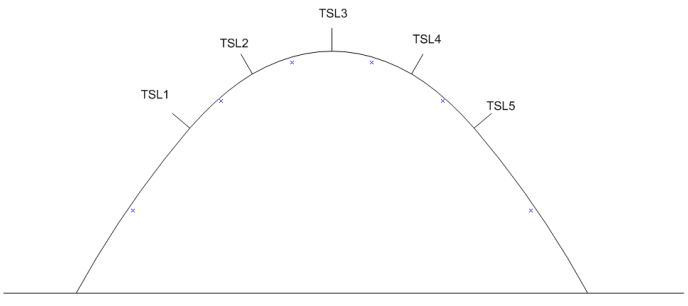
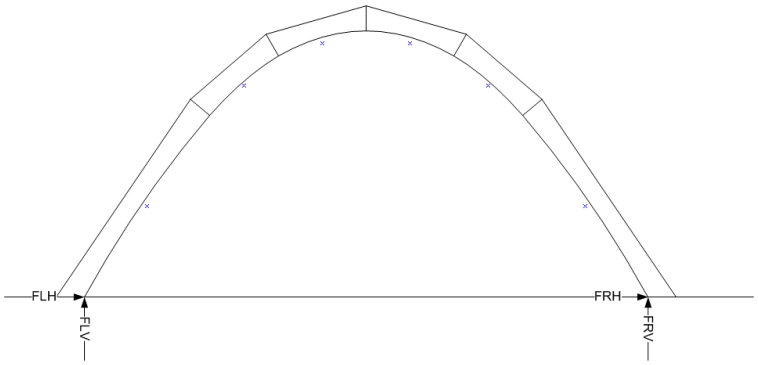
Load combination	 Tendon load (kN)					
Tendon No	**TL1**	**TL2**	**TL3**	**TL4**	**TL5**	**TL6**
Dominant	23.91	24.37	25.35	25.14	24.21	23.38
LC1	23.98	24.44	25.42	25.21	24.27	23.44
LC2	23.98	24.44	25.42	25.22	24.27	23.45
LC3	23.99	24.45	25.43	25.23	24.28	23.46
LC4	24.00	24.46	25.44	25.23	24.29	23.46
LC5	24.01	24.46	25.45	25.24	24.30	23.47
LC6	24.02	24.48	25.46	25.25	24.31	23.48
Max	**24.02**	**24.48**	**25.46**	**25.25**	**24.31**	**23.48**

Table 49: Tendon support loads for 350mm vault with 25kN post-tension in hurricane wind condition.

Load combination	 Tendon support load (kN)

Tendon support No	TSL1	TSL2	TSL3	TSL4	TSL5
Dominant	6.49	9.74	11.97	9.72	7.35
LC1	6.51	9.77	12.01	9.74	7.38
LC2	6.51	9.77	12.01	9.75	7.38
LC3	6.51	9.78	12.01	9.75	7.38
LC4	6.51	9.78	12.02	9.75	7.38
LC5	6.52	9.78	12.02	9.75	7.38
LC6	6.52	9.79	12.03	9.76	7.39
Max	**6.52**	**9.79**	**12.03**	**9.76**	**7.39**

Table 50: Foundation loads for 350mm vault with 25kN post-tension in hurricane wind condition.

Load combination				
	FLH (→)	**FLV (↑)**	**FRH (→)**	**FRV (↑)**
Dominant	22.65	44.86	-22.00	44.24
LC1	16.58	41.92	-26.86	42.25
LC2	16.26	41.97	-26.72	42.08
LC3	16.28	47.22	-26.92	47.40
LC4	16.25	47.12	-26.77	47.22
LC5	15.69	39.69	-26.22	39.82
LC6	15.68	44.84	-26.27	44.96
Max	**15.69**	**47.22**	**-26.92**	**47.40**

Conclusion It was found that a 350mm shell section, post-tension to an effective post-tension force of 25kN, yielded a suitable solution to the problem. This configuration resulted in pure compression of the section under dominant and service load conditions, adequate un-cracked bending moment capacity under the ultimate limit state load conditions, and an adequate cracked moment capacity to safely resist loads generated during hurricane force winds.

The effective shell thickness (although it would have been preferred to be less) is still deemed a practical section thickness, while the effective post-tension requirement is considered achievable.

3.5.4 Buckling Analysis

A buckling analysis was conducted on the five point contact post-tensioned vault discussed under section 3.5.2. This analysis was deemed a requirement to determine a refined critical buckling load of the section as configured in Figure 3.62. Here, Strand7 FEA modelling suit was utilised. Strand7 was selected as the modelling tool of choice based on its powerful fully fledged buckling solver.

Linear Buckling Solver in StaadPro V8i Although StaadPro V8i does provide a linear buckling solver, the solver does not yield buckling load factors when non-linear cable elements are implemented. A possible reason for this may be that in theory, the slightest bit of compressive load will make a cable entity buckle. When the programme therefore reports a buckling factor of zero or approaching zero, it is assumed that the programme behaves correctly and that the structure has a buckling capacity of zero.

Strand7 Buckling Solver Considerations Strand7 overcome the obstacle of non-linear cable elements by analysing the structure by two different solvers opposed to one. The structure was therefore first analysed by a non-linear solver of which the results were then used as initial conditions in the linear buckling solver.

In order to analyse the structure in Strand7, the geometry coordinates, material properties and other boundary conditions had to be converted to a readable format before implementation. As cable elements were used to model the post-tensioned tendon, the model could only be solved by a non-linear solver. The non-linear solver considered the non-linear

geometry of the tendon and iterated through the post-load application in 10% load increments.

It was important to note that the model definition in Strand7 has one small difference to that in StaadPro V8i. In StaadPro V8i, the tendon supports were constructed of short beam elements. These elements were released such that only axial forces could be applied through it to the vault's shell. In Strand7, these supports had to be defined by attachment links, allowing only point force transfer to the shell.

As a result of this small change in the model definition, the results were not expected to by 100% identical. It was, however, expected to see a close correlation between the results from the two models.

Strand7 moreover offers a function which allows the cable tension to remain uniform over its supports by assuming a frictionless pulley for each support condition. This function is called "*string grouping*". The effect of ignoring friction, against taking force variations in the different tendon sections into consideration, was explored.

The buckling characteristics of a five point post-tensioned vault with a 250mm shell thickness were considered. As the vault was optimised to resist the dominant loads in pure compression, little to no bending moment was expected in the results file. Buckling analyses results will be discussed for the following conditions:

1. A vault where the section is under pure compression when subjected to a 300kph wind load as discussed under Section 3.5.33.5.2, *Complete*
2. A vault where the section is under pure compression when subjected to service wind loads as discussed under Section 3.5.3, *Partial Post-tensioning of 250mm Shell Section*

The buckling results for a vault subjected to service and ultimate limit state wind loads will not be discussed. The reason for this is because the latter condition is considered as less conservative to that when the structure is

subjected to hurricane wind load conditions. Such high wind loads will have the highest destabilising effect on any of the two models and are hence considered critical.

Post-tensioned Vault for No Tension under Service Loads The post-tensioned vault as discussed under Section 3.5.3, *Partial Post-tensioning of 250mm Shell Section,* is discussed. From the non-linear analysis in Strand7 where "*string grouping"* was considered, it was determined that a maximum tendon force of 20kN yielded an absolute maximum bending moment of 0.22kNm/m in the section.

Non-linear solver results interpretation Comparing this bending moment to the 0.09kNm/m bending moment determined by the StaadPro V8i model, the result seemed in the correct order of magnitude. It would, however, be beneficial to have the discrepancy between the two models to a minimum. The model was therefore solved without taking "*string grouping*" into consideration in an attempt to determine the effect of this function on the structure.

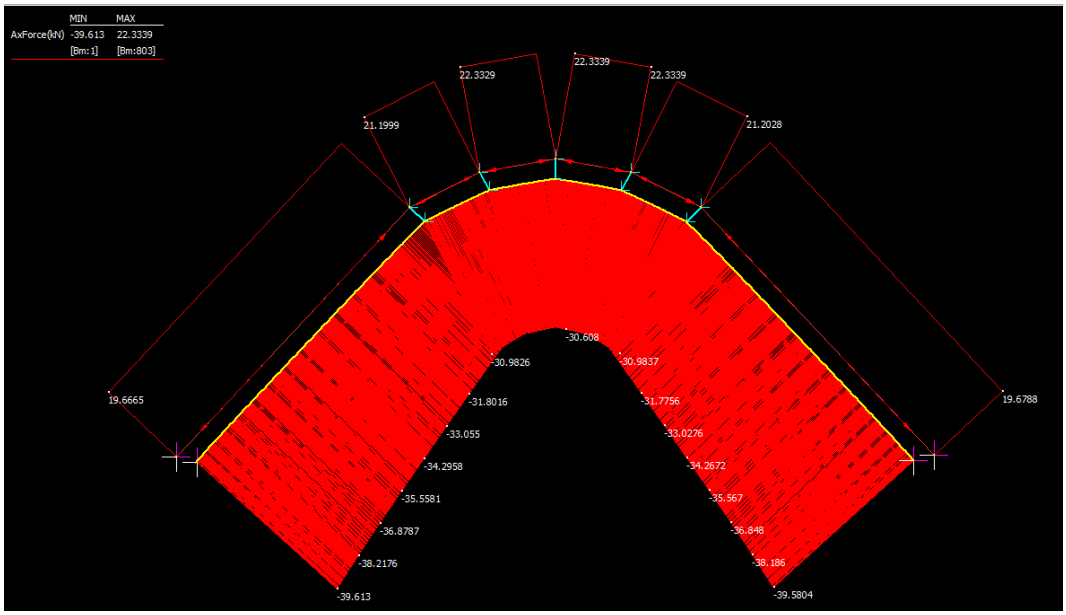


Figure 3.69: Axial force diagram for five point contact post-tensioned vault without string grouping (Strand7).

For the model where "*string grouping*" was ignored, an absolute bending moment of 0.10kNm/m was determined with a maximum tendon load of 22.3kN. These results are listed in Figure 3.69 and Figure 3.70. A comparison of the results to that of the StaadPro V8i model revealed an 8.8% discrepancy between the two models. This discrepancy was deemed acceptable and as a result, the use of "*string grouping*" was discredited. It was moreover felt that this function generated a scenario which will most probably not be achievable in practice, as some friction will realise between the tendon and its supports.

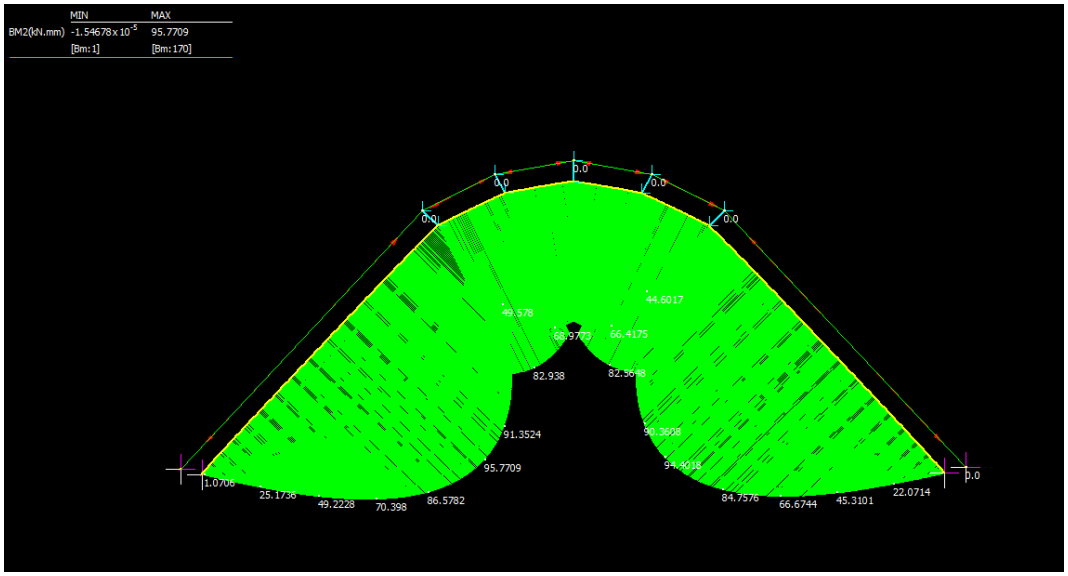


Figure 3.70: Bending moment diagram for five point contact post-tensioned vault without string grouping (Strand7).

Buckling mode shapes As discussed under Section 2.2.2, *Buckling of Arches,* each structure has a critical load at which catastrophic failure will occur. The magnitude of this load is usually reduced in the presence of other destabilizing forces. For each buckling mode shape, a particular critical buckling load factor exists. The critical buckling load is the product of the buckling load factor and the maximum axial compressive force in the section under consideration.

The buckling mode shapes for the dominant load condition of a vault, post-tensioned to accommodate service loads in pure compression, are illustrated in Figure 3.71.

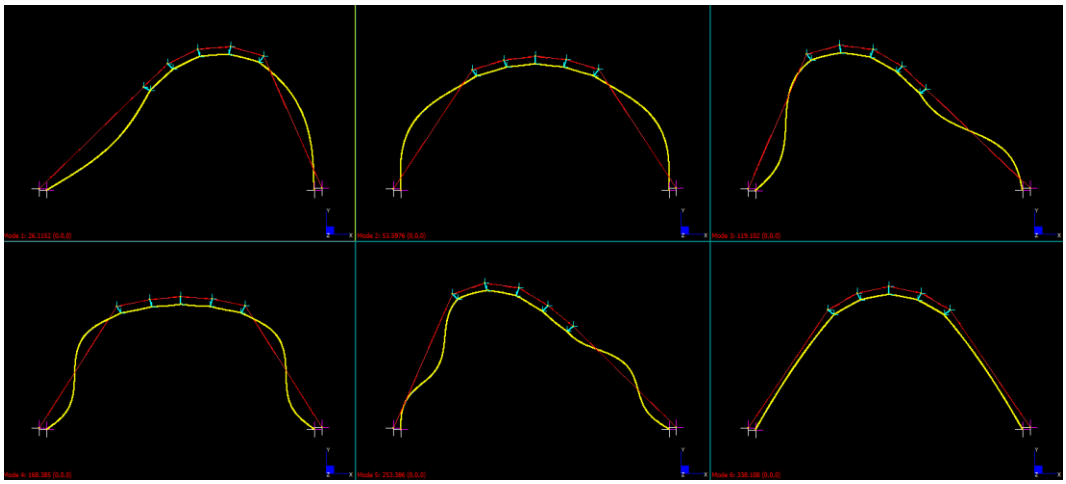


Figure 3.71: Buckling mode shapes for dominant load case of vault post-tensioned to pure compression for service loads (Strand7).

It was determined that the buckling load factor for this configuration started at 26.12. This yielded a critical buckling load of 1034kN. The buckling load factors and their corresponding critical buckling loads per mode shape are listed in Table 51.

Table 51: Critical buckling load factors for dominant load case of vault post-tensioned to pure compression for service loads.

Buckling mode shape #	A. Buckling factor	B. Maximum axial force (kN/m)	Critical buckling load (AxB) (kN/m)

1	26.12	39.60	1034.00
2	53.60	39.60	2122.00
3	119.10	39.60	4716.00
4	168.39	39.60	6668.00
5	253.39	39.60	10034.00
6	338.11	39.60	13389.00

For the dominant load case (self-weight and post-tension force), the structure was found to be safe from buckling. This may however change when the structure is subjected to other load conditions which may lead to destabilisation. The most destabilising conditions were deemed to be present in the event of a hurricane force wind. As a result, the critical buckling load factors for the structure subjected to 300kph wind loads were investigated.

It was determined through this analysis that the critical buckling load of the structure is not significantly affected by the application of excessive wind loads. The buckling mode shapes for this analysis are presented in Figure 3.72.

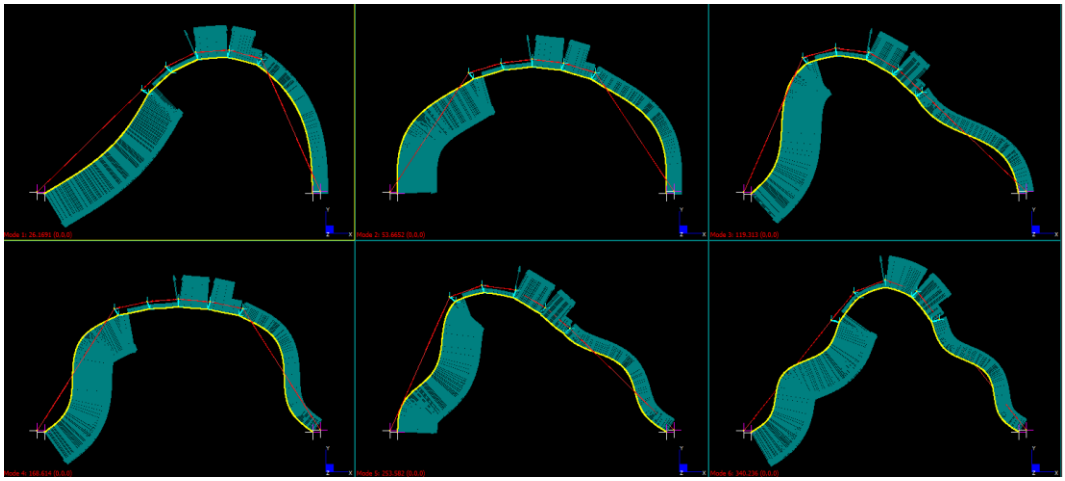


Figure 3.72: Buckling mode shapes for LC6 as per Table 12 for vault post-tensioned to pure compression for service loads (Strand7).

Five Point Contact Vault Post-tensioned for Hurricane Wind Loads

The buckling results from the Strand7 linear buckling solver for this load condition are listed in Figure 3.73, Figure 3.74 and Figure 3.75 for no "*string grouping*".

Non-linear solver results interpretation The absolute maximum bending moment in the dominant load condition was determined at 0.42kNm/m with a maximum shell compressive force of 93kN/m. This result compared well with the results obtained by the StaadPro V8i model. The bending moment obtained by the StaadPro V8i model was 0.42kNm/m at a maximum axial compressive force of 100.4kN/m.

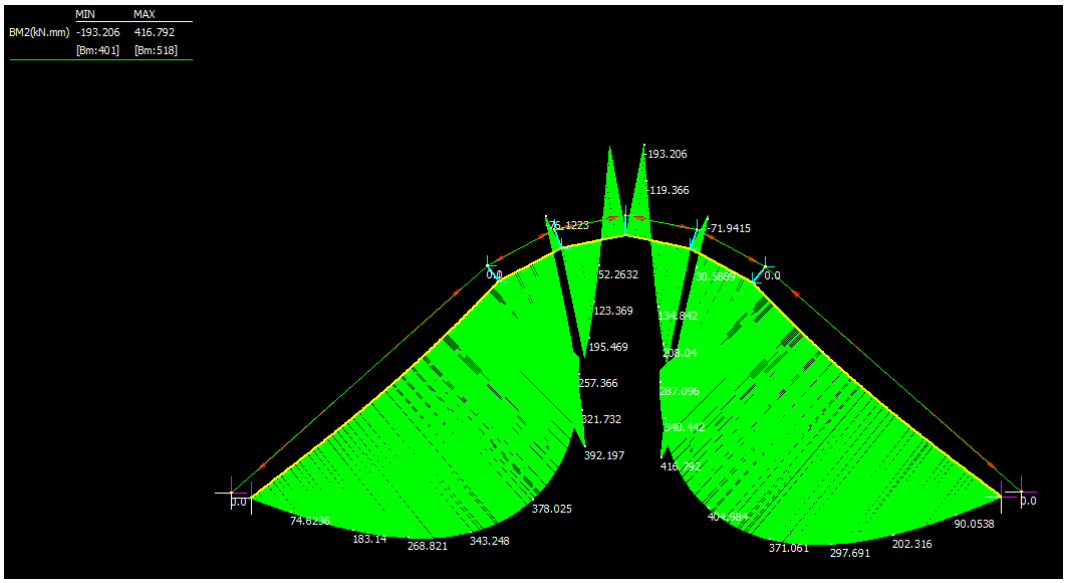


Figure 3.73: Bending moment diagram for five point contact post-tensioned vault with string grouping (Strand7).

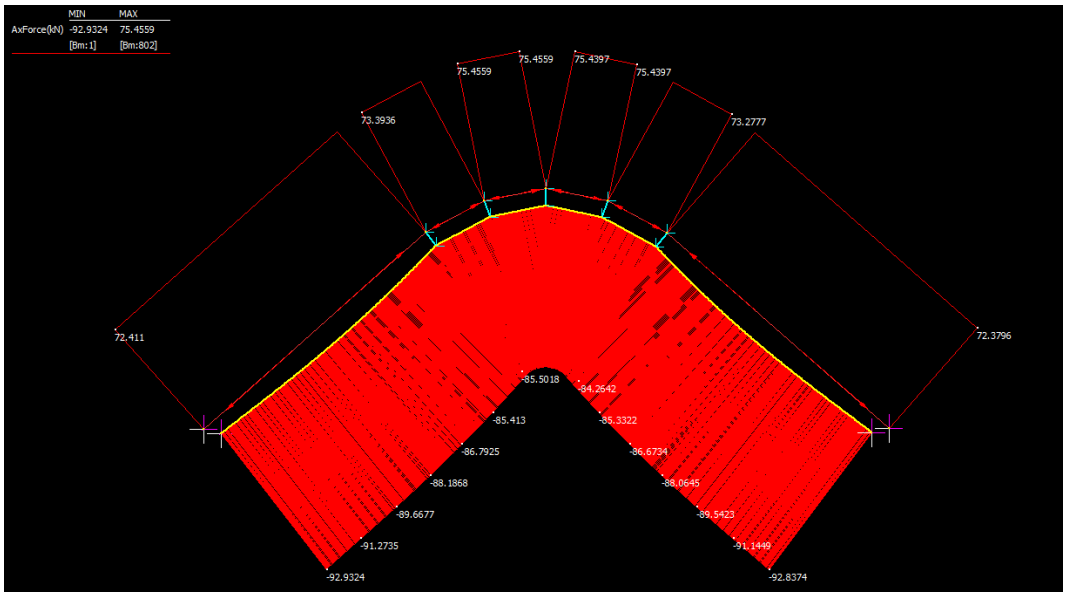


Figure 3.74: Axial force diagram for five point contact post-tensioned vault with string grouping (Strand7).

Buckling mode shapes The buckling mode shapes for the vault as geometrically defined in Section 3.5.3, *Geometry* are illustrated in Figure 3.75. These shapes do not look different to the buckling mode shapes displayed in Figure 3.71. This result was expected as the only variable was the post-tension force applied by the tendon.

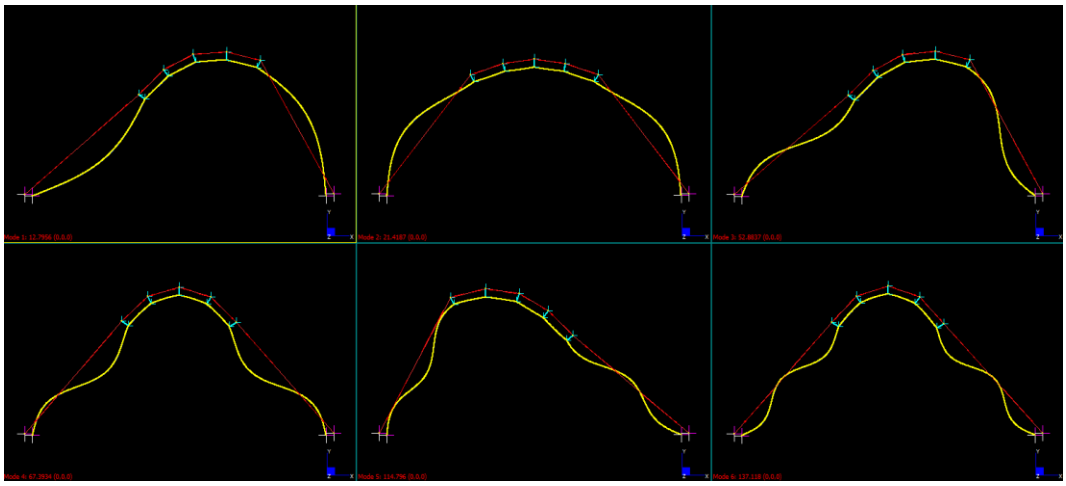


Figure 3.75: Buckling mode shapes for dominant load case of vault post-tensioned to pure compression for 300kph wind loads (Strand7).

For this configuration, the minimum critical buckling load factor was determined at 12.8 which resulted in a critical buckling load of 1189kN/m. The critical buckling load factors and their corresponding critical buckling loads for each mode shape are listed in Table 52.

Table 52: Critical buckling load factors for dominant load case of vault post-tensioned to pure compression for 300kph wind loads.

Buckling mode shape #	A. Buckling factor	B. Maximum axial force (kN/m)	Critical buckling load (AxB) (kN/m)
1	12.80	93.00	1189.00
2	21.42	93.00	1991.00
3	52.88	93.00	4918.00
4	67.39	93.00	6268.00
5	114.80	93.00	10676.00
6	137.12	93.00	12752.00

It was proven that the application of hurricane wind loads do not critically alter the buckling load factors of the structure. The post-tension force in this case was however significantly larger. As a result, it was thought that the effect hurricane wind loads have on the critical buckling factors of the structure should be investigated. The results of this investigation are however illustrated in Figure 3.76, and no significant changes in the critical buckling load factors were observed.

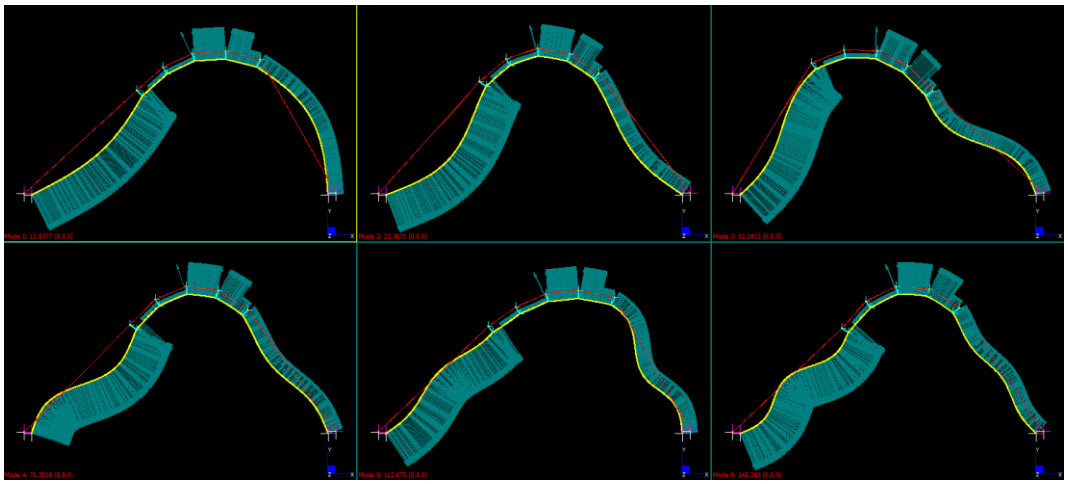


Figure 3.76: Buckling mode shapes for LC6 as per Table 12 for vault post-tensioned to pure compression for 300kph wind loads (Strand7).

Comparison between FEA analysis and manual Calculation In the preceding discussions, the post-tensioned vault was subjected to an FEA analysis in order to determine its critical buckling load. The findings of this investigation revealed a critical buckling load in the order of ±1000kN/m for the first mode of buckling.

It was considered worthwhile to verify this result by means of manual calculation. Three different procedures were utilised in order to determine the most probable critical buckling load of the structure. These procedures are:

A. DIN 18800 Part 2 (German Building and Civil Engineering Standards Committee & German Committee for Structural Steelwork, 1990: 18).
B. Critical buckling of curved bars and arches (Timoshenko & Gere, 1963).
C. The buckling load of catenary arches informed by Eladio Dieste (Pedreschi & Theodossopoulos, 2007).

The theory behind the above mentioned procedures were discussed under Section 2.2, *Buckling of Arches*. It was proven, as will be discussed under Section 4, that a 250mm shell thickness is found to be inadequate in

resisting the loads applied to it. Similarly, it was proven that a 335mm section subjected to a 13kN post-tension force is also inadequate to resist the applied bending moments resulting from hurricane force winds. A 350mm shell at 25kN post-tension force was, however, found to have adequate capacity to resist all loads applied to it during the lifespan of the vault.

As a result, buckling verifications on all three these instances were conducted by means of manual calculation. The results obtained from manual calculation for a 250mm, 335mm and 350mm thick catenary vault are listed in Table 53. It is important to note that these results are applicable to the traditionally shaped catenary vaults. As a result, slight variations compared to that obtained from the FEA analysis were expected. This is the case, as the result from an FEA analysis takes into consideration the complex geometry of the structure which manual calculations negate.

Table 53: Critical buckling loads of 250mm and 335mm thick catenary vault.

Procedure	**Applicable critical buckling load equation**	**Critical buckling load (kN/m) – 250mm shell thickness 22kN post-tension**	**Critical buckling load (kN/m) – 335mm shell thickness 13.5kN post-tension**	**Critical buckling load (kN/m) – 350mm shell thickness 25kN post-tension**
A	Equation (17)	755	1817	2072
B	Equation (18)	1918	4847	5300
C	Equation	611	1328	1580

	(19)			
Average		**1094**	**2664**	**2984**

It is evident that the magnitude of the critical buckling loads obtained by methods A and C are similar in magnitude. Method B yielded a significantly less conservative result. By considering the average critical buckling load obtained between the three methods, a final critical buckling value of 1094kN/m was obtained. This compared fairly well to the determined 1034kN/m and 1189kN/m critical buckling values obtained from the FEA analysis for the two post-tensioned conditions previously discussed.

As discussed in Section 4, a post-tensioned vault will only be viable if the section thickness is increased to 350mm at an effective post-tension force of 25kN. A linear buckling analysis on this geometry was not conducted in an FEA environment as it was not deemed required. Some of the reasons why an FEA analysis was not considered mandatory are:

1. The effective section area is increased significantly with a marginal increase in post-tension force.
2. The critical buckling load factors determined for a 250mm post-tensioned vault started at a minimum value of 12.79.
3. Manual calculations of the mean critical buckling load compared reliably to that determined by the FEA model. It was therefore assumed that the manually determined critical buckling loads for the 335mm and 350mm thick vaults resulted in a reliable indication of the critical buckling loads of the sections.

For more information on the determination of these results, the reader may refer to Appendix B.4 through Appendix B.6.

Conclusion StaadPro V8i proved not to be a viable tool for the determination of the critical buckling load for a five point contact post-tensioned vault. The use of non-linear cable elements in the linear buckling solver yielded questionable buckling results.

A more sophisticated finite element analysis package proved to be of more value. Strand7 allowed the user to conduct a non-linear analysis on a non-linear model, after which the results were implemented as initial conditions to the linear buckling solver. This functionality allowed the user to solve for the critical buckling load factors of a non-linear structural configuration.

For a five point contact post-tensioned vault, configured to accommodate dominant and service wind loads in pure compression, the critical buckling load factor was determined to be 26.12. In the case where a similar vault was post-tensioned to accommodate hurricane wind loads in pure compression, the critical buckling load factor reduced to 12.79. It was therefore found that the vault configuration in both these instances was safe against buckling failure.

Manual calculation of the critical buckling values of the vault's section yielded fairly comparable results to that obtained from the FEA analysis. As a result, it was assumed that the critical buckling load of the vault, as determined by FEA modelling, was reliable. It was furthermore found that the modified vault, with a 350mm shell thickness, had sufficient capacity against critical section buckling.

4. STRUCTURAL DESIGN

4.1 INTRODUCTION

In the previous discussion, attention was given to the optimisation of the vault's geometry and the structural response thereof during pre-defined wind load conditions. It was proven that the geometry can be optimised such that the structure resists service wind loads in pure compression. When the applied loads were factored to ultimate limit state loading conditions, tension development in the shell was observed.

As the shell will be constructed of earth bricks, it was assumed that minimal tension resistance will be provided by the material. As an alternative means of dealing with tension in the section, reinforcement may have to be designed such that it resists these stresses in the ultimate limit state condition. It should furthermore be noted that, for these load conditions, the structure is to remain crack free in order to retain its durability.

Considering hurricane wind loads, an FEA analysis conducted on the model suggested significant bending moments in the vault's shell. As the applied post-tension force was not designed to ensure pure compression of the shell during these load conditions, flexural tension developed at the extreme shell fibres. These stresses were of a significant magnitude and care was taken with regards to the management thereof.

The initial assumption made in Section 3.5.2, *Partial Post-tensioning of 250mm Shell Section,* was that the structure should not collapse under hurricane wind load conditions. It may, however, crack and experience significant damage during the event, but the safeguard of its occupants should remain a key priority.

4.2 DESIGN LOAD SUMMARY

In section 3.3 a feasible geometric shape and structural configuration of the vault was selected. The selected configuration was further investigated in section 3.5 by means of various FEA models; in an attempt to determine the most effective and feasible solution to the problem. It was observed that it will be most suitable to post-tension the vault along its arch to such a degree that no tension development is allowed under service wind load conditions. The effects of the ultimate and hurricane wind load conditions were consequently investigated depending on the configuration under discussion.

Various structural designs were conducted in an attempt to determine an optimal structural configuration. Under Section 4.4, structural designs on various section thicknesses will be discussed. The applicable design loads, as obtained by FEA analysis, are listed in Section 3.5 for the applicable shell thickness under consideration. These loads were implemented, as applicable, in the structural calculations.

4.3 MATERIAL PROPERTIES

The vault was designed under the assumption that it will be constructed out of an earth brick masonry shell; draped under a basalt geogrid mesh. The mesh was assumed to be post-tensioned to the effective design post-tension force. The material properties of typical earth bricks are listed in Table 14, while Table 13 lists the recommended characteristic mechanical properties for a basalt geogrid mat as tested at the University of the Witwatersrand (Surat, D (Personal Communication)).

4.4 DESIGN OF SHELL

The shell was designed to accommodate the axial compressive force and bending moments it will be subjected to during service. Special attention was given to cases where the flexural tension in the section exceeded the applied compressive stress. These scenarios yielded tension at the extreme fibres of the section, where crack formation was expected to occur.

The design of the section addressed how tension in the section can be managed. Effective utilisation of the section's tensile resistance was considered. While considering a section cut from the vault's shell, an internal force distribution, as depicted in Figure 4.1, was considered. It should be noted that significant bending moments and axial forces were observed by the analysis, while shear forces were negligibly small in all configurations.

The shell's capacity to resisting axial compression and bending moments was determined. Curtin *et al* (1995) suggests that it is allowed to assume some tensile capacity of the masonry in the event of tension development when resulting from wind loads. These assumptions were discussed in more detail under section 2.4.2.

Under Section 3.5.4, it was proven by means of FEA analysis and manual calculation that the vault is safe from critical buckling failure.

The following force resistance requirements of the structural section had to be met:

1. A design compressive resistance that exceeded the maximum axial compression induced by service, ultimate and hurricane wind loads
2. An un-cracked bending moment capacity that exceeded the applied moments induced by service and ultimate limit state wind loads.
3. A cracked bending moment capacity that exceeded the absolute bending moment induced by hurricane wind loads.

If any of the above listed requirements were not met, the structure was modified such to accommodate the applied loads.

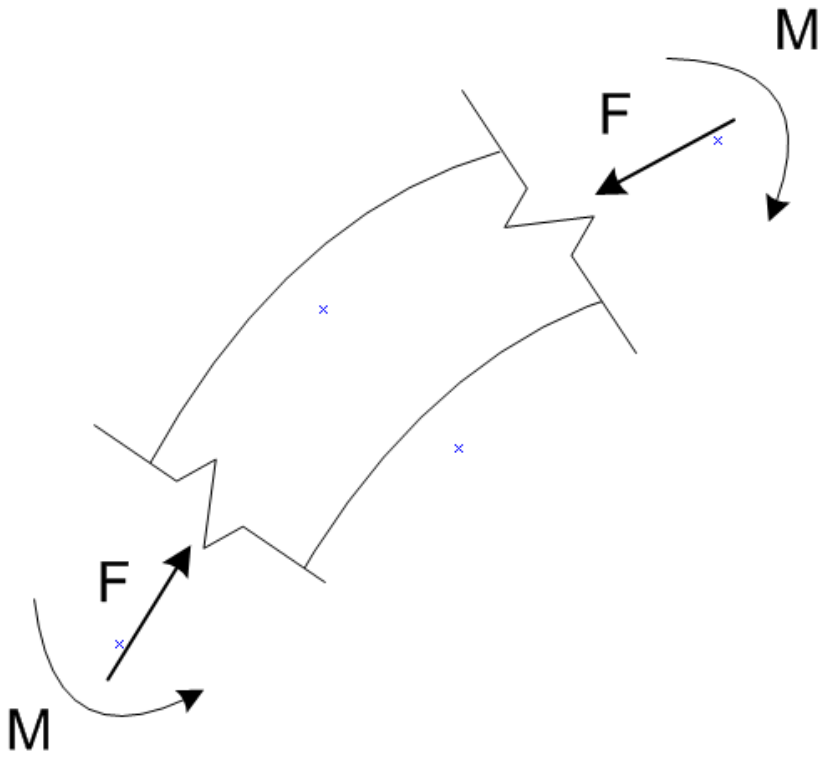


Figure 4.1: Loads applicable to shell section.

4.4.1 250mm Shell Thickness A 250mm shell thickness was deemed practical, as it did not require excessive amounts of material, while still providing a robust shell that was thought not to be easily penetrable by high speed debris. It was moreover considered as a trial section, and cognisance of the fact that custom made bricks will be required should be taken.

By considering the applicable section forces and applying the theory of masonry design as discussed under section 2.4.2, the viability of the section was evaluated. For more details on the physical calculation of the section capacity, the reader may refer to Appendix B.1. A brief description of the design will however be discussed.

Design strength calculation for masonry In order to determine the structural resistance of the masonry as a whole, the mechanical properties of the individual elements (mortar and bricks) needed to be determined. The characteristic 28 day compressive strength of the earth brick modules were taken as 5MPa as recorded in Table 14. As per Figure 2.41, class (iv) mortar was considered the most conservative designation. Considering the mortar class and brick shape factor as per Figure 2.40, the characteristic compressive strength of the masonry was determined according to Figure 2.42 as 4.4MPa.

It should be noted that a reasonable assumption was made that the compressive strength of clay fired bricks and that of earth masonry blocks are similar. This assumption was based on the fact that research into the compressive strength of earth masonry blocks have suggested that masonry bricks typically have lower compressive strength values than that of earth masonry blocks (Walker, 2004).

In order to arrive at the design strength of the masonry, the manufacturing control and workmanship of construction had to taken into consideration. Assuming normal control over brick manufacturing and construction activities, a material factor of 3.5 was selected as per Figure 2.43. The design strength of the masonry was then determined according to equation (32), and yielded a design strength for the masonry of 1.26MPa.

Design resistant capacity of section The design axial resistance of the section was determined according to equation (33). The capacity reduction factor, as per Figure 2.44, was taken as 1.0 in this calculation. This was in result to recognising that the factor takes into consideration the critical buckling resistance of the section, and that critical buckling of the vault was ruled out by FEA analysis as discussed under Section 3.5.4. An axial resistance of 314kN was calculated.

The characteristic flexural strength of the masonry was determined by consulting Figure 2.46. Both perpendicular and parallel bed joint bending

resistance were considered, which yielded 0.4MPa and 1.2MPa characteristic flexural strengths respectively. By assuming no axial compression in the section, equation (35) yielded 0.6kNm/m considering parallel bed joint moment resistance, and 1.79kNm/m considering perpendicular bed joint moment resistance.

Equation (36) took into consideration the presence of axial load in the section, which may be considered beneficial to the design. This axial load is dominantly present due to the self-weight of the vault, as well as the post-tensioning force applied. Considering parallel bed joint moment resistance, a value of 1.96kNm/m was calculated, while the perpendicular bed joint moment resistance was calculated as 3.15kNm/m.

The cracked moment resistance of the section was determined according to equation (38), and yielded 3.68kNm/m resistance.

Conclusion It was determined that the section will be capable of resisting the applied axial loads and bending moments for both the service and ultimate load conditions. The section did however not have enough bending moment capacity to resist the applied bending moment resulting from hurricane wind conditions. A cracked moment resistance capacity of 3.68kNm/m was determined as per Table 54. This was not sufficient to resist the absolute bending moment of 5.84kNm/m induced by a hurricane wind load.

4.4.2 335mm Shell Thickness Upon implementation of a 335mm thick shell, a new FLPC for the vault was derived as discussed under Section 3.5.3, *Partial Post-tensioning of 335mm Shell Section*. The same design process, as discussed under Section 4.4.1, was implemented.

It was determined that this structural configuration was able to resist dominant and service loads in pure compression at a reduced post-tension force, while the un-cracked bending moment resistance was found to adequately resist loads from the ultimate limit state. The increased

internal lever arm yielded a reduced flexural tension and increased bending moment resistance of the section as expected.

Under hurricane wind loads, the cracked bending moment resistance capacity proved to be inferior. It was found that, by decreasing the post-tension force to an optimal level in the dominant and service load condition, the reduced axial force in the section resulted in an inferior internal stabilising moment. It was moreover determined that, by increasing the effective post-tension force to over 32kN, the cracked moment resistance resulted in adequate capacity to resist the applied absolute bending moment generated by hurricane wind forces.

This analysis and limit state design confirmed that a balance between the section thickness and the required effective post-tension force had to be determined. It was therefore decided to determine the most practical section thickness at a practical level of post-tensioning which will result in the most structurally efficient solution. The reader may refer to Appendix B.2 for the detailed set of design calculations.

4.4.3 350mm Shell Thickness From the knowledge gained by analysing and designing the vault with a 250mm and 335mm shell thickness respectively, a final shell thickness of 350mm was selected for design. The structural design procedure adopted was as discussed under Section 4.4.1.

By increasing the shell thickness and effective post-tension force to 350mm and 25kN respectively, adequate section capacity was achieved in all load conditions. A 350mm shell thickness was not considered an un-practical thickness, while 25kN post-tension force was regarded achievable.

Considering other factors which fall beyond the scope of this research, a thicker shell section may also be considered beneficial. During hurricane events, loose standing objects become high speed debris which are notorious for inflicting significant damage to anything in their path. Having

a thick shell may therefore be considered beneficial, as it will protects its occupants from these high speed objects. Another benefit of having a thicker section is the fact that it results in a stiffer shell. Stiff members have a higher natural frequency to that of less stiff elements and are therefore considered a benefit in conditions where low frequency vibration is expected as a result of air flow over the vault. Durability of the structure is also considered key (Davison & Owens, 2008). Thicker shell sections may increase the durability of the structure, as it is generally significantly stronger than the ultimate limit state loads it's designed to resist (C&CI, 2009). As a result, less strain will be experienced by the fibres of the section which will lead to less structural damage due to fatigue effects.

The results of these calculations are listed in Table 55 and the reader may refer to Appendix B.3 for more details.

4.4.4 Normal Reinforcement The option of reinforcing the structure with normal tensile reinforcement was not explored; reason being that a post-tensioned solution, implementing the use of a basalt geogrid mesh, was specifically sought.

Table 54: Section capacity vs applied forces for 250mm effective shell thickness with 22kN post-tension force.

SECTION CAPACITY		SERVICE FORCES		ULTIMATE FORCES		ABSOLUTE FORCES	
Force description	**Magnitude**	**Force description**	**Magnitude**	**Force description**	**Magnitude**	**Force description**	**Magnitude**
Design compressive resistance	**314.3kN/m**	Absolute axial compression	**40.10kN/m**	Absolute axial compression	**40.10kN/m**	Absolute axial compression	**40.10kN/m**
Un-cracked moment capacity parallel to bed joints	**1.96kNm/m**	Service moment	**1.37kNm/m**	Ultimate moment	**1.70kNm/m**	Absolute Moment	**5.84kNm/m**
Un-cracked moment capacity perpendicular to bed joints	**3.15kNm/m**	Service moment	**1.37kNm/m**	Ultimate moment	**1.70kNm/m**	Absolute Moment	**5.84kNm/m**
Cracked moment	**3.68kNm/m**	Service moment	**1.37kNm/m**	Ultimate	**1.70kNm/m**	Absolute	**5.84kNm/m**

capacity				moment		Moment	

Table 55: Section capacity vs applied forces for 350mm effective shell thickness with 25kN post-tension force

SECTION CAPACITY		SERVICE FORCES		ULTIMATE FORCES		ABSOLUTE FORCES	
Force description	**Magnitude**	**Force description**	**Magnitude**	**Force description**	**Magnitude**	**Force description**	**Magnitude**
Design compressive resistance	**440kN/m**	Absolute axial compression	**49.05**	Absolute axial compression	**49.05**	Absolute axial compression	**49.05**
Un-cracked moment capacity parallel to bed joints	**3.46kNm/m**	Service moment	**1.46**	Ultimate moment	**1.77**	Absolute Moment	**6.08**
Un-cracked moment capacity perpendicular to bed joints	**5.8kNm/m**	Service moment	**1.46**	Ultimate moment	**1.77**	Absolute Moment	**6.08**
Cracked moment	**6.24kNm/m**	Service moment	**1.46**	Ultimate	**1.77**	Absolute	**6.08**

capacity				moment		Moment	

.

4.5 POST-TENSION DESIGN

4.5.1 Introduction

In Section 3, an optimal vault configuration was established. It was determined that a 350mm shell, at an effective post-tension force of 25kN, will result in a structure that is regarded as viable, cost effective and most importantly safe. Due to the mechanical characteristics of materials subjected to tensile forces, the final long term post-tension force is usually of a lesser magnitude than that initially applied during construction. This is a result of losses that occur during the initial post-tensioning process, as well as losses that occur over an extended period of time. These losses were discussed in more depth under Section 2.5.

In the preceding sections it was proven that a vault of 350mm cross-sectional thickness had adequate capacity to resist the applied post-tension force of 25kN as required by the design for service, ultimate and hurricane conditions. In order to ensure the required magnitude of effective post-tensioning is achieved, the magnitude of the post-tension force required at transfer needed to be determined. Considering this, in conjunction with the estimated amount of losses, the magnitude of post-tension force at transfer was calculated.

As discussed under Section 2.5.4, sophisticated calculations to determine the amount of post-tension losses are commonly considered redundant by specialists in the field (Marshall & Robberts, 2000; Raju, 2007). It was therefore assumed that a conservative loss of post-tensioning of 20% will be a sufficiently accurate estimation for the purpose of this research. In addition to the assumed long term loss of post-tensioning, the instantaneous loss of post-tension force due to elastic shortening was assumed to be 7.8% as discussed under Section 3.4.1.

4.5.2 Transfer Force Application

As discussed under Section 2.5.4, any structure subjected to post-tensioning needs to be structurally validated to ensure capacity to resist the internal forces generated during transfer and service. In order to ensure that an effective post-tension force of 25kN was achieved, the magnitude of the post-tensioning required at transfer was determined as 31.25kN.

As discussed under Section 2.5.4, 20% post-tensioning losses are generally considered an adequate estimation for the long term stress losses applicable. It is furthermore known that basalt fibres have similar losses to that of steel when subjected to post-tensioning (Pearson *et al.*, 2013). Assuming a material factor of 1.15 for the post-tensioned geogrid, equation (47) yields a post-tensioning force requirement of 31.25kN at transfer. Considering instantaneous losses of 7.8% due to elastic shortening, and applying equation (47) in a similar fashion, the required jacking load was calculated as 33.5kN. This amounts to a geogrid area requirement of 80mm^2/m and an effective transfer stress of 460MPa in the basalt fibres. For more information into the determination of the required post-tension force at transfer, the reader may refer to Appendix B.7.

In order to ensure that minimal loss of post-tensioning force was observed at the tendon supports, post-tension bearing pads were considered. These pads should be custom made to ensure that the force, exerted by the tendon to the shell, remains at the required angle to the horizontal plane. The pads can be constructed of the same material as used for post-tensioning sleeves, and will be discussed in more detail under Section 5.4.

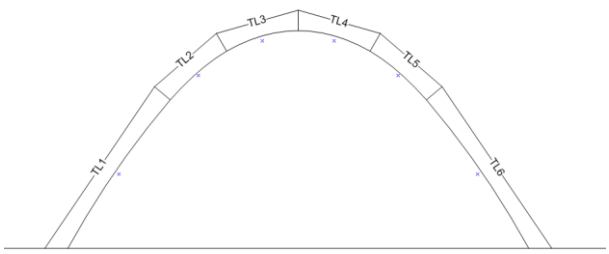
As a final verification, the final vault configuration was subjected to the required post-tension force at transfer. This force was ±25% greater than the effective post-tension force the structure was previously designed to. Due to the increased post-tension force at transfer, the vault will be

subjected to forces it was not optimised to resist in pure compression. As a result, it was expected that bending moments will be generated in the shell. The section will be considered adequate if the generated bending moments at transfer do not exceed the un-cracked bending moment resistance thereof.

4.5.3 Results Interpretation

From an FEA analysis conducted, the applied post-tension force at transfer yielded bending moments and axial loads in the shell section as listed in Table 59. It was observed that these forces do not exceed the section's capacity. The absolute bending moment during transfer was determined as 0.82kNm/m while the section's un-cracked bending moment capacity was 3.46kNm/m. As a result, the vault configuration as assumed was deemed adequate to resist the loads exerted during transfer.

Table 56: Tendon loads for 350mm vault with 33.5kN jacking force.

Load combination	 **Tendon load (kN)**					
Tendon No	**TL1**	**TL2**	**TL3**	**TL4**	**TL5**	**TL6**
Jacking load	32.27	32.94	34.18	33.91	32.63	31.56

The post-tension load in the tendon, tendon supports and shell foundations during jacking are listed under Table 56, Table 57 and Table 58 respectively.

Table 57: Tendon support loads for 350mm vault with 33.5kN jacking force.

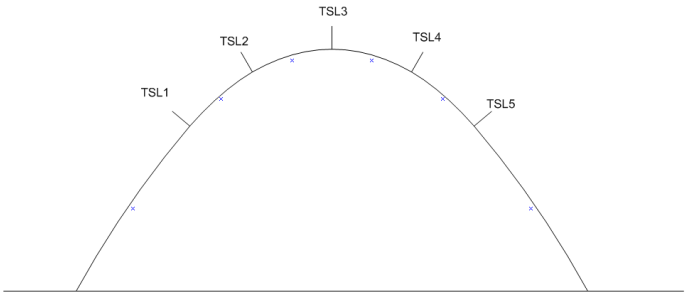
Load combination	 Tendon support load (kN)				
Tendon support No	**TSL1**	**TSL2**	**TSL3**	**TSL4**	**TSL5**
Jacking load	8.76	13.15	16.16	13.11	9.92

Table 58: Foundation loads for 350mm vault with 33.5kN jacking force.

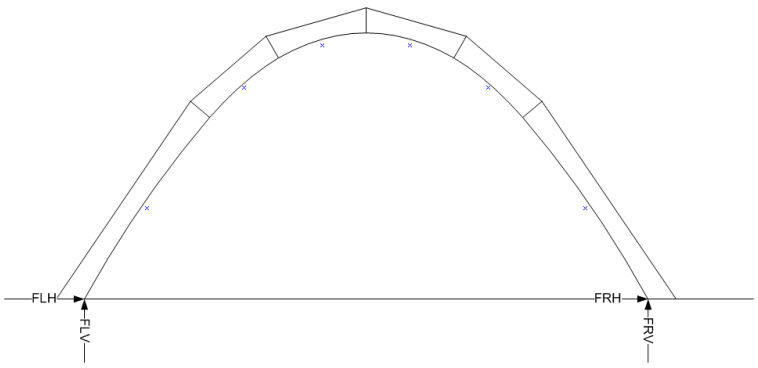
Load combination				
	FLH (→)	**FLV (↑)**	**FRH (→)**	**FRV (↑)**
Jacking load	26.92	51.54	-26.04	50.73

Table 59: Section capacity vs applied forces for 350mm effective shell thickness with 31.25kN transfer post-tension force.

Force/Stress Description	Magnitude	Force/Stress Description	Magnitude
Minimum un-cracked bending moment resistance capacity	3.46kNm/m	Transfer bending moment	**0.82kNm/m**
Design compressive resistance	440kN/m	Maximum axial force at transfer bending moment event	**40.86kN/m**
	440kN/m	Absolute axial compressive force	**58.14kN/m**
Compressive Resistance	1.26MPa	Maximum compressive stress	**0.16MPa**
		Minimum compressive stress	**0.08MPa**
		Maximum tensile stress	**0.00MPa**

5. FINAL SOLUTION

5.1 3D ISOMETRIC MODELLING

In order to assist in the visualization of the proposed solution, the post-tensioned vault, as discussed in previous chapters, was graphically modelled as a three-dimensional model in *Google Sketchup 2015*. Three post-tension solutions were conceptually investigated.

Each solution presented considered the feasibility, possible cost implications as well as the practicality of implementation. The three solution explored does not involve altering the core application of the post-tension force to the vault's shell, but looks into the methods of constructing and post-tensioning the structure to its required parameters.

The generated isometric models created a virtual space where different components of the vault could be visualised. This assisted in the spatial orientation and integration between the sub-surface foundations, post-tensioning equipment, gable end walls, post-tensioned geogrid as well as the vault's shell. It moreover allowed for a better understanding of what the final solution will look like from an architectural perspective.

In the discussions to follow, all isometric representations consisted of nine fundamental components. These components are as depicted in Figure 5.1:

1. A 350mm earth brick shell.
2. A basalt geogrid post-tensioned mesh.
3. Post-tensioned bearing pads.
4. Earth brick gable end walls.
5. A 700mm square window.
6. A front door of standard dimensions (2032mm x 813mm).
7. A concrete floor slab of minimum 200mm thick.
8. Custom tie-downs used for anchoring the post-tensioned basalt geogrid mesh.

9. Custom anchor foundations to which the post-tensioned mesh is anchored.

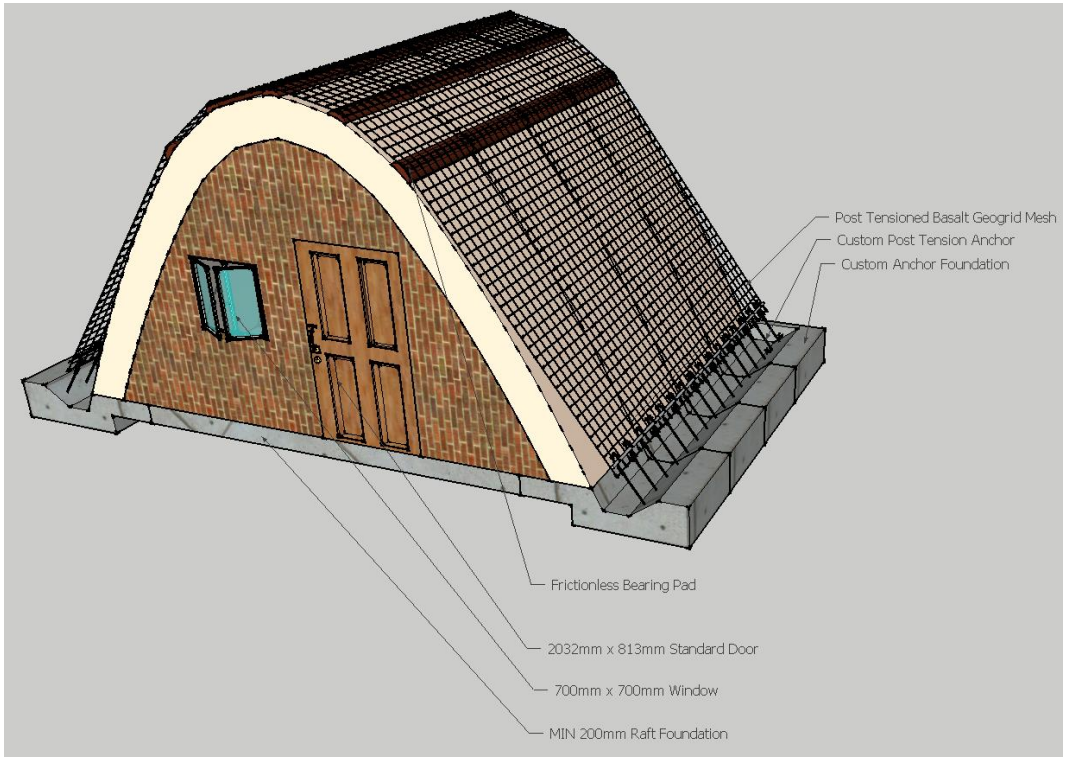


Figure 5.1: Basic components of the final solution in isometric view.

5.2 EXPLORED METHODS OF POST-TENSIONING

As the final solution should ideally be of a low-cost nature, creative ways of obtaining the required post-tension force in the mesh was explored. The cost-effectiveness of each solution presented, however, falls beyond the scope of this research. Future research into the cost-effectiveness of each presented solution is therefore recommended.

The three post-tensioning solutions explored were:

1. Uniform ratchet tensioning.
2. Funicular chain-block tensioning.
3. Uniform electric winder tensioning.

As each post-tensioning system should be designed to exert a 33.5kN jacking force to a 1000mm section of the vault, the basic configuration of

the solution will not be affected. In other words, the only components of the isometric model expected to change was the post-tension anchor mechanism, its anchor foundation and the end-detail of the basalt geogrid mesh.

5.2.1 Uniform Ratchet Tensioning

The uniform ratchet tensioning solution was based on the principle of incrementally increasing the tension in the mesh by cranking a cable come-along ratchet on both ends of the vault. The required jacking force at the ends of the mesh was 33.5kN/m as determined under Section 4.5.2. Depending on the preferred jacking procedure, the size of the required ratchet was selected.

Jacking Process The ratchet configuration is illustrated in Figure 5.2. This configuration does not ensure a uniform distribution of the post-tension jacking load in the absence of some modification, as the ratchets are connected at finite locations along the mesh's edge. In order to ensure a fairly uniform distribution of the jacking force, a load distribution beam (a) will be required. This beam should be designed such that deflection is limited to such an extent that excessive load transfer losses (to the basalt geogrid mesh) are not observed along the beams edge.

The edge of the basalt geogrid mesh, where the load distribution beam is to be installed, should be prepared such that the longitudinal basalt strands wrap around the load distribution beam in loop form. A schematically representation of the proposed edge preparation is depicted in Figure 5.3.

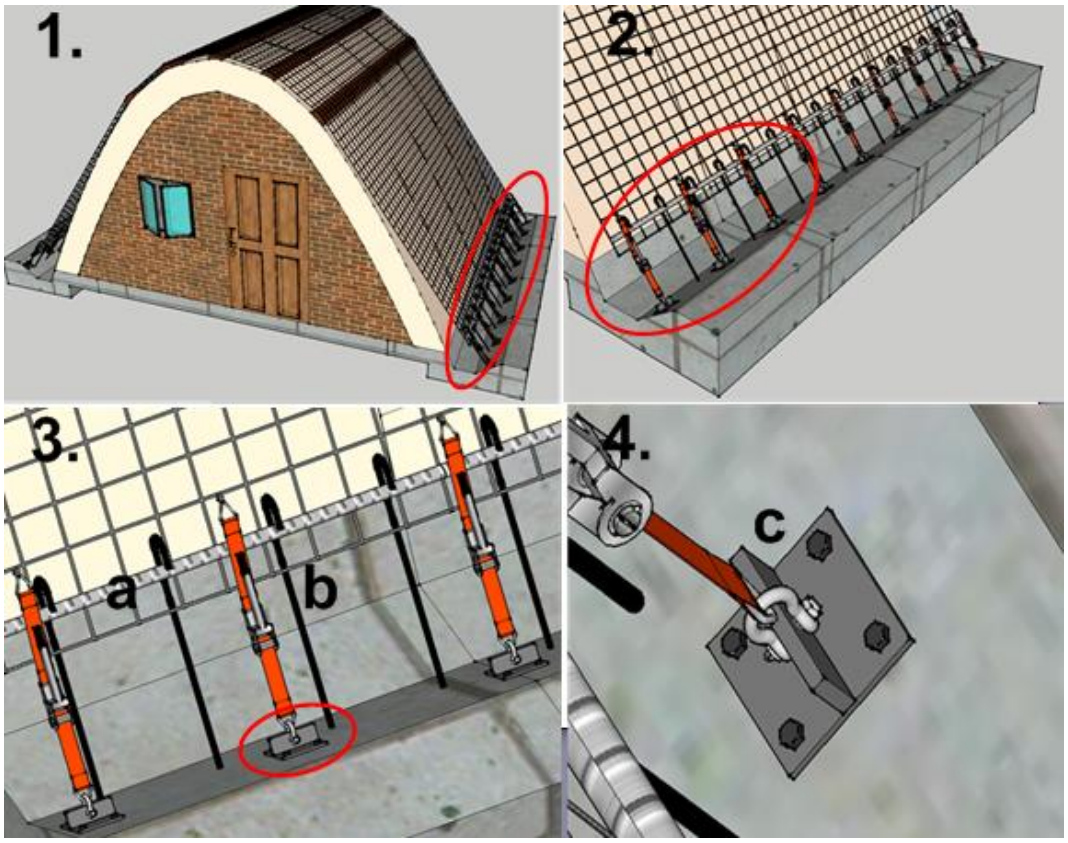


Figure 5.2: Six ratchet post-tensioning jack configuration.

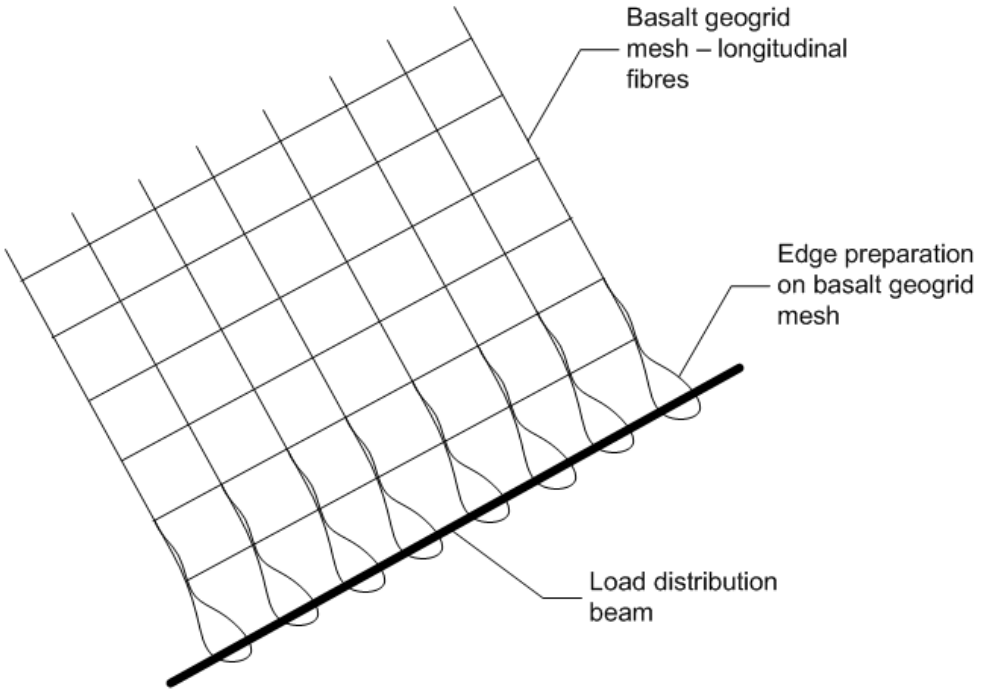


Figure 5.3: Edge preparation of basalt geogrid for effective load transfer from load distribution beam to mesh.

By tensioning the ratchet, the basalt geogrid mesh will elongate up until a point where the anchor hook (b) can be hooked onto the load distribution beam. In order to limit the loss of post-tensioning during the hooking process, it is advised that the hook should be more of a 90degree bend than a hook. To prevent slipping of the load distribution beam from the hook, it can be field welded to one another at transfer.

The ratchets, used to post-tension the mesh, can be re-used for every 1000mm section of the vault. It should be fixed to the anchor foundation by means of a bracket connection (c), which can be removed after the post-tensioning process. The brackets can be installed by means of drilling holes, and bolting it fast onto the concrete anchor foundations. Lugs or similar mechanisms can be used to connect ratchets to the anchor plates.

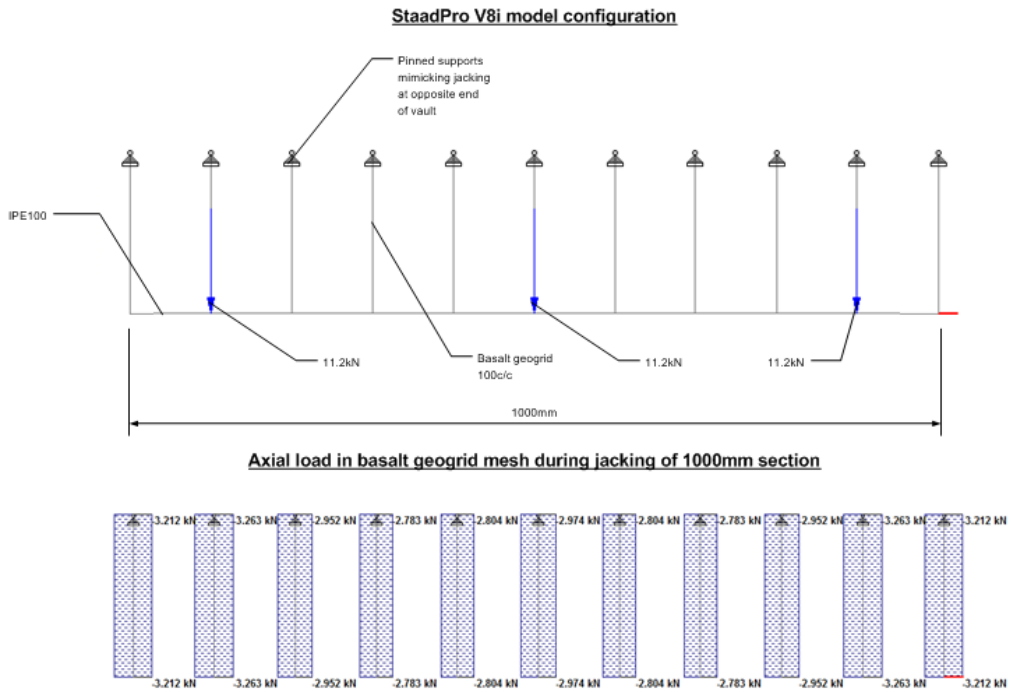


Figure 5.4: Six ratchet post-tensioning jack configuration.

Depending on the amount of ratchets to be used, the size of the load distribution beam can be selected. Should six ratchets per 1000mm section be used, it was determined that an IPE100 load distribution beam will yield an acceptable level of uniform load distribution to the mesh. This was determined by creating an FEA model in StaadPro V8i, as depicted in Figure 5.4. With the use of six ratchets (three on each side of the vault) the jacking force to be exerted by each ratchet was calculated to be 11.2kN. By using load cells between the ratchet-to-bracket connections, this load can be easily monitored.

Due to the amount of ratchets used in the jacking process, space may become a constraint when simultaneous cranking of the ratchets is required. The load distribution beam will however evenly distribute the applied jacking force to the mesh, hence phased cranking can be allowed in 20% load intervals. The load cells should be used to achieve the desired tensile force at each ratchet.

The distributed load variance in the basalt geogrid mesh fibres, as illustrated in Figure 5.4, were determined to be a maximum of approximately 40kg. This can be reduced by increasing the load distribution beam size, or alternatively making use of stiffer truss members. Increased load distribution member stiffness will, however, impact the final cost of the solution and should be taken into consideration.

Ratchet A proposed ratchet, capable of providing 2tons of pull force, is the *Tekton 5541 power puller* as depicted in Figure 5.5 ("2 Ton Power Puller | TEKTON 5541", 2016).



Figure 5.5: 2 Metric ton cable ratchet ("2 Ton Power Puller | TEKTON 5541", 2016)

It is proposed that a ratchet with a working load limit of 2tons is used, regardless of the fact that the maximum jacking force per ratchet is only 1ton. The reason for this is due to the fact that these ratchets are to be used numerous times, and that fatigue of the ratchet as well as the operator will be mitigated by using a higher load rated ratchet.

Anchor Foundations The foundations to be used to anchor the post-tensioned mesh are illustrated in Figure 5.6. The forces to be resisted by the foundation are the jacking force exerted by the post-tensioned mesh (T), the force acting along the vault's shell (F) and the self-weight of the foundation (W).

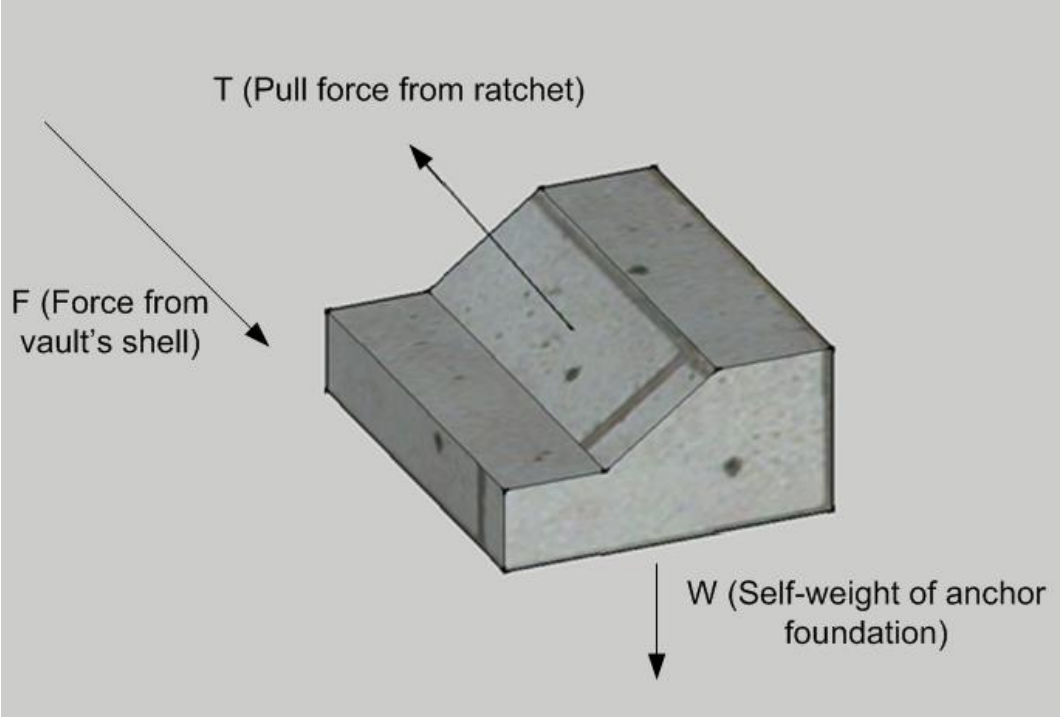


Figure 5.6: Ratchet configuration - anchor foundation.

The angle at which the FLPC of the vault intercept the horizontal is approximately 68degrees. The thrust components obtained during jacking should be considered during the design of the foundation. These loads are as listed under Table 58. For the left hand side foundation, the horizontal thrust towards the anchor foundation was found to be 27kN, while the vertical downward load was 51.5kN. This yielded a resultant thrust force (F) of 58kN. Considering an angle of incidence of 50degrees for the anchors, the 33.5kN jacking force resolved into a 25.66kN vertical uplift and 21.53kN horizontal push force respectively. The vertical uplift of the anchor foundation can be countered by ensuring that the foundation has a volume of approximately $1m^3$, while the horizontal sliding force can be absorbed by friction between the foundation and the soil; introducing a

shear key or considering the embedded soil's resistance against movement.

The characteristic parameters of the founding soil will play a significant role in the design of the foundation and should be determined by means of a geotechnical investigation. After tensioning, the ratchets should be removed and the foundations filled by a layer of top soil.

In order to avoid the loss of post-tensioning due to differential settlement, the foundations of the vault and anchors should be designed to act as a rigid entity. This configuration will allow for possible settlement, but ensure that the anchor foundations remain in position relative to the vault's foundation. The anchor foundations should be tied to one another by means of a tie beam in the direction of the vaults span. These beams will prevent possible kicking at the foot of the vault.

5.2.2 Funicular Chain Block Tensioning

An alternative method of post-tensioning the basalt geogrid mesh is by assuming a funicular or parabolic attachment as anchor. This configuration is illustrated in Figure 5.7.

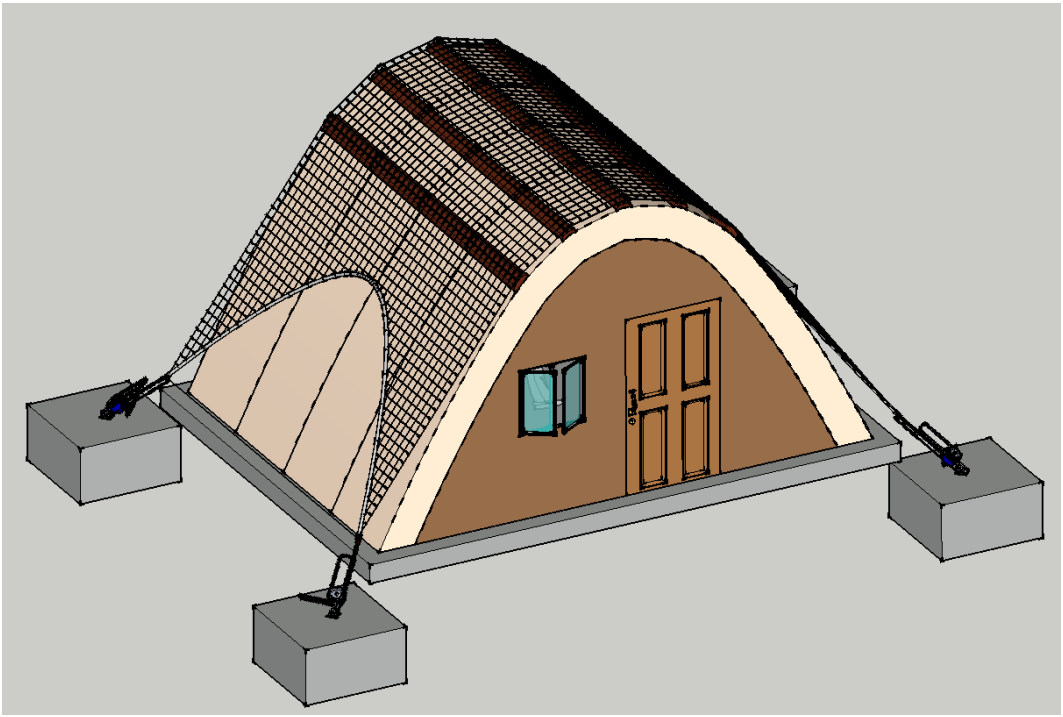


Figure 5.7: Funicular chain block tensioning configuration.

In this configuration, the use of ratchets were replaced by four 8ton rated chain blocks, while the load distribution beam in Section 5.2.1, *Jacking Process,* was replaced by a high tensile strength post-tensioning cable. In order to ensure that the configuration acts at an optimal level, the load path of the steel cable can be designed as funicular for the required load in the basalt geogrid mesh (Allan *et al.*, 2010).

Bow's Notation As it was known that the jacking force required is 33.5kN/m, the load per strand equalled 3.05kN, assuming a mesh of 100mm c/c spacing of its strands. This information was then used in a graphical analysis to determine the most efficient curvature the steel cable needed to assume. As depicted in Figure 5.8, the post-tensioned mesh will exert a constant 3kN force at each strand location. The proposed cable will be anchored at the left and right jacking position. One method of resolving these loads, to be supported in a funicular tension fashion, is to apply bow's notation (Allan *et al.*, 2010).

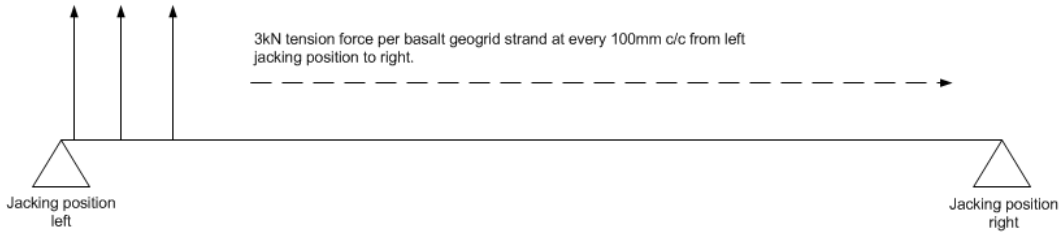


Figure 5.8: Schematic illustration of basalt geogrid mesh's force application under post-tensioning.

Force Diagram Figure 5.9 illustrates the application of Bow's notation on the jacking end of the basalt geogrid mesh. By identifying the space created by subsequent strand forces (with capital letters and in alphabetical order) a force diagram can be constructed (Allan *et al.*, 2010). A force diagram is a graphical representation of the flow of forces in the global system (Allan *et al.*, 2010). As the mesh is to be supported by only two anchors on each side of the vault, the total vertical reaction at each support during jacking was found to be 67kN upwards. By starting the force diagram at +67kN at the left hand anchor, and defining a scale of 1mm:0.033kN, the remainder of the diagram was drafted. Each strand's force reduced the previously recorded load by 3kN in sequential order. Completing the loop from the left anchor position through all of the alphabetical identifiers (including the right hand support) the force diagram closed at the starting point (Allan *et al.*, 2010).

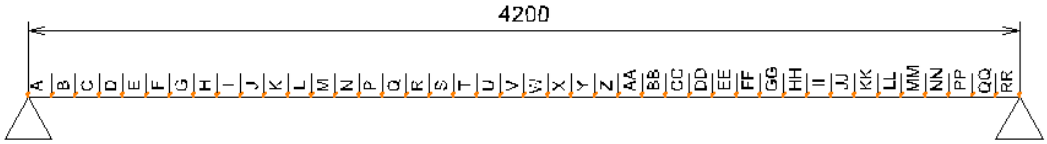


Figure 5.9: Bow's notation on basalt geogrid mesh (Allan *et al.*, 2010).

The force diagram at transfer is presented in Figure 5.10. By noting that the origin in Figure 5.9 was designating the closing string, the line which intercepted the force diagram at "a" in Figure 5.10 should also intercept the closing string at "A" in Figure 5.9 (Allan *et al.*, 2010). In order to ensure a continuous flow of forces between the different segments, the line that intercepted "b" in Figure 5.10 was placed on a line intercepting "A" and the vertical through "B" in Figure 5.9 (Allan *et al.*, 2010). By applying the same procedure to the remaining segments, the funicular curve for the given structural configuration was drafted.

Funicular Form of Cable The funicular form for the post-tensioned cable is illustrated in Figure 5.11. By trial and error, the lowest required jacking force at the anchor foundations was obtained. This was done by noting that the width of the force diagram in Figure 5.10 is an indication of the force magnitude in the post-tensioning cable (Allan *et al.*, 2010). The thinner the force diagram, the shallower the curve's sag and lower the required tension at the jacks (Allan *et al.*, 2010). A thicker force diagram yielded a deeper curve with higher jacking load requirements (Allan *et al.*, 2010). From the spatial layout, it was determined that a 3m sag will yield the lowest jack force at the anchor foundations.

This force could be determined by multiplying the measured length of the line intercepting "a" in Figure 5.10 according to the previously defined scale. This yielded a required jacking force of 74.22kN on each side of the cable. As this line was also the longest line in the force diagram, this load could be used to choose the required post-tension cable for the system. A simple FEA analysis of this configuration yielded 76kN of tension in the cable at the anchors.

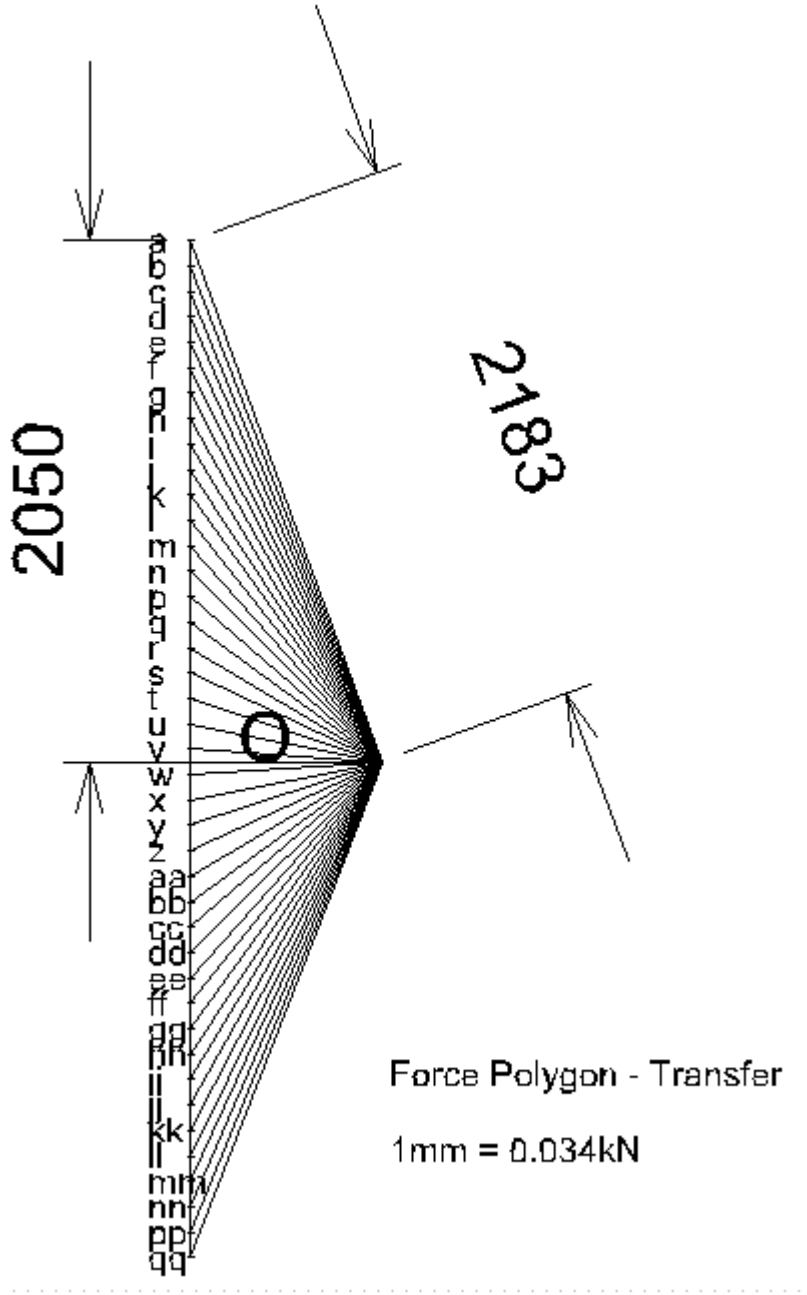


Figure 5.10: Force diagram at transfer.

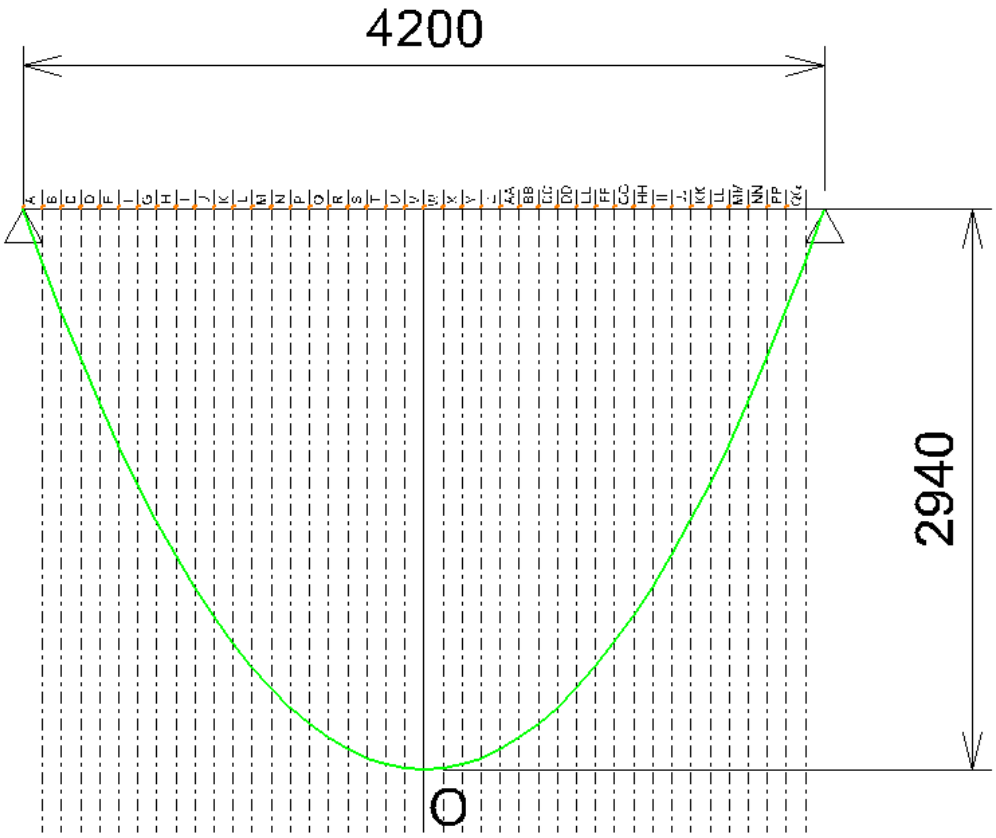


Figure 5.11: Funicular profile for cable tensioning at transfer.

Anchor Foundations The anchor foundations of the structure will have to be designed to resist a resultant jacking force 76kN per foundation. The inclination angle of the anchor rod to the horizontal was found to be approximately 40degrees. This angle was measured from the isometric model, and was based on the parameters of the foundations as will be discussed.

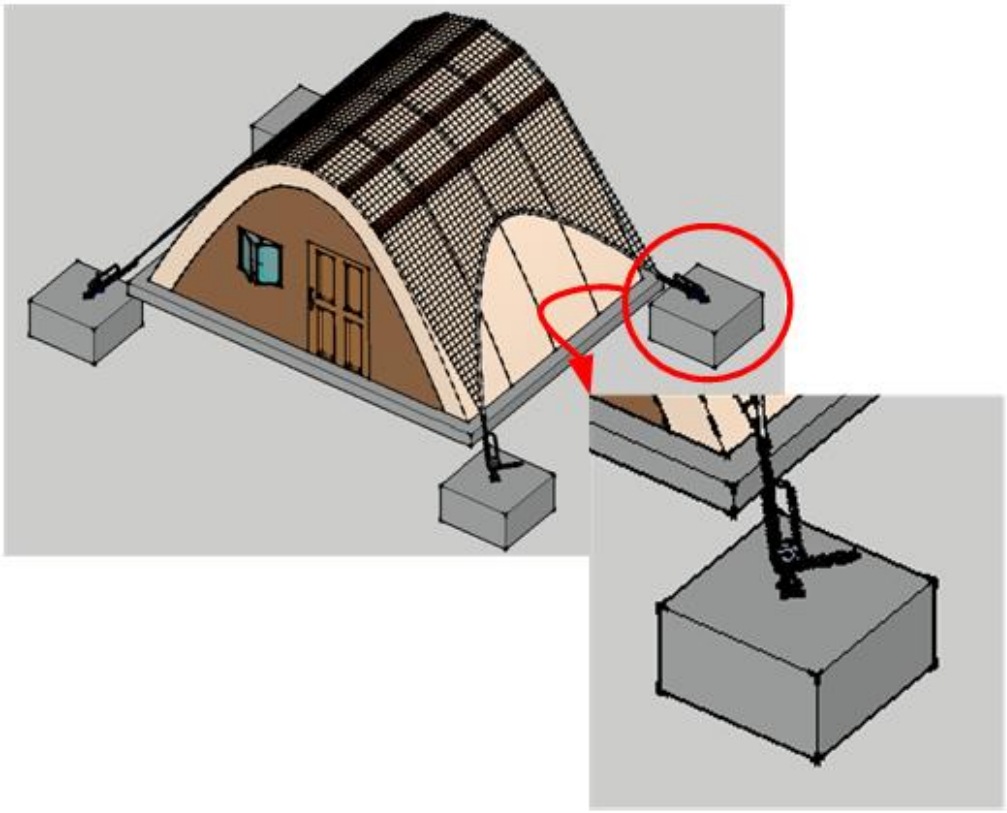


Figure 5.12: Funicular cable tensioning anchor foundations.

Resolving the jacking load into its components, the vertical force to be resisted by each anchor foundation was 48.85kN, while its horizontal component equalled 58.22kN. Assuming a density for concrete of 25kN/m^3, a foundation of at least 2m^3 will be required to resist the upward load per anchor point. The required tension force at the ends of each cable can be achieved by making use of four 8ton rated chain blocks.

It may seem intuitive to reduce the amount of concrete required by placing it underneath the soil and utilising the soils self-weight in countering the uplift force. This can possibly be achieved depending on the chain block type, anchor and space available, but will most probably be cumbersome in executing.

Another concern with regards to this configuration is the possibility of differential settlement of the different foundations. As the structure requires a pre-defined post-tension force in the mesh, possible downward settlement of the vault's foundation and upwards settlement of the anchor foundations may result in a significant loss of post-tensioning. Hence, it may be beneficial to tie the anchor foundations together into strip footings.

In order to eliminate the possibility of differential settlement, the foundation of the vault can effectively be supported by concrete beams on top of the anchor strip footing as depicted in Figure 5.13.

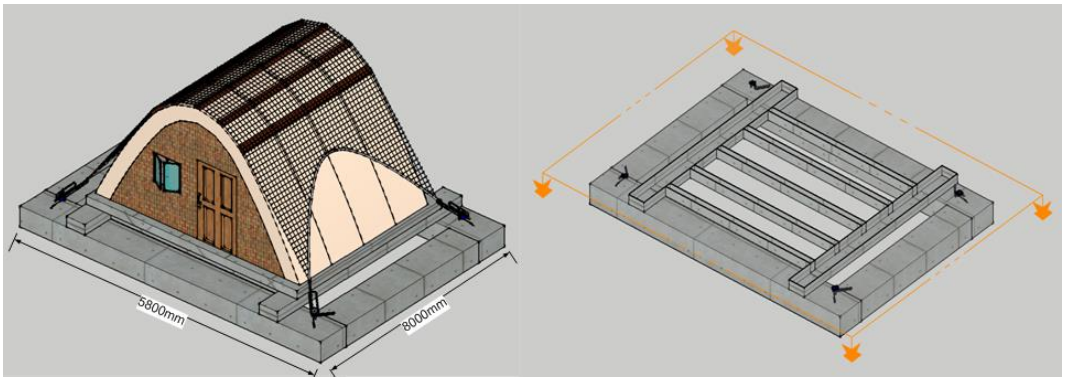


Figure 5.13: Funicular cable tensioning – tied strip footing for anchor foundation and section at foundation level.

The new proposed anchor foundation configuration was assumed to act as a simply supported beam, spanning between the anchor points. As previously discussed, the required volume of concrete to prevent uplift of the foundation was 2m^3 per anchor.

From the model, it was determined that each anchor can be pinned by 6.9m length of foundation. Assuming a width of 800mm, a depth of

360mm was required to overcome the un-factored upward force of 48.85kN, while a minimum effective depth of 540mm was required when a safety factor against uplift of 1.5 was applied (Robberts & Marshall, 2010). This was more than the minimum span/effective depth ratio of 16 for simply supported concrete beams, hence an anchor foundation depth of 550mm was adopted (Robberts & Marshall, 2010).

In order to ensure rigidity of the foundation, top and bottom reinforcement in the raft is suggested. The amount of reinforcement should be determined by considering the geotechnical conditions of the site as well as the total load of the vault onto the beams.

5.2.3 Winch Tensioning

The third alternative in tensioning the basalt geogrid mesh may be to tension it by means of an electrical or mechanical winch.

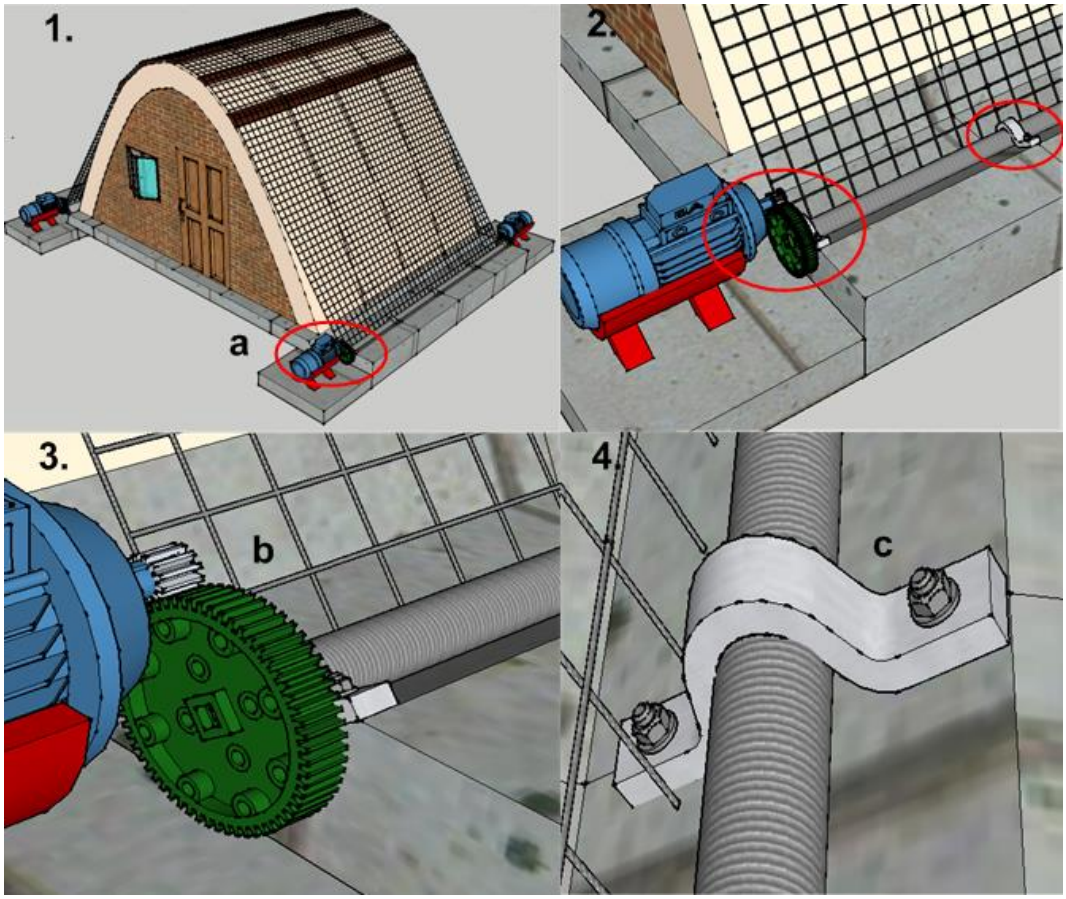


Figure 5.14: Winch tensioning

Winching Methodology The proposed mechanism is illustrated in Figure 5.14. The methodology behind this solution is to tension the mesh uniformly along the length of the vault. This can be achieved by fixing a shaft along each edge of the vault where the basalt geogrid mesh is to be anchored. The shaft can be fixed with anchor bearings (c) to the foundation at 1000mm c/c spacing which should only allow one way rotation of the shaft. Recognising that the shaft will act as a continuous beam under a uniform load of 33.5kN/m at jacking, the shaft will be subjected to a positive bending moment between the support bearings, and a negative bending moment over the supports as illustrated in Figure 5.15. The bending moment at transfer will equal 3.6kNm.

A suitable profile, from a moment resistance perspective, was determined to be a 76.2x2.5mm circular hollow profile with a design bending moment resistance of 4.34kNm. A maximum deflection of 27mm will however be observed during transfer, which is deemed non suitable in this configuration. Assuming the deflection parameter as a governing factor, a 193.7x3.5mm circular hollow section was selected. Assuming a stringent span/600 deflection limit, the maximum deflection in the section at transfer was determined to now be a mere 1.15mm.

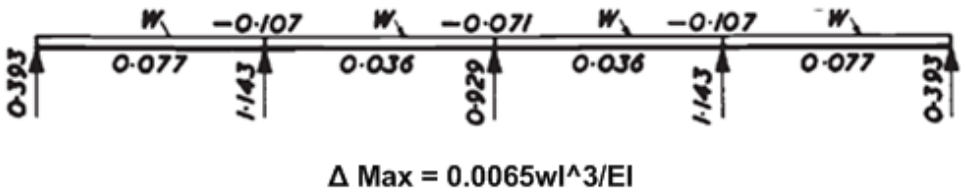


Figure 5.15: Bending moment, reaction and deflection for equal span beams under uniform load (Davison & Owens, 2008).

Winch Motor The shaft is to be propelled by an electric or mechanical winch (a). Four of these winch motors will be required to tension the mesh uniformly. The motors should be temporarily installed and fixed to the foundation. After tensioning, it should be removed for future use.

In order to reduce the winch's torque requirements, it is suggested that a low gear ratio is used. This will allow slow rotation of the shaft, while the load requirement of the winch motor is kept at a minimum. For the current configuration, the torque to be exerted by the shaft in order to obtain the required jacking force in the mesh is approximately 13.2kNm.

The initial attachment between the basalt geogrid mesh and the shaft can be as per the contractor's preference.

Anchor Foundations The foundation type to be used is as depicted in Figure 5.6 and should be designed to resist the loads as discussed under Section 5.2.1, *Anchor Foundations*.

The gears attached to the shafts should be removed after tensioning, and the shaft should be buried under a layer of soil.

In order to avoid the loss of post-tensioning due to differential settlement, the foundations of the vault and winch anchor should be designed to act as a rigid entity. This configuration will allow for possible settlement, but ensure that the winch anchor foundations remain in position relative to the vault's foundation. The winch anchor foundations should be tied to one another in the direction of the vaults span by means of tie beams. These beams will prevent possible kicking of the foot of the vault.

5.3 GABLE END WALLS

The vault may be enclosed by gable walls. These walls should however not have a translational or moment fixed connection to the shell. Should this not be the case, localised bending moments is expected in the shell at these intersections. As the vault is designed to be catenary under the

applied post-tension force and self-weight, any obstruction to the normal deflection of the shell under these loads will result in unwanted bending moments.

A sliding connection between the gable walls and shell may be considered. Such a connection may only transfer loads horizontally along a longitudinal section of the vault. Vertical deflection of the shell should not be altered by the gable end walls and adequate tolerance should hence be provided.

It is suggested that the gable walls be designed as separate entities to the vault. This can be achieved by ensuring that the walls act as cantilevers which do not require lateral support from the vault.

5.4 POST-TENSION BEARING PADS

One of the most critical areas of the structure is deemed the bearing pads. These pads will support the post-tensioned basalt geogrid mesh in service, and should be carefully manufactured in order to ensure that it exerts force onto the vault's shell at the pre-determined inclination angle. General details of what these bearing pads should typically look like are given in Figure 5.16.

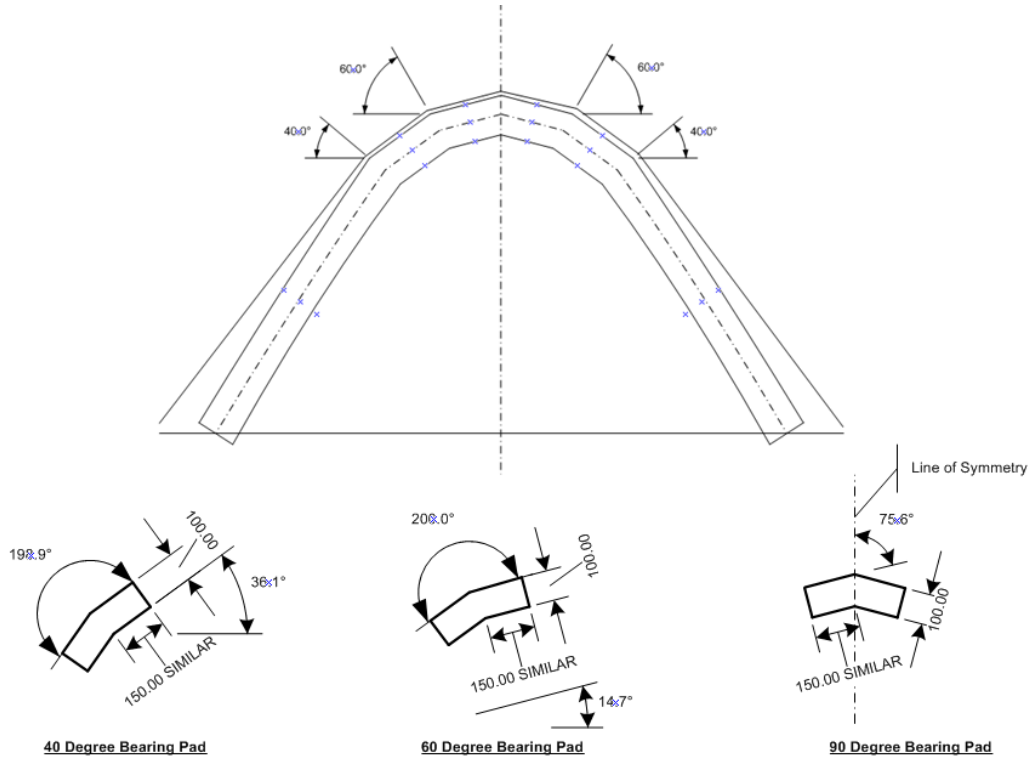


Figure 5.16: Post-tension bearing pad details.

The proposed material out of which these bearing pads should be manufactured is High Density Polyethylene (HDPE). Tests conducted on unoiled post-tension tendons, sleeved in HDPE ducts, measured a coefficient of friction of 0.12 (Wang, Prozzi & Hong, 2006). This value was found to be almost 50% lower than the recommended AASHTO friction coefficient for friction losses in post-tensioning systems (Wang *et al.*, 2006). The oiling of post-tensioning tendons yielded even lower friction coefficients and can therefore be implemented to further improve the loss of post-tensioning force (Wang *et al.*, 2006).

As HDPE is easily mouldable, complex and accurate shapes can be created easily and effectively. Alternative materials may also be considered sufficient, provided that the friction coefficient for the selected material is equal or less than that of HDPE in a post-tensioning configuration.

5.5 ERECTION SEQUENCE

As a result of the optimised geometry of the vault, it is intuitive to assume that the structure may not support itself in pure compression in the absence of a post-tension force. During construction, the shell will be constructed prior to it being post-tensioned to transfer force. It was therefore considered important to verify if the structure requires formwork up until post-tensioning it to transfer.

By modifying the final FEA model of the structure, removal of the post-tension force suggested that the structure will be subjected to a 1.75kNm/m bending moment. This model configuration catered for the scenario where the formwork is removed underneath the vault's shell prior to it being post-tensioned. At an axial compressive force of 19.32kN/m, the force eccentricity was determined to be 90.5mm, which suggested the development of some tensile stress in the extreme fibres of the section. The shell did, however, still show some tensile resistance which may be utilised.

Assuming the 28day characteristic properties of the Earth Brick masonry, the un-cracked bending moment of the section was determined to be 3.46kNm/m. This suggested adequate bending moment capacity for the removal of the formwork prior to the post tensioning operation. For the 28day strength, the factor of safety regarding the bending moment resistance was found to be ±2.00. It was therefore though that the 7 day bending moment resistance may be adequate for removal of the formwork prior to post-tensioning the structure, but is not suggested until more accurate calculation confirms this assumption.

6. CONCLUSIONS AND RECOMMENDATIONS

6.1 FINDINGS

In Section 3 and Section 4, the definition and design of an optimised, post-tensioned catenary vault was respectively discussed. Different solutions were explored which arrived to a final, liveable, structurally efficient and viable solution as illustrated in Figure 6.1.

By implementing Stem Element theory, it was determined that an optimised catenary form of the vault will only be achieved should the vault's shell be excessively thick. This finding suggested that in such a case, excessive self-weight of the structure yielded a funicular line for pure compression which comparatively overlapped one another for all load combinations considered. An excessive section thickness did, however, defeat the purpose of finding a structure which efficiently utilises the material it is constructed of.

In order to minimize the material usage of the vault, post-tensioning of the structure was considered. The two main post-tensioning solutions were to place the post-tensioning tendon coincidental to the shell's geometric centroid, or to drape the structure in a post-tensioned mesh. The latter solution was selected as the most viable solution and three different shell thicknesses at different post-tension magnitudes were considered.

By finite element analysis and analytical designs it was found that a 250mm thick vault, post-tensioned to 22kN post-tension force, yielded adequate axial compressive and un-cracked bending moment capacity to the applied loads. The section did however prove to be inadequate in resisting bending moments generated during hurricane wind load conditions.

Similarly it was proven that a 335mm thick vault, post-tensioned to 13kN post-tension force, failed under the same applied loading. From this investigation it was furthermore found that the required vault thickness

was inversely related to the post-tension force applied. By increasing the section thickness, a reduced effective post-tension force was required to obtain adequate section capacity. Inversely a reduced section thickness required an increased post-tension force in order to obtain the required design section capacity.

The geometry coordinates of the final structural solution are listed in Appendix A.

6.2 ON THE GEOMETRY OF THE VAULT

The vault solution selected has a clear height of 2780mm, a length of 4000mm and a span of 4900mm. A minimum shell thickness of 350mm is required with an effective post-tension force of 25kN. An initial post-tension force at transfer of 31.25kN is required, which will be obtained by jacking the mesh to 33.5kN/m.

At transfer, the geometry is not optimised to resist the loads it is subjected to in pure compression. The structure was therefore modelled and found to have adequate resistance against bending moments and axial loads at transfer.

A graphical representation of the final vault configuration is depicted in Figure 6.1.

6.3 ON THE PERFORMANCE CRITERIA OF THE VAULT

The shell should be constructed of earth bricks laid in general purpose mortar which will be in pure compression during dominant and service load conditions. During the ultimate load condition, bending moments will yield no flexural tension in the extreme fibres of the vault's shell as the FLPC falls within the kern of the section.

During hurricane wind conditions, the structure will be subjected to more elaborate bending moments. These moments will result in relatively high flexural tensile stresses which will govern the extreme fibres of the shell.

The vault's shell was determined to have adequate capacity to resist these forces in the absence of tensile reinforcement. Cracking of the section is however allowed and significant damage is expected to occur. The structure is designed to not catastrophically fail as a result of hurricane wind loads and is expected to protect its occupants against such unpleasant conditions. It should furthermore be noted that, although the structure is expected to remain standing after such an event, it may have to be taken out of service or require significant repair to reinstate it to its original design state.

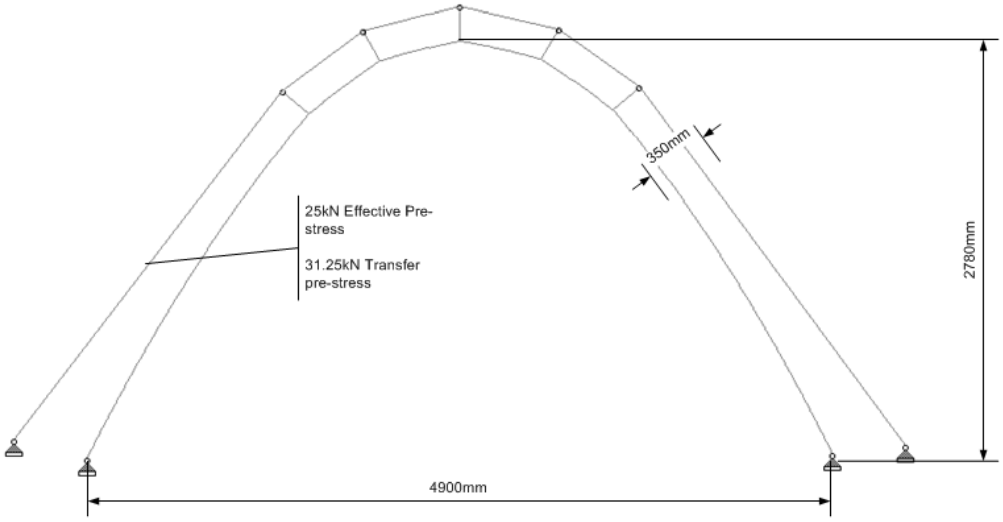


Figure 6.1: Final vault geometry

As previously mentioned, the shell will be constructed of earth bricks laid in general purpose mortar. This will result in the shell having force resistance capacities as listed in Table 55.

It was found that the vault is able to withstand its self-weight in the absence of the designed post-tension force. This is important not only for construction purposes, but also in case the anchors are damages while in service, and a loss of post-tensioning force is observed.

6.4 ON POST-TENSIONING SOLUTIONS

Three post tension solutions were discussed. These involved tensioning the basalt geogrid mesh by means of ratchets, funicular draped high strength cables or winching. The solutions are depicted in Figure 6.2.

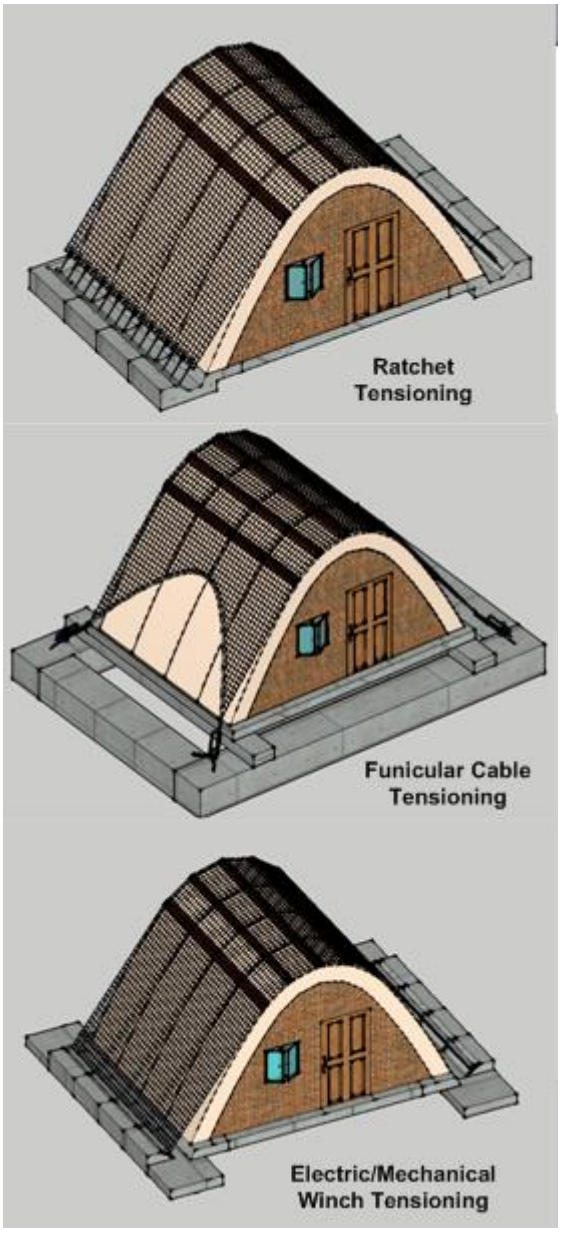


Figure 6.2: Post-tensioning solutions.

6.4.1 Ratchet Tensioning

The ratchet tensioning solution may possibly be the solution with the lowest cost implication to the post-tensioning problem. This statement should, however, be verified by future research into the topic. The tensioning process will, however, be a laborious process which will allow room for error during tensioning and possible fatigue of the labourers involved. It is envisaged that significant post-tension losses will be evident during hooking of the load distribution beam to the anchor hooks, while the ratchet mechanisms are found not to be excessively expensive.

6.4.2 Funicular Cable Tensioning

This solution is considered the most sophisticated solution in the series. In order to ensure that the cable is placed along the pre-determined funicular path, the basalt geogrid mesh will have to be cut and modified accordingly. The cable will then have to be adequately fixed to the basalt geogrid mesh, all of which come at a cost.

It is envisaged that, depending on the preferred anchor used, post-tensioning losses during the hooking process may be higher than desired. It was furthermore determined that the foundations of the structure will have to be modified in order to ensure rigidity thereof. This will require more concrete and possibly steel reinforcing, which increases the cost of the structure.

6.4.3 Winch Tensioning

The winch tensioning method is deemed a midway solution between the anticipated low cost and primitive ratchet tensioning method and sophisticated funicular tensioning method. This method will automate the post-tensioning process, saving on time as well as physical labour. As the shaft will form part of the permanent structure, there is no concern of post-tension losses resulting from hooking.

The winch motors, gears and anchor bearings may be costly; countering the objective of a low cost solution.

6.5 RECOMMENDATIONS

As this research is theoretically based, it is recommended that scale model testing on the suggested configuration is conducted. These tests should be carried out in order to determine the actual wind pressure coefficients on the structure, as well as physical testing of the structures physical strength.

Although the structure is found to be fairly robust under its dominant load condition, it is suggested that care should be taken in the accuracy of the geometric construction thereof. It is therefore recommended that future research should be conducted (in the form of FEA modelling) into the sensitivity of this shape to installation imperfections.

During erection, it is thought that adequate structural resistance, in the absence of a post-tensioning force, is generated by the shell. As a result, it is highly likely that the props, supporting the structure, may be removed prior to post-tensioning thereof. This assumption should, however, be investigated, as the analysis conducted on the erection sequence negated the fact that the earth bricks will most probably not have achieved its 28day design compressive strength.

The tendon supports require careful design. It needs to be ensured that the angle at which the tendon projects its loads onto the shell is at a low tolerance to the intended objective. The bearing pads should furthermore be properly designed in order to resist the loads exerted by the tendon onto them. As it is moreover at this stage unknown what the structure's response to temperature differences are, it is recommended that future research takes into consideration the loss or increase of the post-tension force on the structure due to temperature differentials.

The recommended solution for post-tensioning is post-tensioning by means of winching. This solution will ensure a uniform distribution of the jacking force onto the basalt geogrid mesh. The winching process will furthermore be less laborious in executing, while the motors to be used will be re-useable for other applications after the vault was post-tensioned. The cost of the support bearings may be of concern, and alternative methods of supporting the shaft may be worthwhile to explore.

An investigation into the capital cost of the recommended solution is to be conducted. This cost is then to be compared to the current housing cost of the area in which it is proposed to be implemented. It is furthermore recommended that, should a full scale model be constructed, the solution be discussed with the local community where it is proposed to be implemented. This recommendation is to ascertain what methods of construction will be preferred by the local community.

It is recommended that the foundations of the vault and that of the tendon be thoroughly connected to one another. This configuration is recommended mainly to avoid possible differential settlement, which may result in a significant loss of post-tensioning. The forces in the structure are highly sensitive to the position of its line of thrust. Pertaining to the design of the foundations, the soil's characteristic conditions should first be determined, and should be sized considering the loads applicable, as well as the effective bearing capacity of the soil and post-tensioning solution considered.

In order to ensure a safe and liveable space, the structure may be enclosed by gable walls. It is recommended that these walls are designed as separate entities to that of the vault. The foundations of the walls may be design to tie into the floor slab of the vault. It should be insured that no load transfer at the roof-to-wall interface realise.

APPENDIX A: FINAL GEOMETRY COORDINATES

APPENDIX B: DESIGN CALCULATION

B.1 SECTION CAPACITY VERIFICATION FOR 250MM SHELL THICNKESS WITH 22KN POST-TENSION

B.2 SECTION CAPACITY VERIFICATION FOR 335MM SECTION WITH 13KN POST-TENSION FORCE

B.3 SECTION CAPACITY VERIFICATION FOR 350MM SECTION WITH 25KN POST-TENSION

B.4 BUCKLING LOAD OF 250MM VAULT WITH 22KN POST-TENSION

B.5 BUCKLING LOAD OF 335MM VAULT WITH 13.5KN POST-TENSION

B.6 BUCKLING LOAD OF 350MM VAULT WITH 25KN POST-TENSION

B.7 POST-TENSION DESIGN FOR 350MM VAULT WITH 25KN POST-TENSION FORCE

REFERENCES

2 Ton Power Puller | *TEKTON 5541*. 2016. [Online], Available: http://tekton.com/Pulling_Tools/Power_Pullers/2-Ton-Power-Puller [2016, December 06].

Allan, E., Zaleski, W. & Boston Structures Group. 2010. *Forms and Forces*. 1st ed. Canada: John Wiley & Sons, Inc.

Asian Development Bank Ed. 2009. *Poverty in the Philippines: causes, constraints, and opportunities*. Mandaluyong City, Philippines: Asian Development Bank.

Bradley, R.A. 2011. Wind-tunnel study of cross vault structures. Engineering Research. University of the Witwatersrand. [Online], Available: http://146.141.12.21/handle/10539/10534 [2016, August 08].

Bradley, R.A., Gohnert, M., Goliger, A.M. & Mistry, Y. 2016. Wind loading on catenary vault structures. *Journal of the South African Institution of Civil Engineering= Joernaal van die Suid-Afrikaanse Instituut van Siviele Ingenieurswese*. 58(4):29–47. [Online], Available: https://journals.co.za/content/civileng/58/4/EJC199572 [2017, July 13].

C&CI. 2009. *Fulton's Concrete Technology*. 9th Edition ed. Midrand, South Africa: Cement and Concrete Institute.

Cowan, H.J. 1977. A history of masonry and concrete domes in building construction. *Building and Environment*. 12(1):1–24. [Online], Available: http://www.sciencedirect.com/science/article/pii/0360132377900026 [2016, August 09].

Curtin, W.G., Shaw, G., Beck, J.K. & Bray, W.A. 1995. *Structural Masonry Designer's Manual*. Second ed. Great Britain: Blackwell Science.

Davison, B. & Owens, G.W. 2008. *Steel Designer's Manual*. 6th ed. Blackwell Publishing. [Online], Available: http://onlinelibrary.wiley.com/doi/10.1002/9780470775097.fmatter/summary [2016, December 14].

De Fazio, P. 2011. Basalt fibra: from earth an ancient material for innovative and modern application. *Energia Ambiente e Innovazione*. 1(2):89–96.

Fiore, V., Scalici, T., Di Bella, G. & Valenza, A. 2015. A review on basalt fibre and its composites. *Composites Part B: Engineering*. 74(7):74–94.

German Building and Civil Engineering Standards Committee & German Committee for Structural Steelwork. 1990.

Gohnert, M. 2016. *A Program for the Determination of Catenary Forms Based on Stem Element Theory*. Johannesburg: University of the Witwatersrand.

Gohnert, M. & Bradley, R. 2016. Stem Elements for the Generation of Optimal Structural Forms. *(Article under review)*. 10.

Griffiths, J., Berlinger, J., Westcott, B. & Alexander, R. 2016. Typhoon Haima: Philippines hit by second storm in a week. *CNN*. 20 October. [Online], Available: http://edition.cnn.com/2016/10/18/asia/typhoons-haima-philippines/ [2016, October 24].

Holmes, J.D. 2001. *Wind loading of structures*. London ; New York: Spon Press.

Huerta, F., S. 2001. Mechanics of masonry vaults: the equilibrium approach. *P.B Lourenco & P. Roca (Eds.)*. 47–69. [Online], Available: http://oa.upm.es/569 [2016, August 05].

Jaramillo, J.J. 2013. *Super Typhoon Haiyan Devastates Philippines*. [Online], Available: http://www.slate.com/articles/news_and_politics/photography/2013/11/super_typhoon_haiyan_devastates_philippines_photos.html [2016, December 14].

Jinsan, J. & Yanlin, G. 2002. In-plane elastic buckling of Arch. *Tsingua Science and Technology*. 7(3):322–325.

Katayanagi Hiroshi, S. 2012. *The Forgotten Slums: The Smoky Mountain*. [Online], Available: http://www.jesuitsocialcenter-tokyo.com/eng/?page_id=2987 [2016, August 24].

Marsh, T. 2013. Super Typhoon Haiyan Seen from Space. [Online], Available: http://www.taylormarsh.com/2013/11/super-typhoon-haiyan-seen-space/ [2016, December 14].

Marshall, V. & Robberts, J.M. 2000. *Prestressed Concrete Design And Practice*. 1st ed. Midrand: Concrete Society of South Africa.

Morton, T. & Bennetts, R. 2008. *Earth masonry design and construction guidelines*. Bracknell: IHS BRE Press.

Mullen, J. 2013. Super Typhoon Haiyan, strongest storm of 2013, hits Philippines. 8 November. [Online], Available:

http://edition.cnn.com/2013/11/07/world/asia/philippines-typhoon-haiyan/ [2016, October 24].

Padua, D. 2013. *The 10 deadliest typhoons in the Philippines | The National*. [Online], Available: http://www.thenational.ae/world/southeast-asia/the-10-deadliest-typhoons-in-the-philippines [2016, December 14].

Pearson, M., Donchev, T. & Salazar, J. 2013. Long-Term Behaviour of Prestressed Basalt Fibre Reinforced Polymer Bars. *Procedia Engineering*. 54(4th):261–269.

Pedreschi, R. 2006. The Structural Behaviour and Design of Free-Standing Barrel Vaults of Eladio Dieste. *Proceedings of the Second International Congress on Construction History*. 3:2451–2467. [Online], Available: https://www.researchgate.net/profile/Remo_Pedreschi/publication/263068747_THE_STRUCTURAL_BEHAVIOUR_AND_DESIGN_OF_FREESTANDING_BARREL_VAULTS_OF_ELADIO_DIESTE/links/54c0fb280cf28a6324a4f69c.pdf [2016, August 13].

Pedreschi, R. & Theodossopoulos, D. 2007. The double-curvature masonry vaults of Eladio Dieste. *Proceedings of the Institution of Civil Engineers - Structures and Buildings*. 160(1):3–11.

Perez, J.B. 2016. *Poverty incidence among Filipinos registered at 21.6% in 2015 - PSA*. [Online], Available: https://psa.gov.ph/poverty-press-releases [2016, December 19].

Raju, N.K. 2007. *Prestressed Concrete*. 4th ed. New Dehli: Tata McGraw-Hill.

Robberts, J.M. & Marshall, V. 2010. *Analysis and Design of Concrete Structures*. Pretoria: Nuclear Structural Engineering.

Rowlett, R. & University of North Carolina. 2000. *Saffir-Simpson Hurricane Intensity Scale*. [Online], Available: https://www.unc.edu/~rowlett/units/scales/saffir.html [2016, December 20].

Ryan Bradley. 2011. *Wind Pressure Coefficients on Catenary Vaults*. Johannesburg: University of the Witwatersrand.

SABS. 2011. *Basis of structural design and actions for buildings and industrial structures, SANS 10160-1:2011*. Pretoria: The Council for the South African Bureau of Standards.

Saravanan, D. 2006. Spinning the rocks - Basalt Fibres. *IE(I) Journal-TX*. 86:39–45.

Sengupta, D.A.K. & Menon, P.D. n.d. [Online], Available: http://nptel.ac.in/courses/IIT-MADRAS/PreStressed_Concrete_Structures/pdf/3_Analysis_of_Members/Section3.3.pdf [2016, August 08].

Sim, J., Park, C. & Moon, D.Y. 2005. Characteristics of basalt fiber as a strengthening material for concrete structures. *Composites Part B: Engineering*. 36(6–7):504–512.

Timoshenko, S.P. & Gere, J.M. 1963. *Theory of Elastic Stability*. 2nd ed. Vol. 17. Singapore: McGraw-Hill 'Co-Singapore.

Truesdell, C. 1983. The influence of elasticity on analysis: the classic heritage. *Bulletin of the American Mathematical Society*. 9(3):293–310. [Online], Available: http://www.ams.org/bull/1983-09-03/S0273-0979-1983-15187-X/S0273-0979-1983-15187-X.pdf [2016, August 09].

Vermeltfoort, A.T. 2001. Analysis and Experiments of Masonry Arches. *P.B Lourenco & P. Roca (Eds.)*. (Proceedings of the 3rd International Seminar on Historical Constructions):489–498. [Online], Available: http://www.hms.civil.uminho.pt/sahc/2001/page%20489-498%20_151_.pdf [2016, August 08].

Walker, P.J. 2004. Strength and erosion characteristics of earth blocks and earth block masonry. *Journal of Materials in Civil Engineering*. 16:497–506.

Wang, F., Prozzi, J.A. & Hong, F. 2006. *Evaluation of Equipment, Methods, and Pavement Design Implications for Texas Conditions of the AASHTO 2002 Axle Load Spectra Traffic Methodology: Literature Review and Level 1 Data*. (no. 4510). Center for Transportation Research, University of Texas at Austin.